ALEKSI PALMROTH

Bioresorbable Wireless Resonance Sensors

Materials and processes

ALEKSI PALMROTH (NÉE HÄNNINEN)

Bioresorbable Wireless Resonance Sensors
Materials and processes

ACADEMIC DISSERTATION
To be presented, with the permission of
the Faculty of Medicine and Health Technology
of Tampere University,
for public discussion in the auditorium S2
of the Sähkötalo, Korkeakoulunkatu 3, Tampere,
on 19 November 2021, at 12 o'clock.

ACADEMIC DISSERTATION
Tampere University, Faculty of Medicine and Health Technology
Finland

Responsible supervisor and Custos	Professor Minna Kellomäki Tampere University Finland	
Supervisors	Professor Emeritus Jukka Lekkala Tampere University Finland	Professor Susanna Miettinen Tampere University Finland
Pre-examiners	Professor Diego Mantovani Laval University Canada	PhD Clémentine Boutry EPFL Lausanne Switzerland
Opponent	Professor Reijo Lappalainen University of Eastern Finland Finland	

The originality of this thesis has been checked using the Turnitin OriginalityCheck service.

ACKNOWLEDGEMENTS

I would like to express my gratitude towards Professor Minna Kellomäki for offering me the opportunity to work in her research group in this project. Professor Kellomäki was the main supervisor in this thesis, and I am grateful for her trust, support and guidance throughout the process. I would also like to thank the other supervisors, Professor Jukka Lekkala and Professor Susanna Miettinen for their support, valuable advices, encouragement and permission to work in their laboratories during these years.

I want to express my gratitude to the pre-examiners, Assistant Professor Clémentine Boutry and Professor Diego Mantovani for their efforts in reviewing this thesis. Their constructive comments allowed me to see this thesis from a new perspective, which will benefit me also in the future.

I owe my deepest gratitude to Timo Salpavaara for sharing his knowledge and experience with me. Without your contributions, this thesis would be at least very different, if not non-existent. I also want to thank Niina Ahola for her valuable insights concerning this thesis, as well as for mentoring and supporting me throughout these years.

I would like to thank Maiju Juusela for introducing me into the project and for sharing her expertise with me. I wish to thank co-authors Anni Antniemi, Inari Lyyra, Mart Kroon, Professor Petri Vuoristo, Sanna Karjalainen, Tommi Kääriäinen and Professor Jonathan Massera for their valuable efforts related to the publications.

I am extremely grateful to Heikki Liejumäki, Suvi Heinämäki, Pasi Kauppinen, Thomas Kraft, Anna-Maija Honkala, Miia Juntunen, Sari Kalliokoski, Jukka-Pekka Pirhonen, Nina Sandberg, Jari Viik, Tomi Ryynänen and Marika Janka for the time and effort that they have invested in supporting this project. I also want to thank everyone at Tampere University's ProLab and FabLab for their assistance.

ABSTRACT

Implantable sensors are gaining increasing attention due to their ability to provide local information from inside the body. This information can be used for example to detect complications after a surgical operation. Bioresorbable sensors that are ultimately metabolized by the body are a promising technology for many applications where the monitoring need is only temporary. As these materials are cleared from the body without a removal surgery, they hinder the complication risks related to long-term implantation of non-degradable devices or their removal.

This thesis addresses bioresorbable materials, their performance and fabrication methods related to orthopedic inductor-capacitor circuit-based wireless sensors. The sensing method was chosen due to the wireless readout and simple structure of the sensors. Due to the delicate nature of bioresorbable materials, the project was started by studying sensors made from conventional non-degradable materials. Thereafter, bioresorbable inductor coils were fabricated. Finally, similar fabrication principles were applied to build functional fully bioresorbable sensors.

The conductors were mainly made by evaporating magnesium (Mg) films onto polymeric or glass substrates, but also sputtered zinc (Zn) films and commercial molybdenum (Mo) wire were used. No significant differences in the resistances of the Mg and Zn films of similar thicknesses were noticed. Thus, Zn was estimated to offer a similarly conducting but slower degrading alternative for commonly used Mg. In this study, the thickness of the sputtered Zn conductors was limited due to excessive heating of the polymer substrates.

The sensor substrates used in the study included conventional printed circuit boards, bioresorbable polymeric screws, bioresorbable metallized polymer fibers and sheets, as well as bioactive glass discs. The fabricated bioresorbable sensors were wirelessly readable up to distances of about 15 mm, as compared to the non-degradable sensor with 23 mm. Different measurands included pressure, compression of the screws and complex permittivity of the sensor environment. The polymer-based pressure sensors were most rigorously studied, and their performance was uniform in ambient conditions. One of the pressure sensors was wirelessly readable and responsive to pressure (0-200 mmHg) for 10 days in simulated physiological conditions, but its stability should be improved for practical

applications. The results indicate that the deterioration of the sensor performance was caused by water, which diffused into the sensor substrates and thus corroded the metal conductors, causing dimensional changes to the sensor structure.

In summary, the fabricated devices included simple sensor architectures that could be assembled with only few processing steps. It was shown that depending on the sensor design, different measurements and thus various orthopedic applications could be possible. However, especially the relatively poor stability of the bioresorbable sensors requires attention in the future. In addition, the short-range reading distances may limit potential clinical applications. Nevertheless, the presented results provide a good reference point for choosing the right bioresorbable materials for future studies.

TIIVISTELMÄ

Implantoitavat anturit saavat osakseen kasvavaa huomiota, koska ne pystyvät tuottamaan paikallista tietoa kehon sisältä. Tätä tietoa voidaan käyttää esimerkiksi havaitsemaan komplikaatioita kirurgisen operaation jälkeen. Bioresorboituvat anturit, jotka hajoavat kehon sisällä ja jotka kehon aineenvaihdunta pystyy lopulta poistamaan, ovat lupaava teknologia moniin väliaikaisiin mittauksiin. Koska tällaiset anturit hajoavat kehossa, vältytään ylimääräisiltä komplikaatioriskeiltä, jotka liittyvät pitkäaikaisiin antureihin tai niiden poisto-operaatioihin.

Tämä väitöskirja käsittelee bioresorboituvia materiaaleja ja niiden ominaisuuksia sekä valmistusmenetelmiä langattomissa ortopedisissä antureissa. Työssä käsitellään kela-kondensaattori-värähtelypiireihin perustuvia antureita niiden yksinkertaisen rakenteen ja langattoman lukutekniikan vuoksi. Johtuen bioresorboituvien materiaalien haastavasta prosessoinnista, tutkittiin projektin alussa ensin ei-hajoavista materiaaleista valmistettuja antureita. Tämän jälkeen valmistettiin bioresorboituvia keloja. Vastaavia periaatteita hyödyntäen valmistettiin lopulta langattomia antureita bioresorboituvista materiaaleista.

Anturien johtimet valmistettiin pääosin höyrystämällä kalvoja magnesiumista (Mg) polymeeri- tai lasialustoille, mutta myös sputteroituja sinkkikalvoja (Zn) sekä kaupallista molybdeenilankaa (Mo) tutkittiin. Yhtä paksujen magnesium- ja sinkkikalvojen resistansseissa ei havaittu merkittäviä eroja, joten sinkin pääteltiin tarjoavan hitaammin hajoavan vaihtoehdon yleisesti käytetylle magnesiumille. Tässä tutkimuksessa sinkkikalvojen paksuutta rajoitti kuitenkin polymeerialustan liiallinen lämpeneminen prosessin aikana.

Tutkimuksessa käytettiin anturien alustoina (substraatteina) perinteisiä ei-hajoavia piirilevyjä, bioresorboituvia polymeeriruuveja, bioresorboituvia metalloituja polymeerikuituja ja -levyjä sekä bioaktiivisesta lasista valmistettuja kiekkoja. Bioresorboituvat anturit voitiin lukea korkeintaan noin 15 mm etäisyydeltä, kun taas ei-hajoavien antureiden korkein mahdollinen lukuetäisyys oli 23 mm. Mitattavia suureita olivat paine, ruuvien puristuma sekä anturien ympäristön kompleksinen permittiivisyys. Tarkimmin tutkittiin polymeerialustoille valmistettuja paineantureita, joiden käyttäytyminen oli yhteneväistä tavallisissa huoneolosuhteissa. Yksi antureista oli langattomasti luettavissa ja paineeseen reagoiva (0-200 mmHg) 10 päivän ajan

simuloiduissa kehon olosuhteissa. Sen stabiilisuus ei kuitenkaan ollut riittävällä tasolla käytännön sovelluksiin. Tulosten perusteella anturiin tunkeutunut vesi aiheutti sen toiminnan heilahtelut reagoimalla magnesiumjohtimien kanssa ja aiheuttamalla muutoksia anturin rakenteeseen.

Yhteenvetona voidaan sanoa, että väitöskirjassa valmistettujen antureiden rakenne oli yksinkertainen, mikä mahdollisti niiden kokoamisen vain muutamalla prosessivaiheella. Suunnittelemalla anturin rakenne eri tavoin oli mahdollista tehdä useita erityyppisiä mittauksia, mikä mahdollistaa monia ortopedisiä sovelluksia. Erityisesti anturien melko heikon stabiilisuuden parantaminen vaatii tulevaisuudessa lisätutkimuksia. Lisäksi anturien rajoitettu lukuetäisyys voi rajata mahdollisia käytännön sovelluksia. Tutkimuksen tulokset tarjoavat hyvän vertailukohdan oikeiden bioresorboituvien materiaalien valitsemiseen jatkossa.

CONTENTS

ABBREVIATIONS

AC	Alternating current
ACS	Acute compartment syndrome
ALD	Atomic layer deposition
CVD	Chemical vapor deposition
DC	Direct current
DMEM	Dulbecco's modified eagle medium
di-H_2O	Deionized water
DSC	Differential scanning calorimetry
EBSS	Earle's balanced salt solution
E-beam	Electron beam
EHT	Electron high tension
FBS	Fetal bovine serum
FESEM	Field-emission scanning electron microscope
FIBSEM	Focused ion-beam scanning electron microscope
HBSS	Hank's balanced salt solution
HCl	Hydrochloric acid
ICP	Intracranial pressure
i.v.	Inherent viscosity
LC	Electrical circuit consisting of coil and capacitor
LED	Light-emitting diode
MEM	Minimum essential medium
Micro-CT	Micro-computed tomography
PBTPA	Poly(buthanedithiol 1,3,5-triallyl-1,3,5-triazine-2,4,6 (1H, 3H, 5H)-trione pentenoic anhydride)
PCB	Printed circuit board
PCL	Poly(ε-caprolactone)
PDTEC	Poly(desamino tyrosyl-tyrosine ethyl ester carbonate)
PECVD	Plasma-enhanced chemical vapor deposition
PGS	Poly(glycerol sebacate)
PLCL	Poly(lactide-co-caprolactone)

PLDLA	Poly(L/D-lactide)
PLGA	Poly(lactide-co-glycolide)
PLLA	Poly(L-lactide)
POC	Poly(1,8-octanediol-co-citrate)
Poly(DTE carbonate)	Poly(desamino tyrosyl-tyrosine ethyl ester carbonate)
PoMAC	Poly(octamethylene maleate (anhydride) citrate)
PTMC	Poly(trimethylene carbonate)
PVA	Poly(vinyl alcohol)
PVD	Physical vapor deposition
Q	Quality factor
Q-factor	Quality factor
RF	Radio frequency
RLC	Electrical circuit consisting of resistor, coil and capacitor
SBF	Simulated body fluid
SEM	Scanning electron microscopy

SYMBOLS

C	Capacitance, or capacitor component in a circuit
C_s	Capacitance of the sensor
e	Euler's number
f	Frequency
$f_{\max(Re)}$	Estimate for the frequency of the maximum in the real part of impedance
$f_{\text{phase-dip}}$	Estimate for the frequency of the minimum in the phase of impedance
f_0	Resonance frequency of an inductor-capacitor circuit
L	Inductance, or inductor component in a circuit
L_s	Inductance of the sensor
L_{crit}	Critical sample thickness
R	Resistance, or resistor component in a circuit
R_s	Resistance of the sensor
$Re\ (Z)$	Real part of the impedance
T_g	Glass transition temperature
T_m	Melting temperature
Z	Impedance
δ	Skin depth of a conductor
ϱ	Electrical resistivity of the material
μ_r	Relative permeability
μ_0	Permeability constant

ORIGINAL PUBLICATIONS

Publication I Salpavaara, T.*, Hänninen, A.*, Antniemi, A., Lekkala, J., Kellomäki, M. Non-destructive and Wireless Monitoring of Biodegradable Polymers. Sensors and Actuators B: Chemical (2017) 251, 1018-1025.

Publication II Palmroth, A., Salpavaara, T., Lyyra, I., Kroon, M., Lekkala, J., Kellomäki, M. Bioresorbable Conductive Wire with Minimal Metal Content. ACS Biomaterials Science & Engineering (2018) 5, 1134-1140.

Publication III Palmroth, A., Salpavaara, T., Lekkala, J., Kellomäki, M. Fabrication and Characterization of a Wireless Bioresorbable Pressure Sensor. Advanced Materials Technologies (2019) 4, 1900428.

Publication IV Palmroth, A., Salpavaara, T., Vuoristo, P., Karjalainen, S., Kääriäinen, T., Miettinen, S., Massera, J., Lekkala, J., Kellomäki, M. Materials and Orthopedic Applications for Bioresorbable Inductively Coupled Resonance Sensors. ACS Applied Materials & Interfaces (2020) 12, 31148–31161.

*These authors contributed equally

AUTHOR'S CONTRIBUTIONS

Publication I   The author was responsible for the materials-related parts in writing of the paper and in interpreting the data. The author participated in the electrical measurements of the encapsulated sensors together with the co-authors, as well as fabricated the Parylene coatings onto the sensors.

Publication II   The author wrote the manuscript and analyzed the data as the main author. Together with the co-authors, he planned the study, fabricated the samples, and did the electrical measurements.

Publication III   The author wrote the manuscript as the main author. He was responsible for choosing the polymeric materials and fabricating the sensors. Together with the co-authors, the author planned the study, measured the sensors, and analyzed the data. The presented pressure sensor was designed by Timo Salpavaara.

Publication IV   The author planned the main parts of the study and wrote it as the main author. Together with the co-authors, he fabricated the devices, performed the electrical measurements and material tests, as well as analyzed the results. The presented devices were designed by Timo Salpavaara.

1 INTRODUCTION

Implantable sensors can be used to monitor various physiological conditions for example after an acute trauma or a surgery. Such sensors can complement or even replace conventional diagnosis and imaging methods if they can provide better diagnostic accuracy or detect adverse effects earlier. [1] In the current paradigm, implantable sensors are made from non-degradable materials with the aim of reliable long-term measurements. This mindset was challenged in 2009, when Kim et al. proposed a futuristic idea of fabricating temporary sensors using so called bioresorbable materials [2]. In physiological conditions, these materials are gradually broken down into degradation products that can be eliminated from the body via metabolic pathways.

Medical implants that resorb from the body offer several advantages over their biostable counterparts, including the avoidance of their surgical removal, which was recently indicated as one of the main issues of implantable pressure sensors [3]. Bioresorbable polymers, glasses, ceramics and metals are already being used clinically for example as surgical sutures, orthopedic bone fixation screws and plates, synthetic bone grafts and drug delivery devices. One approach for using bioresorbable sensors could be to integrate a sensor into a bioresorbable orthopedic implant that would be surgically inserted regardless. Such a smart implant would act as a sensor along with its original function, after which the whole system would be metabolized by the body. For example, a bone fixation plate could provide temporary information about bone formation, or cues of possible infections at the fracture site.

Sensors with wireless readout are preferred over skin-penetrating wires that are uncomfortable for the patients and increase the probability of infections. Inductively coupled resonance sensors consisting only of an inductor (L) and a capacitor (C) offer an attractive option for wireless sensors, because they do not require batteries. This decreases their size and complexity. Such passive LC circuits are inductively (magnetically) coupled with a reader device, similarly to electric toothbrushes that are often wirelessly connected with their charger base.

Despite their relatively simple structure, the fabrication and assembly of LC circuits using bioresorbable materials remains a challenge, because conventional

microfabrication methods often involve elevated temperatures, aqueous conditions or chemicals that are detrimental for most bioresorbable materials. In addition, the materials start to degrade upon exposure to physiological conditions in the use phase, which leads to challenges in the reliability and stability of the sensors.

This thesis presents methods for materials processing and sensor assembly, as well as evaluates the materials properties and sensor performance to promote further development of bioresorbable inductively coupled sensors. The presented results provide insight into the potential and limitations of the sensors from a materials perspective, which has been somewhat overlooked in the literature.

2 BACKGROUND

2.1 From non-degradable to bioresorbable orthopedic sensors

Implantable sensors are used to provide real-time in situ information about physiological parameters such as pressure, temperature, pH and others [4]. For example, clinical pressure measurements are made with implantable sensors in the circulatory system, brain, eye, muscle compartments and others [3]. Respective examples of commercialized sensors include the CardioMEMS™ HF System by Abbott for monitoring the pulmonary artery pressure, NEUROVENT-P-tel by Raumedic for monitoring intracranial pressure and Eyemate® by Implandata Ophtalmic Products for eye pressure measurements. This thesis focuses on implantable sensors that are intended for monitoring conditions related to orthopedic trauma, disease or surgery.

Orthopedic sensors have been used for research purposes since the 1960's for example to understand in vivo biomechanics, validate analytical models and optimize bioreactors for tissue engineering. In addition, monitoring the healing time and morphology of bone and cartilage has been performed by attaching sensors onto bone or directly underneath the cartilage layers. Most implantable orthopedic sensors are still used as this kind of research tools, but recent efforts in their development are leading towards increasing clinical success. [5], [6] For example, Verasense™ by OrthoSensor Inc. is used during total knee arthroplasty surgery, where it gives real-time information about the ligament balance and thus helps in the implant positioning [7]. The device is removed and replaced with a plastic spacer after balancing the knee. Similar intraoperative device is being developed for spinal rod strain sensing by Intellirod Spine. In addition, their product pipeline includes an implantable wireless strain sensor (Accuvista™) for postoperative monitoring of lumbar spine fusion. Correspondingly, Ortho-Tag is developing a system that can be used to wirelessly identify orthopedic implants or to detect joint infections early. OrthoDx is a startup company with a functional sensor prototype for monitoring the motion of orthopedic implants, which could be used to detect their loosening. This kind of smart technology may lead to a new era of orthopedic implants that

communicate with the clinician or patient in real-time during or after implantation [8].

In many cases, the health conditions that require monitoring are only temporary. Thus, a sensor removal surgery might be needed to mitigate risks of infections and other complications that may arise from long-term sensor implantation [1]. In addition to their costs, these surgeries pose risks for the patients [9]. Bioresorbable sensors have been proposed for temporary sensing applications as a means to avoid sensor removal surgeries. The idea is that these sensors function in a stable manner for a short time, after which they degrade and are metabolized by the body.

Some practical applications where the monitoring need is only temporary involve pressure measurements. In traumatic brain injuries the life-threatening secondary increase in intracranial pressure (ICP) occurs usually within 3 to 10 days [10]. In acute compartment syndrome (ACS) the pressure inside an osteofascial compartment rises above the intramuscular arteriolar pressure, thus decreasing blood flow and oxygen diffusion in the tissue. If untreated, it may lead to limb amputation or even death. There are multiple causes for ACS, but it is often related to bone fracture and typically occurs within the first 48 hours of injury. [11]–[13] Furthermore, early signs of infection can be monitored for example by sensing pH or temperature at the implantation site. Acidic metabolites of bacteria and immune cells reduce the local pH all the way to 4 in extreme cases like osteomyelitis. Similarly, the local temperature may rise by 2-4 °C in an infection. [9], [14] In the future, the smart implants could also monitor tissue healing. For example, wireless strain sensor readings only one week after operation have been noticed to correlate with long-term bone healing [15]. Another way to observe bone healing could be to monitor changes in the complex permittivity of the sensor environment. This method has been earlier used to distinguish different tissues [16] and could be a highly valuable sensing method for verifying callus formation or implant attachment onto bone.

The sensor technology advancements in power transfer and wireless communications have been partly responsible for the emergence of smart implants [17]. The early implantable sensors utilized transcutaneous wires for both communication and power. Wireless sensors were later developed to increase patient comfort and to reduce the infection risk. Active wireless sensors contain an internal battery, whereas passive sensors are powered with external mechanisms such as electromagnetically or inductively (magnetically) transmitted energy. Due to the limited lifetime and relatively large size of the batteries, passive systems have been considered more practical in implant applications and are likely dominant in the future. [5], [8], [18]

Passive sensors based on electromagnetic coupling contain typically complex circuit elements but on the other hand have longer reading distances compared to inductively coupled resonance sensor systems [18]. However, some of the most popular wireless technologies like Bluetooth rely on complex integrated circuits that are currently not fabricated from bioresorbable materials [9]. In fact, even the fabrication of much simpler bioresorbable circuits and components may be challenging due to poor chemical and thermal resistance of most bioresorbable substrate materials [19], [20]. This limits the use of solvents, processing temperatures and lithographic techniques. Consequently, a simple sensor structure can be expected to provide advantages in the fabrication phase. Resonance sensors based on inductor-capacitor (LC) circuits have a simple structure but still offer passive wireless readout, which makes them highly interesting for implant applications [21]. For example, the CardioMEMS™ and Eyemate® pressure sensors that were mentioned in the first paragraph are based on LC circuits. The next chapter summarizes the operational principle and basic properties of inductively coupled LC circuits to better understand the requirements for bioresorbable materials and their processing methods.

2.2   Inductively coupled inductor-capacitor circuits

Inductively coupled passive resonance sensors utilize magnetic fields for energy and data transmission. They provide a promising technology for implant applications due to their small size, battery-free wireless readout and simplicity. Such sensors may consist of only an inductor (L) and a capacitor (C) and are hence called LC circuit-based sensors, or LC resonator sensors. In addition, the inductor presents a parasitic resistance, due to which the devices are sometimes named RLC resonators in the literature. On the other hand, the RLC circuits may also contain a separate resistor (R) component. [5], [21]

Inductively coupled LC circuits can be wirelessly read using an external reader coil that is typically connected to an impedance analyzer [22]. A low frequency alternating current (AC) in the reader coil is used to generate an alternating magnetic field [23]. Bringing the inductor coil of the LC circuit close to the reader coil allows magnetic coupling of these two and thereby the induction of energy from the reader coil to the LC circuit [24]. When measuring the impedance of the reader coil, the inductively coupled circuit can be detected from a deviant resonance curve [18]. The curve is usually in the form of a peak or dip, depending if the real part of the

impedance (*Re (Z)*) or its phase is measured, respectively. The resonance frequency (f_0) of the LC circuit can be estimated from the maximum value of the peak, or the minimum value of the phase-dip. A simplified illustration of the measurement setup as well as the two measurement options maximum *Re (Z)* and minimum phase-dip are presented in Figure 1.
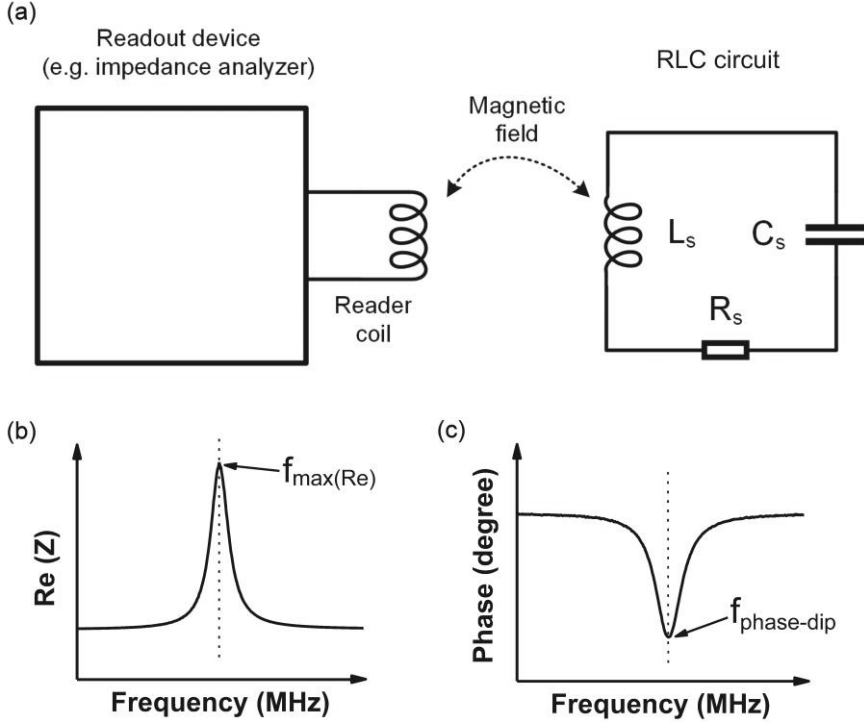
Figure 1. (a) A schematic illustration of typical physical components used for the LC circuit-based measurements. The sensor resistance (R_s) often consists of parasitic resistances alone, but the circuit may contain a separate resistor component as well. (b) A characteristic graph of the Re (Z) measurement, indicating the estimated sensor resonance frequency $f_{max(Re)}$. (c) A corresponding phase measurement graph, showing the estimated sensor resonance frequency $f_{phase-dip}$.

The sensing principle of the RLC circuit-based sensors is related to a shift in their resonance frequency in response to a certain stimulus. The resonance frequency f_0 of the sensors is characterized with respect to their capacitance, inductance, and resistance and can be estimated according to the following equation [18]:

$$f_0 = \frac{1}{2\pi} \sqrt{\frac{1}{L_s C_s} - \frac{R_s^2}{L_s^2}} \tag{1}$$

where L_s, C_s and R_s are the inductance, capacitance and resistance of the sensor, respectively. The effect of parasitic resistance is often neglected, which leads to a simplified estimation in the absence of a resistor component [21]:

$$f_0 = \frac{1}{2\pi\sqrt{L_s C_s}} \qquad (2)$$

Each of the circuit components (capacitor, inductor, or resistor) may respond to a parameter of interest, but in a typical case the capacitor is used as the sensing element. For example, a parallel plate capacitor with an air cavity or an elastomeric dielectric material between the capacitor plates can be used to monitor pressure or force. The measurement is based on capacitance changes as the distance between the capacitor plates is altered. Another example of capacitive measurements involves complex permittivity changes near the interface between the sensor and its environment, which influence the capacitance of the sensor. The method has been proposed e.g. for characterizing different tissues based on their distinct complex permittivity values. In certain cases even parasitic capacitors can be considered as sensing elements, if no external capacitor is connected to the inductor coil. [16], [21], [22], [25], [26]

The most common inductors used in LC circuits can be divided into two main categories, namely planar and solenoidal inductor coils. Inductive sensing applications are often based on alterations of relative permeability, which may be designed to cause a linear inductance change. In addition, alterations in the dimensional parameters of the coil affect the inductance value of the LC circuit. [21] This can be utilized for example in a strain sensor, where the inductance of a solenoidal coil is consistently altered by dimensional changes in the coil [27].

Measurements where resistance variation is used as a means for sensing can be applied for example in temperature monitoring if the conductor material is temperature-sensitive, or in strain sensing using a resistive strain gauge [28], [29]. However, measurements founded upon resistance changes are relatively uncommon, as they involve a change in the quality factor of the sensors, which is often defined using the resistance value [18], [21]:

$$Q = \frac{2\pi f_0 L_s}{R_s} = \frac{1}{R_s}\sqrt{\frac{L_s}{C_s}} \qquad (3)$$

The higher the Q-factor, the narrower is the measured *Re (Z)* or phase curve, thus allowing better discrimination between different resonance frequencies. In addition

to a narrower bandwidth, a higher peak amplitude is found at resonance for high-Q resonators. In other words, a device with an increased Q-factor can acquire more energy via inductive coupling as well as transmit data more effectively. This interpretation means that LC circuits with higher Q-factors have also longer reading distances compared to their lower Q-factor counterparts. Another definition for Q can be formulated as:

$$Q = \frac{f_0}{BW} \tag{4}$$

where BW is the -3 dB bandwidth at resonance. However, these definitions for Q are only valid for high-Q (Q>>1) resonators. [21], [30]–[32]

The distance between the reader coil and the LC circuit, or the reading distance, may affect the resonance frequency of the sensor due to parasitic capacitances in parallel to the reader coil. The coupling distance can be even used as a sensing method for monitoring sensor displacement. However, in many applications this feature is undesirable and should be compensated. [21], [33], [34] This includes many implant applications, where the reading distance might be difficult to control precisely.

Certain environmental factors may affect the characteristics of LC circuit-based sensors. For example, temperature fluctuations in the sensor environment might influence the inductance, capacitance or Q-factor of the device. Thus, temperature changes are a possible error source that may affect the sensitivity of the sensor or its baseline resonance frequency f_0. For instance, changes in the Young's Modulus due to increased temperature of the substrate can cause sensitivity drifts in pressure sensors. Furthermore, the resonance frequency of a capacitive sensor may change if the dielectric material has a temperature-dependent dielectric constant. Separate temperature-sensing compensation structures can be used to eliminate the influence of temperature on other measurements if necessary. [9], [35]–[41]

The conductivity of the environment inside the human body causes losses for implantable LC circuits, resulting in an attenuated resonance curve. In addition, proximity of metallic implants or other objects may interfere with the measurement. Thus, implantable inductively coupled sensors should be ideally located remotely from any metallic implants. [26], [42]–[44]

2.3 Materials for bioresorbable inductor-capacitor circuits

Bioresorbable polymers, ceramics, metals and their composites have been studied for decades for various implant applications. The same materials can be used as substrates, conductors and other components to construct electronic devices that can be broken down and resorbed by the body. [45] This chapter is dedicated to outlining materials and their relevant properties for bioresorbable LC circuits. Depending on the material, these properties may include for example mechanical and thermal properties, degradation rate, chemical resistance, processability, biocompatibility or electrical properties.

2.3.1 Definitions

In a medical context, biodegradable materials can be defined as materials that degrade hydrolytically or by enzymatically accelerated degradation under physiological conditions [46]. However, as virtually all materials show some degradation in such an environment, the distinction between biodegradable and non-degradable materials can be done by comparing the degradation time to the duration of the intended application or for example to human lifetime. In this thesis, materials that degrade significantly slower under physiological conditions than the duration of their intended application are considered non-degradable. [47] These definitions do not specify the nature or the fate of the degradation products, although in an ideal case they are easily cleared from the body [48]. This issue is addressed by the term bioresorbable, which can be attributed to materials that not only degrade in the body, but produce degradation products that are non-toxic and eliminated from the body by metabolic pathways [49]. Thereby, bioresorbable electronics (sometimes transient electronics) refers to electronic devices that are able to completely dissolve or disintegrate into biologically harmless degradation products under physiological conditions [50].

2.3.2 Bioresorbable materials for substrates, dielectrics and water barrier layers

Polymers are typically utilized as substrates in bioresorbable electronics, but they find use also as encapsulation layers, dielectrics and spacers. Furthermore, bioactive glasses and bioceramics provide an interesting yet less investigated substrate

alternative. Table 1 illustrates selected properties of selected polymers poly(L-lactide) (PLLA), poly(ε-caprolactone) (PCL), Poly(desamino tyrosyl-tyrosine ethyl ester carbonate) (PDTEC), poly(ortho ester) IV as well as bioactive glass 45S5 (Bioglass®).

Table 1. A summary of the thermal, mechanical and degradation properties of certain bioresorbable polymers and bioactive glass 45S5

	Glass transition temperature	Melting temperature	Flexural Modulus	Erosion
PLLA	60 °C [51]	174 °C [51]	1.4-3.3 GPa [52]	Bulk erosion
PCL	-60 °C [53]	59-64 °C [53]	0.5 GPa [52]	Bulk erosion
PDTEC	93 °C [54]	Amorphous [55]	2.8 GPa [56]	Bulk erosion
Poly(ortho ester) IV	Up to 110 °C [57]	Amorphous [58]	Tailorable [57]	Predominantly surface erosion [59]
Bioactive glass 45S5	538 °C [60]	>1000 °C [61]	30-50 GPa [61]	Dissolution, remnants left behind* [62]

*In the case of >2 mm particles

Degradation of polymers can be considered as a chemical phenomenon, where the bonds of the polymer chain are cleaved. Correspondingly, erosion refers to a physical process of material loss from the polymer sample. Biodegradable polymers can be divided to bulk or surface eroding polymers depending on their erosion mechanisms. In bulk erosion, water diffuses into the polymer specimen and reaches an equilibrium before mass loss starts. The sample undergoes surface erosion if polymer chains are eroded from a confined reaction zone at the sample surface before water is diffused throughout the specimen. Achieving surface erosion is difficult, and bulk eroding polymers form the majority of biodegradable polymers. The most common surface eroding polymer groups are polyanhydrides and poly(ortho esters). [63], [64]

Immersed bulk eroding polymer samples with thicknesses up to 1 mm become usually saturated with water within a time span from a few hours to a few days. As the hydrolysis proceeds and the molecular weight of the polymer decreases, the amount of chain ends increases. If the chain ends are acidic, a process called

autocatalysis (or autoacceleration) may take place, where the chain ends catalyze the degradation of the adjacent polymer chains. Furthermore, if the degradation products are not able to diffuse from inside the sample into the aqueous solution, the pH inside the sample is further increased, finally resulting in a swollen viscous oligomer solution inside a polymer crust. Characteristic for bulk eroding polymers is that the initial erosion is low or non-existent, after which it spontaneously begins at a later stage of degradation. Therefore, bulk erosion is considered as a more complex process compared to surface erosion. [64]–[66]

2.3.2.1 Poly(a-hydroxy acids)

Poly(α-hydroxy acids) are a family of macromolecules synthesized typically from cyclic diester monomers including glycolide, different enantiomers of lactide and combinations thereof. The properties of the resulting (co)polymers, such as the degradation rate can be adjusted to some extent based on the ratio and stereochemistry of the monomers. In addition, the degradation profiles of poly(α-hydroxy acids) depend on multiple other factors, including molecular weight, degree of crystallinity and the processing history of the sample. These factors need to be considered when comparing degradation studies, even if stereochemically similar materials are investigated. With decades of clinical applications for example as orthopedic fixation implants, poly(α-hydroxy acids) are considered as the most important and widely used bioresorbable polymers. [67]–[70]

Semicrystalline poly(L-lactide) (PLLA) degrades slower compared to amorphous poly(DL-lactides). Considering poly(lactide-co-glycolide) (PLGA) copolymers, the increasing amount of glycolide units typically results in faster degradation except for PLGA 50:50, which is the fastest degrading PLGA type. The cleavage of labile ester bonds of poly(α-hydroxy acids) results in formation of acidic end groups, which may lead to autocatalysis. [70]–[72]

Poly(α-hydroxy acids) are popular substrate materials in bioresorbable electronics. Luo et al. fabricated their first bioresorbable wireless pressure sensor using solvent casted PLLA substrates (200-300 µm) and spacers (30 µm) [73]. Upon examining the immersed sensors, they suggested that the formation of cracks in the substrates was a possible failure pathway for the sensors. In order to accelerate the degradation of the device, the authors tested PLGA 50:50 as an alternative material [74]. However, maintaining appropriate mechanical properties at +37 °C was difficult due to the relatively low T_g (40-47 °C) of PLGA 50:50, which lead to using poly(vinyl alcohol) (PVA) as a mechanical support. Also Boutry et al. used

PLLA layers (50 μm) in their strain and pressure sensors together with other biodegradable polymers and elastomers [75], [76]. Furthermore, appropriate processing of PLLA has been noticed to yield piezoelectric responses (5-15 pC/N), making PLLA a potential sensing material [77]. PLGAs have also been a popular choice with semiconductor devices whose assembly requires transfer printing [20], [78], [79].

2.3.2.2 Poly(desamino tyrosyl-tyrosine ethyl ester carbonate)

Synthetic poly(amino acids) degrade to their natural and non-toxic amino acid building blocks in vitro and in vivo. However, they tend to degrade thermally in the molten state, which has severely limited their application due to processing limitations. To maintain the favorable characteristics of the amino acid building blocks while improving the materials processing possibilities, so-called pseudo-poly(amino acids) have been developed. In pseudo-poly(amino acids), the amino acids are linked by carbonate, ester or other non-amide bonds. [54], [80]

Tyrosine-derived polycarbonates represent a class of pseudo-poly(amino acids) that are synthesized by polymerizing desaminotyrosyl-tyrosine alkyl ester monomers. The aromatic group in the amino acid tyrosine enabled producing polymers with increased stiffness and mechanical strength, which contributed to choosing tyrosine dipeptides as monomers. The four most extensively studied tyrosine-derived polycarbonate polymers are synthesized from monomers containing an ethyl, butyl, hexyl or octyl ester pendant chain. The respective polymers are referred to as poly(DTE carbonate), poly(DTB carbonate), poly(DTH carbonate) and poly(DTO carbonate) as shown in Figure 2. [54], [81] In this study, poly(DTE carbonate) is referred to as PDTEC.
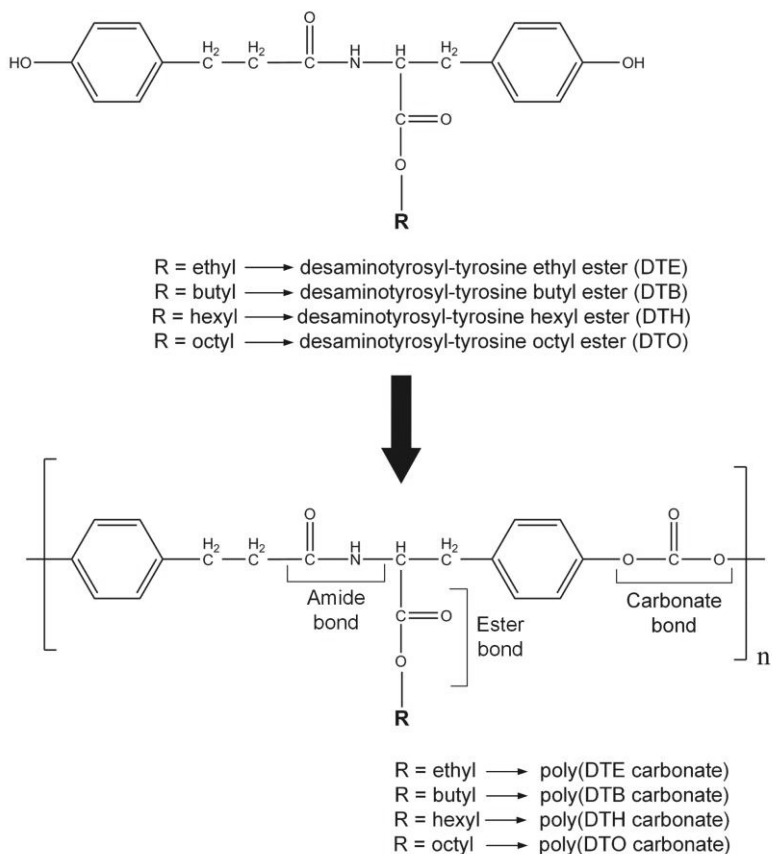
Figure 2. The structural formulae of the monomers and the resulting tyrosine-derived polycarbonates as adapted from [54].

All tyrosine-derived polycarbonates are amorphous. Some of their properties have been shown to correlate to the amount of carbon atoms in the pendant chain. For example, an increase in the length of the pendant chain correlates to a decreasing glass transition temperature (T_g) but increasing hydrophobicity and solubility. On the other hand, no clear correlation was noticed between the pendant chain and the polymer tensile properties, although poly(DTO carbonate) showed more flexible characteristics than the other polymers of the same family. In general, the tensile modulus of thin tyrosine-derived polycarbonate films at 1.2-1.6 GPa was comparable to that of non-reinforced PLLA. Another study has reported poly(DTE carbonate) (PDTEC) and PLLA to have Young's Moduli of 1.9 GPa and 2.7 GPa, respectively. [82], [83] From the perspective of bioresorbable electronics, PDTEC is an interesting material choice due to its relatively high T_g from 81 up to 100 °C [84],

[85], which enables further sensor assembly steps at slightly higher temperatures compared to commonly used lactide- and glycolide-based polymers.

The initial stage of tyrosine-derived polycarbonate degradation consists mostly of the hydrolysis of the carbonate bonds in the polymer backbone with only a small amount of ester bond cleavage in the pendant chain. As a result, the molecular weight of the polymer is reduced but no mass loss is observed, because the degradation products still carry the pendant chain and are thereby virtually insoluble in water. The carbonic acid produced in the hydrolysis of the carbonate bonds is unstable, decomposing further to a phenolic group and CO_2. The mass loss of tyrosine-derived polycarbonates occurs later in the final stage of degradation, where considerable pendant chain ester bond cleavage is observed. The progressive hydrolysis of the ester bonds leads to the formation of free carboxylic acid groups bound to the polymer, thus autocatalyzing the degradation of the backbone carbonate bonds. The degradation of the backbone might be accelerated in vivo by possible enzymatic cleavage of the amide bonds, which were reported to be stable in vitro during the 40 weeks test period. The completion of the whole resorption process may take up to four years. [55], [82], [86]

The spreading, attachment and proliferation of cells on tyrosine-derived polycarbonates has been studied with rat lung fibroblasts. Cell attachment and proliferation were noticed to correlate with the material hydrophobicity, with PDTEC showing the best cell response. The in vivo biocompatibility of PDTEC has been evaluated in rats, dogs and rabbits, where the material has caused only mild foreign body responses. Moreover, it showed a comparable, if not superior tissue response to PLLA. [55], [82], [87]–[90]

2.3.2.3 Poly(ε-caprolactone)

Poly(ε-caprolactone) (PCL) is an aliphatic semicrystalline polymer synthesized typically by ring-opening polymerization of cyclic ε-caprolactone monomers. It has a low T_g of about -60 °C, meaning that it is in the viscous state in room or body temperature. Still, due to its relatively high degree of crystallinity, PCL is stiffer than many soft tissues. The T_m of PCL is between 59-64°C, which enables its melt processing at relatively low temperatures. [53], [91]

PCL is one of the few synthetic polymers that degrade in the outdoor environment by bacteria and fungi. However, suitable enzymes are not present in the human body, due to which PCL degrades hydrolytically in vivo. The degradation occurs by random chain scission of ester bonds in the polymer backbone ultimately

leading to capronic acid by-products. In an in vivo rat study, the low molecular weight PCL particles were phagocytosed and further degraded by macrophages, giant cells and even fibroblasts. In humans, total degradation of PCL takes approximately 2-4 years and the degradation products are cleared from the body by renal secretion or via tricarboxylic acid cycle. [53], [92]–[95]

The popularity of PCL in biodegradable electronics is partly caused by its broad availability, hydrophobicity, bendability and facile processing due to its low T_m [20]. Luo et al. utilized heated PCL (55 °C, 10 bar) as an adhesive layer in their bioresorbable pressure sensor to attach the folded PLLA substrate onto the laser-cut PLLA spacer. Gao et al. exploited the low T_m of electrospun PCL substrates in on-demand destructible electronic components, where resistive heaters enabled a controllable mechanical destruction by shrinking the substrates [96]. Salpavaara et al. compared PCL and poly(L-lactide-co-ε-caprolactone) (PLCL) 70:30 as encapsulation materials for non-degradable resonance circuits, reporting that PCL provided a more stable encapsulation compared to PLCL. However, compression molding of PLCL required higher temperatures and was noted to give more irregular encapsulation outcomes compared to PCL, which could partly explain the results. [97]

2.3.2.4 Biodegradable elastomers

Elastomers are characterized by their ability to recover from high deformation to their initial state. This ability results from a crosslinked network of long polymer chains with a high degree of flexibility. In electronic applications, elastomers can be used for example as substrates for soft tissue incorporated bendable and stretchable devices, or as dielectric layers with fast response times in capacitive pressure sensors. Fabricating biodegradable elastomers often involves crosslinking a liquid pre-polymer mixture. Thus, processing methods like solvent casting, replica molding, 3D printing and photolithography are commonly used. [25], [98]–[101]

Biodegradable elastomers include for example poly(glycerol sebacate) (PGS), poly(octamethylene maleate (anhydride) citrate) (POMaC), poly(1,8-octanediol-co-citrate) (POC) and poly(trimethylene carbonate) (PTMC). [102] Boutry et al. have used micropatterned PGS films as an intermediate dielectric layer between magnesium capacitor plates in their pressure sensor array. The viscoelastic response of PGS was noted to be minimal, thus enabling fast response times. Furthermore, the viscoelastic properties did not change significantly even after seven weeks of immersion in buffer solution. [25] In a later study, POMaC (500 μm) was used as a protective layer for a wired biodegradable strain and pressure sensor, which was

functional after 3.5 weeks of subcutaneous implantation in rats. The mechanical properties of POMaC were noted to be close to those of many soft tissues. [75]

Stretchable sensors would be desirable for many applications, where lamination onto skin or other organs is desired. Optimized semiconductor devices on POC elastomer substrates provided reversible stretching up to strains of 30 %. The degradation of POC occurred within several weeks and can be adjusted based on the crosslinking density of the elastomer. [101]

2.3.2.5 Surface eroding polyanhydrides

Surface eroding polymers have been considered desirable in bioresorbable electronics as they may enhance the water-resistance of the device and avert problems related to the swelling of the material [103], [104]. Still, the majority of studies have utilized bulk eroding polymers. This is probably due to the poor availability of surface eroding polymers and the well-developed processing schemes of bulk eroding polymers such as PLGAs.

Polyanhydrides were initially considered for textile fiber applications, but their hydrolytic instability was found to be insurmountable for industrial use. The fast hydrolysis rate that leads to surface erosion was later considered as an advantage for drug delivery systems, which is nowadays the primary research topic related to polyanhydrides. Commercially used polyanhydride products include the Gliadel™ wafer and the antibacterial Septicin™ implant, which are utilized for intracranial anticancer compound delivery and for chronic bone infection treatment, respectively. Nevertheless, commercial applications of polyanhydrides are limited by the storage, handling and fabrication challenges caused by their hydrolytic susceptibility. [52], [105], [106]

Polyanhydrides constitute a number of different polymers, including aromatic and aliphatic polyanhydrides, as well as anhydride copolymers. Aromatic polyanhydrides have a relatively low molecular weight, high degree of crystallinity and glass transition temperatures between 50-100°C, whereas aliphatic polyesters have significantly lower glass transition temperatures. Multiple studies involve compression molded polyanhydride discs, but other melt processing techniques like injection molding may also be used. Certain aromatic polyanhydrides have high melting temperatures of around 240 °C combined with poor solubility in organic solvents, which makes their processing challenging. [105], [107], [108]

Polyanhydrides show surface erosion with sample thicknesses that are above a critical sample thickness (L_{crit}), which is on average 75 μm for linear polyanhydrides,

but may vary significantly depending on the polymer composition. Below L_{crit} the water diffuses into the sample faster than the anhydride bonds are hydrolyzed, leading to bulk degradation. Aromatic polyanhydrides are generally considered to be among the slowest degrading polyanhydrides, with examples where the process has taken about 90 days. The hydrolysis of anhydride bonds is base catalyzed, whereby pH affects the degradation rate. The degradation products constitute sparingly water-soluble diacidic monomers. This makes their elimination from the body a slow process. Aliphatic monomers are likely metabolized further by β-oxidation pathway, whereas aromatic monomers are removed from the body without metabolic transformation. Insoluble degradation products can be resorbed by inflammatory cells and macrophages. [66], [105], [109]

Kang et al. used a specially synthesized poly(buthanedithiol 1,3,5-triallyl-1,3,5-triazine-2,4,6(1H,3H,5H)-trione pentenoic anhydride) or PBTPA as an encapsulation layer (120 μm) for their wired piezoresistive pressure sensor, which operated in a stable manner for 3 days with encapsulation. The diminishing material thickness was noticed to result in only very small changes in the sensor sensitivity. Furthermore, a PBTPA (120 μm) encapsulated Mg resistor (300 nm) showed a stable resistance for 4 days in vitro before water reached the Mg pattern. Correspondingly, the stable operation time of Mo electrodes was prolonged from a few hours without encapsulation to 6 days with a PBTPA barrier layer. The erosion rate of PBTPA was estimated at 1.3 μm/day. [79]

Polyanhydrides have been also considered for non-medical transient electronic devices, where the polymer substrate degradation was triggered by moisture in air. The acidic degradation products participated as a functional component to the dissolution of the conductor, semiconductor and dielectric materials. The acidic conditions enabled using e.g. metals like Cu, Al and Ni that are considered non-degradable in ambient conditions. The surface erosion process caused practically no mechanical strain onto the functional components, which is a favorable feature for implantable devices as well. [110]

2.3.2.6 Surface eroding poly(ortho esters)

Poly(ortho esters) (POEs) were developed for drug delivery in the early 1970s and form another class of surface eroding polymers along with polyanhydrides. The ortho ester bonds are highly reactive, but water diffusion into the polymer bulk is very limited due to high hydrophobicity of POEs, which makes their erosion very slow. [57]

Poly(ortho esters) constitute four different types of polymers, named from POE I to POE IV. POE IV was considered to be the only one with required attributes for commercialization, as its thermal, mechanical and degradation properties can be adjusted in the synthesis phase. For example, POE IV materials with glass transition temperatures up to 110 °C can be produced. Furthermore, POEs can be processed by conventional melt processing methods like injection molding and extrusion. The predicted L_{crit} of poly(ortho esters) is around 400 µm, which is higher than that of polyanhydrides. [57], [59], [105]

The drawbacks of POEs include their challenging synthesis, which includes unstable intermediates. Moreover, poly(ortho esters) are known to show surface erosion behavior only with certain additives. The irreproducibility of the synthesis method has limited the development of these materials and no reports of POEs in bioresorbable electronic applications have been published. However, new POE synthesis methods utilizing air- and moisture stable precursors were recently reported. [52], [111]

2.3.2.7 Bioceramics and bioactive glasses

Bioceramics are inorganic, nonmetallic materials that can be introduced into living tissue as a part of a medical device [112]. They include a variety of materials, some of which are nearly inert such as Al_2O_3, and others that are bioresorbable like tricalcium phosphate. As a special subcategory, bioactive glasses possess a completely amorphous structure with a more open network compared to conventional glasses. This structure enables bioactive glasses to dissolve and release ions like Ca^{2+} or PO_4^{3-} when exposed to aqueous conditions. The leached ions lead to an apatite surface layer formation, which allows strong glass to bone bonding. [113], [114] Bioactive glasses have not been extensively explored for biodegradable electronic applications, although borate-based glasses have been proposed as dissolvable substrate materials [115], [116].

The biocompatibility and corrosion resistance of bioceramics are typically good [117], which makes them attractive materials for protective water barrier coatings. Furthermore, thin films of silicon dioxide (SiO_2), silicon nitride (Si_3N_4), magnesium oxide (MgO) and their combinations are commonly used as dielectric layers in biodegradable electronic devices. [118] Thin SiO_2 layers dissolve to silicic acid in water according to the following equation:

$$SiO_2 + 2H_2O \rightarrow Si(OH)_4 \tag{5}$$
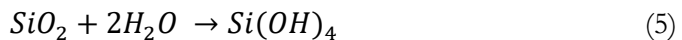
The process is initiated by OH⁻ ions, meaning that a high pH increases the dissolution rate. Correspondingly, Si_3N_4 hydrolyzes in two steps with an oxidation into SiO_2 occurring first:

$$Si_3N_4 + 6\,H_2O \rightarrow 3\,SiO_2 + 4\,NH_3 \qquad (6)$$
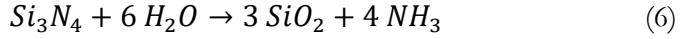
Thereafter, SiO_2 dissolves further according to equation (5). [119], [120] The dissolution of MgO begins according to the following equation [121], [122]:

$$MgO + H_2O \rightarrow Mg(OH)_2 \qquad (7)$$
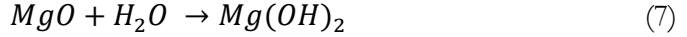
Then, $Mg(OH)_2$ dissolves further as described later in chapter 4.3.1. An encapsulation layer made from MgO has been reported to result in a functional lifetime of approximately 4 days in the case of Mg-based transistors immersed in deionized water (di-H_2O) [122]. However, such thin ceramic layers are considered to undermine the mechanical flexibility of the encapsulated devices [123]. Furthermore, fluid leaks might occur, primarily due to defects such as pinholes. Multilayer structures of both silicon nitrides and oxides may reduce the amount of such defects, improving the performance of the barrier layer. [119]

The performance of different silicon oxide and nitride water barrier films was measured by monitoring the electrical resistance of Mg patterns (300 nm) on glass substrates in di-H_2O at room temperature. The results revealed that single SiO_2 and Si_3N_4 layers (500 nm) protected the Mg for some hours, whereas an additional atomic layer deposited (ALD) SiO_2 (20 nm) layer provided protection for about 5-7 additional days. The best result was achieved with three consecutive (SiO_2 + Si_3N_4) double layers, which preserved the conductivity of the Mg pattern for 10 days. [119] Moreover, thermally grown SiO_2 encapsulation layers have been reported to yield in vivo functional lifetimes of 25 days when applied on wired silicon nanomembrane-based piezoresistive pressure sensors [124].

2.3.3 Biodegradable conductor metals

The most widely used conventional thin film conductor materials are Al, Au, Cu and Ag, which are the four metals with the highest electrical conductivities (2.7×10^{-8} Ω·m, 2.2×10^{-8} Ω·m, 1.7×10^{-8} Ω·m and 1.6×10^{-8} Ω·m at 20 °C, respectively). In bioresorbable electronics, especially Mg, Fe, Zn and Mo have been considered, all of which are elements that a human body necessitates. In addition,

tungsten (W) has been proposed as a biodegradable implantable metal, however, it is not a universal bioelement. [125]–[128]

In bioresorbable electronics, the metals are usually applied as thin films, which denotes that pinholes or other microstructural properties might dominate the material properties. This should be taken into account when interpreting for example corrosion data from the existing literature, where the metals are often in bulk form. [126] The most important characteristics for metals in bioresorbable electronics are related to their electrical properties, corrosion behavior, biocompatibility and processing options [50]. An overview of some important material properties is given in Table 2.

Table 2.   Certain properties of the most investigated metals for bioresorbable electronic applications

	Resistivity (295 °K) [129]	Skin depth (10 MHz)	Skin depth (100 MHz)	Melting point [130]	Corrosion rate* [126]
Mg	4.3×10^{-8} Ω·m	33 μm	10 μm	649 °C	7×10^{-2} μm/h
Zn	5.9×10^{-8} Ω·m	39 μm	12 μm	419 °C	7×10^{-3} μm/h
Fe	9.8×10^{-8} Ω·m	0.7 μm	0.2 μm	1535 °C	1×10^{-2} μm/h [131]
Mo	5.3×10^{-8} Ω·m	37 μm	12 μm	2617 °C	3×10^{-4} μm/h

*In di-H_2O except for Fe, which has been tested in Hanks' solution.

At high frequencies, alternating currents (AC) tend to penetrate only to a limited depth of a conductor [132]. This phenomenon is named as the skin effect. The AC penetration depth, or skin depth, limits the effective conductor thickness and should be considered when choosing the conductor thickness and the related fabrication method. The skin depth (δ) of a conductor is the depth at which the current density is 1/e, or about 37 % of the current density at the surface of the conductor. It is inversely correlated with frequency, leading to larger skin depths at lower frequencies. [133] In this study, the skin depth was approximated using the following equation [134]:

$$\delta = \sqrt{\frac{\rho}{\pi f \mu_0 \mu_r}} \qquad (8)$$

where ϱ is the electrical resistivity of the material, f denotes the given frequency and μ_0 equates to the permeability constant ($4\pi\times10^{-7}$ H/m). The relative permeability μ_r was approximated as 1 for all other metals except for Fe, whose μ_r estimation was 5500 [135].

2.3.3.1 Magnesium (Mg) and its alloys

Magnesium ions (Mg^{2+}) are involved in a wide variety of physiological functions, including muscle contraction, blood pressure and glycemic control. The recommended daily allowance for Mg is 320 mg for adult females and 420 mg for adult males. The kidneys are the primary regulator of Mg homeostasis, and the intestines and bones are involved to a lesser extent. However, most of the magnesium filtered by the kidneys is reabsorbed, with only about 100 mg of Mg excreted in urine daily. [136]

Mg was first studied as an implantable material already more than 100 years ago, but controlling its corrosion was not achieved in a satisfactory manner and intensive investigations were thus discontinued [137]. However, the interest in Mg and its alloys has recently increased significantly and the first commercial products are in clinical use. CE marks have been granted for implantable devices made from Mg alloys containing zirconium and rare earth elements, and bone fixation screws made from Mg-Ca-Zn alloys have been accepted for clinical use by the Korean Food and Drug Administration [138]. In the early reports concerning bioresorbable electronics, Mg was the material choice for interconnects and electrodes due to its rapid degradation, relatively facile processing and biocompatibility [126]. Furthermore, Mg has been held as the most promising candidate for LC resonators due to its higher electrical conductivity compared to other biodegradable metals [139]. The degradation of Mg under physiological conditions is an extremely complex process, whose primary reactions can be simplified as follows [140], [141]:

Anodic reaction: $\qquad Mg \rightarrow Mg^{2+} + 2\,e^-$ $\qquad\qquad\qquad$ (9)

Cathodic reactions: $\quad 2\,H_2O + 2\,e^- \rightarrow 2\,OH^- + H_2$ $\qquad$ (10)

$\qquad\qquad\qquad\quad 2\,H_2O + O_2 + 4\,e^- \rightarrow 4\,OH^-$ $\qquad$ (11)

Product formation: $\quad Mg^{2+} + 2\,OH^- \rightarrow Mg(OH)_2$ $\qquad$ (12)
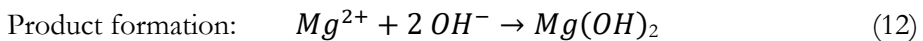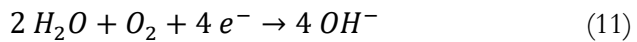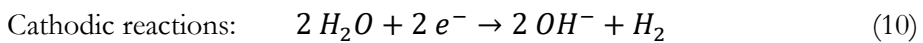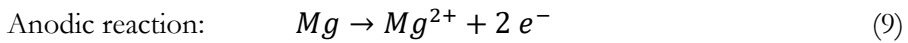
Thus, the corrosion of Mg alkalinizes the environment and generates hydrogen gas. As Mg(OH)$_2$ has a low solubility in water, it precipitates to form the first solid degradation product. The further dissolution of this layer and the formation of other Mg degradation products are strongly dependent on the immersion environment of the sample. For example, precipitated Mg(OH)$_2$ is converted into soluble MgCl$_2$ if the chloride ion concentration is more than 30 mmol/l. For comparison, the in vivo Cl$^-$ concentration is about 150 mmol/l. [141], [142]

$$Mg(OH)_2 + 2\,Cl^- \rightarrow MgCl_2 \qquad (13)$$
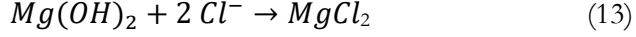
The dissolution of the Mg(OH)$_2$ layer exposes metallic Mg, thus promoting its further corrosion [143]. In addition to Mg(OH)$_2$, also MgO and MgCO$_3$ have been identified as main degradation products in simulated body fluid (SBF), Hank's balanced salt solution (HBSS) and Dulbecco's modified eagle medium (DMEM) [144]. The formation of MgCO$_3$ can be summarized as follows [143]:

$$Mg^{2+} + OH^- +\ HCO_3^- + n\,H_2O \rightarrow MgCO_3 \cdot (n+1)\,H_2O \quad (14)$$
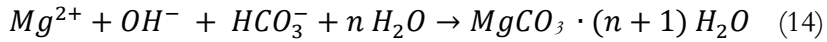
The buffering system of the corrosive media together with its inorganic and organic components have a remarkable effect on the in vitro degradation rate of Mg. Furthermore, the composition of the degradation products may be significantly altered depending on the immersion media. For example, commonly used Tris buffering accelerates the degradation rate of pure Mg tenfold compared to the buffering system in blood plasma. Similarly, small amounts of certain inorganic ions can inhibit or accelerate the degradation process with respect to simple NaCl solutions. The addition of organic components into the solution is advisable for simulating the in vivo conditions. Plasma proteins play a key role in physiological pH regulation and bind a notable amount of Ca^{2+} and Mg^{2+}, which is not the case in simulated body fluids that lack these proteins. Due to these reasons, it is important to refer to the exact buffer solution composition when studying Mg degradation. SBF or Earle's Balanced Salt Solution (EBSS) with CO$_2$/HCO$_3^-$ buffering system are recommended for material screening and degradation rate comparisons, whereas cell culture media with fetal bovine serum (FBS) are suggested for studies where the degradation mechanisms are investigated. [141], [145]

As a result of their fast degradation rate, Mg thin films typically require protection in bioresorbable electronic devices [123]. Nevertheless, rapid conductor resorption can be considered as an advantage in certain applications. The applied Mg film thicknesses have ranged from a few micrometers up to a few hundred

micrometers [37], [146], [147]. For comparison, the electrical resistance of 50 μm thick Mg wires started to distinctly increase after 1 week of immersion in bovine serum [148].

Alloying elements can be used to adjust Mg properties like degradation rate, mechanical properties or electrical conductivity. A common motive for alloying Mg is to slow down its degradation, in order to control the H_2 gas generation rate. Sufficiently slow H_2 generation allows its transportation away from the sites of gas creation in order to avoid the formation of potentially dangerous local gas pockets. [149] Boutry et al. studied LC resonators made from pure Mg and an Mg alloy (with 2 % Ytrium, 1 % Zn, 0.25 % Ca and 0.1 5% Mn), noticing that the DC conductivity of the Mg alloy was approximately 80% of the pure Mg, which resulted in a lower Q-factor in the alloy resonators. [139] Correspondingly, in a study by Yin et al. the decrease in electrical conductivity during hydrolysis was lower in 300 nm thick films made from AZ31B Mg alloys (3 % Al and 1 % Zn) compared to those made from pure Mg. Nonetheless, the corrosion-related deterioration of electrical conductivity was significantly faster in Mg, AZ31B Mg alloy and Zn with respect to Mo, Fe or W films. [126]

The main concerns related to Mg corrosion in vivo are the possible accumulation of H_2 gas bubbles as well as the alkalization of the implant surroundings. The early reports suggested that Mg implants are non-toxic and promote the formation of hard callous. Nevertheless, developing new Mg alloy compositions understandably requires biocompatibility testing. However, in vitro biocompatibility testing using the current ISO 10993 standard series entails several challenges, including the suggested preparation of extracts. Extracts prepared according to the standard expose the investigated cells to an osmotic shock caused by high osmolarity and pH, leading to the classification of almost all Mg alloys as cytotoxic despite contradictory in vivo results. Therefore, standard modifications have been proposed, including diluting the extracts by a factor between 6 and 10 and running alongside tests where the cells are in direct contact with the metal. [142], [150]–[152]

2.3.3.2 Iron (Fe) and its alloys

In the human body, iron (Fe) constitutes many proteins, including hemoglobin, myoglobin and various enzymes. The recommended daily Fe intake ranges from 6 to 20 mg. Although early reports utilizing Fe wires in bone fixation date back centuries, the application of Fe as a purposely biodegradable implantable material stems from the early 2000s, thus being a rather new concept. Fe has been studied

especially for cardiovascular stent applications due to its high ductility. However, based on preclinical in vivo experiments, pure Fe degrades slower than desired. This has led to strategies for accelerating the corrosion process, including tuning the microstructure of the material or using alloying elements such as Mn, W, Si or Sn. [153]–[156]

As opposed to Mg, the degradation of iron does not produce H_2 gas [157]. The degradation obeys the following general processes under physiological conditions [158]:

Anodic reaction: $\qquad Fe \rightarrow Fe^{2+} + 2\,e^-$ $\qquad\qquad\qquad\qquad$ (15)

Cathodic reaction: $\qquad O_2 + 2\,H_2O + 4\,e^- \rightarrow 4\,OH^-$ $\qquad\qquad$ (16)

Product formation: $\qquad Fe^{2+} + 2\,OH^- \rightarrow Fe(OH)_2$ $\qquad\qquad$ (17)
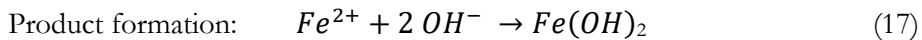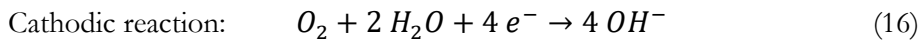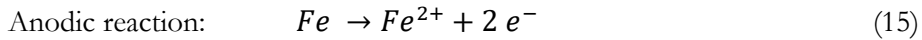
The Fe^{2+} and OH^- ions form iron(II) hydroxide $Fe(OH)_2$, although some of the Fe^{2+} may be transformed to Fe^{3+} and further to ferric hydroxide $Fe(OH)_3$. In addition, iron oxides (Fe_2O_3, Fe_3O_4, or FeO) may be formed in the process. The degradation of e-beam evaporated Fe thin films (150 nm) in di-H_2O has been noticed to proceed in a non-uniform manner from randomly located pitting nucleates, which is in agreement with the corrosion reported for bulk Fe samples. The degradation products of the films included Fe oxides (Fe_2O_3 and Fe_3O_4) and Fe hydroxides. The Fe oxides did not dissolve within the period of one month, which was deemed as an undesirable feature for many bioresorbable electronics applications. [126], [158]

Fe-based materials have been investigated for biodegradable LC resonator applications in 2012. Three different Fe alloys as well as pure Fe were used as raw materials for producing the resonators by electric discharge machining. Compared to Mg and its alloys, the Fe-based materials had significantly lower Q-factors. This was explained by the larger relative permeability of Fe, which in turn results in a low skin depth. Thus, pure Fe has been described as a poor conductor choice for high frequency applications, albeit Fe films have been used as an adhesion layer for other conductor materials like Zn and Mg. [25], [73], [139]

2.3.3.3 Zinc (Zn) and its alloys

Zinc (Zn) is a vital component in numerous enzymes and the mechanisms regulating its absorption and retention are so efficient, that its excessive ingestion has been considered unlikely. Zn is mostly eliminated in the stool with almost negligible

amount of urinary excretion in healthy persons. The recommended dietary allowance for Zn is 15 mg per day and the tolerable upper intake limit in adults is 40 mg per day. [159]–[162]

The development of metallic Zn-based implants is in its early stage compared to those made from Mg or Fe. The focus has been especially in stent applications, but also bone fixation devices have been considered. The corrosion rate of Zn is regarded desirable for implant applications, as it corrodes faster than Fe but slower than Mg. [154] The corrosion occurs according to the following main reactions [163]:

Anodic reaction: $\qquad 2\,Zn \rightarrow 2\,Zn^{2+} + 4\,e^-$ $\qquad\qquad$ (18)

Cathodic reaction: $\qquad O_2 + 2\,H_2O + 4\,e^- \rightarrow 4\,OH^-$ $\qquad$ (19)

Product formation: $\qquad 2\,Zn^{2+} + 4\,OH^- \rightarrow 2\,Zn(OH)_2$ $\qquad$ (20)

$$Zn(OH)_2 \rightarrow ZnO + H_2O \qquad\qquad (21)$$
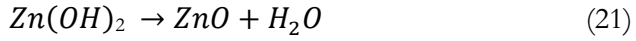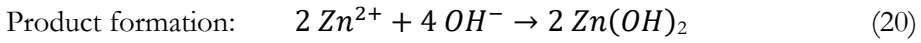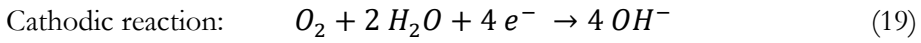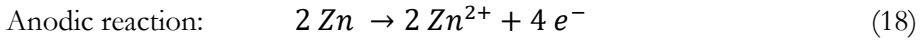
No gas evolution is expected in the corrosion process of Zn [163]. The degradation products $Zn(OH)_2$ and ZnO dissolve further, promoting the corrosion of the exposed Zn. In the presence of a high concentration of Cl- ions, the surface may be converted to soluble $ZnCl_2$ [163] similarly as in the case of Mg:

$$6\,Zn(OH)_2 + \ Zn^{2+} + 2\,Cl^- \rightarrow 6\,Zn(OH)_2 \cdot ZnCl_2 \qquad (22)$$

$$4\,ZnO + 4\,H_2O + \ Zn^{2+} + 2\,Cl^- \rightarrow 4\,Zn(OH)_2 \cdot ZnCl_2 \qquad (23)$$
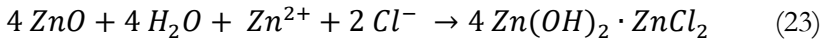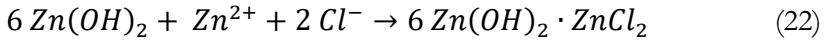
Currently, the motivation for alloying Zn is mostly related to its limited mechanical properties [154]. If the degradation rate of Zn conductors needs to be accelerated, another possibility along with alloying is to couple the conductors onto a nobler metal. This was demonstrated by Luo et al. who used electroplated Zn conductors (50 μm) with a thin Fe adhesion layer (5-10 μm) that was also exploited as an acceleration means for the degradation of the Zn conductors [73].

Low doses of Zn have been shown to correlate with increased osteoblast and mesenchymal stem cell viability, whereas high doses are shown to be cytotoxic [164]. A corresponding behavior has been noticed with human smooth muscle cells during a 24 hour cultivation, where lower Zn^{2+} concentrations (<80 μM) had positive impact on cell proliferation, adhesion and spreading without adverse effects on cell viability, but higher concentrations up to 120 μM inhibited cell viability and

proliferation [165]. In general, the cytotoxicity tests using Zn extracts have produced varying results with many of them reporting cytotoxicity of Zn [166]. This has raised concerns whether the extracts should be diluted, as proposed in the case of Mg.

The in vivo evaluation of Zn has mostly focused on cardiovascular applications showing good biocompatibility. In addition, Zn is known to promote bone growth by promoting osteoblast differentiation while inhibiting osteoclast differentiation. Still, only few studies of Zn-based materials are reported for orthopedic applications, probably due to the insufficient mechanical properties of pure Zn. In conclusion, Zn is a promising biodegradable metal, but more long-term in vivo studies are needed. [166], [167]

2.3.3.4 Molybdenum (Mo)

Molybdenum (Mo) is a trace element that is a central component in several human enzymes, such as xanthine oxidases and sulfite oxidases. The Mo toxicity data in humans is limited, but indicates low toxicity. This can be explained by the reported rapid urinary excretion of Mo at increased intake levels. The tolerable upper intake level of Mo is 2 mg/day based on animal studies. [162], [168]–[170]

The corrosion of magnetron sputtered Mo thin films (40 nm) in di-H_2O has been reported to yield an initial native MoO_3 oxide at the film surface, after which a mixture of valence (Mo^{4+}, Mo^{5+} and Mo^{6+}) oxide dissolution products were observed. After 80 days, Mo^{5+} oxide was formed as a terminal compound. The dissolution of the MoO_x occurred slowly with an estimated rate of 0.2-0.5 nm/day. The electrical resistance of the tested thin films was noticed to decrease faster than their thickness due to the formation of micropores. [126]

The slow dissolution rate of Mo makes it a potential option for devices that require direct contact of electrodes with biological tissues. Previously, Mo has been used for instance as wires (10 µm) for transcutaneous data transfer and as sputtered interconnects (2 µm) between the wires and Si nanomembranes in semiconductor-based sensors. Furthermore, laser-cut molybdenum foil (5 µm) has been used to form inductor coils and resistive heating elements for a biodegradable wireless drug delivery device. These 5 µm thick Mo components were reported to dissolve completely within 6-8 months of in vitro immersion in phosphate-buffered saline (PBS) at +37 °C. [79], [126], [171]

Mo thin films with a thickness of 1 µm have been achieved both by sputtering and evaporating [172]. However, due to the high T_m of Mo (2617°C), the energy needed for Mo evaporation is high, which in turn could lead to undesired heating of

the substrate. Sputtering might therefore provide a more useful physical vapor deposition method for fabricating bioresorbable LC devices.

2.4 Conventional microfabrication methods

Microfabrication techniques are used for fabricating devices with dimensions ranging from sub-microns to millimeters. The fabrication methods often involve silicon or ceramic substrates that are subjected to various thin film deposition and photolithography techniques for defining the film patterns. In addition, soft fabrication methods such as embossing, molding and casting can be considered. [173] This chapter focuses on various film deposition and patterning methods that are commonly used for constructing planar LC circuit components.

2.4.1 Film deposition

Physical vapor deposition (PVD) methods include a variety of thin film deposition methods, of which evaporation- and sputtering-based techniques are the most common. Evaporation has been considered as perhaps the simplest thin film deposition technology; it involves heating the source material under vacuum to either evaporate or sublime it. The vacuum environment is needed to enable a transition of the raw material to gaseous state at a lower temperature compared to atmospheric pressure. Metals like Au, Ag, Cu, Al, Ni and Cr can be easily evaporated. The primary techniques are thermal and electron beam (e-beam) evaporation. In thermal evaporation the whole material and its container are heated, which increases the risk of unwanted reactions or alloying with the crucible material. In e-beam evaporation, a focused high-energy beam of electrons is directed to a limited area to heat the source material. Moreover, the localized e-beam should not heat the crucible, for why the variety of materials that can be e-beam evaporated is larger compared to thermal evaporation. [125], [174]

Sputtering is a PVD process where the deposited material is mechanically removed from a target by bombarding it with high kinetic energy ions. The sputtering process occurs under a constant flow of rare gas like argon (Ar), which is ionized in an intense electric field to generate plasma. The deposition pressure is controlled by the gas flow rate and by a throttle valve located between the deposition chamber and the vacuum pump. The most common sputter source types are diodes

and magnetrons, both of which can be operated utilizing direct current (DC) or radio frequency (RF). Diode sources are cheaper, facilitate a uniform target consumption and can be easily scaled for larger batch sizes. However, magnetron sputtering yields much higher deposition rates due to increased plasma density and enables better control of the electrons by using a magnetic field, thus reducing the ion bombardment at the substrate. In magnetron sputtering, the electrons are confined around a ring at the target center, which results in an uneven target consumption. Certain compound films can be fabricated using reactive sputtering, which involves introducing a reactive gas into the vacuum chamber, where it chemically reacts with the depositing film to form for example oxide or nitride layers. [173], [174]

Electrodeposition is an essential part of the fabrication of many electronic devices and can be used to produce thicker metal films compared to the previously mentioned PVD techniques. Electrodeposition involves depositing desired metals from an ionic solution onto a conducting surface. It usually utilizes external electrical current to enable the reduction reaction at the substrate surface but may also be done in an autocatalytic fashion as a so-called electroless deposition. Not all metals can be electrodeposited, but Au, Cu, Sn and Ag are examples of commonly employed materials. For instance, electrodeposited Cu is often used to provide electrical connections through printed circuit board (PCB) via holes. [125], [173]

Chemical vapor deposition (CVD) methods rely on chemical carrier gases that produce material films by reacting with other gases or by decomposing into stable reaction products at the substrate surface. CVD techniques are usually performed in rough vacuum provided with thermal or plasma energy to enable the chemical reactions. [174] Conformal coatings produced by CVD methods enable filling holes and covering other 3D shapes. However, the methods usually require high temperatures and may utilize toxic chemical precursors or produce toxic by-products. For example, conventional plasma-enhanced chemical vapor deposition (PECVD) processes are often operated around 250-350 °C, although room temperature processes have also been developed. [19], [119], [175] Moreover, the conformity of PECVD layers is more likely to be compromised compared to non-plasma based CVD layers [176].

Atomic layer deposition (ALD) is a special form of CVD, where the reactions are self-limited by the precursors. The precursors are alternated in cycles, producing atomic layer deposits onto the substrate. One ALD cycle may take from 1 s to 1 min depending on the equipment. ALD is typically used to produce thin films composed of two elements, such as metal nitrides and metal oxides. Although conventional

ALD utilizes higher temperatures, certain ALD processes can be performed below 100 °C, thus enabling the usage of polymer substrates. [176]–[178]

Organic polymer thin films used in electronics are usually applied using spin coating. Such films may be temporary, as in the case of photoresists, or permanent, such as dielectric polyimide thin films. Spin coating allows control over the film thickness by adjusting the centrifugal speed or the resin to solvent ratio. Other methods for depositing polymeric films include dip coating, screen-printing, spraying and flow coating, whose variation is extrusion coating. In addition, CVD of polymers is a highly desirable method due to its ability to fully cover assembled circuits, including wire bonds and other detailed structures. However, most organic monomers and polymers decompose before vaporizing, which limits the material options in CVD of polymers. One widely used vapor deposited polymer group are poly(para-xylylenes), better known by their trade name Parylene. Parylene coating involves vaporizing solid xylene dimers under vacuum, after which the dimers are pyrolyzed to form gaseous monomers that are further polymerized on a sample surface near room temperature. [125]

Thin film-based parallel-plate capacitors require the deposition of two electrode plates combined with one dielectric layer. The dielectric material should withstand temperatures of at least 125-150 °C, which is the accepted stress testing range for integrated circuits and other electronic devices. Nevertheless, much higher heat resistance may be required depending on the subsequent assembly steps. Therefore, inorganic films like silicon oxides, silicon nitrides, aluminum oxides and titanium oxides are often preferred over polymeric dielectric films. [125]

2.4.2   Thin film patterning

Conventional rigid PCB-based technologies often utilize passive components like resistors, capacitors and inductors as external off-the-shelf components that can be soldered to electroplated PCBs [179]. However, these components can be also produced with thin film technologies. This chapter summarizes certain conventional methods for patterning thin films.

The simplest method for producing reproducible thin film patterns is using physical shadow masks that protect the areas underneath the mask, leaving only the exposed areas coated. The main limitation of this approach is its rather low resolution [20]. Even though stencil lithography offers a high-resolution shadow

mask technology, it is predominantly limited to simple structures, in contrast to inductor coils and other complex shapes [146].

Photolithographic methods have high resolution capabilities, which have been driving the miniaturization of feature sizes in electronic components. Photolithography involves creating a patterned photosensitive polymer (photoresist) mask onto the substrate. The photoresist is typically spin coated onto a thoroughly cleaned substrate, baked around 75-100 °C to remove the solvent and then selectively exposed to a suitable light source. In the case of negative photoresists, the light-exposed material becomes polymerized or crosslinked and the unexposed low-molecular weight resist can be washed off with a developer solution. Correspondingly, positive photoresists are rendered soluble by the exposure. The developers for positive and negative photoresists are usually aqueous alkaline solutions or organic solutions, respectively. Hard baking may be performed after development to avoid resist breakdown in the subsequent processing steps. [125], [173]

The deposited films can be patterned either by a lift-off method, where the film is deposited through the photoresist mask which is then stripped off, or by applying the mask onto a deposited film and then etching away the unprotected film sections. The etching can be done by dry etching techniques such as reactive ion etching or ion beam milling, or by wet etching using chemical liquids like $FeCl_3$, $CuCl_2$ and alkaline solutions that are used for Cu etching in printed circuit board manufacturing. In the lift-off processes, the film deposition is usually performed utilizing conventional PVD techniques. Depending on the photoresist and the baking conditions, the mask may be removed using a multitude of options. Wet cleaning includes inorganic processes using for example H_2SO_4-based chemicals at elevated temperatures (>100 °C), as well as organic processes using for example acetone. Dry processes can be performed for instance using oxygen plasma ashing, where reactive ions are used to break down the photoresist. [125], [173], [180], [181]

2.5 Processing of bioresorbable materials for electronic applications

New methods are needed for fabricating bioresorbable sensor components and for assembling the sensors, because the sensitivity of these materials considerably constrains the processing temperatures and applicable solvents [19]. The purpose of this chapter is to outline the literature regarding the fabrication of different

bioresorbable circuit components and to introduce the associated constraints. The components that are addressed include substrates, conductors, dielectrics and encapsulation layers.

2.5.1   Bioresorbable substrate fabrication

Substrates function as supporting structures for the electrically functional layers. In many cases, the substrates are also utilized as passivation layers to protect the encapsulated functional layers. The reported bioresorbable substrate materials are typically polymers [50], but also bioactive glasses [115], [116] have been proposed. Even biodegradable thin metal foil substrates with spin-on-glass insulating layers have been considered for semiconductor devices [182]. Metallic substrates are however not practical for LC circuits, as they interfere with the magnetic readout [43].

Solvent casted silk films were the first substrate proposed for bioresorbable electronics due to their non-inflammatory degradation products, tailorable degradation rate and the possibility to process the material in ambient conditions [2]. Nevertheless, the reported silk-based devices have disintegrated in vitro within hours [122], [123], which has led to using synthetic bioresorbable polymers like PLLA or PLGAs in more recent publications [76], [78], [79], [148]. These synthetic materials are relatively easily formed into various shapes using for example solvent casting and melt processing methods. In addition, their tackiness is an advantage if the patterned conductors are transfer printed onto the bioresorbable substrate. These advantages come at a cost of relatively poor thermal stability and possible swelling in water. Most, if any, bioresorbable polymer substrates are not compatible with current photolithographic processes. [20], [182]–[185]

Solvent casting is a commonly used method for producing bioresorbable polymeric substrates [20], [73], as it is simple and does not require expensive equipment. However, producing films with an even thickness might be difficult, which is why spin casting is sometimes utilized. A further solution processing technique electrospinning can be used to produce highly porous substrates [96]. In addition to solution processing, polymers may be melt processed into sheets for example by extrusion or compression molding (hot pressing) [20], [148], [186]. Sub-micrometer features like channels or pillars may be formed onto the substrate using techniques like microcutting, hot embossing or micromolding [185].

Traditional non-degradable glasses are used in electronics as substrates due to their low cost, ease of processing into various shapes, controllable thermal deformability and surface smoothness [125]. Correspondingly, bioactive glass and bioceramic substrates are interesting materials for implantable temporary sensors due to their superior temperature and chemical resistance compared to common bioresorbable polymers. Bioactive glasses and bioceramics are typically processed by melting the resources, pouring the melt into an appropriate mold and cooling it rapidly. Machine finishing like grinding and polishing are often used for subsequent shaping. [187]

2.5.2   Bioresorbable dielectric and encapsulation layer fabrication

Dielectric layers are needed in LC circuits for instance for building capacitors and enabling conductor crossovers. The fabrication of the dielectrics is a critical part of assembling bioresorbable sensors, as harsh processing methods can damage the substrate or underlying conductors in multilayer structures. Commonly used materials include ceramic thin films like SiO_2, MgO and Si_3N_4, as well as various polymer films like PVA or PCL [37], [119], [188]. The same material types are often used as passivation layers to prolong the functional lifetime of the devices under physiological conditions.

Thin oxide films can be deposited for example using evaporation, sputtering, PECVD or ALD methods. [119], [189] E-beam evaporation is among the most common oxide deposition techniques in bioresorbable electronics [79], [110], [122]. In standard evaporation configurations, different vapor pressures and melting points of compounds lead to different evaporation rates between their components [190]. For example, Kang et al. noticed a Si:O ratio of 1:2.2 in e-beam evaporated SiO_2 films as opposed to 1:2 in PECVD and thermal oxidation films [119]. This might partly explain why e-beam evaporated SiO_2 was shown to dissolve 100-fold faster compared to PECVD SiO_2 [191]. On the other hand, porosity or other structural properties could also account for different dissolution rates.

Sputtering can be used to deposit compound films that share the same composition with the material target, because the process involves dislodging particles from a target rather than evaporating or sublimating the material. Still, certain stoichiometric changes were noticed in sputtered bioactive glass films as compared to the target composition [192], [193]. Moreover, sputtered bioactive glass films have not been investigated in bioresorbable electronic applications yet, possibly

due to the operation temperature (150 °C) of the reported technique. In general, sputtering is a non-directional process due to gas-phase scattering of sputtered atoms, as well as short target-to-sample distances combined with large target areas. This leads to the possibility of preparing continuous films over small steps on a substrate as illustrated in a schematic view in Figure 3. [190] Such step coverage is especially important if another conductor layer is deposited onto the dielectric film.
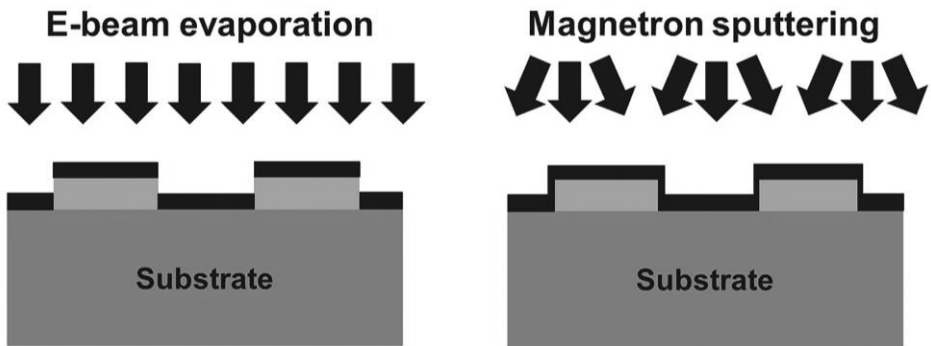
Figure 3. Schematic simplification of differences in step coverage between e-beam evaporation and magnetron sputtering deposition methods, adapted from [194].

PECVD SiO_2 films have been reported in the bioresorbable electronics literature, but as the processes have been performed at 250-350 °C, practiclly all polymeric substrates are excluded from these fabrication steps. However, also room temperature remote PECVD processes where the substrates are located outside the plasma have been reported. Furthermore, pinholes and other defects may be expected with PECVD deposited films, whereas ALD coatings might contain a reduced amount of defects. Low temperature ALD processes (<100 °C) have been studied on biodegradable polymers for packaging applications, but more studies are needed where bioresorbable electronic devices would be tested under immersion. [19], [119], [175], [176], [195], [196]

Processing of insulating polymer films can be done using many techniques, including spin coating, solvent casting or melt processing techniques. In addition, biodegradable waxes have been proposed as encapsulation layers that can be molten and then dip coated onto polymeric PLGA substrates [197]. Further coating advancements can be expected in the future with CVD polymerized biodegradable polymers, whose first proof-of-concept has been recently reported [198].

Although fabricating films from bioresorbable polymers is straightforward, attaching such films onto polymer substrates in the sensor assembly phase might be

a burden. Boutry et al. used PLLA as an insulating layer between two inductor coils in their wireless arterial pulse sensor, because its toughness facilitated an easy assembly [76]. Luo et al. utilized solvent bonding, where an adhesive PCL layer was bonded to a PLLA spacer with a small amount of dichloromethane [73]. A similar approach was used in their faster degrading sensor, where water was used as a solvent to attach the PLGA 50:50 spacer onto PVA before folding and laminating the substrate. Acar et al. have provided insight into the material properties of insulating PVA, concluding that its degradation can be accelerated by adding sucrose into the PVA matrix or decelerated with gelatin [188].

2.5.3   Bioresorbable conductor fabrication

Patterned metal films are a typical conductor choice in bioresorbable electronics. They can be deposited directly onto the substrate or prepared separately and then transfer printed. Direct deposition of the metal onto the substrate should be performed below the T_g of the substrate material, which limits the material options in PVD-based methods [20]. The shadow masks can be prepared for example by etching Kapton film, laser cutting plastic or metal, or 3D printing. In cases where the substrate material is compatible with lithographic methods, sacrificial photoresist masks can be applied directly onto the substrate.

The most suitable conductor deposition process depends on several aspects, including the film thickness and the applied material [174]. For example, the deposition of Mg films is generally done by e-beam evaporation in biodegradable electronics [19], [25], [37], [75], [122], [199], [200], although Mg sputtering has been also reported [122], [148]. Mg sublimes when evaporated, resulting relatively conveniently in films up to several micrometers [200], [201]. On the contrary, the high sublimation rate of Zn combined with its high vapor pressure lead easily to wall deposits that may spoil the vacuum system when evaporated [201]. Sputtering of Zn is therefore usually preferred [126], [202]–[204]. Furthermore, the mechanical nature of sputtering permits depositing Mo films in temperatures well below its melting point [174], which could be an advantage when using heat sensitive substrates. Mo films have been deposited both by evaporation and sputtering [172], but the reports related to bioresorbable electronic devices have mainly utilized sputtered Mo [78], [79], [126].

Printing techniques are considered as a promising conductor fabrication method because they are more easily scalable than the vacuum-based deposition

technologies. Printing of bioresorbable materials is currently under development with only few reports addressing liquid inks based on Zn, Mo, W and Fe nano- or microparticles [205]–[208]. The compatibility of the substrates with the printing conditions and possible post-processing steps are important factors to consider in the development of bioresorbable inks. [50]

Fabricating conductors separately from the substrate and transfer printing them allows circumventing challenges associated with high temperature or harsh chemicals. [50] The fabrication of transferable conductor patterns can be divided into top-down and bottom-up methods, where either metal foils are patterned or the films are additively deposited, respectively. Chemical etching and laser cutting of Mg foils were described by Tsang et al. already in 2013 with exemplary spiral coil and interdigitated comb structures [209]. Koo et al. fabricated inductor coils from Mg foils (~50 μm) by using photolithography and wet etching in diluted hydrochloric acid (HCl : di-H_2O = 1 : 9). The coils were soaked with ethyl acetate and then transferred onto a PLGA 65:35 substrate. In addition, bioresorbable capacitors were manufactured by depositing SiO_2 layers (600 nm) onto patterned Mg foil pieces and laminating two such pieces together. [148] Boutry et al. used laser cutting for fabricating coil structures from Mg foil (50 μm). The laser-cut foil was comprised of two parts that were folded onto each other using PLLA (50 μm) as an insulation between the folded parts. [76] In addition, Lee et al. fabricated detailed Mo conductors including inductive coils and resistors by laser cutting Mo foils (5 μm) attached onto temporary plastic substrates [171].

In addition to the top-down etching and laser cutting methods, Tsang et al. proposed a bottom-up method where Mg (50 μm) was electrodeposited onto a metallized seed layer on a glass substrate. The deposition was performed through patterned SU-8 masks. [209] The first wireless bioresorbable pressure sensor was reported by the same research group, involving Zn conductors (50 μm) electrodeposited onto a Kapton film through a 90 μm thick photoresist mold. [73] Jurgeleit et al. have suggested a magnetron sputtering-based method for depositing thick Fe films (~30 μm) onto a silicon wafer containing a sacrificial Cu layer (0.5 μm). After the sputtering process, the sacrificial layer was wet etched to yield free-standing Fe foils that were further annealed at temperatures ranging from 400 to 800 °C. [210] Rüegg et al. have proposed a fabrication method for detailed Mg patterns on glass substrates. The method was used to fabricate wireless Mg microheaters using thermal evaporation of Mg (2 μm) followed by a photolithographic patterning of a spin coated resist applied onto the Mg film. The Mg film was then ion beam etched, after which the remaining photoresist was stripped using oxygen plasma and acetone.

The method was proposed as an alternative to lift-off technique, which suffers from limitations in the maximum conductor layer thickness. [146]

2.6 Bioresorbable inductively coupled devices

2.6.1 Early bioresorbable non-sensor inductor-capacitor circuits

Kim et al. introduced the first practical concept of bioresorbable electronics in 2009 by constructing silicon nanomembrane semiconductors on silk substrates [2]. During the last decade, the amount of publications based on bioresorbable semiconductors and other wired solutions has increased at a fast pace. Examples of wired sensor applications include monitoring intracranial pressure [79], mapping the electrical activity of the brain [78] and monitoring tendon healing [75]. Nevertheless, the development of wireless bioresorbable devices has been slower. The first bioresorbable LC resonators and other RF devices described in this chapter were powered wirelessly using inductive coupling, but not designed for sensing applications.

Finamore et al. presented a prototype of a bioresorbable LC circuit in 2009 as a part of an envisioned temporary electrical stimulator for bone repair. The circuit was fabricated by milling Mg alloy coupons (250 μm) to form capacitor plates and an inductor. These components were then assembled into a circuit using melt processed polylactide (PLA) as insulating and encapsulation layers. The LC circuit was successfully read from a depth of 1 cm inside pork belly. [211]

In 2012, Boutry et al. published a paper addressing LC resonators made from biodegradable metals (Mg, Fe and their alloys) and from conductive polymer composites (polycaprolactone-polypyrrole and polylactide-polypyrrole). The polymer resonators showed low Q-factors due to their poor conductivity. Furthermore, polypyrrole is considered non-degradable. The resonance frequency of the metal resonators was in the range from 500 MHz to 1 GHz. Mg and Mg alloy (with 2 % Ytrium, 1 % Zn, 0.25 % Ca and 0.15 % Mn) provided the highest Q-factors. Hence, Mg was considered as the most promising material for wireless bioresorbable implants. [212] In their follow-up paper, the authors observed that similar resonators produced a detectable, although largely attenuated resonance peak from a depth of 6 mm of fat or muscle tissue [139].

Hwang et al. proposed an LC resonator design in 2012 based on Mg electrodes, MgO dielectrics and solvent casted silk substrates. In addition, preclinical in vivo results of a thermal therapy device were presented. The device consisted of Si resistors connected to inductor coils, enabling wireless powering of the devices through rat skin. The method was demonstrated to yield 5 °C higher temperatures at the site of the resistors compared to background levels. Moreover, the time scale for functional transience was declared at 15 days. [122] Other bioresorbable examples utilizing inductive coupling for wireless powering of electronic implants include drug delivery devices where an antibiotic or anti-cancer drug release was thermally triggered using remotely heated resistors, as well as electrical nerve stimulation implants for enhancing postoperative nerve regeneration. [148], [213], [214] In 2019, Rüegg et al. reported detailed Mg-based (2 μm) microresonators onto float glass substrates. The resonators with meander resistors were selectively heated using an external RF field. The generated heat was strong enough to induce damage to the protective Parylene layer on top of the resistor. Unprotected Mg patterns were noticed to dissolve completely within 50 minutes in PBS at +37 °C. [146]

A collection of bioresorbable RF circuit components like capacitors, antennas, inductors, resistors and transistors were presented by Hwang et al. in 2013 [199]. Linear dipole antennas were made either from evaporated Mg layers (500 nm) or Mg foils (5-50 μm) that were cut into shape. The antennas were adhered onto silk substrates and were reported to function at frequencies of 950 MHz or 2.4 GHz. By combining an RF antenna, an inductor, a resistor, diodes and capacitors, a fully biodegradable RF power scavenger circuit was realized with an ability to turn on a commercial light-emitting diode (LED) from approximately 2 m. The device disintegration occurred within minutes in di-H_2O at room temperature due to silk substrate dissolution. A similar partly biodegradable LED-powering device was later reported by Lee et al. based on printed Zn inductors. The components were encapsulated in poly(lactide-co-glycolide) (PLGA) (100 μm) and remained functional for several hours in water. [215]

Salpavaara et al. reported an LC resonator based on e-beam evaporated Mg (7 μm) on compression molded PLA substrates. Furthermore, a SiO_2 (50 nm) layer was evaporated onto the Mg patterns, which enabled assembling two of such substrates against each other to create an LC circuit without through hole vias. The $f_{phase-dip}$ of two resonators were 50.8 MHz and 58.9 MHz. The Mg patterns showed no visual signs of Mg corrosion after the first 24 hours of immersion and the resonators were readable up to 51 hours of immersion in 0.9 % saline. [104] The LC

circuit architecture was used as a basis for the wireless pressure sensor in this thesis in publication III.

2.6.2   Bioresorbable inductor-capacitor circuit-based sensors

The first fully bioresorbable wireless pressure sensor was published by Luo et al. in 2014. It was based on a folded poly(L-lactide) (PLLA) substrate (200-300 μm) with Fe/Zn (5-10 μm/50 μm) conductors. The sensor coil was fabricated with lithographic methods and contained 14 turns. The sensor was tested in normal saline (0.9 % NaCl solution) at room temperature from 0 to 150 mmHg. The sensitivity of the sensor in that range was -3.9 kHz/mbar or -5.2 kHz/mmHg. The reading distance used in the wireless measurements was 3 mm and the $f_{phase-dip}$ of the sensor 31.9 MHz in air. Upon immersion in normal saline, the $f_{phase-dip}$ decreased to 30.5 MHz and a slightly reduced sensitivity of -4.7 kHz/mmHg was noticed. The equilibrium state of the immersed sensor was reached after 21 hours, after which the $f_{phase-dip}$ remained at 30.7 ± 0.1 MHz with a stable Q-factor above 9. This period from 21 to 107 hours was considered as the functional lifetime for the sensor. The pressure sensitivity of the sensor remained at -7.2 ± 0.5 kHz/mmHg. After 107 hours of immersion, both the $f_{phase-dip}$ and the Q-factor started to drop rapidly with only a faint resonance between the reader coil and the sensor after 1 week (168 hours). [73]

In order to accelerate the degradation of their pressure sensor, Luo et al. constructed a similar sensor architecture, where the PLLA substrate was replaced with a faster degrading PLGA 50:50 film (250 μm) together with a water-soluble PVA inner support layer (250-300 μm) and a laser-cut PLGA 50:50 spacer. The sensors were tested at a frequency range of 1-100 MHz and pressure range of 0 to 225 mmHg. The sensors showed an initial $f_{phase-dip}$ of 50.7 MHz in air with a pressure sensitivity of -5.8 kHz/mmHg. As opposed to their earlier PLLA-based device, the PLGA-PVA sensor was tested at +37 °C. The immersed sensor showed a significantly faster equilibration phase of only 1.5 hours. The subsequent functional lifetime was from 1.5 to 25 hours, during which the $f_{phase-dip}$ remained at 31.7 ± 0.3 MHz and the pressure sensitivity at 5.6 ± 0.1 kHz/mmHg. After 25 hours, the $f_{phase-dip}$ started to rapidly increase and the Q decreased from 12 to 5 within the next 2 hours. After 30 days of hydrolysis, a virtually complete degradation had occurred with only traces of Zn and PLGA remaining. [74]

Boutry et al. recently described a cuff-type biodegradable pressure sensor for monitoring blood flow in arteries. The sensor could be used for monitoring the functionality of blood vessels after revascularization surgeries. The pressure sensitivity was achieved using patterned PGS elastomer pyramids between magnesium electrodes (50 μm). This enabled fast response times in the millisecond range. Wireless communication relied on coils that were laser-cut from Mg foil (50 μm). The sensor was characterized in vitro but also in vivo. All the components, including structures made from poly(octamethylene maleate (anhydride) citrate) (POMaC), PGS, PLLA and Mg were degraded within 3 months, leaving only polyhydroxybutyrate/polyhydroxyvalerate (PHB/PHV) packaging layers behind. Although a decreased Q-factor was noticed, the sensor was still operational after one week of implantation and showed similar results to an external Doppler ultrasound method. [76]

Lu et al. fabricated a wireless temperature sensor using PLGA 65:35 substrates in combination with conductors fabricated by laser-cutting Mg foils (100 μm). Other components included PLA spacers (50 μm), conductive wax (15:1 weight ratio of tungsten powder and candelilla wax), liquid poly(ethylene glycol) (PEG) dielectric and an encapsulating wax mixture (200 or 500 μm). Water was deemed to penetrate the thicker encapsulation wax after 6 days of immersion in PBS at +37 °C, as noted by a decreasing $f_{max(Re)}$. However, the drifting sensor was still readable for a total of 14 days. Reliable sensor operation in rats was perceived for 4 days. The thinner encapsulation layer enabled a stable in vitro operation for 2 days. [9]

3 AIMS OF THE STUDY

In this thesis, the fabrication and performance of bioresorbable inductively coupled passive resonance sensors was studied from the materials perspective. The working hypothesis was that we could fabricate a fully bioresorbable wireless sensor that functions at least 2 weeks in simulated physiological conditions and does not require an internal energy source.

The most important aims in this thesis were:

1. To develop fabrication methods for bioresorbable electronic devices, as most biodegradable materials do not tolerate the conditions used in conventional microfabrication methods.

2. To identify the most critical material properties regarding the fabrication of bioresorbable electronic devices and their performance in simulated physiological conditions.

3. To fabricate a fully bioresorbable sensor that is functional in simulated physiological conditions for at least 2 weeks.

4 MATERIALS AND METHODS

4.1 Materials and their processing

The materials used in this thesis are presented in Table 3. Poly(L-lactide-co-glycolide) [80:20] (PLGA 80:20), Poly(DL-lactide-co-glycolide) [85:15] (PDLGA 85:15), Poly(L/D-lactide) 96:4 (PLDLA 96:4) and Poly(ε-caprolactone) (PCL) were medical grade materials. As described later in more detail, the bioresorbable polymers were either melt processed or spin coated depending on the application.

E-beam evaporation of Mg pellets was used to fabricate thicker Mg films (7-7.5 µm; Publications II, III and IV), as well as thinner control Mg films (0.5 µm; Publication II). In addition, similar control Cu films (0.5 µm) were evaporated using Cu pellets. The evaporation processes were performed under a vacuum level of less than 7×10^{-6} torr. The substrate holder was rotated with a source-to-substrate distance of 31 cm for the thicker Mg films (7-7.5 µm) and 75 cm for the thin Cu and Mg films (0.5 µm).

DC magnetron sputtering of a Zn target (99.99 %; Kurt J. Lesker Company, UK) was used to prepare the Zn films (Publication IV). The sputtering process involved a vacuum level of 5×10^{-6} torr with a working Ar gas pressure of 10^{-3} torr. The sputtering voltage and current were 560 V and 1 A, respectively. The target-to-substrate distance was 10.5 cm, and no substrate rotation was used.

Solid Parylene C dimer (Galxyl C, Galentis S.r.l., Marcon, Italy) was polymerized under vacuum using LabTop 3000 Parylene Deposition System (Para Tech, Aliso Viejo, California, USA). The dimers were first vaporized at 170 °C, then cleaved via pyrolysis at 650 °C and finally polymerized at room temperature to form conformal CVD coatings (Publications I and IV).

Bioactive glass S53P4 (BonAlive®) was prepared from appropriate amounts of $CaCO_3$, Na_2CO_3, $CaHPO_4 \cdot 2H_2O$ and Belgian Sand for SiO_2. The nominal glass composition of S53P4 is presented in [216]. The raw materials were mixed and then molten at 1450 °C for 3 hours. The molten glass was casted into a rod shaped (Ø = 14 mm; Publication IV) graphite mold and annealed. About 2 mm thick discs were then sliced from the rod and polished.

Table 3.   The raw materials used in this thesis

Material	Abbreviation	Supplier	Publication
Poly(L-lactide-co-glycolide) [80:20]	PLGA 80:20	Corbion Purac, the Netherlands	I
Poly(DL-lactide-co-glycolide) [85:15]	PDLGA 85:15	Corbion Purac, the Netherlands	I
Poly(L/D-lactide) 96:4	PLDLA 96:4	Corbion Purac, the Netherlands	IV
Poly(desamino tyrosyl-tyrosine ethyl ester carbonate)	Poly(DTE carbonate) or PDTEC	Integra LifeSciences, USA	II, III, IV
Poly(ε-caprolactone)	PCL	Corbion Purac, the Netherlands	II, III, IV
Magnesium (99.99 %)	Mg	G-materials, Germany	II, III, IV
Cu (99.99 %)	Cu	G-materials, Germany	II
Zinc (99.99 %)	Zn	Kurt J. Lesker Company, UK	IV
Molybdenum wire	Mo wire	Goodfellow Inc., UK	IV
Parylene C dimer	-	Galentis S.r.l., Italy	I, IV
Bioactive Glass S53P4	S53P4	Molten in-house	IV

4.2   Device fabrication and structure

The structures of all the wireless LC circuits used in this study are shown in Figure 4. In addition to these devices, planar three-turn coils fabricated from the bioresorbable conductive wire (Publication II) were also wirelessly measured. Photographs showing the actual sizes of the pressure sensors (introduced in Figure 4c-d) and the other devices are presented later in Figure 14 and Figure 16, respectively.
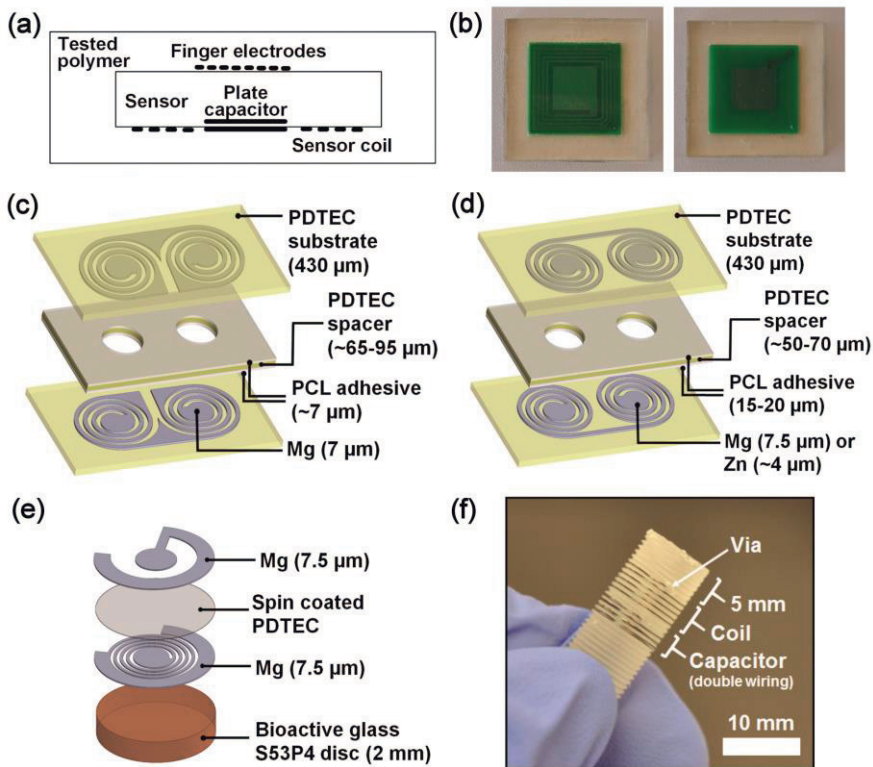
Figure 4. Illustration of the structures of the LC circuits used in this study. (a-b) A schematic cross-sectional view and photographs of the polymer-encapsulated non-degradable sensor (Publication I) used to monitor the degradation of their shell. (c) Schematic structure of the bioresorbable pressure sensor studied in Publication III. These are called type 1 pressure sensors in this thesis. (d) A modified bioresorbable pressure sensor version (Publication IV) with slightly thicker PCL adhesive layers as well as tuned conductor patterns. These devices are termed type 2 pressure sensors in this thesis. (e) The bioactive glass S53P4-based LC resonators (Publication IV) with a diameter of 14 mm. (f) A photograph illustrating the structure of the insulated Mo wire-based compression sensors fabricated onto bioresorbable PLDLA 96:4 screws (Publication IV). In addition to the indicated through hole via, another one can be found between the coil and the capacitor.

4.2.1 Non-degradable LC circuit (Publication I)

A four-layer circuit board design was used for the non-degradable LC circuits. These wireless sensors were commercially manufactured (Prinel Piirilevy Oy, Tuusula, Finland) upon specification and comprised an interdigitated capacitor as a primary sensing component, a parallel-plate capacitor and a coil as shown in Figure 4a.

The number of finger electrodes in the interdigitated capacitor was 24. The thickness of the copper conductors was 35 µm with an approximately 30-40 µm thick electrically insulating solder resist layer on top. In addition to these untreated sensors, four sensors were coated with an approximately 14 µm thick layer of Parylene C. This was done to test the effect of the coating on the consistency of the measurements.

The 20 mm by 20 mm by 1.60 mm sensors were encapsulated in either PLGA 80:20 or PDLGA 85:15 to study the degradation of these copolymers in aqueous conditions. The encapsulation layers were fabricated by compression molding an LC circuit between two 32 mm by 32 mm by 2 mm copolymer sheets to form a single piece.

4.2.2 Bioresorbable conductive wire and planar coil (Publication II)

PDTEC powder was dried in vacuum for 4 days and extruded under nitrogen atmosphere using a microextruder (Gimac, Gastronno, Italy). The resulting monofilament fiber was collected at a rate of 4 m/min using a conveyer. The curvature-containing flat fibers were cleaned with an isopropanol-dampened cloth and metallized by e-beam evaporating Mg pellets to obtain a conductive Mg surface (7.5 µm). Thinner Cu and Mg layers (0.5 µm) were evaporated onto similar fibers as reference materials. During the process, the fibers were attached onto a holder with Kapton tape, resulting in discontinuous metal films on continuous PDTEC fibers. The continuous lengths of the thicker Mg surfaces varied from 9 to 14 cm, whereas those of the control films were 25 cm long. The fibers with thicker Mg layers (7.5 µm) were extrusion coated with PCL using a crosshead die with a nozzle diameter of 2 mm. The coated wire was collected with the conveyer at a rate of 3 m/min.

Three similar planar coils with three turns were formed by coiling bioresorbable conductor wires around a template pillar (Ø = 7 mm). The insulating PCL layer was melted with a soldering iron and cooled to adhere the coil turns into each other. In the original study, three reference coils were made from commercial insulated Cu wire (Flexi-E 0.10, Stäubli Group, Switzerland) using the same template and super glue to attach the coil turns.

4.2.3 Bioresorbable pressure sensors (Publications III and IV)

The LC circuit-based pressure sensors were fabricated by first extruding PDTEC rods with a twin-screw extruder (Mini ZE 20*11.5 D, Neste Oy, Finland) and compression molding (ZB110, NIKE Hydraulics Ab, Eskilstuna, Sweden) about 430 μm thick substrates from the rod pieces. The compression was done against glass to enable low surface roughness for the substrates. Conductor patterns were then formed either by e-beam evaporating Mg (7.0-7.5 μm) or by DC magnetron sputtering Zn (~4 μm). The Mg-based pressure sensors presented in Publication III are termed type 1 pressure sensors in this thesis, whereas type 2 pressure sensor indicates the slightly modified sensors that were studied in Publication IV. The differences in the sensors are illustrated in Figure 4c-d.

The conductor patterns in the type 1 sensors were defined by 3D printed plastic masks, as opposed to laser-cut metal sheets in the type 2 devices. The sensors were assembled by attaching two substrates onto a PDTEC spacer with two laser-cut holes in it. The attachment was done by melting spin coated (Type 1; Publication III) or compression molded (Type 2; Publication IV) PCL adhesive layers between the spacer and the substrates.

The adhesive PCL films were first placed on both sides of the spacer, molten and then cooled back to room temperature. Thereafter, excessive PCL was removed from the spacer holes. The substrate-spacer-substrate sandwich was then heated to 80 °C under gentle pressure to melt the PCL adhesive again and to thereby adhere the substrates onto the spacer. Finally, the sides of the sensor were heat sealed (Hawo HPL ISZ, Obrigheim, Germany) and trimmed with scissors to yield approximately 35 mm by 25 mm by 1 mm sized sensors.

4.2.4 Other resonance circuits (Publication IV)

A bioactive glass S53P4-based LC circuit was fabricated by first preparing the S53P4 substrate discs. After melting the glass, cutting discs and polishing them, an e-beam evaporated Mg coil (7.5 μm) was deposited through 3D printed PLA masks. A subsequent dielectric layer was fabricated by spin coating 12 % PDTEC in cyclohexanone solvent at 3000 rpm. Thereafter, a further Mg layer (7.5 μm) was deposited to complete the resonator as illustrated in Figure 4e. To protect the Mg conductors in aqueous conditions, the bioactive glass resonators were coated with Parylene C (~13 μm). A similar method with spin coated dielectric layers on an e-

beam evaporated Mg spiral was experimented with PDTEC and PLDLA 96:4 substrates, but the conductors were noticed to crack during the solvent drying phase.

Wireless compression sensors on threaded PLDLA 96:4 screws were fabricated using biodegradable Mo wire (200 µm) as the conductor. The wire was insulated with Parylene C (~10 µm) to avoid short-circuits in the structure. The coil was formed by winding Mo wire around the PLDLA screw. The capacitor consisted of a double strand of the insulated wire in each screw thread (Figure 4f). The coil and the capacitor were connected by drilled through hole vias on the PLDLA screw.

4.3 Material characterization

Unless otherwise stated, all the immersion tests were performed at +37 °C using Sörensen phosphate buffer solution (pH 7.46-7.49) that was prepared according to the standard "ISO 15814:1999(E): Implants for surgery – Copolymers and blends based on polylactide – In vitro degradation testing".

4.3.1 Water uptake and mass loss of polymers (Publications I, II, IV)

Water uptake of PLGA 80:20 and PDLGA 85:15 (Publication I) was evaluated at time points of 2, 4, 6 and 8 weeks by drying the immersed samples (n=4) gently with tissue paper, weighing them and then drying them first in a fume hood and then in a vacuum chamber. The dried samples were weighed, and the water uptake of the samples was calculated using the following equation:

$$Water\ uptake\ (\%) = \frac{wet\ weight - dry\ weight}{dry\ weight} \times 100\ \% \qquad (24)$$

In comparison, the water uptake properties of PCL and PDTEC were evaluated from thoroughly dried $0.4 \times 10 \times 50\ mm^3$ sized samples (n=5) by comparing the measured wet weights to the initial dry weight that was measured before immersing the samples. The effect of mass loss was considered negligible due to the slow degradation rates of these polymers [86], [217]. The tested samples were weighed after the test periods to ensure that no significant mass loss had occurred.

4.3.2 Mechanical testing (Publications I, II, IV)

The flexural properties of PLGA 80:20 and PDLGA 85:15 were tested after 0, 2, 4, 6 and 8 weeks of immersion using a three-point bending setup (Publication I). The size of the test specimens was approximately $32 \times 11 \times 3.8$ mm³. The mechanical testing equipment (Instron 4411, High Wycombe, England) was operated with a 5 kN load cell, 5 mm/min crosshead speed and 22 mm span length. The loading edge radius was 1.5 mm. The tests were performed in ambient conditions immediately after taking the sample out from the buffer solution.

The flexural characteristics of $50 \times 10 \times 0.9$ mm³ sized PDTEC samples (n=3) were also tested using the three-point bending setup (Publication IV). The equipment (Instron Electropuls E1000, High Wycombe, UK) was operated with a 50 N load cell, 5 mm/min crosshead speed and a span length of 30 mm. The loading edge radius was 1 mm. Only the 0-day time point was tested in ambient conditions at +21 °C, whereas all the latter time points were tested while the samples were immersed in Sörensen buffer at +37 °C. In addition, the stress relaxation behavior of PDTEC was investigated under the wet conditions by bending the samples to a 2 mm displacement and recording the changes in the stress needed to hold the displacement during a 3-hour time period.

The tensile properties of the PDTEC fibers (n=10), as well as PCL coated PDTEC fibers (n=10) were studied using the Instron 4411 testing equipment equipped with a 500 N load cell (Publication II). The distance between the pneumatic grips was 50 mm and the crosshead speed 10 mm/min. The fiber cross sections were approximated as rectangles in the calculations. Tensile strength, elongation at break as well as Young's Moduli were calculated based on the measurements.

4.3.3 Thermal analysis (Publications I, II and III)

The onset glass transition temperatures (T_g) of all bioresorbable polymers, as well as the melting temperatures (T_m) of the semi-crystalline polymeric samples were characterized using differential scanning calorimetry (DSC; Q1000, TA Instruments, Delaware, USA). Moreover, in Publication I the T_g of the PLGA 80:20 and PDLGA 85:15 samples were measured after 2, 4, 6 and 8 weeks of immersion. This was done to track the degradation of these polymers, because the T_g of PLGAs is a function of the molecular weight at appropriately low molecular weights. The DSC tests were performed using two parallel samples. The samples in Publication I were first heated

from 0 to 220 °C at 5 °C/min, then cooled back to 0 °C at 50 °C/min and finally heated again at 20 °C/min. Other DSC runs were performed by first heating from 0 to 200 °C at 20 °C/min, cooling back to 0 °C at 50 °C/min and then heating to 200 °C again at 20 °C.

4.3.4 Inherent viscosity measurements (Publications I and II)

The inherent viscosity (*i.v.*) is a viscometric measure of the molecular size in dl/g. In this analysis, the sample pieces were dissolved in chloroform and analyzed using an automated Ubbelohde viscometer (LAUDA, Lauda-Königshofen, Germany) in ambient conditions. Two parallel samples were measured per time point.

In Publication I, the PLGA 80:20 and PDLGA 85:15 copolymer samples were first dried at pre-determined time points, after which pieces of 20 ± 0.8 mg were cut from the core of the samples. Correspondingly, in Publication II the *i.v.* of PDTEC raw material, as well as extruded PDTEC fiber were analyzed from 20 ± 0.6 mg samples.

4.3.5 Scanning electron microscopy (Publications II and IV)

The cross-sectional scanning electron microscopy (SEM) images of the conductive wire (Publication II) were taken with a field-emission scanning electron microscope (FESEM; JSM-7610F, JEOL Ltd., Japan). The wire was first immersed in methanol to promote a brittle behavior during cutting, then frozen in liquid nitrogen and freeze fractured under liquid nitrogen immersion. Finally, the wire cross section was coated with a thin Cr layer.

A high-resolution field emission SEM (FESEM; Zeiss UltraPlus) was used for imaging the surface of the Mg (7.5 μm) and Zn (~4 μm) thin films (Publication IV). A working distance of 5.0 ± 0.2 mm with an electron high tension (EHT) of 1.5 kV was used. Furthermore, the cross-sectional view of the metal films was imaged with a focused ion-beam scanning electron microscope (FIBSEM; Zeiss CrossBeam 540). A Pt cover was applied onto the films before focused gallium ion milling. A working distance of 5.2 mm with an EHT of 3.0 kV was used.

4.3.6 Electrical resistance measurements and mean bulk resistivity calculations (Publications II and IV)

The resistance values of the e-beam evaporated metals on PDTEC fibers were measured using a digital multimeter (AxioMET AX-572) equipped with sharp tipped lead probes. The metal coatings involved Mg (0.5 μm, n=18 and 7.5 μm, n=21) and Cu (0.5 μm, n=18). The extrusion coated wires were measured by melting the PCL coating and peeling off the excessive melt. Then, the multimeter probes were pressed through the residual PCL film. This measurement was done in order to assess the effect of the extrusion coating to the wire resistance divided by its length (R/L in Ω/cm).

The mean resistances of the evaporated Mg (1.7 μm and 7.5 μm; n=6) and sputtered Zn films (1.7 μm; n=6) on glass substrates were studied with 4-wire measurements (Publication IV) using a digital multimeter (Agilent 34401A). The resistances were then divided by the distance of the inner lines of the 4-wire patterns to obtain electrical resistance per conductor length (Ω/cm). These values were averaged. Mean bulk resistivities ($\Omega \cdot$m) were approximated by multiplying the mean R/L values with the estimated cross-sectional area of the conductor. The width of the Mg conductor films was estimated at 1 mm and the cross-sectional area of the Zn films to be equal to that of the Mg films. Both were 1.7 μm thick. These area estimates were based on the profilometer data (Figure 3b in Publication IV).

The changes in electrical resistance of the PCL coated conductive wire (Publication II) as well as 200 μm thick Mo wires (Publication IV) were also evaluated under immersion. Both types of wires (n=5) were attached to perforated caps of 50 ml falcon tubes, leaving the tips of the wires in air and the rest immersed in buffer solution inside the tubes. In case of the Mg-based conductive wire, two layers of conductive silver epoxy adhesive (8331−14G; MG Chemicals, Canada) at the tips of the wires were used to provide more reliable contacts for the measurements. The multimeter equipped with hook clip probes was used to measure the wire resistances. Again, the resistance values were divided by the length of each wire and averaged. The buffer solution was changed every four weeks in the case of the Mo wires.

4.3.7 Thin film corrosion tests (Publication IV)

The corrosion behavior of unprotected Mg and Zn thin films were assessed in cell culture conditions as suggested in [141]. The medium consisted of Minimum

Essential Medium (MEM; Sigma Aldrich, UK) supplemented with 10 % fetal bovine serum (FBS; Gibco by Life Technologies, UK) and 1 % antibiotics (100 U/ml penicillin; 100 U/ml streptomycin; Lonza, Switzerland). The tests where cell medium was used were performed under 5 % CO_2 supply. For comparison, Mg films were also tested in di-H_2O and Sörensen buffer solution with and without 5 % CO_2. All tests were done at +37 °C and 25 ml of solution was used per sample. The corrosion of the metal films was assessed visually by taking photographs at pre-determined time points.

4.3.8   Micro-computed tomography (Publication III)

Micro-computed tomography (Micro-CT; Xradia MicroXCT-400, Zeiss, USA) imaging was performed for pressure sensors to compare the distance of the capacitor electrodes (Publication III) before and after 24 hours of immersion in Sörensen buffer (100 ml). The imaged area was 10 mm by 10 mm and the corresponding pixel size 20 µm. In addition, 2 mm by 2 mm images with a 2 µm pixel size were taken to evaluate the distance between the capacitor plates more accurately.

4.3.9   Cell response (Publication IV)

PDTEC and PLDLA 96/4 polymer discs (Ø = 14 mm) were punch-cut from compression molded sheets, washed briefly in 2-propanol (VWR Chemicals) and sterilized by g-irradiation (BBF Sterilisationsservice GmbH, Kernen im Remstal, Germany) with a minimum dose of 25 kGy. Human foreskin fibroblasts (ATCC, CRL-2429) at passage 12 were seeded onto discs using polystyrene 24-well plates (Ø = 15 mm; Nunc, Roskilde, Denmark) as a control. The seeding was done by adding 1 ml of cell culture medium onto the wells, after which 50 µl of cell suspension including 1000 cells was added. The medium was based on DMEM/F-12 (DMEM/F-12 1:1; Gibco by Life Technologies, United Kingdom) and supplemented with 10 % fetal bovine serum (FBS; Gibco by Life Technologies), 1 % L-glutamine (GlutaMAX I; Thermo Fischer Scientific, USA) and 1 % antibiotics (100 U/ml penicillin; 100 U/ml streptomycin; Lonza, Switzerland). The cell culture was done at +37 °C with a 5 % CO_2 supply. The medium was changed twice a week.

Live/Dead (Invitrogen Molecular Probes, USA) staining probes were used to assess cell viability on the discs at time points of 1, 3, 7 and 14 days. The cells were incubated in 0.25 mM EthD-1 (Molecular Probes) and 0.5 mM calcein AM

(Molecular Probes) in Dulbecco's Phosphate Buffered Saline (DPBS; Sigma Aldrich, United Kingdom) for 45 minutes. Thereafter, the stained cells were imaged with a phase-contrast microscope (Olympus IX51, Japan) equipped with fluorescence optics. In addition, comparison of the cell numbers was done using a previously reported quantitative crystal violet staining method with slight modification.[218] The fibroblasts were fixed with 5% glutaraldehyde in 0.1 M PBS, washed, dried and stained with 250 µl of 0.1 % crystal violet stain (Merck) in H_2O (milli-Q). After thorough washing with H_2O, the polymer substrates were dried.

The samples were photographed before the dye bound in the cell nuclei was solubilized in 10 % acetic acid (J.T. Baker, Deventer, the Netherlands). The amount of acetic acid was calculated based on the culture area, using 100 µl for a 96-well plate (Ø = 6.4 mm) as a basis.[219] The optical density (590 nm) of the samples was measured using Victor 1420 multilabel plate reader (Wallac, Turku, Finland), providing relative cell numbers given as absorbance units. The mean optical densities ± standard deviations were calculated for each material (n = 8). The optical densities of stained substrates without any cells were subtracted from the adjacent measurements containing cells.

4.4   Wireless measurements

The LC resonator and the bioresorbable planar coil were measured by inductively coupling them with a reader coil, whose real part of the impedance, or its phase was measured. The signal processing such as estimating the resonance frequencies from the measured data was performed as described in [18]. In this thesis, the resonance frequency f_0 is used to refer to both $f_{\max(\mathrm{Re})}$ and $f_{\text{phase-dip}}$ from the original publications.

4.4.1   Measurement setups

The wireless readout of the LC devices was performed using three main setups. Setup I consisted of a custom-made portable reader device [18] equipped with a reader coil (Figure 5a). The portable reader was smaller and capable of faster measurements compared to an impedance analyzer. Setup II involved a double-turn rectangular reader coil (Figure 5b) connected to an impedance analyzer (Agilent 4396B). Lastly, in Setup III the reader coil located inside an oven and was connected to the impedance analyzer with a cable (Figure 5c). All the pressure measurements

in this thesis were done through a glass bottle from a reading distance of approximately 6 mm. An external pressure calibrator was used to quantify the amount of applied pressure inside the bottle. Although Setup III was used in both Publication III and Publication IV, the oven was different in these studies.
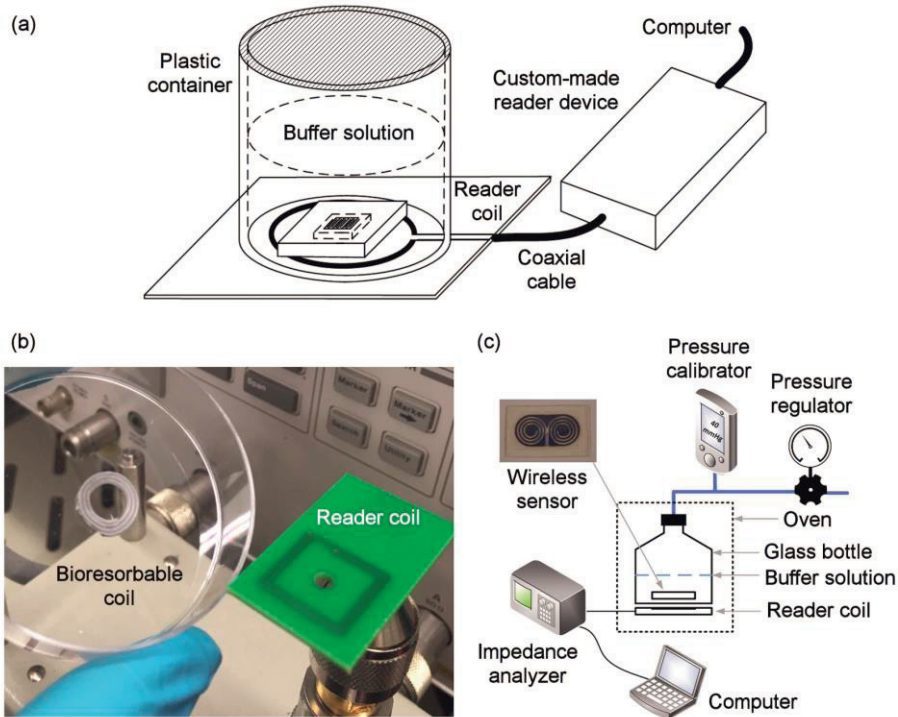
Figure 5. The main measurement setups used in this thesis. (a) Setup I consisted of a custom-made reader device connected to a computer and a reader coil. (b) Setup II utilized a rectangular reader coil with two turns. The coil was connected to an impedance analyzer. (c) Setup III was used for the pressure measurements and utilized a reader coil (Ø = 33 mm) inside an oven. The coil was connected to the impedance analyzer with a cable. Furthermore, pressurized air was guided into a glass bottle from outside the oven.

Table 4 summarizes different setups used for measuring the LC devices in this thesis. The reader coils used in Setups I and III were circular single-turn Cu coils with a diameter of 33 mm, except for the compression response measurements (Publication IV), where a single-turn Al coil with a diameter of 30 mm was used. The reader coil in Setup II was a rectangular double turn Cu coil on a printed circuit board (Figure 5b), where the diameter of the coil was approximately 20 mm. The self-resonance frequencies of the coils were not at the measured frequency ranges in any of the measurements.

Table 4. A summary of the setups used for different wireless measurements. Unless otherwise stated, the real part of the impedance *Re (Z)* was measured.

Publication	Resonator	Subject of interest	Setup
I	Non-degradable LC circuit*	Temperature sensitivity	I***
		Reading distance**	II
		All others	I
II	Bioresorbable three-turn coil	Resonance frequency estimate and peak shape	II
III	Type 1 bioresorbable pressure sensor	All others	III
		System rise time	I
		Reading distance**	II
IV	Type 2 bioresorbable pressure sensors	Pressure response	III
		Reading distance	II
	Bioactive glass resonator	Surrounding medium	II
		Reading distance	II
	Mo wire-based compression sensor*	Compression response	I
		Reading distance	II

*Phase was measured instead of *Re (Z)*

**Unless otherwise stated in the results section, Setup II was used

***In oven

4.4.2 Wireless measurements in air

The reading distances of the LC devices were estimated using Setup II as a basis and adding microscopy slides (1 mm) stepwise between the reader coil and the LC device. The measurements were performed after each microscopy slide addition until the device was not detected anymore. In this thesis, also the type 1 Mg pressure sensor (Publication III) was measured using Setup II. However, the effect of reading distance on the f_0 was analyzed from the original Publication III data, where a similar measurement was performed using a larger reader coil.

The pressure response of the pressure sensors was tested from 0 to 200 mmHg and back at intervals of 20 mmHg in ambient conditions. The type 1 sensors were

subjected to three measurement cycles from 0 to 200 to 0 mmHg, whereas only one cycle was conducted with the type 2 sensors.

The type 1 pressure sensors were also tested under stepwise static pressure from 0 to 100 mmHg and back to 0 mmHg at intervals of 50 mmHg. The pressure was kept constant for 1 hour in each step, during which 60 measurements were recorded. Furthermore, 100 measurement samples were recorded and averaged immediately before and after each 1-hour step. The initial resonance frequency was chosen as the average of the first 100 measurements in ambient conditions. The pressure sensitivities obtained from the linear approximations of the pressure responses were used to translate the obtained resonance frequencies into pressure values.

The temperature response of the type 1 pressure sensors was tested by recording 100 measurement samples at set test points ranging from room temperature to 40 °C. In addition, the sensor response to room temperature changes was studied during a 40-hour period by recording a measurement sample every 5 minutes and comparing the data against temperature changes that were measured with an indoor weather station (Netatmo, France).

Complementary error source measurements performed with the type 1 pressure sensors involved placing a sensor into the middle of the reader coil, moving it 1 mm at a time and measuring it at each position. This effect of the displacement between the sensor and the reader coil was studied in X- and Y-directions (Figure S3a, Supporting Information in Publication III), as well as in Z-direction, or in other words as a function of reading distance.

The compression sensor (Publication IV) was measured using a modified setup I, where the reader coil (Ø = 30 mm) was attached to a vise with an electrically insulating Teflon block between the vise jaw and the reader coil. The sensors were axially compressed in the vise and the compression was measured with a digital caliper.

4.4.3   Wireless measurements under aqueous conditions

The immersion tests in Publication I were done by first attaching the polymer-encapsulated LC circuit onto the bottom of plastic containers. Then, 100 ml of pre-warmed Sörensen buffer solution was added into the containers. The sensors were wirelessly measured through the containers and stored in an incubator (+37 °C) between the measurements. The buffer was changed every two weeks. The

measurement period was 8 weeks except for the Parylene-coated sensors encapsulated with PLGA 80:20, which were measured for 120 days.

The performance of the immersed pressure sensors (Publications III and IV) was evaluated after first studying them in air at room temperature. The sensors were attached onto the bottom of a glass bottle from two corners using Kapton tape, after which pre-warmed Sörensen buffer (100 ml) was added. The f_0 was recorded every 15 or 30 minutes and the pressure response was measured at pre-determined time points similarly to the measurements that were done in air. In Publication IV, one Mg pressure sensor was immersed in MEM solution to see if the different composition of the buffer solution affects the corrosion of the conductors. The pressure response of the sensor immersed in MEM was not tested in order to decrease the contamination risk.

The temperature response of the immersed non-degradable sensors (Publication I) was tested to evaluate temperature as a possible error source. The test was performed by first immersing a PLGA-encapsulated sensor into Sörensen buffer at room temperature for 18 hours to equilibrate the system. Thereafter, the sensor response was recorded at several test points from room temperature to 45 °C.

The bioactive glass-based LC resonators (n=2) were encapsulated with non-degradable Parylene C by chemical vapor deposition as described earlier in section 4.2.1. This was done to enable stable testing of the sensor characteristics under aqueous conditions. The sensor was placed on a Petri dish with a 1 mm thick bottom and immersed in various media. All the bioactive glass sensor tests were done at room temperature. The media included air, di-H_2O, Sörensen buffer, DMEM with high glucose (Sigma Aldrich, Hampshire, UK) and 96 % ethanol (VWR Chemicals). 200 measurements were recorded in each condition. The sensor was rinsed with di-H_2O and dried with tissue paper between each condition. In addition, the response of the sensor to an increasing ionic content was tested by immersing it in 9 ml of di-H_2O and adding 9 % NaCl solution stepwise until a NaCl concentration of 4.5 % was reached. The measurement samples were recorded in di-H_2O and then after each NaCl addition step.

5 RESULTS

5.1 Materials characterization

5.1.1 Bioresorbable polymers

The main bioresorbable polymers used in the study were PLGA 80:20, PDLGA 85:15, PDTEC and PCL. Their inherent viscosity (*i.v.*) values were measured, because *i.v.* can be used as a viscometric variable for estimating the size of the polymer molecules. Table 5 summarizes the main polymeric materials used in this thesis along with their T_g, T_m and inherent viscosity.

Compression molding of PLGA 80:20 and PDLGA 85:15, as well as extrusion of PDTEC were noticed to result in polymer degradation. The relative *i.v.* in PDLGA 85:15, PLGA 80:20 and PDTEC decreased 53 %, 19 % and 33 % during melt processing, respectively. In addition, changes in the *i.v.* and T_g of immersed PLGA 80:20 and PDLGA 85:15 samples were monitored at intervals of 2 weeks (Figure 4 in Publication I). The T_g of PDLGA 85:15 decreased only slightly from 54 °C to 50 °C for the first 4 weeks, after which a steeper decrease was noticed, resulting to a T_g of about 30 °C at 8 weeks. During the test period, the maximum and minimum T_g values of the PLGA 80:20 samples were 61 °C and 57 °C, respectively. Nevertheless, the *i.v.* values in both polymers decreased throughout the test period, showing the cleavage of the polymer chains.

Table 5.   A summary of the bioresorbable polymers used in the thesis, including their glass transition temperature (T_g), melting temperature (T_m) and inherent viscosity values

Polymer	T_g	T_m	Inherent viscosity
PDLGA 85:15			
Raw material	54 °C	amorphous	3.2 dl/g*
Compression molded	-	-	1.5 dl/g
PLGA 80:20			
Raw material	61 °C	amorphous	5.8 dl/g
Compression molded	-	-	4.7 dl/g
PLDLA 96:4			
Raw material	61 °C	157 °C	6.0 dl/g
PDTEC			
Raw material	99 °C	amorphous	0.9 dl/g
Extruded fiber	-	-	0.6 dl/g
PCL			
Raw material	-60 °C**	57 °C	1.2 dl/g*

*As stated by the manufacturer
**Literature value [53]

The water uptake of the polymers is shown in Figure 6. The amount of diffused water in PLGA 80:20 remained around 1.0 wt-% throughout the 8 weeks measurement period, whereas that of PDLGA 85:15 was 1.7 % after 2 weeks and increased up to 10 % at 8 weeks, when the samples appeared significantly swollen. By contrast, the water uptake percentage of PDTEC equilibrated at 3.0 % in a few days and remained there during the whole 100 days test period. Similarly, PCL showed a constant water uptake of about 0.3 % throughout the 30 days test period.
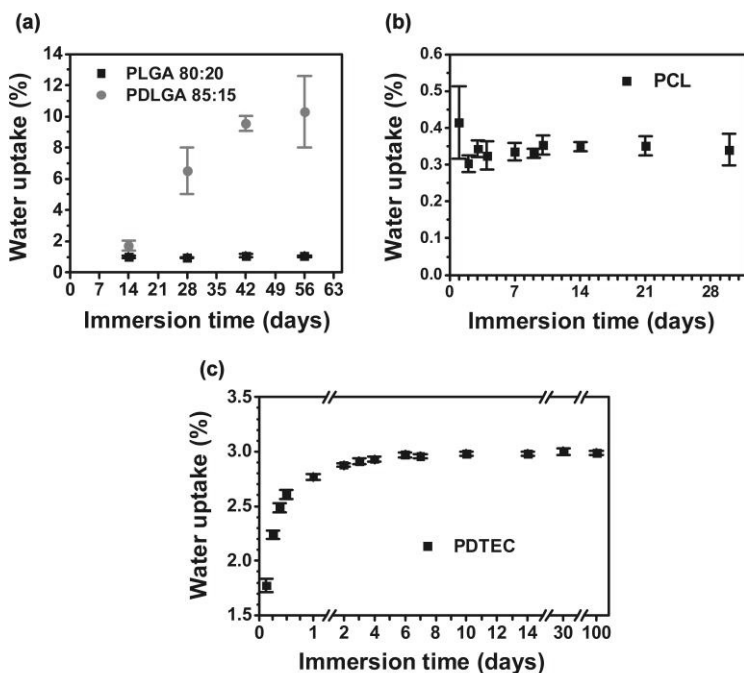
Figure 6. Water uptake of various bioresorbable polymers immersed in Sörensen buffer solution at +37 °C. (a) PLGA 80:20 and PDLGA 85:15 (Publication I), (b) PCL (Publication II) and (c) PDTEC (Publication IV).

Visual changes in PDLGA 85:15 and PLGA 80:20 copolymer capsules during hydrolysis are presented in Figure 7. After 56 days, the PDLGA 85:15 capsules are almost fully degraded, whereas hardly any visual changes are seen in the PLGA 80:20 samples. A prolonged hydrolysis showed cracks in PLGA 80:20 at 159 days, after which the buffer solution was not changed anymore. Nevertheless, the sample was imaged after 2 years, showing white, opaque polymer material. The pH of the buffer solution was 2.9 at this point.
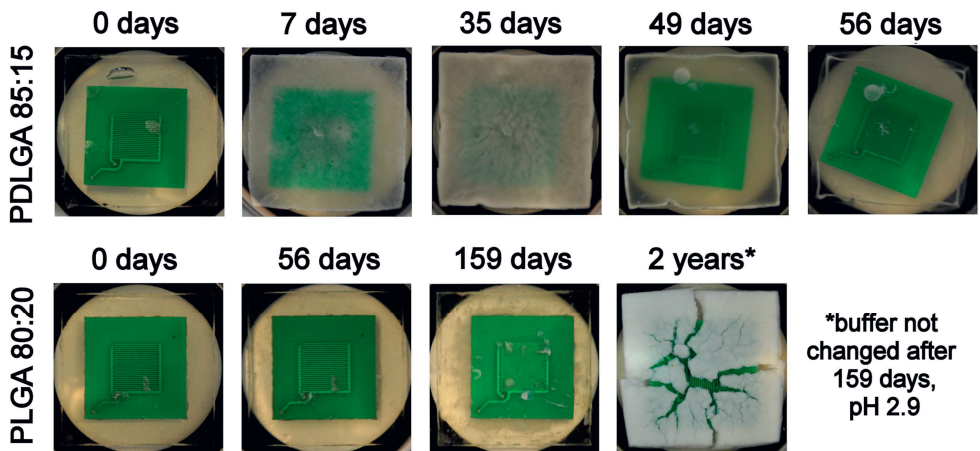
Figure 7. Photographs showing the degradation of the bioresorbable polymer capsules as a function of immersion time.

The mechanical properties of the bioresorbable polymers are outlined in Table 6. Flexural moduli of compression molded PLGA 80:20, PDLGA 85:15 and PDTEC materials were also tested at various time points after immersion. These results are presented in Figure 8. The changes in the moduli of the polyester samples were in line with the other degradation tests, showing relatively rapid loss of mechanical properties in PDLGA 85:15, while those of PLGA 80:20 remained near the initial value throughout the 8 weeks.

Table 6. Mechanical properties (mean ± standard deviation) of various polymer specimens in air at ambient conditions

Material	Processing	Test method	Flexural Modulus	Stress at maximum load
PDLGA 85:15 (n=4)	Compression molded	3-point bending	3.4±0.2 GPa	114±3 MPa
PLGA 80:20 (n=4)	Compression molded	3-point bending	3.4±0.1 GPa	142±3 MPa
PDTEC (n=3)*	Compression molded	3-point bending	2.8±0.1 GPa	82±3 MPa

Material	Processing	Test method	Young's Modulus	Stress at maximum load
PDTEC fiber (n=5)	Extruded	Tensile testing	1.9±0.1 GPa	56±3 MPa
PCL coated PDTEC fiber (n=5)	Extruded and extrusion coated	Tensile testing	0.9±0.1 GPa	25±3 MPa

*Please note that the PDTEC sample thickness was 0.9 mm, as opposed to 3.8 mm thick PDLGA and PLGA samples

The PDTEC samples were tested during immersion in buffer solution (+37 °C). The test period was only one week, as the motivation was to investigate possible changes in the mechanical properties of the sensor substrate material. A modest increasing trend between days 1 and 7 was noticed. However, the mean flexural moduli of all the immersed samples remained within the standard deviation of the dry samples.
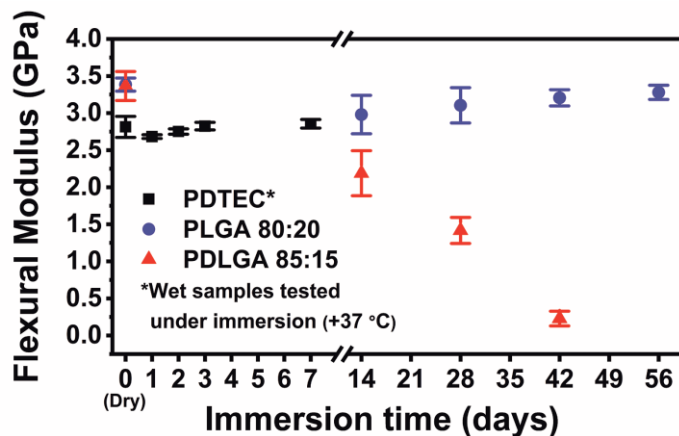
Figure 8. The flexural moduli of PDTEC (Publication IV) compared with PLGA 80:20 and PDLGA 85:15 (Publication I) during hydrolysis in Sörensen buffer solution. The PDTEC samples were tested while immersed (+37 °C), whereas the other sample types were tested in ambient conditions after taking the samples out from the immersion container.

The cell culture results (Figure S1, Supporting Information in Publication IV) showed that the human fibroblast proliferation on PDTEC discs was comparable if not superior to that of the polystyrene well plate and PLDLA 96:4 reference materials. The cell shape was rather spherical on all substrates during the first days of culture, but after 1 week a more elongated shape was prevalent. No dead cells (stained red) were noticed in the Live/Dead images, where live cells were stained green.

5.1.2   Bioresorbable conductors

The SEM images from the e-beam evaporated Mg films (7.5 μm) and DC magnetron sputtered Zn films (4 μm) are illustrated in Figure 9. The cross-sectional structure of the Mg films was columnar. The Zn films appeared denser, with a slightly sparser structure in the upper part of the film. The surface of the Mg films appeared to consist of tabular crystallites, as compared to the granular appearance of the Zn film surface. The largest Zn particles were approximately 2 μm. The cross-sectional profiles of the films showed some differences; the evaporated Mg films contained almost vertical side walls as compared to the rounder shape of the Zn films (Figure 3b in Publication IV).
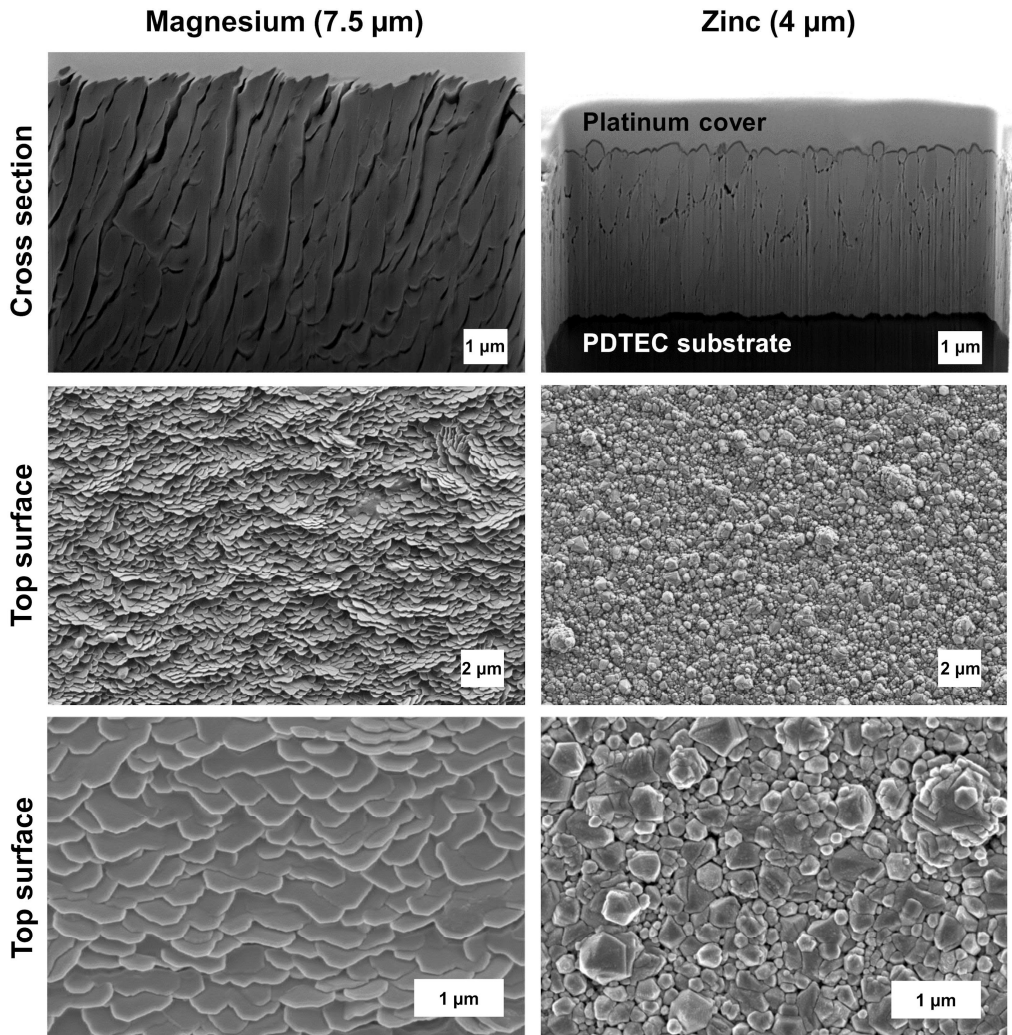
Magnesium (7.5 μm)   **Zinc (4 μm)**

Figure 9. Cross-sectional FIB-SEM and surface FESEM images of the Mg (7.5 μm) and Zn (4 μm) films on bioresorbable PDTEC substrates.

In Publication II, Mg was e-beam evaporated onto PDTEC fibers, after which they were extrusion coated using PCL. Figure 10 illustrates a set of SEM images showing the structure of the wire. The Mg layer covered the grooves of the fiber evenly, but certain areas of the Mg layer had detached during the extrusion coating process. In these areas, the Mg layer was adhered onto the PCL coating.
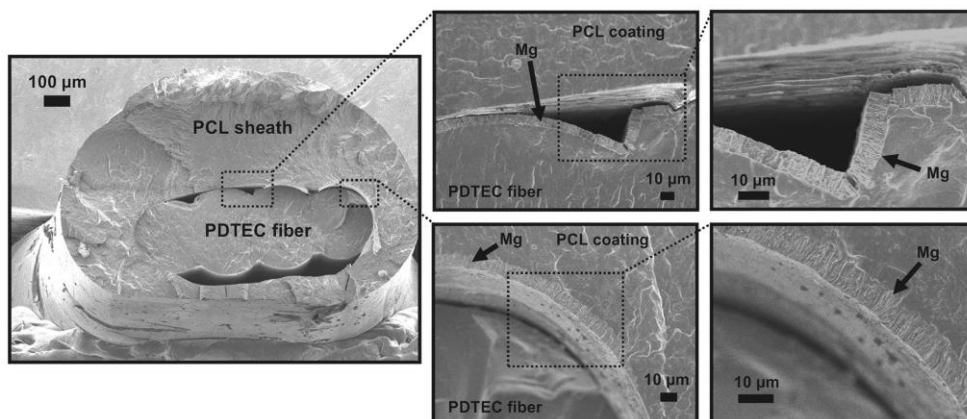

Figure 10. SEM images of the bioresorbable conductive wire showing the whole cross section as well as selected zoomed areas.

Comparing the electrical resistance of the metal films (Figure 11) on various substrates reveals that the conductive fibers had significantly higher resistances compared to Mg layers of similar thickness (7.5 μm) on glass. On the other hand, the 0.5 μm thick Cu layer on a PDTEC fiber was almost as conductive as a 7.5 μm Mg layer on a smooth glass surface. The 1.7 μm thick Zn and Mg films had comparable resistances of just over 1 Ω/cm. A thin Mg film of 0.5 μm on a PDTEC fiber had a resistance of 10 Ω/cm, which was about 10-fold larger compared to the 7.5 μm Mg layer on a similar fiber substrate. The mean bulk resistivity was estimated for the films deposited on glass; the respective values for the Zn (1.7 μm), thinner Mg (1.7 μm) and thicker Mg (7.5 μm) films were 180, 200 and 290 nΩ·m.
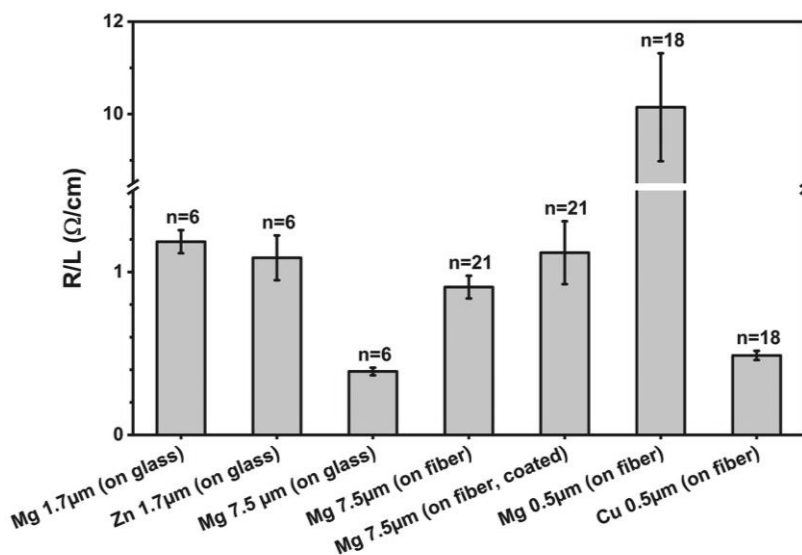
Figure 11. Comparison of the mean electrical resistance per conductor length (Ω/cm) of various conductors used in this study.

The bioresorbable conductive wires, whose metallized (7.5 μm Mg) inner fiber was protected with a PCL coating were submerged into Sörensen buffer solution at +37 °C (n=5), yet leaving the tips of the wires in air to ensure more reliable contact points. During the first immersion day, the mean resistance per length increased from 1.6 to 2.5 Ω/cm and remained at that level throughout the first 3 days (Figure 12a). An upward trend in the mean resistance was noticed between the 6-day and 9-day time points from 3.1 to 5.3 Ω/cm. After 10 days of immersion, two of the wires had lost their conductivity. The test was terminated after 14 days, at which time two of the wires were still conductive.

In addition to the samples with metal thicknesses ranging from 0.5 to 7.5 μm, the mean electrical resistance of a dry 200 μm thick Mo wire was evaluated at 0.024 Ω/cm in ambient conditions and 0.027 Ω/cm immediately after placing the wires (n=5) into Sörensen buffer. The degradation of the Mo wires under immersion proceeded slowly in a consistent manner, where the surface of the wires turned dark, then flaked away usually during the buffer solution change after every 4 weeks. This flaking revealed an Mo wire surface of the original color, which turned dark again under immersion and finally flaked. Despite this behavior, the electrical resistance showed negligible changes during the first 4 weeks of immersion, after which it was increased to around 0.04 Ω/cm. Significant resistance increases were seen after

10 weeks and the first two wires broke after 14 weeks of immersion. The last intact wire broke at the 16-week time point during the buffer change.
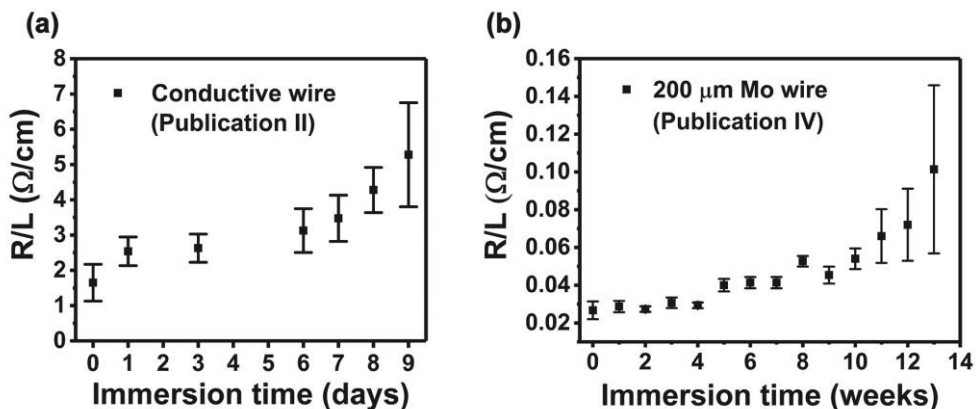

Figure 12. The changes in the mean electrical resistance per conductor length of (a) the conductive wire with 7.5 µm thick Mg on a PDTEC fiber, extrusion coated with PCL (Publication II) and (b) an uncoated Mo wire (200 µm; Publication IV). Both tests were performed in Sörensen buffer solution at +37 °C and the 0-day sample was measured immediately after the samples were partly immersed. The error bars denote standard deviations (n=5).

Comparing the corrosion rates of the 7.5 µm thick Mg films in different conditions (Figure 13) revealed that the 5 % CO_2 supply accelerated the degradation process significantly in di-H_2O. The Mg film was intact in ambient air after 24 hours, although black precipitates were seen at the surface. The dissolution was the quickest in Sörensen buffer, where only thin traces of the Mg film were left after 6 hours. Furthermore, the degradation appeared to proceed from the sides of the film towards the middle. The cell culture medium (Minimum Essential Medium supplemented with 10 % fetal bovine serum and 1 % Penicillin-Streptomycin) caused gas bubble formation immediately after immersing the Mg samples. The corrosion had clearly begun after 3 hours, which was noticed as dark precipitates on the surface. 24 hours of immersion in cell culture conditions resulted in clear pitting corrosion, but the Mg pattern was otherwise intact. After 3 days, only dark film precipitates were left. In conclusion, the corrosion behavior of Mg was evidently different depending on the environment.
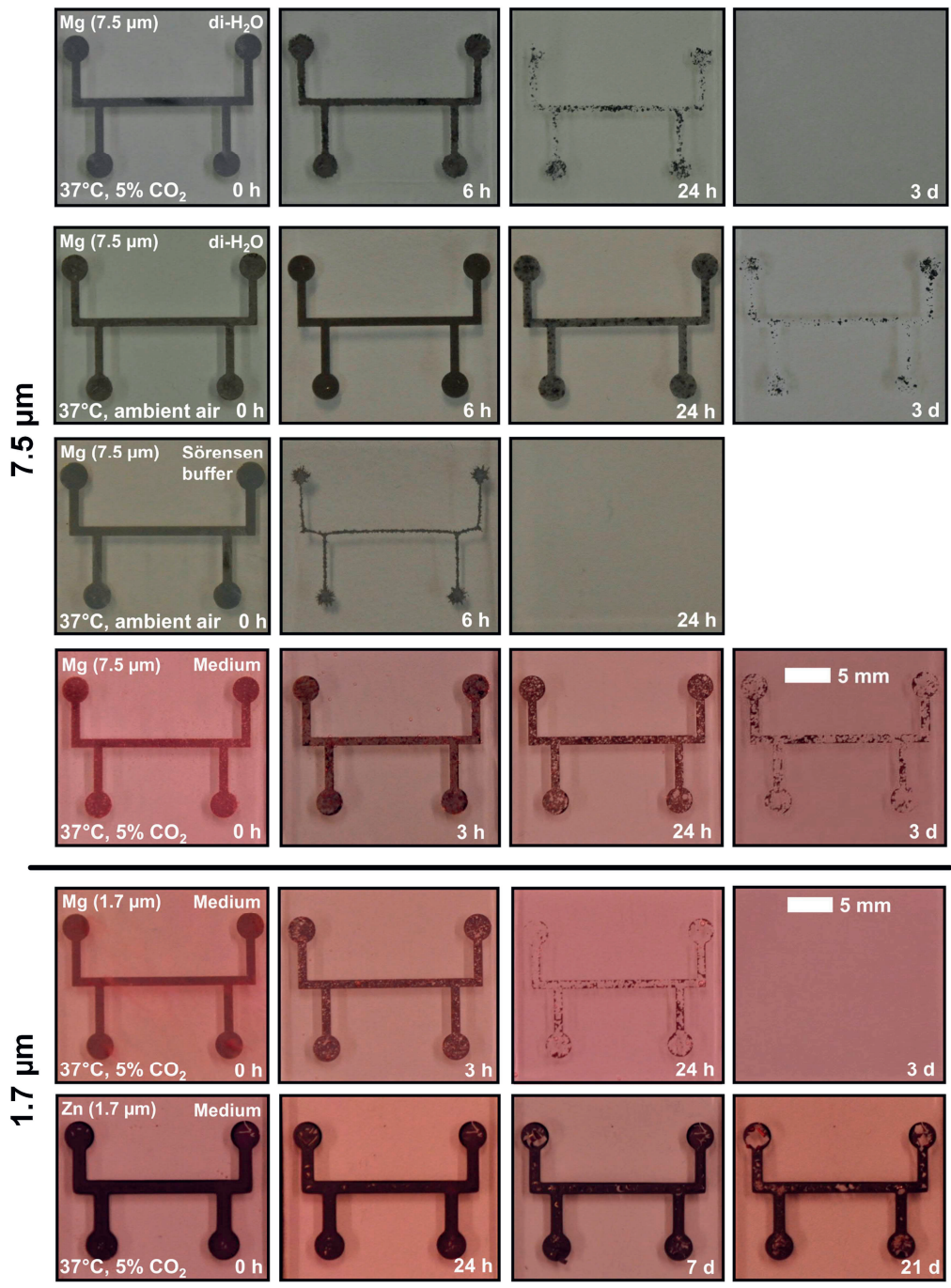
Figure 13. Optical images of 7.5 μm thick Mg films as well as 1.7 μm thick Mg and Zn films on glass substrates, showing their corrosion behavior in different conditions.

The corrosion behavior testing of 1.7 μm thick Mg and Zn films was performed in cell culture conditions, as suggested by Gonzalez et al. due to the appropriate HCO_3^-/CO_2 buffering system as well as adequate inorganic ingredients and organic components [141]. These thinner Mg films (1.7 μm) showed otherwise similar corrosion behavior as the thicker (7.5 μm) films, but the dissolution of the metal occurred faster as could be expected. After 24 hours, only black precipitates were left. The whole film was dissolved at 3 days. The Zn films on the other hand showed flaking after 24 hours, but most of the Zn remained even after 7 days. The Zn film showed significant deterioration at the 21-day time point. Nevertheless, most of the film had still not dissolved, demonstrating a significantly slower dissolution behavior than Mg.

The dissolution behavior of encapsulated Mg (7.5 μm) and Zn (~4 μm) conductor patterns as parts of immersed type 2 pressure sensors are shown in Publication IV (Figure S3, Supporting Information). Mg showed clear signs of corrosion after 2 weeks and the metallic appearance was lost after 3 months. Even after 1 year, white degradation products were found from inside the pressure sensor. In the case of Zn, the dissolution was clearly slower and there were metallic Zn remnants left inside the sensor after 1 year of immersion in Sörensen buffer.

5.2   Wireless inductor-capacitor resonator measurements

Different bioresorbable pressure sensors are presented in Figure 14 along with their resonance curves with increasing reading distance. Rescaled graphs of the *Re (Z)* spectra of type 2 Mg and Zn pressure sensors at higher reading distances are illustrated in Publication IV (Figure 4b and Figure 4d, respectively).

Both Mg-based sensor types showed a maximum reading distance of about 15 mm with only a slightly less attenuated resonance peak in the improved type 2 design (Publication IV). However, at smaller reading distances the height of the peak in these type 2 sensors was clearly larger compared to the type 1 sensor. The maximum reading distance of the Zn pressure sensors in air was approximately 10 mm.
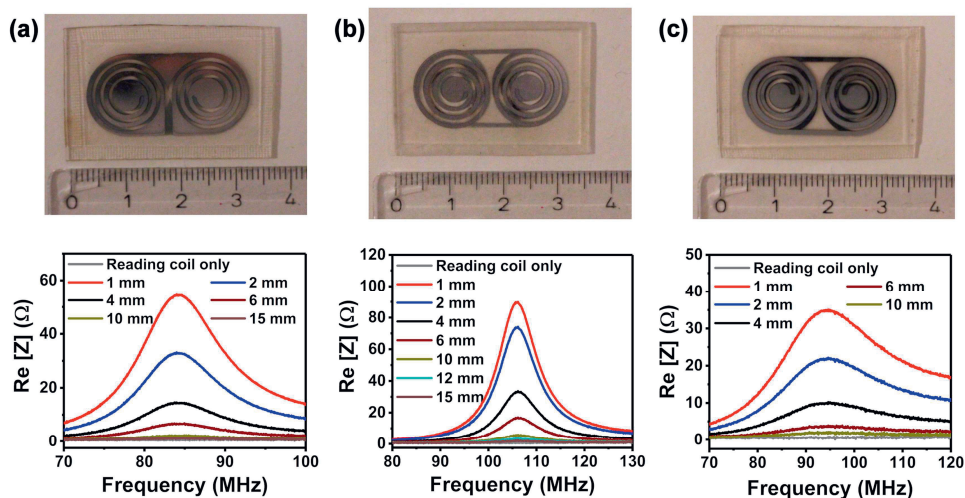
Figure 14. Photographs of various bioresorbable wireless pressure sensors and their measured real part of the impedance spectra with increasing reading distances. (a) Type 1 Mg pressure sensor (Publication III). (b) Type 2 Mg pressure sensor where the conductor patterns differ from the type 1 sensors (Publication IV). (c) Type 2 Zn pressure sensor (Publication IV).

The pressure sensitivities of the different pressure sensor samples are illustrated in Table 7. The pressure responses of the type 1 Mg sensors (n=8) are plotted in Publication III (Figure 1d) and those of the type 2 Mg and Zn sensors (n=3) in Publication IV (Figure 4a and Figure 4c). In addition, the static pressure response of type 1 sensors is presented in Publication III (Figure 2a-b).

Table 7. Pressure sensitivities and initial resonance frequencies (f_0) of the wireless pressure sensor samples

Sensor sample	Initial resonance frequency in air	Pressure sensitivity
Type 1 Mg sensor #1	91.50 MHz	-6.5 kHz/mmHg
Type 1 Mg sensor #2	81.85 MHz	-6.7 kHz/mmHg
Type 1 Mg sensor #3	83.98 MHz	-3.3 kHz/mmHg
Type 1 Mg sensor #4	76.96 MHz	-5.7 kHz/mmHg
Type 1 Mg sensor #5	89.04 MHz	-5.8 kHz/mmHg
Type 1 Mg sensor #6	94.20 MHz	-6.0 kHz/mmHg
Type 1 Mg sensor #7	92.28 MHz	-5.3 kHz/mmHg
Type 1 Mg sensor #8	84.49 MHz	-5.9 kHz/mmHg
Type 2 Mg sensor #1	106.57 MHz	-7.2 kHz/mmHg
Type 2 Mg sensor #2	99.57 MHz	-6.7 kHz/mmHg
Type 2 Mg sensor #3	98.67 MHz	-5.4 kHz/mmHg
Type 2 Zn sensor #1	84.58 MHz	-5.1 kHz/mmHg
Type 2 Zn sensor #2	95.79 MHz	-7.2 kHz/mmHg
Type 2 Zn sensor #3	88.32 MHz	-9.4 kHz/mmHg

The baseline resonance frequency (f_0) of the immersed Mg-based pressure sensors was noticed to change, as illustrated in Figure 15. The type 1 sensors showed fluctuating changes for the first 14-18 hours, after which the f_0 of all the three sensors started to rapidly increase. The immersion tests concerning type 1 sensors were terminated after 24 hours. The resonance frequency of both type 2 sensors was similar for the first 12 hours, during which it decreased about 2 MHz from the initial value. Also the type 2 sensors showed increasing $f_{max(Re)}$ values after about 14 hours, but the changes were not as steep compared to the type 1 sensors. In fact, the $f_{max(Re)}$ rise in the type 2 sensor #3 showed an increase of only about 2 MHz in MEM as compared to about 10 MHz regarding sensor #2 in Sörensen. After this, the sensor #3 in MEM showed a gently descending $f_{max(Re)}$ from day 1 to day 10, whereas the sensor #2 showed a steeper $f_{max(Re)}$ decrease between 48 and 96 hours. The tests for the type 2 Mg sensor samples #2 and #3 were terminated after 10 and 12 days (or 240 and 288 hours), respectively, due to the severe attenuation of the resonance peaks. The Zn sensors were not reliably readable in these simulated physiological conditions.
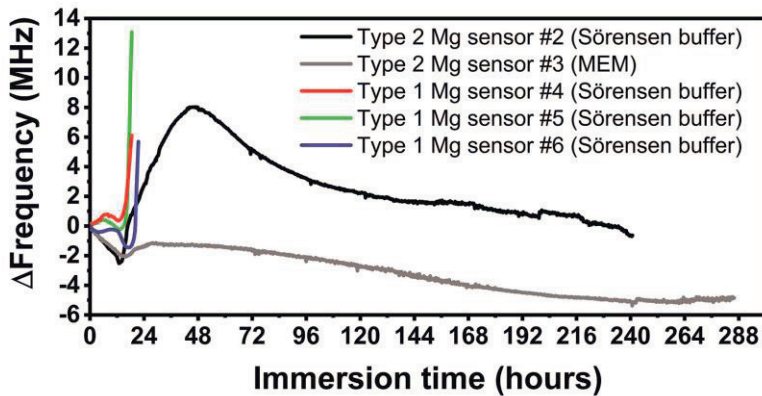
Figure 15. Drifting of the resonance frequencies of different pressure sensor samples under immersion without any applied pressure.

The dimensions of the pressure-sensing cavities in the type 1 sensors were evaluated before and after 24 hours of immersion using micro-CT. The micro-CT images (Figure 5 in Publication III) revealed that the capacitor plates were further apart from each other after immersion, which is in agreement with the data showing increased f_0 values. Moreover, the substrate was noticed to be partly detached from the spacer.

The photographs of the other LC resonators as well as their resonance peaks with different reading distances are shown in Figure 16. The f_0 of the coil that was fabricated from the bioresorbable wire was successfully approximated from up to 7 mm. The coil was seemingly sensitive to changes in the reading distance. The bioactive glass-based LC resonator, whose dimensions were comparable to the bioresorbable coil, showed a similar reading distance of 8 mm. Interestingly, the LC resonator made using Mo wire (200 μm) showed somewhat comparable resonance characteristics compared with a reference device made using commercial Cu wire (180 μm). The Mo wire-based resonance sensor was readable up to 17 mm, which includes the 5 mm thick polymer screw tip that is not taken into account in the distances given in Figure 16c. The non-degradable PCB based sensor showed the highest reading distance of up to 23 mm.
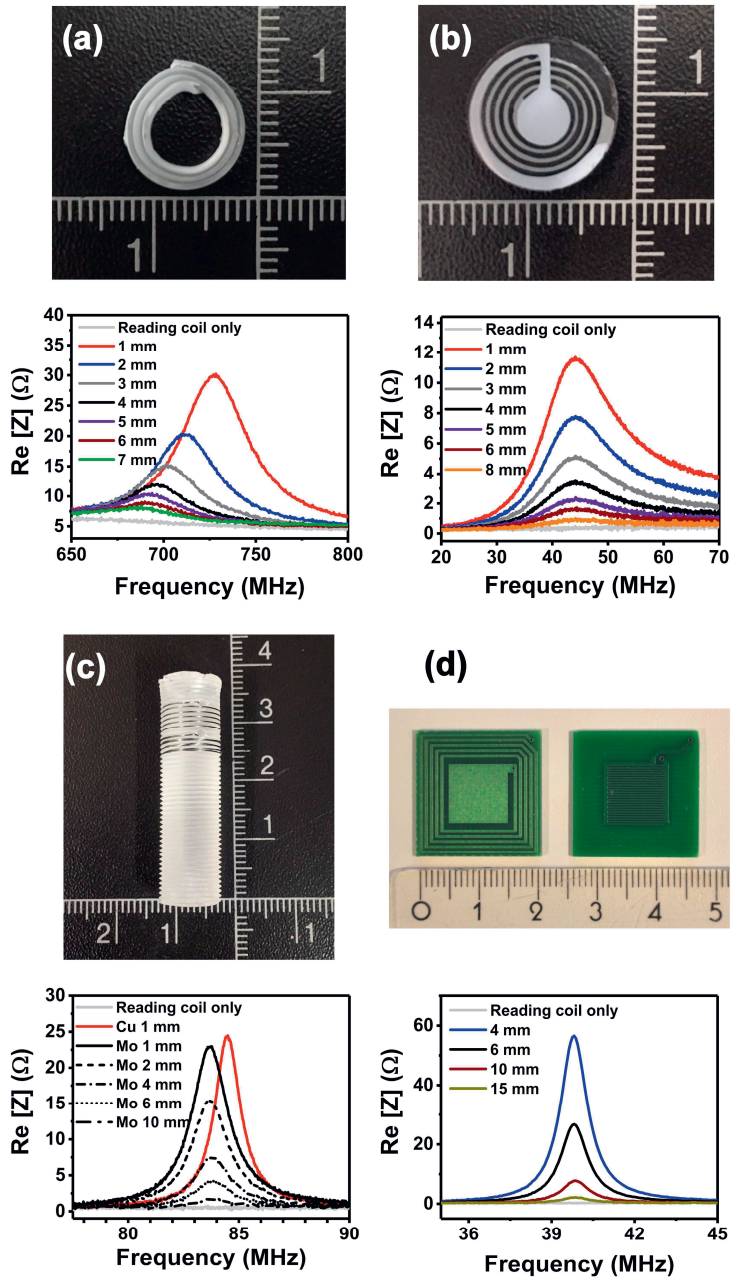
Figure 16. LC resonators and their measured real part of the impedance spectra with increasing reading distances. (a) Planar coil fabricated from a bioresorbable conductive wire (b) Bioactive glass-based LC resonator (c) Molybdenum wire-based resonator on a PLDLA 96:4 screw after compression (d) Non-degradable complex permittivity sensor.

The responses of the LC circuit-based sensors to different parameters of interest are summarized in Figure 17. By immersing a Parylene-protected bioactive glass-based LC circuit in di-H_2O and stepwise adding 9% NaCl solution, a non-linear decreasing resonance frequency was noticed along with an increasing ionic content (Figure 17a). Correspondingly, various media were distinguished from each other by measuring the response of the immersed sensor in different immersion environments (Figure 17b). The response of the Mo wire based solenoidal resonator to compression was tested in a vice jaw, showing an $f_{phase-dip}$ decrease of -0.8 MHz and a further change of -0.5 MHz upon 0.7 % and 1.4 % axial compression of the polymer screw, respectively (Figure 17c).
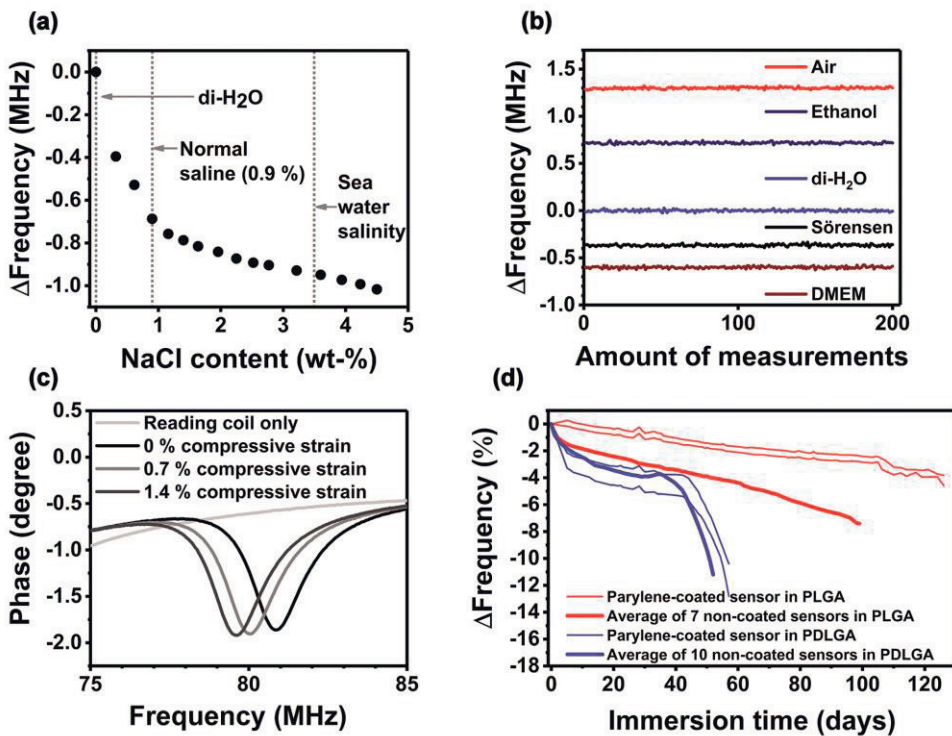
Figure 17. Responses of various LC resonator sensors on different measurands. (a) The bioactive glass-based LC circuit was Parylene-coated and immersed in di-H_2O, after which NaCl was added stepwise into the solution. (b) The same glass-based circuit was immersed in different solutions, which were detected based on the resonance frequency of the sensor. (c) The response of the compression sensor to various compressive strains. (d) The response of the non-degradable LC circuits (Publication I) onto the hydrolytic degradation of their polymer capsules.

The non-degradable sensors encapsulated in compression molded PLGA 80:20 and PDLGA 85:15 polymers showed decreasing resonance frequencies upon immersion of the samples. The resonance frequency of the sensors encapsulated in faster degrading PDLGA 85:15 decreased steeper during the first days of immersion, after which a more gently sloping period was noticed. Finally, around 40 days a steeper resonance frequency drop began and lasted until the end of the measurement period. The other Parylene-coated sensor showed a steeper resonance frequency drop during the first days, but otherwise their behavior was similar to the non-coated sensors embedded in PDLGA 85:15. In the case of PLGA 80:20 encapsulations, the resonance frequency of the Parylene-coated sensors decreased in a gentler manner compared to the non-coated sensors. After 100 days, a steeper f_0 drop was seen in both of the Parylene-coated sensors that were embedded into PLGA 80:20.

5.3   Possible error sources in implantable inductively coupled resonance sensors

Depending on the sensor environment, employed readout method and sensor architecture, inductively coupled resonance sensors may be subject to several error sources. One possible factor that may adversely affect sensor accuracy is an uncontrolled distance between the sensor and the reader coil [220]. Figure 18 illustrates the effect of changing reading distance on the f_0 of three different devices. The bioresorbable coil (Publication II) showed an f_0 decrease of approximately 40 MHz when the reading distance was increased from 1 to 7 mm, whereas the f_0 of the bioactive glass-based resonator decreased only about 150 kHz within the same distance range. However, the uncertainty in approximating the f_0 of the bioactive glass-based resonator increased distinctly along with the increasing reading distance. The type 1 Mg pressure sensor showed an initial f_0 decrease upon increasing reading distance, as measured in Publication III using Setup III. After 6 mm the sensor's f_0 values started to rise and this trend continued until the end of the measurement at 14 mm. In addition, the uncertainty in approximating the f_0 started to increase more clearly after 6 mm.
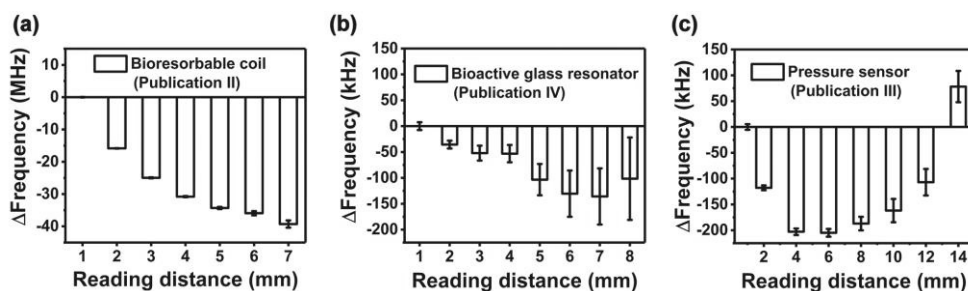
Figure 18. The effect of reading distance on the estimated resonance frequency of (a) the coil fabricated from the bioresorbable conductive wire (Publication II, n=10) (b) the bioactive glass-based resonator (Publication IV, n=100) and (c) the type 1 Mg pressure sensor (Publication III, n=100). Please note that this measurement data stems from the original Publication III and has been performed with a different reader coil (Setup III) compared to the bioresorbable coil and bioactive glass-based resonators (Setup II). In all graphs, the columns together with the error bars denote mean ± SD.

In addition to the vertical reading distance, the planar displacement between the resonator coil and the reader coil may also affect the resonance frequency. In this study, the f_0 of the bioresorbable Type 1 pressure sensor stayed within 50 kHz with displacements of 3 mm in either x- or y-direction, but a 5 mm displacement from the center of the reader coil results in a resonance frequency drift of more than 100 kHz (Figure S2a, Supporting Information in Publication III). The temperature response of an immersed PLGA 80:20 encapsulated non-degradable LC circuit was tested after 18 hours of immersion in order to allow the system to equilibrate. The temperature response of the system was nearly linear with an approximately 400 kHz f_0 decrease over the temperature increase from room temperature to 45 °C. The type 1 Mg pressure sensors showed non-linear temperature responses, where the f_0 values increased along with increasing temperatures. The total f_0 increase in the range from room temperature to 40 °C was about 400 kHz in two of the three tested sensors, whereas one of them was more sensitive to temperature with an about 800 kHz increase.
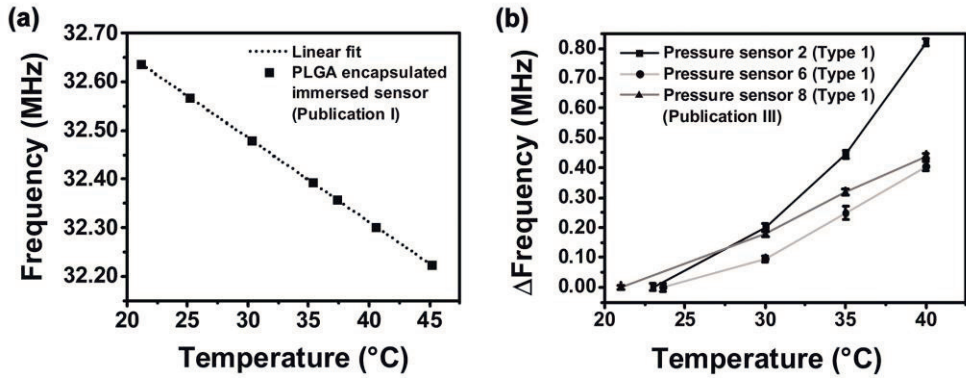
Figure 19. The temperature responses of (a) an immersed PLGA encapsulated non-degradable LC circuit (Publication I) and (b) a set of type 1 Mg pressure sensors in air (Publication III).

Changes in the complex permittivity of the sensor environment may cause changes in the capacitance of the sensor [26]. This can be used as a method for sensing changes in the immediate sensor environment but may also function as an undesirable error source. Figure 20a shows the measured real part of the impedance spectra of a type 1 Mg pressure sensor in air and in Sörensen buffer solution at +37 °C. Upon immersion into the buffer solution, the resonance peak shifted towards lower frequencies and attenuated compared to the measurement performed in air.
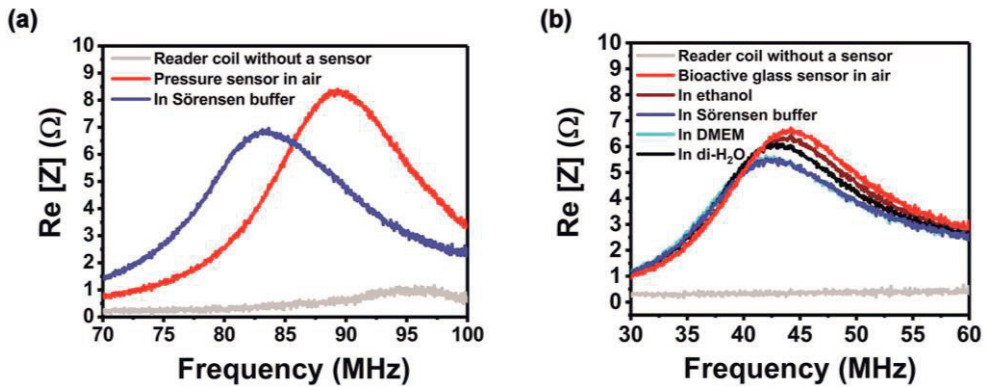
Figure 20. The effect of the surrounding media on the measured real part of the impedance spectra. (a) The wireless pressure sensor (Publication III) measured in air and in pre-warmed (+37 °C) buffer solution through a glass bottle with a reading distance of approximately 6 mm (b) The bioactive glass resonator, measured through a Petri dish with a reading distance of approximately 1 mm (Publication IV).

The Parylene-coated bioactive glass-based LC resonator showed the highest resonance peak in air (Figure 20b). The f_0 of the sensor decreased upon immersion into ethanol and even more in di-H_2O. Still, the lowest f_0 values and the most attenuated resonance peaks were found upon immersion in Sörensen buffer and DMEM. The relative differences in the estimated f_0 of this bioactive glass-based resonator in different conditions were earlier presented in Figure 17b. In addition, similar bioactive glass-based resonance sensors were demonstrated to distinguish different NaCl concentrations from their surroundings when embedded into di-H_2O, as presented earlier in Figure 17a.

6   DISCUSSION

6.1   Fabrication of inductor-capacitor resonators

Printed circuit boards (PCBs) are used to mechanically support and electrically connect electronic components in various commercial electronic devices. Conventional rigid PCBs typically consist of an organic resin like epoxy or polyimide, reinforced with around 50-70 % of woven glass fiber. Cu sheets etched through photoresist masks usually define the conductor patterns. [125], [205], [221] In this thesis, commercially manufactured PCB-based resonance sensors (Publication I) were first tested as a proof-of-concept for wirelessly monitoring the degradation of bioresorbable polymers. The multilayer structure included an inductor coil, interdigitated and parallel-plate capacitors, as well as via through holes. This sensor architecture gives an idea about the structural features that can be fabricated in large quantities using conventional materials. It can thus be used as a comparison reference for bioresorbable devices.

The first step towards fabricating an LC circuit using bioresorbable materials was a conductor wire (Publication II), which was used to form planar coils. In fact, the coils themselves can be considered as resonators whose capacitance consists of parasitic capacitances between the coil turns. This kind of coils can be used for example as sensors [21], [222] or as wirelessly powered microheaters if a meander resistor is connected to the coil [146]. More sensing options can be achieved by pairing two coils with a dielectric layer in between [223]–[225]. PDTEC was chosen as the core fiber material due to its thermal properties (T_g = 99 °C) that enable melting the PCL (T_m = 57 °C) coating onto the core fiber without severely damaging it. It was shown that the evaporated Mg layer on the core fiber remained almost as conductive after the PCL melting process than before, which was a crucial advancement towards realizing a bioresorbable wireless pressure sensor.

The wireless pressure sensors (Publications III and IV) consisted of two similar metallized PDTEC substrates that were attached onto a holed spacer using PCL films as an adhesive. The substrates were melt processed to enable better control over the substrate thickness and surface roughness, as compared to solvent casting which has been commonly used for preparing bioresorbable substrates for electronic

devices [73], [199], [226], [227]. The patterning of the e-beam evaporated Mg (7.0-7.5 μm) or magnetron sputtered Zn (~4 μm) conductors was based on an earlier work by Salpavaara et al. [104]. In the type 2 pressure sensors, laser-cut metal masks replaced the 3D printed plastic masks to prevent sputtered Zn from permeating under the mask. This kind of blurring has been described earlier as a result of non-directional sputtering deposition and may lead to short-circuits if the shadow masks are not in good contact with the substrate [228].

The operation of the pressure sensors was based on bending of the substrates towards each other in the holes of the spacers as pressure was applied. This brought the metallized capacitor plates closer to each other, which changed the capacitance of the LC circuit and thereby the resonance frequency of the device. We showed that with one exception, the sensor sensitivities and initial resonance frequencies between different sensors (n=8) were consistent, even with a manual fabrication process.

The sensor architecture was designed to avoid through hole vias or other galvanic contacts between the conductor layers. This was the main advantage of the presented pressure sensors, along with the possibility to construct the sensors from two identical metallized substrates. In the literature, Luo et al. avoided the challenge of fabricating through hole vias by folding a single substrate that contained an electrical interconnect between the inductor coil and the upper capacitor plate [73], [74]. Boutry et al. used microstructured PGS pyramids between the pressure-sensitive capacitor plates to shorten the response time of their sensor [76]. Furthermore, their inductor coils were laminated on a dielectric PLLA film (50 μm) to separate them from the region of pressure-sensitive capacitors.

The main goal in all the reported sensor architectures was to keep their complexity and the required processing steps as low as possible. During this thesis, another pressure sensor architecture was also tested, where Mg was deposited directly onto a dielectric PCL layer. The pressure-responsive capacitor was created by hot embossing a round cavity onto the upper PDTEC substrate (or lid) and evaporating Mg onto the bottom of this cavity [37]. These endeavors were abandoned due to more complex fabrication procedures and poorer sensor performance compared to the presented sensors.

To summarize the position of our bioresorbable pressure sensors with respect to existing literature, it needs to be first emphasized that the used materials, fabrication methods and sensor architectures vary significantly between different studies. Direct comparison is therefore difficult. In this study, the simple Mg pressure sensor architecture with two similar metallized substrates required only two different, easy-to-manufacture components (holed multilayer spacer and metallized polymer

substrates). The resulting simple assembly process is the main asset of our pressure sensors compared to other reported bioresorbable wireless pressure sensors. In this study, the multilayer spacer was manually assembled from compression molded polymer sheets, but on a commercial scale it could be extruded as a continuous multilayer sheet and then cut into shape. Other bioresorbable pressure sensors in the literature include transfer printing of electrodeposited conductors and folding a single substrate to provide galvanic connections between the two layers [73], [74], or stacking numerous layers of different materials [76], [229].

Bioactive glasses are under-represented as substrate materials for biodegradable electronics and contain a lot of potential for photolithographic methods and other post-processing methods that are being used with conventional non-degradable wafers. Previous studies have evaluated borate-based glasses as sensor substrates, demonstrating their fast dissolution profile with mass loss measurements and wired electrical measurements of prototype devices [115], [116]. In this study, S53P4 (Bonalive®) bioactive glass discs were introduced as substrates that have a better chemical and thermal resistance compared to typical biodegradable polymers. S53P4 is a silicate based bioactive glass composition, which has been commercially used as a synthetic bone graft material in orthopedic surgery [60]. The discs used in this study enabled spin coating an insulating PDTEC layer onto a metallized Mg layer, which was used to demonstrate its chemical resistance. Another option would be to sputter deposit or evaporate dielectric layers (e.g. SiO_2) onto the glass, as done by Unda et al. [115]. This kind of inorganic dielectric layers would be thermally more resistant compared to their polymeric counterparts, which should enable depositing an inorganic water barrier layer onto the final resonator structure. In this study, the highly water-sensitive Mg conductors on the insulating PDTEC layer were protected with non-degradable Parylene to enable studying the sensors under immersion. As a conclusion, the robust glass substrates allowed fabricating the resonator structure step by step without damaging the underlying layers.

The compression sensors (Publication IV) were prepared onto PLDLA 96:4 screws using Parylene-insulated Mo wire to demonstrate a scheme for fabricating solenoidal resonator structures. Although the Parylene coating was not biodegradable, similar chemical vapor deposition methods have been recently developed for biodegradable polymers as well [198]. Extrusion coating the Mo wire could provide a further option. Karipott et al. have earlier reported an approach, where a non-degradable temperature sensor has been mounted into a hollow orthopedic screw [39]. This kind of modular approach could be beneficial in terms

of device assembly, if the sensor part could be fabricated separately and then installed into e.g. an injection molded screw.

6.2 Characteristics of the bioresorbable materials

This chapter discusses the materials used in this thesis. Especially materials processing as well as degradation behavior, such as the water uptake properties of polymers or corrosion of biodegradable metal conductors are addressed. The effect of these material properties on the performance of LC resonators is discussed later in chapter 6.3.

6.2.1 Processing and properties of biodegradable polymers

Biodegradable polymers are known to be more prone to thermal degradation during melt processing than conventional commodity polymers [230]. In the case of lactide-based copolymers, the presence of moisture, residual monomers, oligomers and especially catalytic metal components are known to cause increased thermal degradation [231]. In this study, the inherent viscosity measurements revealed polymer chain cleavage during processing in all the tested polymers. Compared to the raw materials, the *i.v.* of the compression molded PDLGA 85:15 and PLGA 80:20 decreased 53 % and 19 %, respectively, and that of the extruded PDTEC 33 %. These results are in line with an earlier study on PLGA 85:15, where extruded fibers showed relative *i.v.* decreases from 29 % to 56 % compared to the raw material [232]. Because the decreased molecular weight and thermally generated monomers undermine the mechanical properties and may accelerate polymer degradation, mitigating thermal degradation is often desired. This can be done by drying the raw materials carefully prior to processing, using nitrogen atmosphere and low processing temperatures.

After immersing the biodegradable polymers in buffer solution, water starts to diffuse into the polymer matrix. This diffused water is highly significant in bioresorbable electronic applications, as it may plasticize the polymeric substrates [233], contribute to their dimensional changes like swelling [182] and corrode polymer-encapsulated bioresorbable conductor metals. The effect of diffused water on the performance of bioresorbable devices is addressed in chapter 6.3 in detail.

The water uptake of PLGA 80:20 (1.0 wt-%) and PDLGA 85:15 (1.7 wt-%) after 2 weeks of immersion were in agreement with the literature stating about 1 wt-% water uptake for polyesters [64]. The slightly higher amount of diffused water in PDLGA samples was likely caused by polymer degradation, which was evident visually and in the *i.v.* measurements already at 2 weeks [234].

The equilibrium water uptake of PDTEC (~3 wt-%) was reached after a few days of immersion and remained at the same level throughout the 100 days test period, which is in agreement with an earlier report, which estimated that the total bioresorption of PDTEC might take up to 4 years [86]. The unchanged water uptake indicates that no water-soluble degradation products have been formed during the 100 days period, because the ester bonds in the pendent chain are hydrolyzed much slower compared to the backbone carbonate bonds. The water absorption into the PCL matrix was only 0.35 wt-%, probably due to its high degree of crystallinity [235].

The changes in the mechanical properties of the substrates might need to be considered in some applications. For example, Luo et al. explained the small sensitivity change between their immersed and non-immersed pressure sensor with the plasticizing effect of the buffer solution on the polymer substrate [73]. Furthermore, Kang et al. tested surface eroding polyanhydride substrates in a pressure sensor and concluded that a small loss of accuracy was caused by the eroding substrate material over several days [79]. Nevertheless, in their sensor architecture, the error was within the standards of the Association for the Advancement of Medical Instrumentation (AAMI) for pressure monitoring.

The substrate materials used in biodegradable electronic devices have often involved polymers of lactide or lactide-glycolide based copolymers [20], [73], [74], [79]. On the other hand, biodegradable elastomers have also been considered in applications where their flexibility and fast recovery from under stress are appreciated [75], [101]. In this study, PLGA and PDLGA possessed similar mean flexural moduli (3.4 GPa) in ambient conditions, whereas PDTEC (2.8 GPa) was slightly softer. When tested at +37 °C under immersion in Sörensen buffer, the moduli of the PDTEC samples remained within the standard deviation of the samples measured in ambient conditions, although a slightly increasing trend was noticed during the first week. For comparison, the flexural modulus of faster degrading PDLGA dropped from 3.4 to 2.2 GPa during two weeks of immersion.

The substrate material is typically in contact with the surrounding tissues and should therefore be biocompatible. Copolymers of lactide and glycolide have been successfully used in clinical applications for decades [69]. PDTEC on the other hand is less studied due to its slow degradation rate [86]. Earlier results have shown that

the response of rat lung fibroblasts on PDTEC was comparable to glass and hydrophilic modified polystyrene [82]. In addition, only modest foreign body reactions were noticed during the 52-week test periods when PDTEC membranes were implanted into the mandibular angles and subcutaneous pouches of rabbits [89], [90]. In this study, the in vitro cell response of human foreskin fibroblasts to PDTEC discs was at least comparable, if not superior to the PLDLA 96:4 discs and polystyrene well plates. This gives further evidence to the good biocompatibility of PDTEC.

To conclude this chapter, the processing method has an effect on the material properties and should be therefore carefully chosen. In addition, the properties of bioresorbable polymers change dynamically during exposure to physiological conditions. These dynamic changes may contribute to the device performance, as discussed in more detail in chapter 6.3. Finally, the biocompatibility of the substrates should be acknowledged. This is especially important in cases where novel materials are used.

6.2.2 Processing, electrical properties and corrosion of biodegradable metal conductors

Choosing the right conductor material and fabrication technique are among the most important decisions when designing bioresorbable LC resonators. Firstly, the electrical conductivity of the material should be high in order to obtain high Q-factor resonators [21]. Secondly, the corrosion behavior of the conductors may have an influence on the functional lifetime and performance of the device as well as on its biocompatibility. The AC resistance of the conductors can be decreased to some extent by increasing their cross-sectional area, typically by preparing thicker conductor films. However, in practical RF applications, the effective maximum thickness is limited by the skin effect [236], which might pose constraints for the conductor design and fabrication.

Bulk Mg has a lower electrical resistivity (4.3×10^{-8} $\Omega \cdot$m) compared to other biodegradable metals like Zn, Mo or Fe. Mg has thus been considered as the most promising conductor material for LC resonators [139]. Therefore, it was chosen as the primary conductor material in this thesis as well. For comparison, conventional conductor metals like Cu (1.7×10^{-8} $\Omega \cdot$m) or Ag (1.6×10^{-8} $\Omega \cdot$m) show much lower resistivities [135].

E-beam evaporation was chosen as the fabrication method to enable depositing films directly onto the bioresorbable substrates. Several reports have described evaporated Mg films with thicknesses up to a few micrometers [146], [199], [237]. The maximum Mg thickness that could be conveniently evaporated with our equipment was about 7.5 μm. Significantly thicker patterned Mg conductors have been formed by electroplating, as well as by patterning Mg foils with laser cutting or wet etching processes [76], [148], [209]. These methods typically require transfer printing, but on the other hand enable thicknesses of several tens of micrometers or even higher, as well as photolithography-based patterning. Still, as the skin depth of bulk Mg at 100 MHz is around 10 μm, conductors much thicker than 50 μm do not significantly increase the Q-factor of the resonator at this frequency. This approximation is based on the rule-of-thumb, according to which the conductor thicknesses of up to 4-5 times the skin depth are reasonable in high frequency applications [238].

Sputtered Zn was tested in Publication IV as an alternative for Mg. Sputtering was chosen due to the high vapor pressure of evaporated Zn, which easily leads to wall deposits that may spoil the vacuum system [201]. 4 μm thick Zn layers were achieved on PDTEC substrates at most, because an extended sputtering time was noticed to damage the PDTEC substrates due to excessive heating. By contrast, no adverse changes were noticed in the Mg evaporation process even with PLDLA 96:4 (T_g = 61 °C) substrates.

Comparing the cross-sectional FIBSEM images of the metal films illustrates the columnar structure of Mg in contrast to the denser Zn films. This could explain why the Zn films (1.7 μm) showed similar if not lower electrical resistivity compared to their Mg counterparts. Correspondingly, e-beam evaporated large-area Mo films (~1 μm) have been earlier reported to have higher electrical resistivity than their DC sputtered counterparts [172]. The Mo surface morphology was not dependent on the deposition technique. Correspondingly, recently reported DC magnetron sputtered Mg films (2 μm) were noticed to possess similar tabular Mg crystallites [239] than on the top surface of our e-beam evaporated Mg films. Ion beam sputtered Zn films have showed increasing particle sizes on the film surface along with increasing ion beam energies; the highest beam energy (16 keV) yielded films with a particle size 0.7-1 μm [240]. This film morphology appeared similar to that of the sputtered Zn films in this study.

Increasing the thickness of the Mg films from 1.7 μm to 7.5 μm increased the respective mean bulk resistivity estimates from about 200 to 290 nΩ·m, compared to bulk Mg with 43 nΩ·m. This indicates that the thicker films would be of inferior

quality than the thinner films. As a further comparison, 2 μm thick thermally evaporated Mg films (~100 nΩ·m) have been reported earlier on float glass substrates [146]. The estimated mean bulk resistivity of the Zn films was about 180 nΩ·m, as opposed to the literature value of bulk Zn with 59 nΩ·m. Therefore, it appears that in this study the microstructure of the films dominated the intrinsic electrical properties of Mg and Zn. This indicates that the electrical resistivity literature values of bulk metals should not be used as a basis when choosing thin film conductor materials for LC resonators. Due to this reason, the mindset of choosing Mg as the primary conductor material deserves to be challenged. On the other hand, the recently utilized top-down practice of patterning commercial metal foils could provide lower resistivity values compared to evaporated or sputtered thin films [9], [76], [171]. In any case, approximating and reporting the bulk resistivity of the conductor films would be recommended to compare different conductor materials between studies.

Molybdenum offers a slow degrading conductor option for bioresorbable electronic devices [126]. Mo wires have been used for example in energy transmission in bioresorbable devices [79], [148]. The studies have shown negligible changes in the electrical resistance of Mo wires (10 μm) for over one week of immersion in artificial cerebrospinal fluid and bovine serum at physiological temperatures, whereas thicker Mg wires (50 μm) started to show rapidly increasing resistances around one week. In this thesis, no significant resistance changes were seen in the partly immersed unprotected Mo wires (200 μm) during the first 4 weeks in Sörensen buffer solution. Lee at al. used 5 μm thick Mo foil in their inductively coupled drug delivery device and reported that the foil degraded within 6-8 months in PBS at +37 °C [171]. These results encourage further testing of Mo conductors in biodegradable electronics.

The metallized PDTEC fibers (Publication II) were proposed as a bioresorbable conductor wire for applications, where only a minimal amount of biodegradable metals would be desired. An only 0.5 μm thick Cu layer on the PDTEC fiber was noticed to result in a lower resistance compared to 7.5 μm of Mg. This is a harsh practical example of the differences between conventional conductor materials and biodegradable metals, even though in this example, the differences in the evaporation process may partly explain the result.

Immersing the central parts of the extrusion coated Mg based wires in Sörensen buffer was noticed to increase the resistance of the wires already after 1 day, but all the five tested wires were still conductive after 9 days. This result gave a reason to believe that evaporated Mg films encapsulated inside protective bioresorbable

polymer layers might be used in LC resonator structures with functional lifetimes of more than 1 week despite the extremely fast corrosion rate of unprotected Mg.

The corrosion testing environments in the literature are diverse to say the least, for why they need to be critically examined in this thesis as well. In addition to varying corrosion environments, most of the literature addresses bulk metals, which may have different properties compared to thin films that are often used in bioresorbable electronics. For example, Tsang et al. noticed that their electroplated Mg conductors were less resistant to corrosion compared to commercial Mg foil [147].

The physiological environment is extremely complex with a wide variety of parameters that have an effect on the corrosion of these metals [241], [242]. Realistic in vitro corrosion testing of biodegradable metals has been therefore proven difficult. Gonzalez et al. have suggested using cell culture medium supplemented with FBS at +37 °C with 5 % CO_2 supply for in vitro testing of Mg corrosion behavior. However, SBF or Earle's Balanced Salt Solution (EBSS) with a CO_2/HCO_3^- buffering system could be used for material screening purposes [141]. The authors suggest that a suitable simulated solution contains the appropriate organic and inorganic ingredients combined with a CO_2/HCO_3^- buffering system instead of e.g. Tris. Furthermore, they refer to tests performed in saline as far off or even contradictory with in vivo results. Correspondingly to Mg, in vitro corrosion of Zn has been shown to be dependent on the corrosive fluid, where whole blood or plasma was suggested for short term testing and Ringer's solution over PBS for longer term studies [164].

In this study, the effect of the testing environment on thin metal films was demonstrated by immersing unprotected Mg films (7.5 μm) in different conditions. The appearance of the samples in di-H_2O, Sörensen buffer and cell culture medium indicated that Mg may have corroded via different mechanisms depending on the environment. Adding 5 % CO_2 into the testing atmosphere accelerated the corrosion of di-H_2O immersed samples significantly; the corrosion of the films seemed to be at the same stage at 1-day and 3-day time points depending if CO_2 supply was used or not, respectively. This was probably caused by diffusion of CO_2 into the water, which formed carbonic acid (H_2CO_3) and lowered the pH of the solution, thus promoting Mg dissolution [243]. This kind of pH decrease between 6 and 12 hours has been reported in the presence of CO_2, indicating that di-H_2O acquires some buffering capacity in such conditions [244]. A 5 % CO_2 supply has been also reported to strongly influence the degradation of an Fe alloy [245].

The recommended conditions with cell culture media lead to slower corrosion compared to Sörensen buffer. The presence of Cl^- ions in cell culture media should accelerate Mg corrosion by destabilizing the protective $Mg(OH)_2$ layer and exposing more metallic Mg. On the other hand, the lack of Cl^- might explain why the corrosion of Mg films in Sörensen buffer proceeded from the edges of the films instead of pitting corrosion, which occurred in cell culture conditions. High phosphate ion ($H_2PO_4^-$ and HPO_4^{2-}) levels in Sörensen could be expected to retard Mg corrosion by promoting a magnesium phosphate precipitation layer on the sample surface, whereas the role of highly soluble Na^+ and K^+ ions has been considered small in the literature. The presence of proteins in cell culture media is known to affect both the corrosion rate and the degradation products, although the mechanism is still unclear. Proteins have been reported to form a corrosion-inhibiting layer, but there are also results indicating they could act as corrosion promoters. [141], [142], [243], [244], [246], [247]

The addressed factors encompass only some of the possible parameters that may affect the corrosion outcome, but the slower degradation rate in cell culture media could be mostly attributed to the adsorbed proteins on the Mg surface and the different buffering system. However, using cell culture media and CO_2 supply complicates the test setup and increases the risk for bacterial contaminations, due to which measurements where the Mg layers were encapsulated within polymer substrates may be performed in simpler solutions like Sörensen buffer or PBS. When testing immersed LC resonators, di-H_2O should be only accepted with good reasoning as it does not cause similar dielectric losses compared to conductive buffer solutions [26].

The degradation of Mg is known to occur much faster compared to Zn, Fe or Mo [126], which can be considered as an advantage in applications where fast material clearance from the body is desired. The respective dissolution rates for bulk Mg and Zn samples in SBF (pH 7) have been estimated at 220 μm and 50 μm per year, or about 0.60 μm and 0.14 μm per day [161]. Our Zn films (1.7 μm) corroded slower than this in cell culture conditions, as significant proportions of the films remained after 21 days. On the contrary, only remnants of our Mg films (1.7 μm) were left after 24 hours of immersion, which indicates faster degradation compared to the referenced study. These comparisons illustrate the effect of the whole test system and the differences are most likely an interplay between the microstructure of the metal and its environment. For example, the observed sparse structure of the Mg films probably contributed to its fast dissolution.

6.3 The effect of bioresorbable materials in the performance of implantable wireless sensors

The operating environment is one of the main differences that separates implantable electronics from consumer electronics. One of the main hurdles that need to be overcome before clinical application of bioresorbable sensors is to achieve stable operation throughout their intended lifetime, considering that the materials start to degrade upon implantation. This is far from a trivial obstacle, as water absorption into the sensors is considered a challenge even with non-degradable materials. Another important feature limiting potential indications is the reading distance (or interrogation distance) of the sensor. [4], [5], [21] In this chapter, these themes are discussed from the materials perspective. In addition, the most common error sources for passive resonance sensors are briefly addressed.

The reading distance of inductively coupled passive resonance sensors is dependent on several parameters, including the geometry of the sensor coil and the reader coil. In general, a larger coil enables longer reading distances. This thesis focuses on the material perspective, where decreasing the resistance of the conductors is the key procedure for enhancing the reading distance. [18], [21] Unless otherwise stated, all the reading distance tests in this thesis were made using the same rectangular double-turn reader coil with a diameter of about 20 mm.

The non-degradable PCB based LC circuit with Cu conductors (35 µm) provided a reference point for the bioresorbable wireless sensors with a reading distance of about 23 mm. The skin depth of Cu at 35 MHz is 11 µm, which means that increasing the thickness of the conductors much further would have had only a limited effect on the effective RF resistance of the LC circuit. For comparison, Chen et al. have reached a reading distance of 15 mm in air with miniaturized 4 × 4 mm² sensors based on Cu conductors [248]. The intraocular pressure sensor described by Collins in 1967 achieved reading distances of about 30 mm [223]. These examples are in line with the statement of Boutry et al., indicating that inductively coupled LC circuits are not sufficient for distances above several centimeters, and alternative approaches may thus need to be sought for deep-tissue applications [76].

The literature concerning the reading distances of bioresorbable LC circuit-based sensors is scarce. Luo et al. tested their biodegradable pressure sensor from a distance of 3 mm [73], but no results using longer distances were reported. The resonance frequency of the type 2 Mg pressure sensors reported in this thesis was identified from a maximum distance of 15 mm, whereas the corresponding distance for the Zn pressure sensors was 10 mm. The differences in the sensor characteristics were likely

caused by different conductor thicknesses (Mg 7-7.5 μm, Zn 4 μm) that lead to lower resistances in the thicker Mg conductors.

Higher quality resonators can be formed by increasing the conductor thickness [199], as long as the skin effect is taken into account. However, the thicker evaporated Mg films (7.5 μm) in this study were noticed be of inferior quality compared to the thinner films (1.7 μm), as indicated by the higher estimated bulk resistivity of the thicker films. Our secondary pressure sensor architecture [37] was noticed to be readable at 6 mm, which was close to its maximum reading distance. A similar sensor architecture was recently published by Lu et al., where the Mg coil was laser-cut from a Mg foil (100 μm), leading to vertical operating ranges of 6 mm, 12 mm and 22 mm, depending if the coil diameter was 8 mm, 12 mm or 16 mm, respectively [9]. Although the sensor architectures between these studies were not identical, this practical example shows that patterning thick Mg foils by etching or laser cutting is a useful fabrication method for increasing the reading distance of the device. The disadvantage of this strategy is that it typically requires transfer printing of the conductors onto a bioresorbable substrate, which might be a challenge for example with glass substrates.

The bioactive glass-based LC circuit (Ø = 14 mm) was detected from a distance of 8 mm, which is explained by its smaller dimensions compared to the pressure sensors. The planar coils (Publication II) with a similar diameter were readable at 7 mm. The compression sensor (Ø = 10 mm) fabricated using an insulated Mo wire (200 μm) provided an example, where the conductor thickness was about 5 times its skin depth (41 μm at 80 MHz). This enabled comparable reading distances to the larger Mg based pressure sensors (25 × 35 mm²).

Immersing bioresorbable LC resonators into simulated physiological conditions affects their performance in a multitude of ways. Firstly, the immediate environment of the sensor has an effect on the capacitance of the system [18], which was noticed as a drop in the resonance frequency of all the immersed sensors in this study. Secondly, the dielectric losses of conductive buffer solutions are known to increase the width of the resonance curve (or decrease the quality factor of the sensor), thus decreasing the accuracy of the resonance frequency estimates [26], [73]. For example, such dielectric losses were detrimental for the immersed Zn based pressure sensors. On the other hand, both the increasing width of the resonance curve and a diminishing Q-factor can be used to intentionally monitor the environment of the sensor [21], [56], [249].

After immersion, water starts to diffuse into bulk eroding polymers. This may contribute to the dynamic changes in the baseline resonancy frequency of the

immersed sensors. In the beginning, it may be noticed as an increasing capacitance (or decreasing resonance frequency), as noticed in the case of the non-degradable sensors that were encapsulated into bioresorbable polymers (Publication I). Similar effect was seen in the Mg pressure sensors, except for type 1 Mg sensors #4 and #5. The initial increasing resonance frequency in these devices may have been caused by the temperature sensitivity of the pressure sensors combined with the temperature overshooting of the oven (after closing the door) that was used for testing the type 1 sensors. On the other hand, this kind of initial increase and subsequent decrease in f_0 was also reported by Luo et al. in saline at room temperature [73], whereas their faster degrading pressure sensor showed decreasing resonance frequency for the first 1.5 hours at +37 °C [74].

After diffusing into the substrate, water reaches the interior of the sensor. At worst, this may lead to an untimely device failure, most often caused by dissolution of conductors, their fracture, or disintegration of the device structure [20], [50], [182]. In this study, the wireless type 1 Mg pressure sensors were intact for less than 24 hours (Publication III), but type 2 Mg pressure sensors thicker adhesive PCL layers were wirelessly readable and pressure-responsive for up to 10 days in Sörensen buffer solution (Publication IV). However, the baseline resonance frequency (f_0) of the immersed type 2 pressure sensors drifted during the whole measurement period both in Sörensen and in MEM. The drifting was probably an interplay between many factors like diffused water, H_2 evolution as a side product of Mg corrosion which may have led to dimensional changes in the substrates, decreasing resistance of the conductors, as well as possible delamination of the adhesive layers from the substrates. In general, the corrosion of the conductors leads to an increasing electrical resistance in the LC circuit, which may be seen as a wider and lower resonance peak, but may also lead to a decreasing resonance frequency [21], [56]. The effect of increasing resistance on the resonance frequency is often neglected in conventional sensor applications, but it should be taken into consideration with biodegradable conductors where the resistance changes can be large [56].

The type 2 Mg pressure sensor that was tested in Sörensen buffer showed also varying pressure sensitivity during immersion. Altered mechanical properties of the substrate could have an influence on the sensitivity of pressure sensors that are based on deflecting polymer substrates [73], [233], [250]. However, in our case, the flexural modulus of the PDTEC substrate material showed only minor changes during the first week of immersion, which suggests that the effect of changing substrate stiffness is not the cause for the drifting pressure sensitivity. Together with the observed changes in the baseline resonance frequency, the results indicate that the

physical sensor structure underwent changes during immersion. Thus, we concluded that the water diffusion into the substrate should be prevented during its functional lifetime. The lifetime of the bioresorbable conductive wire and the type 2 Mg pressure sensor were at the same scale, which indicates that the diffused water corrodes the Mg conductors in a similar manner regardless of the tenfold higher water uptake of PDTEC compared with PCL. Thus, it seems that if bulk eroding polymers are used as substrates, an encapsulation layer is needed to control water diffusion.

As discussed in Publication IV, encapsulation layers like atomic layer deposited (ALD) coatings or biodegradable waxes are an option for increasing the stability of the devices. Mechanical fragility of inorganic coatings combined with flexible polymer substrates may lead to unsatisfactory results, but are promising with rigid inorganic substrates such as bioactive glasses [56], [119], [251]. Therefore, biodegradable waxes have been proposed as water barrier materials for polymeric substrates. The wax encapsulation (500 μm) of the wireless temperature sensor of Lu et al. was reported to result in a stable sensor performance between 1 and 6 days of immersion in PBS at +37 °C, as denoted by single f_0 measurements on days 1, 2, 5 and 6 [9]. The sensor was readable up to 14 days, but after 6 days the sensitivity and baseline resonance frequency of the sensor started to drift. A thinner wax layer (200 μm) enabled a stable operation period of 2 days.

Boutry et al. reported that their wireless arterial pulse sensor was still functional after one week of implantation in a rat model, although the Q-factor of the signal had diminished [76]. Possible changes in the f_0 were not reported, as they can be considered insignificant in a pulse-monitoring application. The pressure sensor of Luo et al. remained functional for 4 days in saline at room temperature, after which the device failed, probably due to cracks in the PLLA substrates [73]. Their Zn based wireless pressure sensor was relatively stable for 86 hours after an initial 21-hour equilibration period. A year later in 2015, Luo et al. published a follow-up study, where the polymeric materials were replaced with faster degrading alternatives like PLGA 50:50 [74]. This sensor was tested in saline at +37 °C and functioned for approximately 25 hours with a rather stable f_0 (31.7 ± 0.3 MHz) after the initial equilibration period of 1.5 hours. Other literature concerning the drifting of f_0 in bioresorbable wireless sensors is scarce.

The faster degrading sensor of Luo et al. showed shorter functional lifetime compared to their anterior sensor, but the work contained an important overture towards using materials that degrade shortly after the intended lifetime of the device. Philosophically speaking, individually implanted sensors that function for a few days

but take years to fully degrade may not fulfill the definition of biodegradability, if it is defined as a material that degrades soon after its intended application. On the other hand, the situation is essentially different if the sensor is a part of an orthopedic implant that is used for a longer period. For example, a bioresorbable bone fixation plate, whose lifetime endures from months to a few years could be equipped with an embedded sensor that monitors its performance during the first days or weeks. In this case, the degradation time would be in line with the application of the bone fixation plate.

Based on the results in this study and in the literature, the next necessary step would be to discover the exact mechanisms that cause drifting in the sensitivity and f_0 of a given sensor in order to circumvent these challenges. For instance, the differences in the behavior of our wireless pressure sensors and those of Luo et al. may arise from the testing conditions, substrate materials, substrate processing methods, sensor architecture or the conductor materials and their corrosion. For example, 1 mg of Mg produces 1 mL of hydrogen gas upon corrosion [252], which could potentially lead to pressure inside the sensor and associated dimensional changes in the sensor. The corrosion of Zn, which was used in the sensors of Luo et al. [73], [74], is much slower and has reported to lead to smaller amounts of hydrogen gas during the first weeks in HBSS [253]. Another more straightforward way for stabilizing the sensor performance would be to simply prevent water from diffusing into the sensor during its operational lifetime. However, this option includes an assumption that preventing water diffusion would neglect all the causes for sensor drifting. In addition to various encapsulation layers, using bioactive glass or bioceramic substrates contains a lot of unexplored potential in this regard due to their different degradation behavior compared to polymers.

As shown in this thesis, certain systemic effects may cause false interpretation of the sensor readings if not taken into account. For example, temperature changes may affect the dielectric constant or mechanical properties of the sensor substrate [41]. We demonstrated the temperature sensitivity of the bioresorbable polymer-encapsulated non-degradable sensor circuit and the type 1 Mg pressure sensor. Temperature was not a substantial error source in the non-degradable sensors, where an almost linear resonance frequency change of about -0.05% per °C was noticed [234]. The wireless pressure sensors showed a more significant and non-linear temperature dependency, which might have been caused by dimensional changes in the sensor structure upon heating. The results indicate that the temperature response of inductively coupled sensors should be tested and potentially compensated in practical sensor applications. Although typical body temperatures

remain between 36.5-37.2 °C [1], the local temperature may rise up to 4 °C in case of an infection [9] or fever.

The application and the implant location in the body may also have an indirect effect on the sensor performance. For example, any bending or compressive forces may change the geometry of an LC circuit and thereby affect its resonance frequency. Such forces are not uncommon in orthopedic applications. Furthermore, the tissues that are in direct contact with the sensor might have an effect on the capacitance of the system [16] or on the device degradation depending on the vascularization of the physiological compartment where the sensor is located [4]. Finally, the metallic objects like other fixation devices near the LC circuits may cause distortions and energy losses [6].

7 SUMMARY AND CONCLUSIONS

Fabricating wireless implantable sensors from bioresorbable materials can be considered as a futuristic approach for a good reason. Processing of bioresorbable materials, assembling the devices, as well as sensor performance and reliability face more serious challenges compared to conventional non-degradable devices. Furthermore, optimal clearance of the materials from the body adds up to the list of challenges before widespread clinical application. In this thesis, inductively coupled inductor-capacitor (LC) circuit-based resonance sensors were studied due to their simple construction and capability for short-range wireless measurements. The objectives of the thesis were to bring new insights into fabrication and assembly of bioresorbable LC circuits, and to identify the most critical material properties related to device fabrication and performance.

The first aim was to develop fabrication methods for bioresorbable electronic devices. It was shown that bioresorbable poly(ε-caprolactone) (PCL) could be melt processed onto bioresorbable poly(desamino tyrosyl-tyrosine ethyl ester carbonate) (PDTEC) substrates with negligible damage to the metal films on the substrate. This method was used to extrusion coat metallized PDTEC fibers to form bioresorbable coils, and to attach two identical metallized PDTEC sheets onto a holed spacer to construct simple wireless bioresorbable pressure sensors.

The primary conductor fabrication methods in this thesis involved evaporation and sputtering. Both techniques are viable options for conductor fabrication, but they have different requirements for example for the shadow masks. Furthermore, biodegradable Mo wires coiled around a polymeric screw were used to form compression sensors with a solenoidal architecture. Finally, bioactive glass substrates were introduced as a more thermally and chemically resistant substrate option for bioresorbable polymers. Miniaturized bioactive glass-based resonators (Ø = 14 mm) were fabricated from two evaporated Mg layers with a spin-coated dielectric layer in between. All the three layers were deposited directly on top of each other, which was not possible using polymer substrates.

The second aim was to identify the most critical material properties related to the fabrication and performance of the LC circuits. It was noticed that physical vapor deposited (PVD) Mg and Zn conductors showed significantly higher bulk resistivity

estimates (up to 290 nΩ·m) compared to bulk literature values (43 nΩ·m for Mg and 59 nΩ·m for Zn). The conductor thickness and bulk resistivity affect its resistance and are thus crucial to the resonator performance. Both parameters could potentially be improved by patterning metal foils instead of depositing the conductors via PVD. In this study, the PVD methods yielded several micrometers thick metal conductors, which translated into wireless pressure sensor readout from distances up to 15 mm using our setup in ambient conditions.

Metal corrosion was a further key element in the device performance under simulated physiological conditions. It was suggested that the decreasing resistance and the generated hydrogen gas of the fast-corroding Mg conductors were partly responsible for the challenges in the pressure sensor stability. Based on these findings, the role of Mg as the primary conductor material deserves to be challenged. For example, slower corroding metals like Zn or Mo could provide more stable sensor operation. Moreover, the microstructure of the films dominated the resistance in the metal films, suggesting that the literature bulk resistivity values should not be used to compare metals in this kind of applications.

Bioactive glass provides a highly interesting substrate material due to its better thermal and chemical resistance compared to bioresorbable polymers. The polymer properties have forced scientists to innovate and design circuits without through hole vias (Publication III and Publication IV) or transfer print conductors that are prepared separately from the substrate. Furthermore, significant water diffusion into the polymer substrates is an undesirable feature, which indirectly caused the device failure in all the immersed sensors.

The third aim in the study was to fabricate a sensor that would function for 2 weeks under simulated physiological conditions. This aim was not fully reached, although the type 2 Mg pressure sensors were wirelessly readable and pressure-responsive up to 10 days in Sörensen buffer solution at physiological temperatures. However, the baseline resonance frequency as well as the pressure sensitivity of the sensor were noticed to drift. This was likely attributed to the diffused water inside the sensor, which caused dimensional changes in the sensor and resistance decreases in the conductors.

In my opinion, future academic efforts should be directed towards finding material solutions and sensor architectures that enable a stable functional lifetime for the bioresorbable LC circuits. Especially the drifting of the baseline resonance frequency deserves more attention. The key to stable operation could be found in bioresorbable encapsulation layers, or in substrate materials that prevent the diffusion of water into the sensor during its intended lifetime. In addition, the role

of metal corrosion on the drifting of the sensors should be addressed in a systematic manner. Especially the effects of conductor corrosion on the electrical resistance of the LC circuit as well as gas generation inside the sensor were deemed as probable causes for drifting in our wireless pressure sensors.

A critical practical matter concerning the future of bioresorbable sensors is finding clinically and economically attractive applications for the sensors. Pressure sensors provide a good starting point for studying bioresorbable sensors, but their clinical applications are often related to detecting life-threatening conditions like elevated intracranial pressure or acute compartment syndrome. Such applications require undisputed sensor operation, which is not an easy task even with non-degradable materials. Thus, added diagnostic value could be first sought from less critical applications. A clinical breakthrough could be achieved first with applications like detecting incipient bacterial infections or monitoring parameters that are relevant to the performance of the fixation device, such as bone attachment onto the implant.

REFERENCES

[1]   M. De Santis and I. Cacciotti, "Wireless implantable and biodegradable sensors for postsurgery monitoring: current status and future perspectives.," *Nanotechnology*, vol. 31, no. 25, p. 252001, Apr. 2020, doi: 10.1088/1361-6528/ab7a2d.

[2]   D. Kim *et al.*, "Silicon electronics on silk as a path to bioresorbable, implantable devices," *Appl. Phys. Lett.*, vol. 95, no. 13, p. 133701, Sep. 2009, doi: 10.1063/1.3238552.

[3]   Y. Honjol *et al.*, "Current view and prospect: Implantable pressure sensors for health and surgical care," *Med. Devices Sensors*, vol. 3, no. 3, p. e10068, Jun. 2020, doi: 10.1002/mds3.10068.

[4]   B. S. Klosterhoff *et al.*, "Implantable Sensors for Regenerative Medicine," *J. Biomech. Eng.*, vol. 139, no. 2, pp. 210091–2100911, Feb. 2017, doi: 10.1115/1.4035436.

[5]   E. H. Ledet, D. D'Lima, P. Westerhoff, J. A. Szivek, R. A. Wachs, and G. Bergmann, "Implantable Sensor Technology: From Research to Clinical Practice," *J. Am. Acad. Orthop. Surg.*, vol. 20, no. 6, 2012, doi: 10.5435/JAAOS-20-06-383.

[6]   S. S. Karipott, B. D. Nelson, R. E. Guldberg, and K. G. Ong, "Clinical potential of implantable wireless sensors for orthopedic treatments," *Expert Rev. Med. Devices*, vol. 15, no. 4, pp. 255–264, Apr. 2018, doi: 10.1080/17434440.2018.1454310.

[7]   S. Risitano, B. Karamian, and P. F. Indelli, "Intraoperative load-sensing drives the level of constraint in primary total knee arthroplasty: Surgical technique and review of the literature," *J. Clin. Orthop. Trauma*, vol. 8, no. 3, pp. 265–269, 2017, doi: 10.1016/j.jcot.2017.06.004.

[8]   A. P. Baumann *et al.*, "FDA public workshop: Orthopaedic sensing, measuring, and advanced reporting technology (SMART) devices," *J. Orthop. Res.*, vol. 39, no. 1, pp. 22–29, Aug. 2020, doi: 10.1002/jor.24833.

[9]   D. Lu *et al.*, "Bioresorbable, Wireless, Passive Sensors as Temporary Implants for Monitoring Regional Body Temperature," *Adv. Healthc. Mater.*, vol. 9, no. 16, p. 2000942, Aug. 2020, doi: 10.1002/adhm.202000942.

[10]   L. Rangel-Castilla, S. Gopinath, and C. S. Robertson, "Management of intracranial hypertension," *Neurol. Clin.*, vol. 26, no. 2, pp. 521–541, May 2008, doi: 10.1016/j.ncl.2008.02.003.

[11]   G. Partal, A. Furey, and O. Robert, "Fasciotomy of the Leg for Acute Compartment Syndrome," in *Operative Techniques in Pediatric Orthopaedic Surgery*, 2nd ed., J. M. Flynn, W. N. Sankar, and S. W. Wiesel, Eds. Wolters Kluwer Health, 2015, pp. 342–343.

[12]   C. Martin, "An unusual presentation of compartment syndrome," *J. Am. Acad. Physician Assist.*, vol. 28, no. 5, pp. 36–39, 2015, doi: 10.1097/01.JAA.0000460920.82885.67.

[13]   A. H. Schmidt, "Acute compartment syndrome," *Injury*, vol. 48, pp. S22–S25, 2017, doi: 10.1016/j.injury.2017.04.024.

[14]   U. Uzair, D. Benza, C. J. Behrend, and J. N. Anker, "Noninvasively Imaging pH at the Surface of Implanted Orthopedic Devices with X-ray Excited Luminescence Chemical Imaging," *ACS Sensors*, vol. 4, no. 9, pp. 2367–2374, Sep. 2019, doi: 10.1021/acssensors.9b00962.

[15]   B. S. Klosterhoff *et al.*, "Wireless sensor enables longitudinal monitoring of regenerative niche mechanics during rehabilitation that enhance bone repair," *Bone*, vol. 135, p.

115311, 2020, doi: 10.1016/j.bone.2020.115311.

[16] M. Yvanoff and J. Venkataraman, "A Feasibility Study of Tissue Characterization Using LC Sensors," *IEEE Trans. Antennas Propag.*, vol. 57, no. 4, pp. 885–893, 2009, doi: 10.1109/TAP.2009.2016073.

[17] E. H. Ledet, B. Liddle, K. Kradinova, and S. Harper, "Smart implants in orthopedic surgery, improving patient outcomes: a review," *Innov. Entrep. Heal.*, vol. 5, pp. 41–51, 2018, doi: 10.2147/IEH.S133518.

[18] T. Salpavaara, *Inductively Coupled Passive Resonance Sensors: Readout Methods and Applications*. Tampere University of Technology, 2018.

[19] S.-W. Hwang *et al.*, "Materials and Fabrication Processes for Transient and Bioresorbable High-Performance Electronics," *Adv. Funct. Mater.*, vol. 23, no. 33, pp. 4087–4093, 2013, doi: 10.1002/adfm.201300127.

[20] S.-W. Hwang *et al.*, "High-Performance Biodegradable/Transient Electronics on Biodegradable Polymers," *Adv. Mater.*, vol. 26, no. 23, pp. 3905–3911, 2014, doi: 10.1002/adma.201306050.

[21] Q. A. Huang, L. Dong, and L. F. Wang, "LC Passive Wireless Sensors Toward a Wireless Sensing Platform: Status, Prospects, and Challenges," *J. Microelectromechanical Syst.*, vol. 25, no. 5, pp. 822–841, 2016, doi: 10.1109/JMEMS.2016.2602298.

[22] K. G. Ong, C. a. Grimes, C. L. Robbins, and R. S. Singh, "Design and application of a wireless, passive, resonant-circuit environmental monitoring sensor," *Sensors Actuators A Phys.*, vol. 93, no. 1, pp. 33–43, 2001, doi: 10.1016/S0924-4247(01)00624-0.

[23] K. Bazaka and V. M. Jacob, "Implantable Devices: Issues and Challenges," *Electronics* , vol. 2, no. 1. 2013, doi: 10.3390/electronics2010001.

[24] H. Kim, H. Hirayama, S. Kim, K. J. Han, R. Zhang, and J. Choi, "Review of Near-Field Wireless Power and Communication for Biomedical Applications," *IEEE Access*, vol. 5, pp. 21264–21285, 2017, doi: 10.1109/ACCESS.2017.2757267.

[25] C. M. Boutry, A. Nguyen, Q. O. Lawal, A. Chortos, S. Rondeau-Gagné, and Z. Bao, "A Sensitive and Biodegradable Pressure Sensor Array for Cardiovascular Monitoring," *Adv. Mater.*, vol. 27, no. 43, pp. 6954–6961, 2015, doi: 10.1002/adma.201502535.

[26] T. Salpavaara *et al.*, "Passive resonance sensor based method for monitoring particle suspensions," *Sensors Actuators B. Chem.*, vol. 219, pp. 324–330, 2014, doi: 10.1016/j.snb.2015.04.121.

[27] J. C. Butler, A. J. Vigliotti, F. W. Verdi, and S. M. Walsh, "Wireless, passive, resonant-circuit, inductively coupled, inductive strain sensor," *Sensors Actuators A Phys.*, vol. 102, no. 1, pp. 61–66, 2002, doi: 10.1016/S0924-4247(02)00342-4.

[28] M. Nabipoor and B. Y. Majlis, "A new passive telemetry LC pressure and temperature sensor optimized for TPMS," *J. Phys. Conf. Ser.*, vol. 34, pp. 770–775, 2006, doi: 10.1088/1742-6596/34/1/127.

[29] M. Bona, E. Sardini, M. Serpelloni, B. Andò, and C. O. Lombardo, "Study on a telemetrie system that works with an inkjet-printed resistive strain gauge," in *2016 IEEE Sensors Applications Symposium (SAS)*, 2016, pp. 1–6, doi: 10.1109/SAS.2016.7479869.

[30] D. Kajfez, "Q-Factor," in *Encyclopedia of RF and Microwave Engineering*, 2005.

[31] R. Abdolvand, B. Bahreyni, E.-Y. J. Lee, and F. Nabki, "Micromachined Resonators: A Review," *Micromachines* , vol. 7, no. 9. 2016, doi: 10.3390/mi7090160.

[32] C. Li *et al.*, "Review of Research Status and Development Trends of Wireless Passive LC Resonant Sensors for Harsh Environments," *Sensors (Basel).*, vol. 15, no. 6, pp. 13097–13109, Jun. 2015, doi: 10.3390/s150613097.

[33] M. Demori, M. Baù, M. Ferrari, and V. Ferrari, "Interrogation Techniques and Interface Circuits for Coil-Coupled Passive Sensors," *Micromachines* , vol. 9, no. 9. 2018, doi: 10.3390/mi9090449.

[34] M. Demori, M. Masud, M. Bau, M. Ferrari, and V. Ferrari, "Passive LC sensor label with distance-independent contactless interrogation," in *2017 IEEE Sensors*, 2017, pp. 1–3, doi: 10.1109/ICSENS.2017.8234410.

[35] C. Zheng, W. Li, A.-L. Li, Z. Zhan, L.-Y. Wang, and D.-H. Sun, "Design and Manufacturing of a Passive Pressure Sensor Based on LC Resonance," *Micromachines*, vol. 7, no. 5, p. 87, 2016, doi: 10.3390/mi7050087.

[36] P. Chen, S. Saati, R. Varma, M. S. Humayun, and Y. Tai, "Wireless Intraocular Pressure Sensing Using Microfabricated Minimally Invasive Flexible-Coiled LC Sensor Implant," *J. Microelectromechanical Syst.*, vol. 19, no. 4, pp. 721–734, 2010, doi: 10.1109/JMEMS.2010.2049825.

[37] A. Hänninen, T. Salpavaara, J. Lekkala, and M. Kellomäki, "An Inductively Coupled Biodegradable Capacitive Pressure Sensor," *Proceedings of Eurosensors 2018*, vol. 2, no. 13. 2018, doi: 10.3390/proceedings2130914.

[38] D. Yan *et al.*, "Low-Cost Wireless Temperature Measurement: Design, Manufacture, and Testing of a PCB-Based Wireless Passive Temperature Sensor," *Sensors*, vol. 18, no. 2. 2018, doi: 10.3390/s18020532.

[39] S. S. Karipott, P. M. Veetil, B. D. Nelson, R. E. Guldberg, and K. G. Ong, "An Embedded Wireless Temperature Sensor for Orthopedic Implants," *IEEE Sens. J.*, vol. 18, no. 3, pp. 1265–1272, 2018, doi: 10.1109/JSEN.2017.2780226.

[40] Q. Ren, L. Wang, and Q. Huang, "Temperature dependence of the quality factor in LC-type passive wireless temperature sensors," in *2015 IEEE Sensors*, 2015, pp. 1–4, doi: 10.1109/ICSENS.2015.7370242.

[41] L. Qin *et al.*, "A Wireless Passive LC Resonant Sensor Based on LTCC under High-Temperature/Pressure Environments," *Sensors (Basel).*, vol. 15, no. 7, pp. 16729–16739, Jul. 2015, doi: 10.3390/s150716729.

[42] R. M. Fish and L. A. Geddes, "Conduction of electrical current to and through the human body: a review," *Eplasty*, vol. 9, p. e44, Oct. 2009.

[43] F. Burny *et al.*, "Concept, design and fabrication of smart orthopedic implants," *Med. Eng. Phys.*, vol. 22, no. 7, pp. 469–479, 2000, doi: 10.1016/S1350-4533(00)00062-X.

[44] M. Maaß, A. Griessner, V. Steixner, and C. Zierhofer, "Reduction of eddy current losses in inductive transmission systems with ferrite sheets," *Biomed. Eng. Online*, vol. 16, no. 1, p. 3, Jan. 2017, doi: 10.1186/s12938-016-0297-4.

[45] X. Huang, *Bioresorbable Materials and Their Application in Electronics*. Cambridge: Cambridge University Press, 2017.

[46] Y. Ohya, "Biodegradable Materials," in *Encyclopedia of Polymeric Nanomaterials*, S. Kobayashi and K. Müllen, Eds. Berlin, Heidelberg: Springer Berlin Heidelberg, 2014, pp. 1–8.

[47] A. Göpferich, "Mechanisms of Polymer Degradation and Elimination," in *Handbook of Biodegradable Polymers*, A. J. Domb, J. Kost, and D. M. Wiseman, Eds. CRC Press, 1997.

[48] R. Song, M. Murphy, C. Li, K. Ting, C. Soo, and Z. Zheng, "Current development of biodegradable polymeric materials for biomedical applications," *Drug Des. Devel. Ther.*, vol. 12, pp. 3117–3145, Sep. 2018, doi: 10.2147/DDDT.S165440.

[49] A. R. Santos Jr., "Bioresorbable polymers for tissue engineering," in *Tissue Engineering*, D. Eberli, Ed. Intech, 2010, p. 536.

[50] X. Yu, W. Shou, B. K. Mahajan, X. Huang, and H. Pan, "Materials, Processes, and Facile Manufacturing for Bioresorbable Electronics: A Review," *Adv. Mater.*, vol. 30, no. 28, p. 1707624, Jul. 2018, doi: 10.1002/adma.201707624.

[51] E.-H. A. Mohamed, "The Effect of Annealing Treatments on Spherulitic Morphology and Physical Ageing on Glass Transition of Poly Lactic Acid (PLLA)," *Mater. Sci. Appl.*, vol. 02, no. 05, pp. 439–443, 2011, doi: 10.4236/msa.2011.25058.

[52] I. Engelberg and J. Kohn, "Physico-mechanical properties of degradable polymers used in medical applications: A comparative study," *Biomaterials*, vol. 12, no. 3, pp. 292–304, 1991, doi: 10.1016/0142-9612(91)90037-B.

[53] M. A. Woodruff and D. W. Hutmacher, "The return of a forgotten polymer—Polycaprolactone in the 21st century," *Prog. Polym. Sci.*, vol. 35, no. 10, pp. 1217–1256, Oct. 2010, doi: 10.1016/j.progpolymsci.2010.04.002.

[54] V. Tangpasuthadol, A. Shefer, K. A. Hooper, and J. Kohn, "Thermal properties and physical ageing behaviour of tyrosine-derived polycarbonates," *Biomaterials*, vol. 17, no. 4, pp. 463–468, 1996, doi: 10.1016/0142-9612(96)89665-7.

[55] K. A. Hooper, N. D. Macon, and J. Kohn, "Comparative histological evaluation of new tyrosine-derived polymers and poly (L-lactic acid) as a function of polymer degradation," *J. Biomed. Mater. Res.*, vol. 41, no. 3, pp. 443–454, Sep. 1998, doi: 10.1002/(SICI)1097-4636(19980905)41:3<443::AID-JBM14>3.0.CO;2-J.

[56] A. Palmroth *et al.*, "Materials and Orthopedic Applications for Bioresorbable Inductively Coupled Resonance Sensors," *ACS Appl. Mater. Interfaces*, vol. 12, no. 28, pp. 31148–31161, Jul. 2020, doi: 10.1021/acsami.0c07278.

[57] J. Heller and J. Barr, "Poly(ortho esters) From Concept to Reality," *Biomacromolecules*, vol. 5, no. 5, pp. 1625–1632, Sep. 2004, doi: 10.1021/bm040049n.

[58] S. Dumitriu and V. I. Popa, *Polymeric Biomaterials: Structure and Function*, Third Edit. CRC Press, 2013.

[59] J. Heller, J. Barr, S. Y. Ng, K. S. Abdellauoi, and R. Gurny, "Poly(ortho esters): synthesis, characterization, properties and uses," *Adv. Drug Deliv. Rev.*, vol. 54, no. 7, pp. 1015–1039, 2002, doi: 10.1016/S0169-409X(02)00055-8.

[60] J. R. Jones, "Review of bioactive glass: From Hench to hybrids," *Acta Biomater.*, vol. 9, no. 1, pp. 4457–4486, 2013, doi: 10.1016/j.actbio.2012.08.023.

[61] A. R. Boccaccini, D. S. Brauer, and L. Hupa, *Bioactive Glasses: Fundamentals, Technology and Applications*. The Royal Society of Chemistry, 2016.

[62] N. C. Lindfors, I. Koski, J. T. Heikkilä, K. Mattila, and A. J. Aho, "A prospective randomized 14-year follow-up study of bioactive glass and autogenous bone as bone graft substitutes in benign bone tumors," *J. Biomed. Mater. Res. Part B Appl. Biomater.*, vol. 94B, no. 1, pp. 157–164, Jul. 2010, doi: 10.1002/jbm.b.31636.

[63] J. A. Tamada and R. Langer, "Erosion kinetics of hydrolytically degradable polymers," *Proc. Natl. Acad. Sci. USA*, vol. 90, no. 2, pp. 552–556, Jan. 1993, doi: doi.org/10.1073/pnas.90.2.552.

[64] S. Lyu and D. Untereker, "Degradability of polymers for implantable biomedical devices," *Int. J. Mol. Sci.*, vol. 10, no. 9, pp. 4033–4065, 2009, doi: 10.3390/ijms10094033.

[65] S. M. Li, H. Garreau, and M. Vert, "Structure-property relationships in the case of the degradation of massive aliphatic poly-(α-hydroxy acids) in aqueous media," *J. Mater. Sci. Mater. Med.*, vol. 1, no. 3, pp. 123–130, 1990, doi: 10.1007/BF00700871.

[66] F. von Burkersroda, L. Schedl, and A. Göpferich, "Why degradable polymers undergo surface erosion or bulk erosion," *Biomaterials*, vol. 23, no. 21, pp. 4221–4231, 2002, doi: 10.1016/S0142-9612(02)00170-9.

[67] S. M. Li, H. Garreau, and M. Vert, "Structure-property relationships in the case of the degradation of massive aliphatic poly-(α-hydroxy acids) in aqueous media - Part 1: Poly(dl-lactic acid)," *J. Mater. Sci. Mater. Med.*, vol. 1, no. 3, pp. 123–130, 1990, doi: 10.1007/BF00700871.

[68] N. Ashammakhi, A. M. Gonzalez, P. Törmälä, and I. T. Jackson, "New resorbable bone fixation. Biomaterials in craniomaxillofacial surgery: present and future," *Eur. J. Plast. Surg.*, vol. 26, no. 8, pp. 383–390, 2004, doi: 10.1007/s00238-003-0568-8.

[69] R. Zamora, A. Jackson, and D. Seligson, "Correct techniques for the use of

bioabsorbable implants in orthopaedic trauma," *Curr. Orthop. Pract.*, vol. 27, no. 4, pp. 469–473, 2016, doi: 10.1097/BCO.0000000000000378.

[70] L. N. Woodard and M. A. Grunlan, "Hydrolytic Degradation and Erosion of Polyester Biomaterials," *ACS Macro Lett.*, vol. 7, no. 8, pp. 976–982, Aug. 2018, doi: 10.1021/acsmacrolett.8b00424.

[71] S. Chatterjee, M. Saxena, D. Padmanabhan, M. Jayachandra, and H. J. Pandya, "Futuristic medical implants using bioresorbable materials and devices," *Biosens. Bioelectron.*, p. 111489, 2019, doi: 10.1016/j.bios.2019.111489.

[72] H. K. Makadia and S. J. Siegel, "Poly Lactic-co-Glycolic Acid (PLGA) as Biodegradable Controlled Drug Delivery Carrier," *Polymers (Basel).*, vol. 3, no. 3, pp. 1377–1397, Sep. 2011, doi: 10.3390/polym3031377.

[73] M. Luo, A. W. Martinez, C. Song, F. Herrault, and M. G. Allen, "A Microfabricated Wireless RF Pressure Sensor Made Completely of Biodegradable Materials," *Journal of Microelectromechanical Systems*, vol. 23, no. 1. pp. 4–13, 2014, doi: 10.1109/JMEMS.2013.2290111.

[74] M. Luo, W. Shen, and M. G. Allen, "Microfabricated PLGA/PVA-based completely biodegradable passive RF pressure sensors," in *2015 Transducers - 2015 18th International Conference on Solid-State Sensors, Actuators and Microsystems (TRANSDUCERS)*, 2015, pp. 101–104, doi: 10.1109/TRANSDUCERS.2015.7180871.

[75] C. M. Boutry *et al.*, "A stretchable and biodegradable strain and pressure sensor for orthopaedic application," *Nat. Electron.*, vol. 1, no. 5, pp. 314–321, 2018, doi: 10.1038/s41928-018-0071-7.

[76] C. M. Boutry *et al.*, "Biodegradable and flexible arterial-pulse sensor for the wireless monitoring of blood flow," *Nat. Biomed. Eng.*, vol. 3, no. 1, pp. 47–57, 2019, doi: 10.1038/s41551-018-0336-5.

[77] E. J. Curry *et al.*, "Biodegradable Piezoelectric Force Sensor," *Proc. Natl. Acad. Sci.*, vol. 115, no. 5, pp. 909–914, 2018, doi: 10.1073/pnas.1710874115.

[78] K. J. Yu *et al.*, "Spatiotemporal mapping of electrical activity from the cerebral cortex," *Nat. Mater.*, vol. 15, pp. 782–791, 2016, doi: 10.1038/NMAT4624.

[79] S.-K. Kang *et al.*, "Bioresorbable silicon electronic sensors for the brain," *Nature*, vol. 530, no. 7588, pp. 71–76, Feb. 2016, doi: 10.1038/nature16492.

[80] S. Pulapura and J. Kohn, "Tyrosine-derived polycarbonates: Backbone-modified 'pseudo'-poly(amino acids) designed for biomedical applications," *Biopolymers*, vol. 32, no. 4, pp. 411–417, Apr. 1992, doi: 10.1002/bip.360320418.

[81] J. Kemnitzer and J. Kohn, "Degradable Polymers Derived from the Amino Acid L-Tyrosine," in *Handbook of Biodegradable Polymers*, A. J. Domb, J. Kost, and D. Wiseman, Eds. CRC Press, 1998, pp. 251–272.

[82] S. I. Ertel and J. Kohn, "Evaluation of a series of tyrosine-derived polycarbonates as degradable biomaterials," *J. Biomed. Mater. Res.*, vol. 28, no. 8, pp. 919–930, Aug. 1994, doi: 10.1002/jbm.820280811.

[83] K. A. Hooper, J. D. Cox, and J. Kohn, "Comparison of the effect of ethylene oxide and γ-irradiation on selected tyrosine-derived polycarbonates and poly(L-lactic acid)," *J. Appl. Polym. Sci.*, vol. 63, no. 11, pp. 1499–1510, Mar. 1997, doi: 10.1002/(SICI)1097-4628(19970314)63:11<1499::AID-APP12>3.0.CO;2-Y.

[84] S. L. Bourke and J. Kohn, "Polymers derived from the amino acid l-tyrosine: polycarbonates, polyarylates and copolymers with poly(ethylene glycol)," *Adv. Drug Deliv. Rev.*, vol. 55, no. 4, pp. 447–466, 2003, doi: 10.1016/S0169-409X(03)00038-3.

[85] K. A. Aamer, C. M. Stafford, L. J. Richter, J. Kohn, and M. L. Becker, "Thin Film Elastic Modulus of Degradable Tyrosine-Derived Polycarbonate Biomaterials and Their Blends," *Macromolecules*, vol. 42, no. 4, pp. 1212–1218, Jan. 2009, doi:

10.1021/ma802115b.

[86] V. Tangpasuthadol, S. M. Pendharkar, R. C. Peterson, and J. Kohn, "Hydrolytic degradation of tyrosine-derived polycarbonates, a class of new biomaterials. Part II: 3-yr study of polymeric devices," *Biomaterials*, vol. 21, no. 23, pp. 2379–2387, Dec. 2000, doi: 10.1016/S0142-9612(00)00105-8.

[87] J. Choueka *et al.*, "Canine bone response to tyrosine-derived polycarbonates and poly(L-lactic acid)," *J. Biomed. Mater. Res.*, vol. 31, no. 1, pp. 35–41, May 1996, doi: 10.1002/(SICI)1097-4636(199605)31:1<35::AID-JBM5>3.0.CO;2-R.

[88] K. James, H. Levene, J. Russell Parsons, and J. Kohn, "Small changes in polymer chemistry have a large effect on the bone–implant interface:: evaluation of a series of degradable tyrosine-derived polycarbonates in bone defects," *Biomaterials*, vol. 20, no. 23, pp. 2203–2212, 1999, doi: 10.1016/S0142-9612(99)00151-9.

[89] A. Asikainen *et al.*, "Tyrosine-derived polycarbonate membrane in treating mandibular bone defects. An experimental study," *J. R. Soc. Interface*, vol. 3, no. 10, pp. 629–635, Oct. 2006, doi: 10.1098/rsif.2006.0119.

[90] A. Asikainen *et al.*, "In vivo degradation of poly(DTE carbonate) membranes. Analysis of the tissue reactions and mechanical properties," *J. Mater. Sci. Mater. Med.*, vol. 19, no. 1, pp. 53–58, 2008, doi: 10.1007/s10856-007-3134-2.

[91] X. Yang, C. Cui, Z. Tong, C. R. Sabanayagam, and X. Jia, "Poly(ε-caprolactone)-based copolymers bearing pendant cyclic ketals and reactive acrylates for the fabrication of photocrosslinked elastomers," *Acta Biomater.*, vol. 9, no. 9, pp. 8232–8244, 2013, doi: 10.1016/j.actbio.2013.06.005.

[92] M. Vert, "Degradable and bioresorbable polymers in surgery and in pharmacology: beliefs and facts," *J. Mater. Sci. Mater. Med.*, vol. 20, no. 2, pp. 437–446, 2009, doi: 10.1007/s10856-008-3581-4.

[93] L. A. Bosworth and S. Downes, "Physicochemical characterisation of degrading polycaprolactone scaffolds," *Polym. Degrad. Stab.*, vol. 95, no. 12, pp. 2269–2276, 2010, doi: 10.1016/j.polymdegradstab.2010.09.007.

[94] S. C. Woodward, P. S. Brewer, F. Moatamed, A. Schindler, and C. G. Pitt, "The intracellular degradation of poly(ε-caprolactone)," *J. Biomed. Mater. Res.*, vol. 19, no. 4, pp. 437–444, Apr. 1985, doi: 10.1002/jbm.820190408.

[95] H. Kweon *et al.*, "A novel degradable polycaprolactone networks for tissue engineering," *Biomaterials*, vol. 24, no. 5, pp. 801–808, 2003, doi: 10.1016/S0142-9612(02)00370-8.

[96] Y. Gao, K. Sim, X. Yan, J. Jiang, J. Xie, and C. Yu, "Thermally Triggered Mechanically Destructive Electronics Based On Electrospun Poly(ε-caprolactone) Nanofibrous Polymer Films," *Sci. Rep.*, vol. 7, no. 1, p. 947, 2017, doi: 10.1038/s41598-017-01026-6.

[97] T. Salpavaara, J. Lekkala, S. Khan, V. Ellä, and M. Kellomäki, "Biodegradable encapsulation for inductively measured resonance circuit," in *2012 IEEE 12th International Conference on Bioinformatics & Bioengineering (BIBE)*, 2012, pp. 323–327, doi: 10.1109/BIBE.2012.6399644.

[98] M. C. Serrano, E. J. Chung, and G. A. Ameer, "Advances and Applications of Biodegradable Elastomers in Regenerative Medicine," *Adv. Funct. Mater.*, vol. 20, no. 2, pp. 192–208, Jan. 2010, doi: 10.1002/adfm.200901040.

[99] E. Bat, Z. Zhang, J. Feijen, D. W. Grijpma, and A. A. Poot, "Biodegradable elastomers for biomedical applications and regenerative medicine," *Regen. Med.*, vol. 9, no. 3, pp. 385–398, May 2014, doi: 10.2217/rme.14.4.

[100] H. Ye, K. Zhang, D. Kai, Z. Li, and X. J. Loh, "Polyester elastomers for soft tissue engineering," *Chem. Soc. Rev.*, vol. 47, no. 12, pp. 4545–4580, 2018, doi: 10.1039/C8CS00161H.

[101] S.-W. Hwang *et al.*, "Biodegradable Elastomers and Silicon

Nanomembranes/Nanoribbons for Stretchable, Transient Electronics, and Biosensors," *Nano Lett.*, vol. 15, no. 5, pp. 2801–2808, May 2015, doi: 10.1021/nl503997m.

[102]   Q. Liu, L. Jiang, R. Shi, and L. Zhang, "Synthesis, preparation, in vitro degradation, and application of novel degradable bioelastomers—A review," *Prog. Polym. Sci.*, vol. 37, no. 5, pp. 715–765, 2012, doi: 10.1016/j.progpolymsci.2011.11.001.

[103]   G. Lee *et al.*, "Fully Biodegradable Microsupercapacitor for Power Storage in Transient Electronics," *Adv. Energy Mater.*, vol. 7, no. 18, p. 1700157, Sep. 2017, doi: 10.1002/aenm.201700157.

[104]   T. Salpavaara, V. Ellä, M. Kellomäki, and J. Lekkala, "Biodegradable Passive Resonance Sensor: Fabrication and Initial Testing," in *BIODEVICES 2015 - 8th International Conference on Biomedical Electronics and Devices*, 2015, pp. 127–131, doi: 10.5220/0005255901270131.

[105]   A. Basu and A. J. Domb, "Recent Advances in Polyanhydride Based Biomaterials," *Adv. Mater.*, vol. 30, no. 41, p. 1706815, Oct. 2018, doi: 10.1002/adma.201706815.

[106]   A. J. Domb, S. Amselem, J. Shah, and M. Maniar, "Polyanhydrides: Synthesis and characterization," in *Biopolymers I - Advances in Polymer Science*, 1993, pp. 93–141, doi: 10.1007/BFb0027552.

[107]   A. Conix, "Aromatic polyanhydrides, a new class of high melting fiber-forming polymers," *J. Polym. Sci.*, vol. 29, no. 120, pp. 343–353, Jun. 1958, doi: 10.1002/pol.1958.1202912002.

[108]   A. Göpferich and J. Tessmar, "Polyanhydride degradation and erosion," *Adv. Drug Deliv. Rev.*, vol. 54, no. 7, pp. 911–931, 2002, doi: 10.1016/S0169-409X(02)00051-0.

[109]   R. Ghadi, E. Muntimadugu, A. J. Domb, W. Khan, and X. Zhang, "Synthetic biodegradable medical polymer: Polyanhydrides," in *Science and Principles of Biodegradable and Bioresorbable Medical Polymers*, X. Zhang, Ed. Woodhead Publishing, 2017, pp. 153–188.

[110]   Y. Gao *et al.*, "Moisture-triggered physically transient electronics," *Sci. Adv.*, vol. 3, no. 9, p. e1701222, Sep. 2017, doi: 10.1126/sciadv.1701222.

[111]   M. J.-L. Tschan, N. S. Ieong, R. Todd, J. Everson, and A. P. Dove, "Unlocking the Potential of Poly(Ortho Ester)s: A General Catalytic Approach to the Synthesis of Surface-Erodible Materials," *Angew. Chem. Int. Ed. Engl.*, vol. 56, no. 52, pp. 16664–16668, Dec. 2017, doi: 10.1002/anie.201709934.

[112]   H. Bakht Khosh Hagh and F. Farshi Azhar, "Reinforcing materials for polymeric tissue engineering scaffolds: A review," *J. Biomed. Mater. Res. Part B Appl. Biomater.*, vol. 107, no. 5, pp. 1560–1575, Oct. 2018, doi: 10.1002/jbm.b.34248.

[113]   L. L. Hench, "Bioceramics: From Concept to Clinic," *J. Am. Ceram. Soc.*, vol. 74, no. 7, pp. 1487–1510, Jul. 1991, doi: 10.1111/j.1151-2916.1991.tb07132.x.

[114]   D. S. Brauer, "Bioactive Glasses—Structure and Properties," *Angew. Chemie Int. Ed.*, vol. 54, no. 14, pp. 4160–4181, Mar. 2015, doi: 10.1002/anie.201405310.

[115]   K. Unda, A. Mohammadkhah, K. Lee, D. E. Day, M. J. O'Keefe, and C. Kim, "Sensor substrates based on biodegradable glass materials," in *2016 IEEE Sensors*, 2016, pp. 1–3, doi: 10.1109/ICSENS.2016.7808408.

[116]   S. Adnan, K.-M. Lee, M. T. Ghasr, M. J. O'Keefe, D. E. Day, and C.-S. Kim, "Water-Soluble Glass Substrate as a Platform for Biodegradable Solid-State Devices," *J. Electron Devices Soc.*, vol. 4, no. 6, pp. 490–494, 2016, doi: 10.1109/JEDS.2016.2606340.

[117]   G. Kaur, O. P. Pandey, K. Singh, D. Homa, B. Scott, and G. Pickrell, "A review of bioactive glasses: Their structure, properties, fabrication and apatite formation," *J. Biomed. Mater. Res. Part A*, vol. 102, no. 1, pp. 254–274, Jan. 2014, doi: 10.1002/jbm.a.34690.

[118]   H. Cheng and V. Vepachedu, "Recent development of transient electronics," *Theor. Appl.*

Mech. Lett., vol. 6, no. 1, pp. 21–31, 2016, doi: 10.1016/j.taml.2015.11.012.

[119] S.-K. Kang *et al.*, "Dissolution Behaviors and Applications of Silicon Oxides and Nitrides in Transient Electronics," *Adv. Funct. Mater.*, vol. 24, no. 28, pp. 4427–4434, Jul. 2014, doi: 10.1002/adfm.201304293.

[120] K. G. Knauss and T. J. Wolery, "The dissolution kinetics of quartz as a function of pH and time at 70°C," *Geochim. Cosmochim. Acta*, vol. 52, no. 1, pp. 43–53, 1988, doi: 10.1016/0016-7037(88)90055-5.

[121] K. Refson, R. A. Wogelius, D. G. Fraser, M. C. Payne, M. H. Lee, and V. Milman, "Water chemisorption and reconstruction of the MgO surface," *Phys. Rev. B*, vol. 52, no. 15, pp. 10823–10826, Oct. 1995, doi: 10.1103/PhysRevB.52.10823.

[122] S.-W. Hwang *et al.*, "A Physically Transient Form of Silicon Electronics," *Science*, vol. 337, no. 6102, pp. 1640–1644, Sep. 2012, doi: 10.1126/science.1226325.

[123] M. A. Brenckle *et al.*, "Modulated Degradation of Transient Electronic Devices through Multilayer Silk Fibroin Pockets," *ACS Appl. Mater. Interfaces*, vol. 7, no. 36, pp. 19870–19875, Sep. 2015, doi: 10.1021/acsami.5b06059.

[124] J. Shin *et al.*, "Bioresorbable pressure sensors protected with thermally grown silicon dioxide for the monitoring of chronic diseases and healing processes," *Nat. Biomed. Eng.*, vol. 3, no. 1, pp. 37–46, 2019, doi: 10.1038/s41551-018-0300-4.

[125] W. Alvino *et al.*, *Electronic Materials & Processes Handbook*, 2nd ed. McGraw-Hill, 1993.

[126] L. Yin *et al.*, "Dissolvable Metals for Transient Electronics," *Adv. Funct. Mater.*, vol. 24, no. 5, pp. 645–658, Feb. 2014, doi: 10.1002/adfm.201301847.

[127] M. Peuster, C. Fink, C. von Schnakenburg, and G. Hausdorf, "Dissolution of tungsten coils does not produce systemic toxicity, but leads to elevated levels of tungsten in the serum and recanalization of the previously occluded vessel," *Cardiol. Young*, vol. 12, no. 3, pp. 229–235, 2002, doi: 10.1017/S1047951102000513.

[128] A. Shah Idil and N. Donaldson, "The use of tungsten as a chronically implanted material," *J. Neural Eng.*, vol. 15, no. 2, p. 21006, 2018, doi: 10.1088/1741-2552/aaa502.

[129] G. T. Meaden, "The Meaning of Electrical Resistance and Its Importance," in *Electrical Resistance of Metals*, G. T. Meaden, Ed. Boston, MA: Springer US, 1965, pp. 1–11.

[130] R. Seppänen *et al.*, *MAOL-taulukot*. Otava, 2000.

[131] J. Cheng, B. Liu, Y. H. Wu, and Y. F. Zheng, "Comparative in vitro Study on Pure Metals (Fe, Mn, Mg, Zn and W) as Biodegradable Metals," *J. Mater. Sci. Technol.*, vol. 29, no. 7, pp. 619–627, 2013, doi: 10.1016/j.jmst.2013.03.019.

[132] H. A. Wheeler, "Formulas for the Skin Effect," *Proc. IRE*, vol. 30, no. 9, pp. 412–424, 1942, doi: 10.1109/JRPROC.1942.232015.

[133] T. Jariyanorawiss and C. Thumkanon, "Optimization of Coating Material Selection Using the Skin Depth Approximation," in *2018 IEEE International WIE Conference on Electrical and Computer Engineering (WIECON-ECE)*, 2018, pp. 114–117, doi: 10.1109/WIECON-ECE.2018.8783199.

[134] A. H. Shaltout and S. Gregori, "Conformal-mapping model for estimating the resistance of polygonal inductors," in *2016 IEEE International Symposium on Circuits and Systems (ISCAS)*, 2016, pp. 1274–1277, doi: 10.1109/ISCAS.2016.7527480.

[135] T. C. Edwards and M. B. Steer, "Appendix B: Material Properties," in *Foundations for Microstrip Circuit Design*, John Wiley & Sons, Ltd, 2016, pp. 635–642.

[136] A. M. Al Alawi, S. W. Majoni, and H. Falhammar, "Magnesium and Human Health: Perspectives and Research Directions," *Int. J. Endocrinol.*, vol. 2018, p. 9041694, Apr. 2018, doi: 10.1155/2018/9041694.

[137] F. Witte, "The history of biodegradable magnesium implants: A review," *Acta Biomater.*, vol. 6, no. 5, pp. 1680–1692, 2010, doi: 10.1016/j.actbio.2010.02.028.

[138] H.-S. Han *et al.*, "Current status and outlook on the clinical translation of biodegradable

metals," *Mater. Today*, vol. 23, pp. 57–71, 2019, doi: 10.1016/j.mattod.2018.05.018.

[139] C. M. Boutry, H. Chandrahalim, P. Streit, M. Schinhammer, A. C. Hänzi, and C. Hierold, "Characterization of miniaturized RLC resonators made of biodegradable materials for wireless implant applications," *Sensors Actuators A Phys.*, vol. 189, pp. 344–355, 2013, doi: 10.1016/j.sna.2012.08.039.

[140] N. Sezer, Z. Evis, S. M. Kayhan, A. Tahmasebifar, and M. Koç, "Review of magnesium-based biomaterials and their applications," *J. Magnes. Alloy.*, vol. 6, no. 1, pp. 23–43, 2018, doi: 10.1016/j.jma.2018.02.003.

[141] J. Gonzalez, R. Q. Hou, E. P. S. Nidadavolu, R. Willumeit-Römer, and F. Feyerabend, "Magnesium degradation under physiological conditions – Best practice," *Bioact. Mater.*, vol. 3, no. 2, pp. 174–185, 2018, doi: 10.1016/j.bioactmat.2018.01.003.

[142] F. Witte *et al.*, "Degradable biomaterials based on magnesium corrosion," *Curr. Opin. Solid State Mater. Sci.*, vol. 12, no. 5, pp. 63–72, 2008, doi: 10.1016/j.cossms.2009.04.001.

[143] Y. Zheng, *Magnesium Alloys as Degradable Biomaterials*. Boca Raton: CRC Press, 2015.

[144] D. Tie, F. Feyerabend, N. Hort, R. Willumeit, and D. Hoeche, "XPS Studies of Magnesium Surfaces after Exposure to Dulbecco's Modified Eagle Medium, Hank's Buffered Salt Solution, and Simulated Body Fluid," *Adv. Eng. Mater.*, vol. 12, no. 12, pp. B699–B704, Dec. 2010, doi: 10.1002/adem.201080070.

[145] N. A. Agha, F. Feyerabend, B. Mihailova, S. Heidrich, U. Bismayer, and R. Willumeit-Römer, "Magnesium degradation influenced by buffering salts in concentrations typical of in vitro and in vivo models," *Mater. Sci. Eng. C*, vol. 58, pp. 817–825, 2016, doi: 10.1016/j.msec.2015.09.067.

[146] M. Rüegg, R. Blum, G. Boero, and J. Brugger, "Biodegradable Frequency-Selective Magnesium Radio-Frequency Microresonators for Transient Biomedical Implants," *Adv. Funct. Mater.*, vol. 29, no. 39, p. 1903051, Aug. 2019, doi: 10.1002/adfm.201903051.

[147] M. Tsang, A. Armutlulu, F. Herrault, R. H. Shafer, S. A. B. Allen, and M. G. Allen, "Development of Electroplated Magnesium Microstructures for Biodegradable Devices and Energy Sources," *J. Microelectromechanical Syst.*, vol. 23, no. 6, pp. 1281–1289, 2014, doi: 10.1109/JMEMS.2014.2360201.

[148] J. Koo *et al.*, "Wireless bioresorbable electronic system enables sustained nonpharmacological neuroregenerative therapy," *Nat. Med.*, vol. 24, no. 12, pp. 1830–1836, 2018, doi: 10.1038/s41591-018-0196-2.

[149] S. Virtanen, "Biodegradable Mg and Mg alloys: Corrosion and biocompatibility," *Mater. Sci. Eng. B*, vol. 176, no. 20, pp. 1600–1608, 2011, doi: 10.1016/j.mseb.2011.05.028.

[150] M. P. Staiger, A. M. Pietak, J. Huadmai, and G. Dias, "Magnesium and its alloys as orthopedic biomaterials: A review," *Biomaterials*, vol. 27, no. 9, pp. 1728–1734, 2006, doi: 10.1016/j.biomaterials.2005.10.003.

[151] O. Jung *et al.*, "Improved In Vitro Test Procedure for Full Assessment of the Cytocompatibility of Degradable Magnesium Based on ISO 10993-5/-12," *Int. J. Mol. Sci.*, vol. 20, no. 2, p. 255, Jan. 2019, doi: 10.3390/ijms20020255.

[152] J. Wang *et al.*, "Recommendation for modifying current cytotoxicity testing standards for biodegradable magnesium-based materials," *Acta Biomater.*, vol. 21, pp. 237–249, 2015, doi: 10.1016/j.actbio.2015.04.011.

[153] J.-M. Seitz, M. Durisin, J. Goldman, and J. W. Drelich, "Recent Advances in Biodegradable Metals for Medical Sutures: A Critical Review," *Adv. Healthc. Mater.*, vol. 4, no. 13, pp. 1915–1936, Sep. 2015, doi: 10.1002/adhm.201500189.

[154] H. Li, Y. Zheng, and L. Qin, "Progress of biodegradable metals," *Prog. Nat. Sci. Mater. Int.*, vol. 24, no. 5, pp. 414–422, 2014, doi: 10.1016/j.pnsc.2014.08.014.

[155] M. Peuster *et al.*, "A novel approach to temporary stenting: degradable cardiovascular stents produced from corrodible metal—results 6–18 months after implantation into

New Zealand white rabbits," *Heart*, vol. 86, no. 5, pp. 563–569, Nov. 2001, doi: 10.1136/heart.86.5.563.

[156]   M. Peuster, C. Hesse, T. Schloo, C. Fink, P. Beerbaum, and C. von Schnakenburg, "Long-term biocompatibility of a corrodible peripheral iron stent in the porcine descending aorta," *Biomaterials*, vol. 27, no. 28, pp. 4955–4962, 2006, doi: 10.1016/j.biomaterials.2006.05.029.

[157]   F. Zivic *et al.*, "Biodegradable Metals as Biomaterials for Clinical Practice: Iron-Based Materials," in *Biomaterials in Clinical Practice: Advances in Clinical Research and Medical Devices*, F. Zivic, S. Affatato, M. Trajanovic, M. Schnabelrauch, N. Grujovic, and K. L. Choy, Eds. Cham: Springer International Publishing, 2018, pp. 225–280.

[158]   R. Gorejová, L. Haverová, R. Oriňaková, A. Oriňak, and M. Oriňak, "Recent advancements in Fe-based biodegradable materials for bone repair," *J. Mater. Sci.*, vol. 54, no. 3, pp. 1913–1947, 2019, doi: 10.1007/s10853-018-3011-z.

[159]   B. L. Vallee and K. H. Falchuk, "The biochemical basis of zinc physiology," *Physiol. Rev.*, vol. 73, no. 1, pp. 79–118, Jan. 1993, doi: 10.1152/physrev.1993.73.1.79.

[160]   R. A. McCance and E. M. Widdowson, "The absorption and excretion of zinc," *Biochem. J.*, vol. 36, no. 7–9, pp. 692–696, Sep. 1942.

[161]   D. Vojtěch, J. Kubásek, J. Šerák, and P. Novák, "Mechanical and corrosion properties of newly developed biodegradable Zn-based alloys for bone fixation," *Acta Biomater.*, vol. 7, no. 9, pp. 3515–3522, 2011, doi: 10.1016/j.actbio.2011.05.008.

[162]   Institute of Medicine (US), *Dietary Reference Intakes for Vitamin A, Vitamin K, Arsenic, Boron, Chromium, Copper, Iodine, Iron, Manganese, Molybdenum, Nickel, Silicon, Vanadium, and Zinc*. Washington, DC: The National Academies Press, 2001.

[163]   G. Katarivas Levy, J. Goldman, and E. Aghion, "The Prospects of Zinc as a Structural Material for Biodegradable Implants—A Review Paper," *Metals*, vol. 7, no. 10. pp. 1–18, 2017, doi: 10.3390/met7100402.

[164]   K. Törne, M. Larsson, A. Norlin, and J. Weissenrieder, "Degradation of zinc in saline solutions, plasma, and whole blood," *J. Biomed. Mater. Res. Part B Appl. Biomater.*, vol. 104, no. 6, pp. 1141–1151, Aug. 2016, doi: 10.1002/jbm.b.33458.

[165]   J. Ma, N. Zhao, and D. Zhu, "Bioabsorbable zinc ion induced biphasic cellular responses in vascular smooth muscle cells," *Sci. Rep.*, vol. 6, p. 26661, Jun. 2016, doi: 10.1038/srep26661.

[166]   J. Venezuela and M. S. Dargusch, "The influence of alloying and fabrication techniques on the mechanical properties, biodegradability and biocompatibility of zinc: A comprehensive review," *Acta Biomater.*, vol. 87, pp. 1–40, 2019, doi: 10.1016/j.actbio.2019.01.035.

[167]   Y. Su *et al.*, "Zinc-Based Biomaterials for Regeneration and Therapy," *Trends Biotechnol.*, vol. 37, no. 4, pp. 428–441, Apr. 2019, doi: 10.1016/j.tibtech.2018.10.009.

[168]   R. Hille, T. Nishino, and F. Bittner, "Molybdenum enzymes in higher organisms," *Coord. Chem. Rev.*, vol. 255, no. 9–10, pp. 1179–1205, May 2011, doi: 10.1016/j.ccr.2010.11.034.

[169]   A. Vyskočil and C. Viau, "Assessment of molybdenum toxicity in humans," *J. Appl. Toxicol.*, vol. 19, no. 3, pp. 185–192, May 1999, doi: 10.1002/(SICI)1099-1263(199905/06)19:3<185::AID-JAT555>3.0.CO;2-Z.

[170]   J. R. Turnlund, W. R. Keyes, and G. L. Peiffer, "Molybdenum absorption, excretion, and retention studied with stable isotopes in young men at five intakes of dietary molybdenum," *Am. J. Clin. Nutr.*, vol. 62, no. 4, pp. 790–796, 1995, doi: 10.1093/ajcn/62.4.790.

[171]   C. H. Lee *et al.*, "Biological lipid membranes for on-demand, wireless drug delivery from thin, bioresorbable electronic implants," *Npg Asia Mater.*, vol. 7, p. e227, Nov. 2015, doi: 10.1038/am.2015.114.

[172] M. A. Martínez and C. Guillén, "Comparison between large area dc-magnetron sputtered and e-beam evaporated molybdenum as thin film electrical contacts," *J. Mater. Process. Technol.*, vol. 143–144, pp. 326–331, 2003, doi: 10.1016/S0924-0136(03)00436-9.

[173] S. Saliterman, *Fundamentals of BioMEMS and Medical Microdevices*. SPIE - The International Society for Optical Engineering, 2006.

[174] F. Abulfotuh *et al.*, *Thin Film Technology Handbook*. McGraw-Hill, 1998.

[175] J. C. Alonso, A. Ortiz, and C. Falcony, "Low temperature SiO2 films deposited by plasma enhanced techniques," *Vacuum*, vol. 43, no. 8, pp. 843–847, 1992, doi: 10.1016/0042-207X(92)90149-Q.

[176] J. Schmitz, "Low temperature thin films for next-generation microelectronics," *Surf. Coatings Technol.*, vol. 343, pp. 83–88, 2018, doi: 10.1016/j.surfcoat.2017.11.013.

[177] N. D. Hoivik, J. W. Elam, R. J. Linderman, V. M. Bright, S. M. George, and Y. C. Lee, "Atomic layer deposited protective coatings for micro-electromechanical systems," *Sensors Actuators A Phys.*, vol. 103, no. 1, pp. 100–108, 2003, doi: 10.1016/S0924-4247(02)00319-9.

[178] K. Lahtinen, P. Maydannik, P. Johansson, T. Kääriäinen, D. C. Cameron, and J. Kuusipalo, "Utilisation of continuous atomic layer deposition process for barrier enhancement of extrusion-coated paper," *Surf. Coatings Technol.*, vol. 205, no. 15, pp. 3916–3922, 2011, doi: 10.1016/j.surfcoat.2011.02.009.

[179] J. Vanfleteren *et al.*, "Printed circuit board technology inspired stretchable circuits," *MRS Bull.*, vol. 37, no. 3, pp. 254–260, 2012, doi: 10.1557/mrs.2012.48.

[180] S. A. Patil and R. P. Yadav, "A Review of Issues Related to Copper Etchant," *IOSR J. Eng.*, vol. 04, no. 07, pp. 40–43, 2014.

[181] M. Toofan and J. Toofan, "A Brief Review of the Cleaning Process for Electronic Device Fabrication," in *Developments in Surface Contamination and Cleaning*, R. Kohli and K. L. Mittal, Eds. Oxford: William Andrew Publishing, 2015, pp. 185–212.

[182] S.-K. Kang *et al.*, "Biodegradable Thin Metal Foils and Spin-On Glass Materials for Transient Electronics," *Adv. Funct. Mater.*, vol. 25, no. 12, pp. 1789–1797, 2015, doi: 10.1002/adfm.201403469.

[183] V. R. Feig, H. Tran, and Z. Bao, "Biodegradable Polymeric Materials in Degradable Electronic Devices," *ACS Cent. Sci.*, vol. 4, no. 3, pp. 337–348, Mar. 2018, doi: 10.1021/acscentsci.7b00595.

[184] S. Verma, Gaganjot, J. Tripathi, M. Katiyar, and V. Verma, "Biodegradable photolithography compatible substrate for transparent transient electronics and flexible energy storage devices," *Appl. Mater. Today*, vol. 13, pp. 83–90, 2018, doi: 10.1016/j.apmt.2018.08.010.

[185] F. Umbrecht, M. Wendlandt, D. Juncker, C. Hierold, and J. Neuenschwander, "A wireless implantable passive strain sensor system," in *2005 IEEE Sensors*, 2005, p. 4, doi: 10.1109/ICSENS.2005.1597627.

[186] P. Anbukarasu, D. Sauvageau, and A. Elias, "Tuning the properties of polyhydroxybutyrate films using acetic acid via solvent casting," *Sci. Rep.*, vol. 5, p. 17884, Dec. 2015, doi: 10.1038/srep17884.

[187] Y. Tanaka and K. Yamashita, *Bioceramics and their Clinical Applications*. Woodhead Publishing Limited, 2008.

[188] H. Acar, S. Çınar, M. Thunga, M. R. Kessler, N. Hashemi, and R. Montazami, "Study of Physically Transient Insulating Materials as a Potential Platform for Transient Electronics and Bioelectronics," *Adv. Funct. Mater.*, vol. 24, no. 26, pp. 4135–4143, Jul. 2014, doi: 10.1002/adfm.201304186.

[189] S.-H. Jeong, J.-K. Kim, B.-S. Kim, S.-H. Shim, and B.-T. Lee, "Characterization of SiO2 and TiO2 films prepared using RF magnetron sputtering and their application to anti-

reflection coating," *Vacuum*, vol. 76, no. 4, pp. 507–515, 2004, doi: 10.1016/j.vacuum.2004.06.003.

[190] S. M. Rossnagel, "Thin film deposition with physical vapor deposition and related technologies," *J. Vac. Sci. Technol. A*, vol. 21, no. 5, pp. S74–S87, Sep. 2003, doi: 10.1116/1.1600450.

[191] R. Li, L. Wang, and L. Yin, "Materials and Devices for Biodegradable and Soft Biomedical Electronics," *Mater. (Basel, Switzerland)*, vol. 11, no. 11, p. 2108, Oct. 2018, doi: 10.3390/ma11112108.

[192] G. E. Stan *et al.*, "Bioactive glass thin films deposited by magnetron sputtering technique: The role of working pressure," *Appl. Surf. Sci.*, vol. 256, no. 23, pp. 7102–7110, 2010, doi: 10.1016/j.apsusc.2010.05.035.

[193] G. E. Stan *et al.*, "Highly adherent bioactive glass thin films synthetized by magnetron sputtering at low temperature," *J. Mater. Sci. Mater. Med.*, vol. 22, no. 12, pp. 2693–2710, 2011, doi: 10.1007/s10856-011-4441-1.

[194] M. Spindler *et al.*, "Chemical etching of Tungsten thin films for high-temperature surface acoustic wave-based sensor devices," *Thin Solid Films*, vol. 612, pp. 322–326, 2016, doi: 10.1016/j.tsf.2016.04.035.

[195] T. O. Kääriäinen, P. Maydannik, D. C. Cameron, K. Lahtinen, P. Johansson, and J. Kuusipalo, "Atomic layer deposition on polymer based flexible packaging materials: Growth characteristics and diffusion barrier properties," *Thin Solid Films*, vol. 519, no. 10, pp. 3146–3154, 2011, doi: 10.1016/j.tsf.2010.12.171.

[196] K. Lahtinen, P. Johansson, T. Kääriäinen, and D. C. Cameron, "Adhesion of extrusion-coated polymer sealing layers to a fiber-based packaging material with an atomic layer deposited aluminum oxide surface coating," *Polym. Eng. Sci.*, vol. 52, no. 9, pp. 1985–1990, Sep. 2012, doi: 10.1002/pen.23148.

[197] S. M. Won *et al.*, "Natural Wax for Transient Electronics," *Adv. Funct. Mater.*, vol. 28, no. 32, p. 1801819, Aug. 2018, doi: 10.1002/adfm.201801819.

[198] F. Xie *et al.*, "Backbone-Degradable Polymers Prepared by Chemical Vapor Deposition," *Angew. Chemie Int. Ed.*, vol. 56, no. 1, pp. 203–207, Jan. 2017, doi: 10.1002/anie.201609307.

[199] S.-W. Hwang *et al.*, "Materials for Bioresorbable Radio Frequency Electronics," *Adv. Mater.*, vol. 25, no. 26, pp. 3526–3531, 2013, doi: 10.1002/adma.201300920.

[200] A. Palmroth, T. Salpavaara, I. Lyyra, M. Kroon, J. Lekkala, and M. Kellomäki, "Bioresorbable conductive wire with minimal metal content," *ACS Biomater. Sci. Eng.*, vol. 5, no. 2, pp. 1134–1140, Dec. 2018, doi: 10.1021/acsbiomaterials.8b01292.

[201] Peter M. Martin, *Handbook of Deposition Technologies for Films and Coatings: Science, Applications and Technology*. William Andrew, 2009.

[202] C. J. Lee, C. H. Hsieh, H. S. Huang, and J. C. Huang, "Improved mechanical properties of sputtered and evaporated Zn films deposited on a flexible substrate with an adhesive layer of amorphous ZrCu film," *Scr. Mater.*, vol. 69, no. 1, pp. 5–8, 2013, doi: 10.1016/j.scriptamat.2013.03.024.

[203] R. Kuzel, V. Valvoda, M. Chládek, J. Musil, and J. Matous, "XRD microstructural study of Zn films deposited by unbalanced magnetron sputtering," *Thin Solid Films*, vol. 263, no. 2, pp. 150–158, 1995, doi: 10.1016/0040-6090(95)06575-X.

[204] A. K. Abduev *et al.*, "Gas-phase clusterization of zinc during magnetron sputtering," *Crystallogr. Reports*, vol. 62, no. 1, pp. 133–138, 2017, doi: 10.1134/S1063774517010023.

[205] X. Huang *et al.*, "Biodegradable Materials for Multilayer Transient Printed Circuit Boards," *Adv. Mater.*, vol. 26, no. 43, pp. 7371–7377, Nov. 2014, doi: 10.1002/adma.201403164.

[206] B. K. Mahajan, X. Yu, W. Shou, H. Pan, and X. Huang, "Mechanically Milled Irregular

Zinc Nanoparticles for Printable Bioresorbable Electronics," *Small*, vol. 13, no. 17, p. 1700065, May 2017, doi: 10.1002/smll.201700065.

[207]   W. Shou *et al.*, "Low-Cost Manufacturing of Bioresorbable Conductors by Evaporation–Condensation-Mediated Laser Printing and Sintering of Zn Nanoparticles," *Adv. Mater.*, vol. 29, no. 26, p. 1700172, Jul. 2017, doi: 10.1002/adma.201700172.

[208]   S. Lee *et al.*, "Metal microparticle – Polymer composites as printable, bio/ecoresorbable conductive inks," *Mater. Today*, vol. 21, no. 3, pp. 207–215, 2018, doi: 10.1016/j.mattod.2017.12.005.

[209]   M. Tsang, F. Herrault, R. H. Shafer, and M. G. Allen, "Methods for the microfabrication of magnesium," in *2013 IEEE 26th International Conference on Micro Electro Mechanical Systems (MEMS)*, 2013, pp. 347–350, doi: 10.1109/MEMSYS.2013.6474249.

[210]   T. Jurgeleit, E. Quandt, and C. Zamponi, "Magnetron sputtering a new fabrication method of iron based biodegradable implant materials," *Adv. Mater. Sci. Eng.*, vol. 2015, p. 9, 2015, doi: 10.1155/2015/294686.

[211]   B. Finamore *et al.*, "Development of an Implantable Biodegradable Electrical Stimulator for Bone Repair - Poster in Biomedical Engineering Society Fall Meeting 2009," 2009.

[212]   C. M. Boutry, H. Chandrahalim, P. Streit, M. Schinhammer, A. C. Hänzi, and C. Hierold, "Towards biodegradable wireless implants," *Philos. Trans. R. Soc. A Math. Phys. Eng. Sci.*, vol. 370, no. 1967, pp. 2418–2432, Apr. 2012, doi: 10.1098/rsta.2011.0439.

[213]   H. Tao *et al.*, "Silk-based resorbable electronic devices for remotely controlled therapy and in vivo infection abatement," *Proc. Natl. Acad. Sci. USA*, vol. 111, no. 49, pp. 17385–17389, Dec. 2014, doi: 10.1073/pnas.1407743111.

[214]   H. Li *et al.*, "Biodegradable Flexible Electronic Device with Controlled Drug Release for Cancer Treatment," *ACS Appl. Mater. Interfaces*, vol. 13, no. 18, pp. 21067–21075, Apr. 2021, doi: 10.1021/acsami.1c04653.

[215]   Y. K. Lee, J. Kim, Y. Kim, J. W. Kwak, Y. Yoon, and J. A. Rogers, "Room Temperature Electrochemical Sintering of Zn Microparticles and Its Use in Printable Conducting Inks for Bioresorbable Electronics," *Adv. Mater.*, vol. 29, no. 38, p. 1702665, Oct. 2017, doi: 10.1002/adma.201702665.

[216]   J. Massera, S. Fagerlund, L. Hupa, and M. Hupa, "Crystallization Mechanism of the Bioactive Glasses, 45S5 and S53P4," *J. Am. Ceram. Soc.*, vol. 95, no. 2, pp. 607–613, Feb. 2012, doi: 10.1111/j.1551-2916.2011.05012.x.

[217]   C. X. F. Lam, D. W. Hutmacher, J.-T. Schantz, M. A. Woodruff, and S. H. Teoh, "Evaluation of polycaprolactone scaffold degradation for 6 months in vitro and in vivo," *J. Biomed. Mater. Res. Part A*, vol. 90A, no. 3, pp. 906–919, Jul. 2008, doi: 10.1002/jbm.a.32052.

[218]   W. Kueng, E. Silber, and U. Eppenberger, "Quantification of cells cultured on 96-well plates," *Anal. Biochem.*, vol. 182, no. 1, pp. 16–19, 1989, doi: 10.1016/0003-2697(89)90710-0.

[219]   S. Miettinen *et al.*, "Role of 24-hydroxylase in vitamin D3 growth response of OVCAR-3 ovarian cancer cells," *Int. J. Cancer*, vol. 108, no. 3, pp. 367–373, Jan. 2004, doi: 10.1002/ijc.11520.

[220]   M. Baù, M. Demori, M. Ferrari, and V. Ferrari, "Contactless Readout of Passive LC Sensors with Compensation Circuit for Distance-Independent Measurements," *Proceedings of Eurosensors 2018*, vol. 2, no. 13. 2018, doi: 10.3390/proceedings2130842.

[221]   M. Kaya, "Recovery of Metals and Nonmetals from Waste Printed Circuit Boards (PCBs) by Physical Recycling Techniques," in *Energy Technology 2017*, L. Zhang, J. W. Drelich, N. R. Neelameggham, D. P. Guillen, N. Haque, J. Zhu, Z. Sun, T. Wang, J. A. Howarter, F. Tesfaye, S. Ikhmayies, E. Olivetti, and M. W. Kennedy, Eds. Cham: Springer International Publishing, 2017, pp. 433–451.

[222] A. Yousaf, F. A. Khan, and L. M. Reindl, "Passive Wireless Sensing of Micro coil parameters in fluidic environments," *Sensors Actuators, A Phys.*, vol. 186, pp. 69–79, 2012, doi: 10.1016/j.sna.2012.01.032.

[223] C. Collins, "Miniature Passive Pressure Transensor for Implanting in the Eye," *IEEE Trans. Biomed. Eng.*, vol. BME-14, no. 2, pp. 74–83, 1967, doi: 10.1109/TBME.1967.4502474.

[224] J. F. Drazan *et al.*, "Archimedean Spiral Pairs with no Electrical Connections as a Passive Wireless Implantable Sensor," *J. Biomed. Technol. Res.*, vol. 1, no. 1, 2014.

[225] F. Wang, X. Zhang, M. Shokoueinejad, B. J. Iskandar, J. G. Webster, and J. E. Medow, "Spiral planar coil design for the intracranial pressure sensor," *Med. Devices Sensors*, vol. 1, no. 3, p. e10012, Jun. 2018, doi: 10.1002/mds3.10012.

[226] M. A. Brenckle *et al.*, "Methods and Applications of Multilayer Silk Fibroin Laminates Based on Spatially Controlled Welding in Protein Films," *Adv. Funct. Mater.*, vol. 26, no. 1, pp. 44–50, Jan. 2016, doi: 10.1002/adfm.201502819.

[227] Q. Zheng *et al.*, "Biodegradable triboelectric nanogenerator as a life-time designed implantable power source," *Sci. Adv.*, vol. 2, no. 3, p. e1501478, Mar. 2016, doi: 10.1126/sciadv.1501478.

[228] S. Morishita, M. Kubota, and Y. Mita, "A blur-range test structure of collimation-controller-integrated silicon shadow mask for three-dimensional surface patterning with sputtering," in *2012 IEEE International Conference on Microelectronic Test Structures*, 2012, pp. 66–70, doi: 10.1109/ICMTS.2012.6190615.

[229] D. Lu *et al.*, "Bioresorbable Wireless Sensors as Temporary Implants for In Vivo Measurements of Pressure," *Adv. Funct. Mater.*, vol. 30, no. 40, p. 2003754, Oct. 2020, doi: 10.1002/adfm.202003754.

[230] G. Y. H. Choong and D. S. A. De Focatiis, "A method for the determination and correction of the effect of thermal degradation on the viscoelastic properties of degradable polymers," *Polym. Degrad. Stab.*, vol. 130, pp. 182–188, 2016, doi: 10.1016/j.polymdegradstab.2016.06.018.

[231] K. Paakinaho, V. Ellä, S. Syrjälä, and M. Kellomäki, "Melt spinning of poly(l/d)lactide 96/4: Effects of molecular weight and melt processing on hydrolytic degradation," *Polym. Degrad. Stab.*, vol. 94, no. 3, pp. 438–442, 2009, doi: 10.1016/j.polymdegradstab.2008.11.010.

[232] K. Paakinaho, H. Heino, J. Väisänen, P. Törmälä, and M. Kellomäki, "Effects of lactide monomer on the hydrolytic degradation of poly(lactide-co-glycolide) 85L/15G," *J. Mech. Behav. Biomed. Mater.*, vol. 4, no. 7, pp. 1283–1290, 2011, doi: 10.1016/j.jmbbm.2011.04.015.

[233] K. Paakinaho, H. Heino, M. Pelto, M. Hannula, P. Törmälä, and M. Kellomäki, "Programmed water-induced shape-memory of bioabsorbable poly(d,l-lactide): activation and properties in physiological temperature," *J. Mater. Sci. Mater. Med.*, vol. 23, no. 3, pp. 613–621, 2012, doi: 10.1007/s10856-011-4538-6.

[234] T. Salpavaara, A. Hänninen, A. Antniemi, J. Lekkala, and M. Kellomäki, "Non-destructive and wireless monitoring of biodegradable polymers," *Sensors Actuators B Chem.*, vol. 251, pp. 1018–1025, 2017, doi: 10.1016/j.snb.2017.05.116.

[235] M. Correlo, Vitor, D. Pinho, Elisabete, I. Pashkuleva, M. Bhattacharya, M. Neves, Nuno, and L. Reis, Rui, "Water Absorption and Degradation Characteristics of Chitosan-Based Polyesters and Hydroxyapatite Composites," *Macromol. Biosci.*, vol. 7, no. 3, pp. 354–363, Mar. 2007, doi: 10.1002/mabi.200600233.

[236] A. Waygood, *An Introduction to Electrical Science*, 1st ed. Routledge, 2013.

[237] C. H. Lee *et al.*, "Wireless Microfluidic Systems for Programmed, Functional Transformation of Transient Electronic Devices," *Adv. Funct. Mater.*, vol. 25, no. 32, pp.

5100–5106, Aug. 2015, doi: 10.1002/adfm.201502192.

[238] Z. Awang, *Microwave Systems Design*. Springer Science & Business Media, 2013.

[239] F. Moens, I. C. Schramm, S. Konstantinidis, and D. Depla, "On the microstructure of magnesium thin films deposited by magnetron sputtering," *Thin Solid Films*, vol. 689, p. 137501, 2019, doi: 10.1016/j.tsf.2019.137501.

[240] L.-C. Chao, C.-F. Lin, and C.-C. Liau, "Effect of surface morphology of metallic zinc films deposited by ion beam sputter deposition on the formation of ZnO nanowires," *Vacuum*, vol. 86, no. 3, pp. 295–298, 2011, doi: 10.1016/j.vacuum.2011.06.020.

[241] Y. Ding, C. Wen, P. Hodgson, and Y. Li, "Effects of alloying elements on the corrosion behavior and biocompatibility of biodegradable magnesium alloys: a review," *J. Mater. Chem. B*, vol. 2, no. 14, pp. 1912–1933, 2014, doi: 10.1039/C3TB21746A.

[242] H. Hermawan, "Updates on the research and development of absorbable metals for biomedical applications," *Prog. Biomater.*, vol. 7, no. 2, pp. 93–110, Jun. 2018, doi: 10.1007/s40204-018-0091-4.

[243] S. Johnston, M. Dargusch, and A. Atrens, "Building towards a standardised approach to biocorrosion studies: a review of factors influencing Mg corrosion in vitro pertinent to in vivo corrosion," *Sci. China Mater.*, vol. 61, no. 4, pp. 475–500, 2018, doi: 10.1007/s40843-017-9173-7.

[244] L. Yang, N. Hort, R. Willumeit, and F. Feyerabend, "Effects of corrosion environment and proteins on magnesium corrosion," *Corros. Eng. Sci. Technol.*, vol. 47, no. 5, pp. 335–339, Aug. 2012, doi: 10.1179/1743278212Y.0000000024.

[245] E. Mouzou *et al.*, "CO2-rich atmosphere strongly affects the degradation of Fe-21Mn-1C for biodegradable metallic implants," *Mater. Lett.*, vol. 181, pp. 362–366, 2016, doi: 10.1016/j.matlet.2016.06.017.

[246] S. Höhn, S. Virtanen, and A. R. Boccaccini, "Protein adsorption on magnesium and its alloys: A review," *Appl. Surf. Sci.*, vol. 464, pp. 212–219, 2019, doi: 10.1016/j.apsusc.2018.08.173.

[247] R. Hou, F. Feyerabend, and R. Willumeit-Römer, "Proteins and medium-flow conditions: how they influence the degradation of magnesium," *Surf. Innov.*, vol. 8, no. 4, pp. 224–233, 2020, doi: 10.1680/jsuin.19.00064.

[248] L. Y. Chen *et al.*, "Continuous wireless pressure monitoring and mapping with ultra-small passive sensors for health monitoring and critical care," *Nat. Commun.*, vol. 5, p. 5028, Oct. 2014, doi: 10.1038/ncomms6028.

[249] T. Salpavaara, A. Antniemi, A. Hänninen, J. Lekkala, and M. Kellomäki, "Inductively coupled passive resonance sensor for monitoring biodegradable polymers in vitro," in *Procedia Engineering*, 2016, pp. 1304–1307, doi: 10.1016/j.proeng.2016.11.353.

[250] C. X. F. Lam, M. M. Savalani, S.-H. Teoh, and D. W. Hutmacher, "Dynamics of in vitro polymer degradation of polycaprolactone-based scaffolds: accelerated versus simulated physiological conditions," *Biomed. Mater.*, vol. 3, no. 3, p. 34108, 2008, doi: 10.1088/1748-6041/3/3/034108.

[251] Q. Yang *et al.*, "Materials, Mechanics Designs, and Bioresorbable Multisensor Platforms for Pressure Monitoring in the Intracranial Space," *Adv. Funct. Mater.*, vol. 30, no. 17, p. 1910718, Mar. 2020, doi: 10.1002/adfm.201910718.

[252] D. Noviana, D. Paramitha, M. F. Ulum, and H. Hermawan, "The effect of hydrogen gas evolution of magnesium implant on the postimplantation mortality of rats," *J. Orthop. Transl.*, vol. 5, pp. 9–15, 2016, doi: 10.1016/j.jot.2015.08.003.

[253] L. Liu *et al.*, "Degradation Rates of Pure Zinc, Magnesium, and Magnesium Alloys Measured by Volume Loss, Mass Loss, and Hydrogen Evolution," *Applied Sciences*, vol. 8, no. 9. 2018, doi: 10.3390/app8091459.

PUBLICATIONS

Publication I   Salpavaara, T.*, Hänninen, A.*, Antniemi, A., Lekkala, J., Kellomäki, M. Non-destructive and Wireless Monitoring of Biodegradable Polymers. Sensors and Actuators B: Chemical (2017) 251, 1018-1025.

Publication II   Palmroth, A., Salpavaara, T., Lyyra, I., Kroon, M., Lekkala, J., Kellomäki, M. Bioresorbable Conductive Wire with Minimal Metal Content. ACS Biomaterials Science & Engineering (2018) 5, 1134-1140.

Publication III   Palmroth, A., Salpavaara, T., Lekkala, J., Kellomäki, M. Fabrication and Characterization of a Wireless Bioresorbable Pressure Sensor. Advanced Materials Technologies (2019) 4, 1900428.

Publication IV   Palmroth, A., Salpavaara, T., Vuoristo, P., Karjalainen, S., Kääriäinen, T., Miettinen, S., Massera, J., Lekkala, J., Kellomäki, M. Materials and Orthopedic Applications for Bioresorbable Inductively Coupled Resonance Sensors. ACS Applied Materials & Interfaces (2020) 12, 31148–31161.

*These authors contributed equally

PUBLICATION
I

Non-destructive and Wireless Monitoring of Biodegradable Polymers

Timo Salpavaara*, Aleksi Hänninen*, Anni Antniemi, Jukka Lekkala,
Minna Kellomäki

ELSEVIER

SENSORS and ACTUATORS B Chemical

Non-destructive and wireless monitoring of biodegradable polymers

CrossMark

Timo Salpavaara [a],[1], Aleksi Hänninen [b],[*],[1], Anni Antniemi [b], Jukka Lekkala [a], Minna Kellomäki [b]

[a] BioMediTech Institute and Faculty of Biomedical Sciences and Engineering, Sensor Technology and Biomeasurements Group, Tampere University of Technology, Korkeakoulunkatu 10, Tampere 33720, Finland
[b] BioMediTech Institute and Faculty of Biomedical Sciences and Engineering, Biomaterials and Tissue Engineering Group, Tampere University of Technology, Korkeakoulunkatu 10, Tampere 33720, Finland

ARTICLE INFO

ABSTRACT

A method for monitoring changes in biodegradable polymers during hydrolysis is proposed. This wireless and non-destructive method is based on inductively coupled passive resonance sensors embedded in the polymer shell. In this study, we prepared specimens using two poly(lactide-co-glycolide) copolymers possessing different degradation profiles. The copolymer embedded sensors were immersed in buffer solution and their resonance features were compared with periodically performed conventional polymer characterization methods. A clear difference was noticed in the wirelessly measured signals between the two tested copolymer materials. Also the reference methods showed clear differences between the degradation profiles of the copolymers. The wirelessly measured signals are likely to correlate to the structural changes in the materials during the hydrolysis. In the future, this technique could be used in the laboratory to provide easy-to-access *in situ* information about the polymers. Even the state of biodegradable polymer implants could be wirelessly monitored.

© 2017 Elsevier B.V. All rights reserved.

1. Introduction

Implants made of biodegradable polymers are used as temporary support structures in orthopedics and tissue engineering. For example, different types of bone fractures can be repaired with biodegradable fixation plates and screws. Ultimately, these polymers are cleared from the body via metabolic routes. This prevents the need for removal operations as well as chronic inflammatory responses associated with biostable implants. The degradation rate of the implant is affected by many factors, including the chemical structure and molecular weight of the polymer as well as the processing history, size and shape of the implant. Even if all these elements were carefully standardized, different enzymatic systems between individuals or different target tissues in a patient might lead to diverse degradation rates [1]. Therefore, there is a need for monitoring the degradation rate of the polymers to ensure the proper behavior of the implants.

There are many well-defined characterization techniques for polymer degradation which can be carried out in the laboratory. Gel permeation chromatography (GPC, also called size exclusion chro-

matography, SEC) for example separates the polymer chains based on their length and thus determines the molecular weight distribution of the polymer [2], which is the most important parameter for tracking polymer degradation [3]. Differential scanning calorimetry (DSC) is a commonly used thermoanalytical technique: by using modern DSC, several parameters related to polymer degradation such as crystallinity and glass transition temperature can be determined. Furthermore, the mechanical properties of the polymers can be analyzed by applying e.g. shear, flexural and tensile tests. In many applications it is crucial for the implants to retain their mechanical properties before starting to transfer the stress to the surrounding tissue by degrading [4].

A common drawback of all of the above-mentioned methods is that they are destructive to the sample [2]. Thus, they are discontinuous and require a set of parallel samples at each time point. Moreover, the methods are not applicable to *in vivo* measurements. Consequently, a wireless and non-destructive method for monitoring the degradation of poly(lactide-co-glycolide)s has been studied based on a fluorescent labeling technique [5]. However, the use of costly imaging methods and fluorescent markers might compromise the cost-effectiveness and safety of the method.

Inductively coupled passive resonance sensors with interdigital capacitive sensing elements have been previously used to detect changes in various materials and applications. Ong et al. tested it as a general way to monitor many environmental parameters

* Corresponding author.
  E-mail address: aleksi.hanninen@tut.fi (A. Hänninen).
[1] Equal contribution authors.

Table 1
A list of the samples.

Encapsulation copolymer	Resonance sensor	Number of samples	Sample codes
PLGA	Yes	10	PLGA 1-10
PDLGA	Yes	10	PDLGA 1-10
PLGA	Yes (parylene coated)	2	PLGA P1-P2
PDLGA	Yes (parylene coated)	2	PDLGA P1-P2
PLGA reference samples	No	12	PLGA R1-R12
PDLGA reference samples	No	12	PDLGA R1-R12

like the temperature, humidity and complex permittivity of the surrounding material [6]. Applications for the method include the assessment of frying oil degradation [7] and water content in civil engineering materials [8]. Also an implantable sensor for tissue characterization has been proposed [9]. These types of sensors enable short range wireless measurements, which can be utilized in applications where the target to be measured is in a closed container or under the skin. Also the simple structure of the sensor is a benefit in *in vivo* applications, especially if the sensor should be fabricated from biodegradable materials.

A wireless online monitoring system capable of detecting day-to-day changes in biodegradable polymer materials could be used *in vitro* as an alternative to destructive and time consuming testing methods. Before using biodegradable sensor structures like presented in [10], we aim to acquire background information about the suitability of this measurement method for this application. Thus, we embedded inductively coupled passive resonance sensors into two biodegradable poly(lactide-co-glycolide)s with different degradation profiles to see if this kind of wireless measurement provides useful information about the degradation of these copolymers.

2. Materials and methods

The degradation of two copolymer materials in buffer solution was investigated for eight weeks. A reference degradation series was done using conventional polymer characterization methods. The other set of samples was wirelessly monitored utilizing inductively coupled passive resonance sensors embedded in the tested copolymers. The measured signals were then compared with the results of the reference series. The method is based on detecting changes in the relative permittivity of the material during hydrolysis by using interdigital capacitors. The capacitors were connected to RLC circuits whose characteristics were measured outside the container.

2.1. Resonance sensor

The resonance sensors used in this study were fabricated using a four-layer circuit board design. The 20 mm by 20 mm by 1.60 mm sized inductively coupled sensors (Fig. 1) comprised an interdigital capacitive sensing structure, a parallel-plate capacitor, and a coil. The operation principle of this sensor is similar to methods discussed in [6,9]. The measurable resonance characteristics of the sensor are modified by the permittivity and conductivity of the tested material. The geometry of the sensor was not optimized or studied in detail due to the different focus of this study.

The total number of fingers in the capacitor was 24. The copper layer thickness was 35 μm. The fabrication process of the printed circuit board (PCB) included an electrically isolating solder resist layer (approximately 30–40 μm) on top of conductive areas.

Due to the noticed variation in the regular sensor series, four sensors were coated by polymerizing an approximately 14 μm thick layer of parylene C (Galxyl C, Galentis S.r.l., Marcon, Italy) onto them using a LabTop 3000 Parylene Deposition System (Para
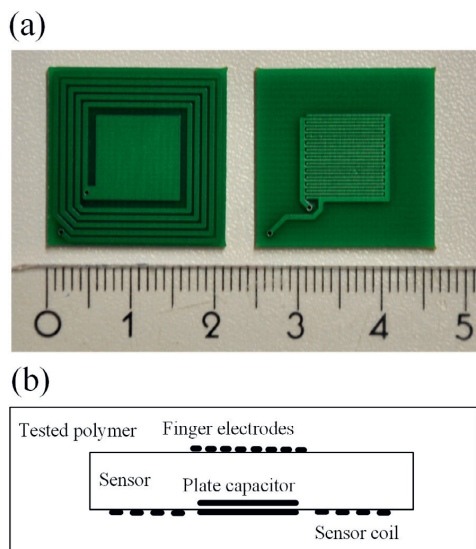

Fig. 1. (a) RLC resonance circuits with interdigital capacitive sensing elements were used to monitor biodegradable polymers. (b) The cross-section of the encapsulated sensor.

Tech, Aliso Viejo, California, USA) to increase the consistency of the measurements.

2.2. Sensor encapsulation and hydrolysis

Hydrolytically degradable poly(lactide-co-glycolide)s are commonly copolymerized from D,L-lactide or L,L-lactide together with glycolide [11]. Amorphous poly(L-lactide-co-glycolide) [80:20] (PLGA) and poly(DL-lactide-co-glycolide) [85:15] (PDLGA) were both obtained from Purac Biochem B.V. (Gorinchem, the Netherlands). The tested copolymer types were chosen based on their different degradation rates, as the presence of D-units into the poly(L-lactide) chain is known to increase the degradation rate [12]. Thus, the degradation of PDLGA was expected to be faster than that of PLGA.

After drying the materials in a vacuum chamber, copolymer sheets of 32 mm by 32 mm by 2 mm were compression molded from the raw material granules using a custom-made metallic mold. Seamless capsules were formed by placing one resonance sensor between two copolymer sheets and compression molding them into one piece (Fig. 1b). Two parylene coated sensors per copolymer type were encapsulated. The full list of all the samples is presented in Table 1.

Samples were fixed 1 mm above the bottom of the container by using plastic 3D printed holders. The amount of Sörensen phosphate buffer per container was 100 ml. The buffer solution was prepared according to the "ISO 15814:1999(E): Implants for surgery
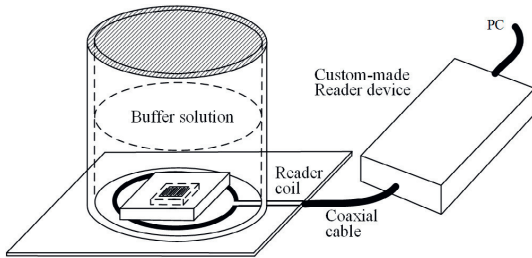
Fig. 2. The measurement of the resonance sensor in a buffer solution container by using an external reader coil and a custom-made reader device.
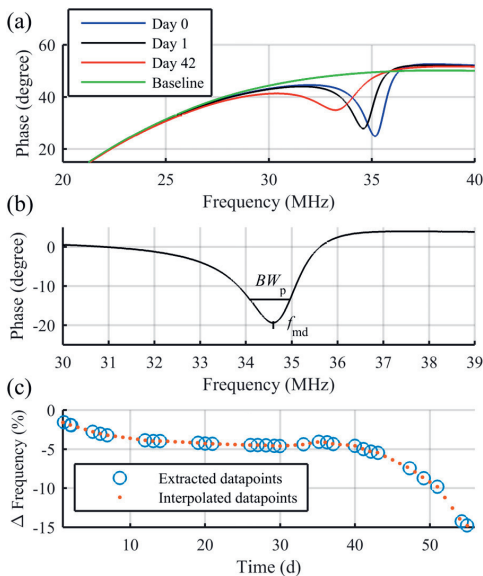

Fig. 3. (a) Examples of raw data measured at the beginning of the hydrolysis (Day 0), after one day, and after 42 days. The baseline of the measurement is also shown. (b) The features f_{md} and BW_p were extracted from the dip in the phase curve. (c) Illustration of interpolation of the data points.

– Copolymers and blends based on polylactide – *In vitro* degradation testing" standard and its pH was 7.46–7.49. All samples were held in an incubator at +37 °C and the buffer solution was changed every other week. Similar hydrolysis procedure was applied for the reference samples.

2.3. Conventional polymer tests for reference

Compression molding was also used to produce the reference test samples from both copolymer types. The reference samples were tested at the time points of 0, 2, 4, 6 and 8 weeks. This time period was assumed to show differences between the copolymers and the number of the parallel samples remained moderate. The 0-week samples were tested dry, whereas the rest were tested wet after taking them out from the buffer solution.

Water absorption measurements were done by taking the samples from the buffer solution, rinsing them with distilled water, wiping gently with tissue paper and then weighing them using an analytical scale. Four samples per material were measured at each time point. The resulting wet weights were then compared with the dry weights, that were measured after drying the samples for
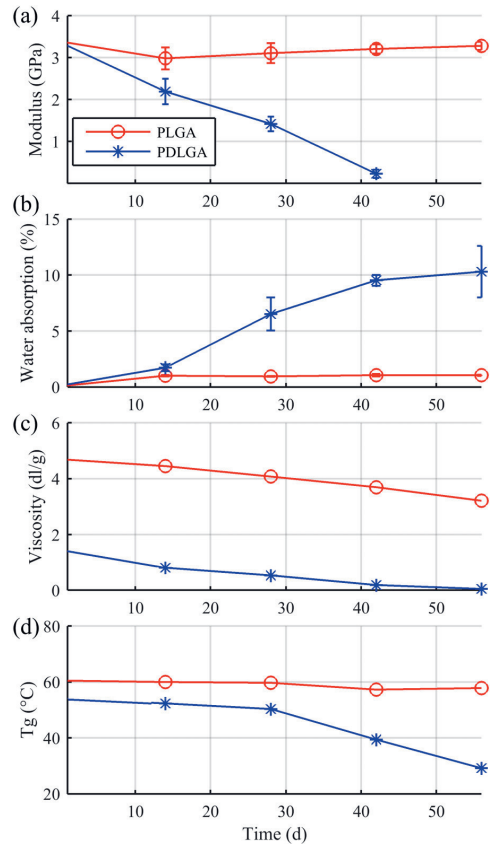

Fig. 4. Reference measurements indicating changes in the material properties of the copolymer samples. The two last graphs lack error bars, since only two parallel samples were measured in the *i.v.* and T_g tests.

three days under a fume hood and then one week in a vacuum chamber. The water absorption percentage was calculated using the equation: *water absorption* (%) = [(*wet weight* – *dry weight*)/*dry weight*] × 100%.

Mechanical testing comprehended three-point bending tests (Instron 4411, Intron Ltd., High Wycombe, England) according to the "SFS-EN ISO 178 Plastics – Determination of flexural properties" standard at ambient conditions. Four parallel samples per time point per material were tested. The mean values and standard deviations of the flexural modulus were calculated in gigapascals (GPa).

The glass transition temperature (T_g) of the samples was measured utilizing differential scanning calorimetry (DSC) (Q1000, TA Instruments, New Castle, Delaware, USA) by analyzing two parallel samples per time point. The T_g corresponds to a reversible transit from a glassy state to a more viscous state. At lower molecular weights, the T_g of poly(lactide-co-glycolide)s is a function of the molecular weight. A decrease in T_g indicates a decrease in molecular weight when at appropriate level, and thus T_g can be used to show the degradation of biodegradable polymers. Only amorphous polymers or the amorphous portions of semicrystalline polymers undergo the glass transition.

An automated Ubbelohde viscometer (LAUDA, Lauda-Königshofen, Germany) was used to assess the inherent viscosity
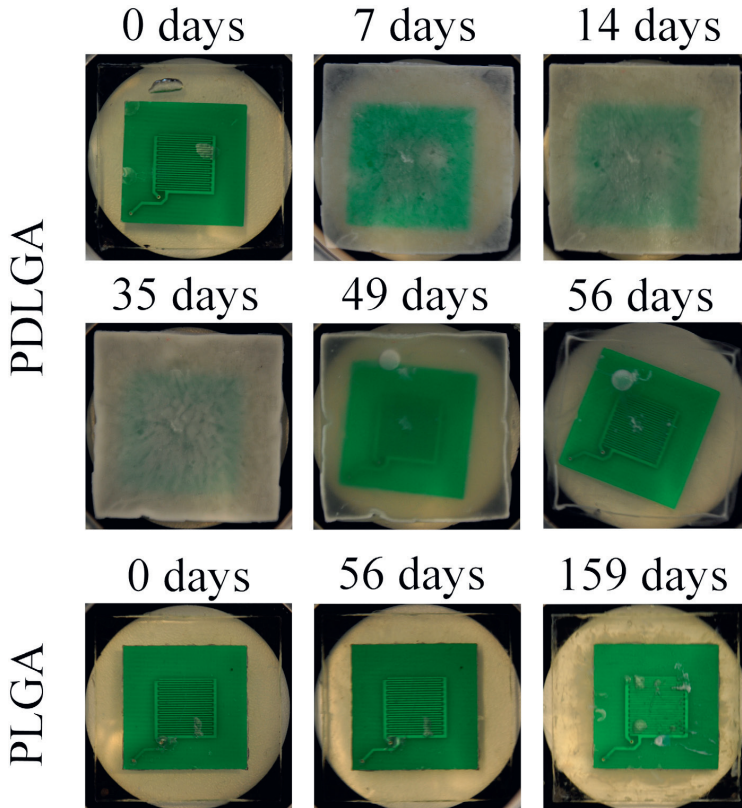
Fig. 5. A visual presentation of the copolymer capsule degradation at different time points, starting from the day when the buffer solution was added. The green sensor can be seen inside the capsules, which are held still with the black 3D printed holders. The last PLGA picture (159 days in buffer solution) is taken from a different sample than the two previous pictures.

(*i.v.*) of the copolymers, which is a viscometric measure of the molecular size utilizing the unit dl/g. After drying the samples, 20 ± 0.8 mg sized pieces were cut from the sample core and dissolved in 20 ml of chloroform overnight. The test was performed in ambient conditions and two parallel samples per time point were measured.

2.4. Resonance measurements

The resonance characteristics of the sensors were inductively measured by using a reader coil and custom-made reader device [13]. The illustration of the measurement arrangement is given in Fig. 2.

The reader device makes frequency sweeps and measures a phase shift against a reference channel. In this setup, the resonance circuit around the reader coil shows as a dip in the measured signal (Fig. 3a). The measurements in the lengthy test series were carried out during working days of the week at non-uniform intervals. Each test point consisted of the multiple frequency sweeps measured within 30 s at the sampling rate of one sweep per second. The frequency sweeps were first averaged and then the measured baseline of the reader coil was subtracted from the measurements.

Next, the resonance characteristics of the RLC circuit were extracted from the data. The feature extraction was done by modeling the measured dip by using a 3rd order polynomial regression model. The features f_{md} and BW_p used in the model, estimate the frequency and the width of the measured dip (Fig. 3b), respectively. The extraction process was similar to the method used in [14]. However, in this case, the measured phase signal was used instead of the measured gain signal because the form of the phase dip was more suitable for the feature extraction. Initially, all resonance circuits had slightly different resonance frequencies. Thus the phase changes were compared with the initial values at the beginning of the hydrolysis. The results of the inductively coupled measurements were given as a change in the features f_{md} and BW_p which are linked to the resonance frequency and losses of the RLC circuit. The average signal for each copolymer type was calculated after interpolating daily estimates for each sample (Fig. 3c).

3. Results

3.1. Conventional polymer characterization methods

The conventional polymer testing methods were used to get reference signals indicating the hydrolytic degradation of the tested copolymers. The changes in the flexural modulus, water absorption percentage, inherent viscosity (*i.v.*) and glass transition temperature (T_g) of the biodegradable copolymers are shown in Fig. 4.

After the second week follow-up, PLGA samples were saturated and did not absorb more water during the test period. PLGA also retained its mechanical properties (the flexural modulus indicates the stiffness of the material). However, the decreasing *i.v.* values
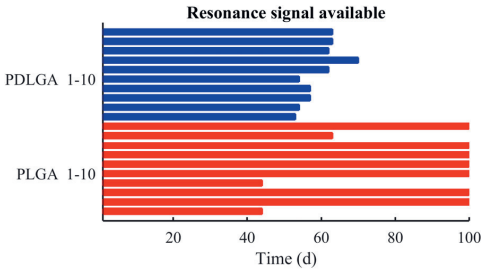
Fig. 6. A diagram showing the availability of the resonance signals of each individual PDLGA and PLGA encapsulated sensors.

indicated that the molecule chains were cleaved due to the presence of water. Also the *i.v.* values of PDLGA decreased throughout the test period. As the hydrolysis proceeded, the values decreased to such a low level, that drawing detailed conclusions becomes difficult. In addition, PDLGA lost its mechanical properties completely already after six weeks. The water absorption of PDLGA was noticed to increase rapidly after the second week follow-up. The T_g of PDLGA was detected to decrease sharply between the 4- and 6-week follow-ups, whereas this was not observed in the case of PLGA.

A visual illustration of the degradation of PDLGA and PLGA is presented in Fig. 5. The clear PDLGA copolymer turned into a white, opaque block soon after starting the hydrolysis. After a few weeks, it started to lose its original shape. The swelling phase occurred later, followed by bursting of the capsule, leaving only a thin copolymer film behind. On the contrary, the dimensions of the PLGA samples were hardly changed during eight weeks in buffer solution.
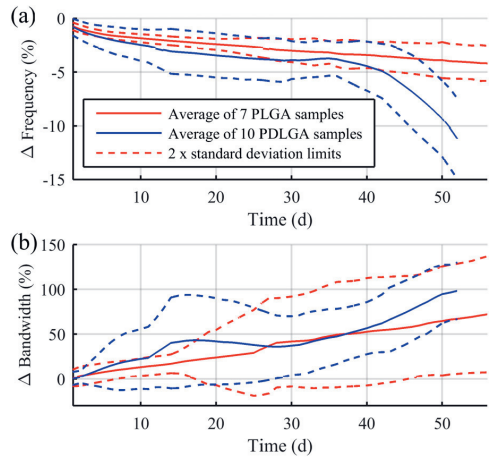

Fig. 7. The average of the changes in the feature f_{md} and (b) BW_p during the test period.

Cracks were noticed in the PLGA samples after prolonged hydrolysis indicating the progress of degradation.

3.2. Resonance measurements

The measured phase dip diminished as the hydrolysis progressed (Fig. 3a). The days when the signal from each individual sample was detectable are illustrated in Fig. 6. The resonance signal of the PDLGA samples faded to an undetectable level after most of the copolymer had dissolved after seven weeks. In general, the
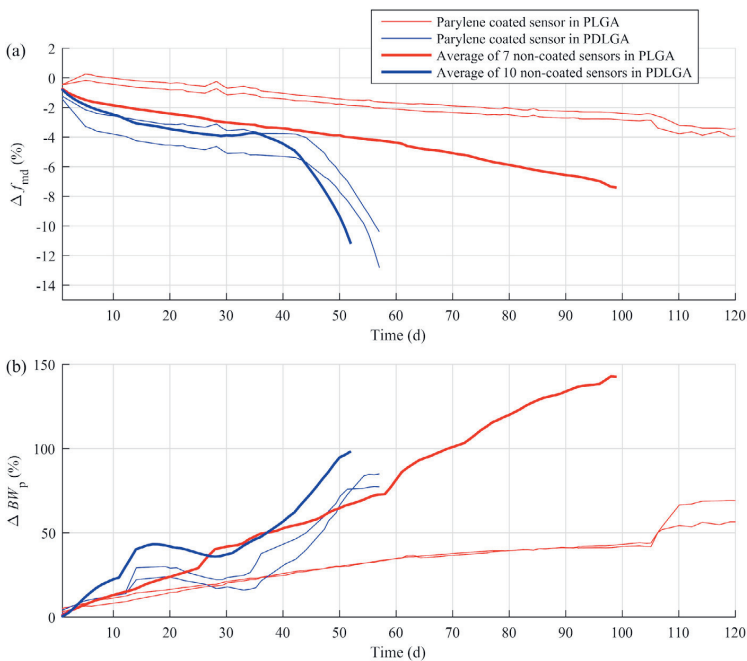

Fig. 8. The resonance features (f_{md} and BW_p) of two parallel parylene coated sensors encapsulated in PLGA and PDLGA. The averages of the non-coated sensors are presented for comparison.
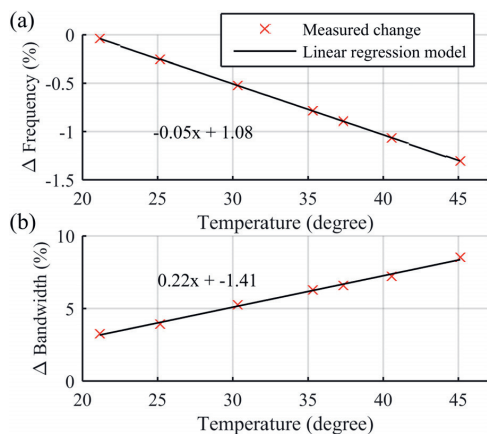
Fig. 9. The change of (a) resonance frequency (f_{md}) and (b) bandwidth (BW_p) as a function of temperature.

sensors in PLGA were detectable over 100 days. Three samples in PLGA samples were noticed to stop providing adequate resonance signals already after six weeks. These samples were excluded from the analysis.

The averages of the changes in the frequency (f_{md}) and bandwidth (BW_p) are presented in Fig. 7. In the case of PDLGA samples, a significant drop in the feature f_{md} was noticed after five weeks of hydrolysis. The signal from the PLGA samples showed only a minor drift. The feature BW_p of PDLGA samples had multiple phases: first, it increased for two weeks and then decreased until day 30. After that point, the feature began to increase again. The BW_p feature from the PLGA samples within this time scale was mainly an increasing drift.

The changes in the features f_{md} and BW_p of the parylene coated samples are presented in Fig. 8. In addition, average signals of the non-coated sensors in PLGA and PDLGA are given to help comparison. In general, the changes of the signals were greater in the non-coated samples. The parylene coating was not noticed to affect the behavior of the f_{md} feature in the PDLGA encapsulated sensors. The shift of the BW_p was greater in the case of non-coated sensors. It was noticed that the transitions in the signals from all the sensors in PDLGA occurred simultaneously.

Signals from the parylene coated sensors in PLGA were detectable at least 120 days. Both coated and non-coated sensors in PLGA showed a monotonic decreasing f_{md} and an increasing BW_p drift, which was steeper in the case of non-coated sensors. The parylene coated PLGA samples revealed a stepwise change in both f_{md} and BW_p around 110 days.

3.3. The effect of temperature

The effect of temperature on the extracted features was tested. This measurement was done using a PLGA sample that was kept in hydrolysis for 18 h. Fig. 9 presents the change in the features f_{md} and BW_p as the temperature was varied. According to the measurements, the temperature sensitivity of the feature f_{md} was $-0.053\%/°C$ and the temperature sensitivity of the feature BW_p was $0.22\%/°C$.

4. Discussion

We encapsulated resonance circuits with interdigital capacitive sensing elements in biodegradable PLGA and PDLGA copolymers

and measured their response during the 8-week hydrolysis in buffer solution. The extracted resonance features (f_{md}) and (BW_p) were compared with the reference measurements that were performed using conventional polymer degradation characterization methods. According to the reference measurements, PLGA did not show any significant signs of degradation during eight weeks of hydrolysis. This expected result is consistent with the findings in the literature [15]. Respectively, the inductively measured resonance features from these samples showed only a slight drift. However, PDLGA was noticed to degrade almost completely in eight weeks. The feature f_{md} from the PDLGA encapsulated sensors showed a significant consistent decrease roughly after five weeks of follow-up. The behavior of the feature BW_p was not monotonic. The temperature dependency of the method was tested and it was not found to be a substantial error source.

Poly(lactide-co-glycolide)s used in this study degrade via bulk erosion [11]. These materials become saturated with water during the first few days in hydrolysis [1]. The water molecules start to cleave ester bonds, causing the molecular weight to decrease without any mass loss at this point. In some cases, the molecular weight keeps decreasing as the number of acidic chain ends becomes so large that their ability to catalyze the cleavage of polymer bonds becomes significant (autocatalysis). The mass loss starts when some of the polymer molecules reach a small enough size to become soluble in water. Typically, these low-molecular-weight components keep dissolving to the solution until the specimen has completely degraded [11,1].

During the 8-week hydrolysis, our PDLGA samples degraded virtually completely and the inductively measured phase dip diminished to an undetectable level after seven weeks. Previously, PDLGA [85:15] discs of 200–250 μm thickness have been estimated to degrade in 6–12 months [16]. We assume that the reason for fast degradation in our test was autocatalysis, which was an unintended but consistent result due to the thickness of our samples. Our PDLGA specimens were seen to soften and eventually turn into a viscous liquid with a harder outer shell. Similar autocatalytic behavior with thick samples has been reported and explained in [17]. As opposed to the PDLGA samples, no signs of autocatalysis were seen in the slower degrading PLGA samples during the test period.

There was an easily detectable drop in the f_{md} of PDLGA samples after five weeks. However, we interpret that the mechanical performance of the PDLGA samples was compromised already after four weeks in buffer solution. This indicates that tested feature cannot be used to predict the mechanical performance of PDLGA. In fact, the flexural modulus of PDLGA was lowered already after two weeks of hydrolysis. Part of this is explained by the fact, that the 0-week samples were tested dry: absorbed water acted as a plasticizer in polymers, thus reducing the modulus. The mechanical performance continued to drop significantly and at the 8-week time point the samples were already so deformed and soft that their testing was impossible.

On the other hand, the easily detectable f_{md} drop of PDLGA samples occurred within the same time frame than the decrease in the T_g values. Additionally, the opacity of PDLGA started to fade after approximately five weeks and the material turned to blurred but transparent substance as seen in Fig. 5. We suggest that the easily detectable change especially in f_{md} might result from the joint effect of the dissolution of the small copolymer degradation products and the following water absorption into the samples. We propose that the outer layer of the PDLGA sample acted as an osmotic membrane, which did not allow the permeation of salts.

Typically, the BW_p of PDLGA samples increased for two weeks, after which a decrease of 2–3 weeks was observed. Finally, the BW_p turned again into an upswing. The behavior of the feature BW_p may provide additional information about the degradation but definite

conclusions cannot be drawn without more extensive studies. We speculate that such a behavior may be related to the outer layer of the specimen and changes in the distribution and size of the polymer chains.

In the consideration of the resonance measurements, the PLGA encapsulated sensors produced an initial frequency drop during the first few days in buffer solution. This drop is again expected to result from the penetration of water into the copolymer matrix. After that, a steadily decreasing f_{md} average was observed, whereas the BW_p average kept increasing. The signal from some sensor samples in PLGA was lost or significantly reduced during hydrolysis. This was probably due to the infiltration of buffer solution onto the interdigital capacitor (after drying the samples, the signals were recovered). We expect this infiltration to occur due to stress cracking, as clear cracks were seen in the PLGA samples. Especially in amorphous polymers, absorbed water can reduce the molecular anchoring of the polymer chains, causing accelerated cracking [1]. The cracking of the copolymer might partly explain the rather large deviation in inductively measured signals especially in the PLGA samples. It is also critical, that the encapsulation process is reliable and the polymer material stays in contact with the sensor.

To test if the monitoring method could be made more consistent, a parylene coating covering the sensor was introduced. The slopes of the signals from the non-coated sensors in PLGA were steeper compared to the parylene coated sensors. Thus, the parylene coating was observed to decrease the sensitivity of the sensors resulting from the thicker isolating layer. However, the overall performance of the parylene coated sensors was similar to the non-coated ones. Accordingly, the parylene coating did not dominate the measurements. We presume that the parylene coated sensors give more consistent signals, which is more important than the slightly greater sensitivity of the non-coated sensors.

Both coated sensors in PLGA provided a detectable signal for at least 120 days. This prolonged measurement period revealed a change in both extracted features in both parallel samples around 110 days. For comparison, Alexis et al. noticed an increase in water absorption with their PLGA films around 100 days of hydrolysis, after which the mass loss started to slowly occur [15]. This suggests that the changes in the features might result from structural changes in the copolymers.

In comparison to the golden standard characterization methods, our approach provides means to observe changes in biodegradable polymers in a non-destructive, wireless manner. In practice, coating the sensors with parylene seemed to provide better results in terms of a longer measurement period and more consistent signals. However, a biodegradable alternative for parylene is needed for biodegradable applications. Ultimately, using for example bioactive glass as a circuit board material and biodegradable magnesium or zinc as conductors, an implantable completely bioresorbable sensor chip could be manufactured. This chip could then be embedded into compression or injection molded biodegradable implants to enable *in vivo* measurements.

The encapsulation methods of the sensors should be improved in the future studies. Based on this study, the suitability of the presented method on predicting the mechanical strength of the implants in general is still uncertain. Since polymer degradation and its effect on the complex permittivity are complicated processes, more studies are needed to investigate the parameters affecting the measurement and the resulting resonance features. For example, a test series where samples made from the same material are divided into sets of normal and accelerated degradation could be performed. More information about the effects of the buffer solution on the resonance features could be obtained by immersing one set of samples in buffer solution and another into distilled water. Furthermore, the presented monitoring method could be automated to make the measurement continuous.

5. Conclusions

Inductively coupled passive resonance sensors with interdigital capacitive sensing elements were used to monitor changes in two biodegradable poly(lactide-co-glycolide)s during an 8-week testing period. The inductively measured signals showed a clear difference between the tested materials, which was verified with the reference methods. However, the inductively measured signals cannot be linked to any of the tested parameters without ambiguity. It was also noticed that the encapsulation process and coating of the sensors are critical for achieving consistent results. This has to be taken account when testing fully biodegradables sensors.

References

[1] S. Lyu, D. Untereker, Degradability of polymers for implantable biomedical devices, Int. J. Mol. Sci. 10 (9) (2009) 4033–4065.
[2] S. Mukherjee, A. Gowen, A review of recent trends in polymer characterization using non-destructive vibrational spectroscopic modalities and chemical imaging, Anal. Chim. Acta 895 (2015) 12–34.
[3] A. Göpferich, Mechanisms of polymer degradation and erosion, Biomaterials 17 (2) (1996) 103–114.
[4] S.O. Adeosun, G.I. Lawal, O.P. Gbenebor, Characteristics of biodegradable implants, J. Miner. Mater. Charact. Eng. 2 (2) (2014) 88–106.
[5] K. Bardsley, I. Wimpenny, Y. Yang, A.J. El Haj, Fluorescent, online monitoring of PLGA degradation for regenerative medicine applications, RSC Adv. 6 (50) (2016) 44364–44370.
[6] K.G. Ong, C.a. Grimes, C.L. Robbins, R.S. Singh, Design and application of a wireless, passive, resonant-circuit environmental monitoring sensor, Sens. Actuators A: Phys. 93 (1) (2001) 33–43.
[7] A.Y. Khaled, S.A. Aziz, F.Z. Rokhani, Capacitive sensor probe to assess frying oil degradation, Inf. Process. Agric. 2 (2) (2015) 142–148.
[8] G. Stojanović, M. Radovanović, M. Malešev, V. Radonjanin, Monitoring of water content in building materials using a wireless passive sensor, Sensors 10 (5) (2010) 4270–4280.
[9] M. Yvanoff, J. Venkataraman, A feasibility study of tissue characterization using LC sensors, IEEE Trans. Antennas Propag. 57 (4) (2009) 885–893.
[10] M. Luo, A.W. Martinez, C. Song, F. Herrault, M.G. Allen, A microfabricated wireless RF pressure sensor made completely of biodegradable materials, Journal of Microelectromechan. Syst. 23 (1) (2014) 4–13.
[11] L.S. Nair, C.T. Laurencin, Biodegradable polymers as biomaterials, Prog. Polym. Sci. 32 (8–9) (2007) 762–798.
[12] A. Höglund, K. Odelius, A.-C. Albertsson, Crucial differences in the hydrolytic degradation between industrial polylactide and laboratory-scale poly(L-lactide), ACS Appl. Mater. Interfaces 4 (May (5)) (2012) 2788–2793.
[13] T. Salpavaara, J. Verho, P. Kumpulainen, J. Lekkala, Readout methods for an inductively coupled resonance sensor used in pressure garment application, Sens. Actuators A: Phys. 72 (1) (2011) 109–116.
[14] T. Salpavaara, M. Järveläinen, S. Seppälä, T. Yli-Hallila, J. Verho, M. Vilkko, J. Lekkala, E. Levänen, Passive resonance sensor based method for monitoring particle suspensions, Sens. Actuators B: Chem. 219 (2014) 324–330.
[15] F. Alexis, S. Venkatraman, S.K. Rath, L.H. Gan, Some insight into hydrolytic scission mechanisms in bioerodible polyesters, J. Appl. Polym. Sci. 102 (4) (2006) 3111–3117.
[16] A. Huhtala, T. Pohjonen, L. Salminen, A. Salminen, K. Kaarniranta, H. Uusitalo, In vitro biocompatibility of degradable biopolymers in cell line cultures from various ocular tissues: extraction studies, J. Mater. Sci. Mater. Med. 19 (2) (2008) 645–649.
[17] S.M. Li, H. Garreau, M. Vert, Structure–property relationships in the case of the degradation of massive poly(α-hydroxy acids) in aqueous media – Part 2. Degradation of lactide-glycolide copolymers: PLA37.5GA25 and PLA75GA25, J. Mater. Sci. Mater. Med. 1 (3) (1990) 131–139.

Biographies

Timo Salpavaara received his M.Sc. degree in electrical engineering from Tampere University of Technology (TUT), Finland, in 2005. Currently, he is working at the Faculty of Biomedical Sciences and Engineering at Tampere University of Technology.

His research activities include inductively coupled resonance sensors, capacitive sensing and readout electronics.

Aleksi Hänninen received his M.Sc. degree in biotechnology in 2015 from Tampere University of Technology (TUT), Finland. His research interests include processing and characterization of biomaterials as well as cell technology. Currently, he is working at the Faculty of Biomedical Sciences and Engineering (TUT) with biodegradable electronics.

Anni Antniemi did her Bachelor's Thesis on biodegradable electronics and received her B.Sc. degree in materials engineering from Tampere University of Technology (TUT), Finland, in 2014. She completed her Master's Thesis in the Biomaterials and Tissue Engineering Group, receiving her M.Sc. degree from TUT in 2016.

Jukka Lekkala is a Professor of Automation Engineering at Tampere University of Technology (TUT), Finland. He received his M.Sc.(Eng) degree in electronics and D.Sc.(Eng) degree in biomedical engineering from TUT, in 1979 and 1984, respectively. During 1985–2001 Lekkala worked as a Senior Research Scientist at VTT (Technical Research Centre of Finland) in different research units developing biosensor technology and sensor materials. In 1991, he was appointed a Docent of bioelectronics at the University of Oulu and a Docent of biomedical engineering at TUT. Currently, he is the Vice-Dean of the Faculty of Biomedical Sciences and Engineering (TUT-BMT) at TUT and in addition leads his research group of Sensor Technology and Biomeasurements. Prof. Lekkala has more than 166 scientific papers and ten patents. Lekkala's main research activities include sensors, biosensing systems, sensor materials, instrumentation, and modeling.

Minna Kellomäki (Dr. Tech., FBSE) has a professor chair in TUT and she is also dean of Faculty of Biomedical Sciences and Engineering and leader of BioMediTech, a joint institute of Tampere University of Technology and University of Tampere. Her professorship is at large in biomaterials, specialized in tissue engineering scaffolds and materials. The main interest is in biodegradable polymers and composites, combinational and hybrid materials, in the processing and characterization of them. The research field is highly interdisciplinary and thus most of the work is done in national and international collaboration with other research groups and companies.

PUBLICATION
II

Bioresorbable Conductive Wire with Minimal Metal Content

Aleksi Palmroth, Timo Salpavaara, Inari Lyyra, Mart Kroon, Jukka Lekkala, Minna Kellomäki

Bioresorbable Conductive Wire with Minimal Metal Content

Aleksi Palmroth,*,† Timo Salpavaara,† Inari Lyyra,† Mart Kroon,† Jukka Lekkala,† and Minna Kellomäki†,‡

†BioMediTech Institute and Faculty of Biomedical Sciences and Engineering, Tampere University of Technology, Tampere 33720, Finland

‡BioMediTech Institute and Faculty of Medicine and Life Sciences, University of Tampere, Tampere 33104, Finland

S Supporting Information

ABSTRACT: The emergence of transient electronics has created the need for bioresorbable conductive wires for signal and energy transfer. We present a fully bioresorbable wire design where the conductivity is provided by only a few micrometers thick electron-beam evaporated magnesium layer on the surface of a polymer fiber. The structure is electrically insulated with an extrusion coated polymer sheath, which simultaneously serves as a water barrier for the dissolvable magnesium conductor. The resistance of the wires was approximately $1\ \Omega\ cm^{-1}$ and their functional lifetime in buffer solution was more than 1 week. These properties could be modified by using different conductor materials and film thicknesses. Furthermore, the flexibility of the wires enabled the fabrication of planar radio frequency (RF) coils, which were wirelessly measured. Such coils have the potential to be used as wireless sensors. The wire design provides a basis for bioresorbable wires in applications where only a minimal amount of metal is desired, for example, to avoid toxicity.

KEYWORDS: transient electronics, bioresorbable, biodegradable, conductive wire, extrusion, RF coil
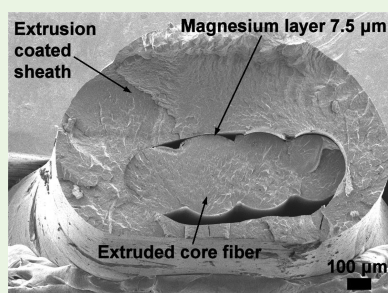
■ INTRODUCTION

Implantable conductive wires and cables provide the means for accessing difficult sensing and stimulation locations inside the body,[1] for example, in cases where the working distance for wireless devices is too long. In addition, conductors are needed in fabricating radio frequency (RF) coils, which can be used in resonating sensor structures[2] or to transmit power wirelessly to implantable medical devices.[3] Implantable wires typically comprise metal-alloy-based core conductors and an insulating layer protecting the conductors from biological fluids.[1] In long-term applications, their robustness and durability are crucial. On the other hand, the emergence of bioresorbable implantable devices[4] for monitoring or treating acute health conditions has created a need for conductive wires that disappear from the body after functioning for a defined time period.

In conductive wire and cable applications, biodegradable materials have often been used only in the sheath. Previous studies include for example an extrusion-coated poly(L-lactide) sheath on a copper wire[5] and cellulose sheaths around carbon nanotube cores.[6] On the contrary, preclinical studies on biodegradable implantable sensors have been conducted using biodegradable transcutaneous molybdenum-based wires for signal transfer.[7,8]

An implantable conductive wire with only minimal bioresorbable metal content might be useful in applications where excessive amounts of metals could cause problems. For example, the corrosion of magnesium produces hydrogen gas,

which might lead to complications in vivo.[9] Zinc, on the other hand, is known to be neurotoxic and hinder bone development at immoderate quantities.[10] Furthermore, some bioresorbable metals like iron dissolve very slowly and are even noticed to cause similar problems that are observed with permanent implants.[11] These issues might be solved by depositing metallic thin films on bioresorbable polymer fibers to achieve conductivity. Depending on the application and the conductivity of the used metal, the metal thickness could be for example from a few hundred nanometers to a few micrometers. The resulting wire can be extrusion-coated without destroying the conductivity, if the glass-transition temperature of the core fiber is distinctly higher than the melting temperature of the coating material. The mechanical properties of such conductive wires are largely defined by the polymer materials, but at the same time constrained by the integrity of the conductive metal layer.

In this study, prototype wires were fabricated using bioresorbable poly(desamino tyrosyl-tyrosine ethyl ester carbonate), or poly(DTE carbonate) as the core fiber material because of its relatively high glass-transition temperature. After depositing magnesium onto the core fiber, it was extrusion-coated using bioresorbable poly(caprolactone) (PCL). The obtained wires were characterized by demonstrating their

 1134

conductivity, flexibility, and lifetime in aqueous conditions. Furthermore, their application as wirelessly readable RF coils was shown. Such coils could be used, for example, as sensors to detect changes in their environment.

■ EXPERIMENTAL SECTION

Wire Fabrication. Poly(desamino tyrosyl-tyrosine ethyl ester carbonate) (poly(DTE carbonate); Integra LifeSciences, New Jersey, USA) with a measured inherent viscosity (i.v.) of 0.89 dL/g was dried in vacuum for 4 days in room temperature before processing. A flat poly(DTE carbonate) monofilament fiber was extruded under nitrogen atmosphere using Gimac microextruder (Gimac, Gastronno, Italy) with a screw diameter of 12 mm. The shape and dimensions of the extrusion die are presented in Figure S1. The flat shape was chosen to prevent any unintentional twisting of the fibers during the subsequent metal deposition process. The fiber was collected with a conveyer at a speed of 4 m/min. The thickness and width of the poly(DTE carbonate) core fiber and the complete conductive wire were measured from different points ($n = 50$) using a digital caliper.

Continuous poly(DTE carbonate) fibers were cleaned using isopropanol dampened clean room wipes and then coiled around a holder plate using Kapton tape for attachment. Magnesium thin films with a thickness of 7.5 μm were e-beam evaporated onto the fibers. This was close to the maximum Mg thickness that could be conveniently evaporated during one process using our system. The e-beam evaporation rate was 2.0 Å/s with a vacuum level in the order of 1×10^{-6} Torr. After evaporation, the Kapton tapes were removed, resulting in poly(DTE carbonate) fibers with various lengths (9−14 cm) of continuous magnesium coating limited by the tape. The fibers with a magnesium layer were extrusion coated with medical grade poly(caprolactone) (PCL; Corbion Purac, The Netherlands) having an i.v. of 1.18 dL/g as stated by the manufacturer. The extrusion was performed with the Gimac microextruder under nitrogen atmosphere using a crosshead die with an output diameter of 2 mm. The resulting wire was collected with a conveyer at a speed of 3 m/min.

Materials Characterization. The thermal transitions of the poly(DTE carbonate) and PCL raw materials were determined using a differential scanning calorimeter (DSC Q1000; TA Instruments, USA). The data was analyzed from the second heating using TA Universal Analysis software.

The inherent viscosity measurements of the extruded poly(DTE carbonate) core fiber and the respective raw material were performed to evaluate the degradation of the material during processing. The analysis was done in ambient conditions using an automated Ubbelohde viscometer (LAUDA, Lauda-Königshofen, Germany). Samples of 20 ± 0.6 mg were weighed and dissolved in 20 mL of chloroform overnight before the measurement. Two parallel samples for both the raw material and the fiber were measured.

Compression molded poly(caprolactone) sheets (n = 5) with a size of $10 \times 50 \times 0.4$ mm^3 were used to study the water uptake properties of the PCL extrusion coating material. The samples were dried in a vacuum chamber at room temperature for 1 week, after which their mass was weighed using an analytical scale. The samples were then immersed in Sörensen buffer solution (Table S1), which was prepared according to the "ISO 15814:1999(E): Implants for surgery − Copolymers and blends based on polylactide − In vitro degradation testing" standard. The immersed samples were stored at +37 °C and weighed at predetermined time points by gently wiping the excessive liquid from the samples with tissue paper and immediately weighing them. The wet weights were compared to the initial dry weight using eq 1:

$$\text{water uptake } (\%) = \left(\frac{\text{wet weight} - \text{dry weight}}{\text{dry weight}} \right) 100\% \tag{1}$$

The possible error caused by the mass loss of PCL during hydrolysis was considered negligible, as virtually no molecular weight changes and an average mass loss of only 0.12% per month have been reported for the first 6 months of PCL hydrolysis.[12]

The tensile properties of both the plain core fibers and the PCL coated fibers ($n = 10$) were studied using Instron 4411 materials testing equipment (Instron Ltd., England) with a 500 N load cell. The distance between pneumatic grips was 50 mm and the crosshead speed was 10 mm/min. The cross sectional areas of the fibers were approximated using a rectangular shape as a basis. Tensile strength, elongation at break, and Young's modulus were calculated from the measured data.

Scanning Electron Microscopy. The scanning electron microscopy (SEM) images were taken from the cross section of the conductive wire. The wire was first immersed in methanol to fill the material (meso)pores and thus promote brittleness during cutting.[13] After the methanol treatment, the wire was freeze fractured in liquid nitrogen, coated with a thin layer of chromium, and imaged using a field-emission SEM (JSM-7610F; JEOL Ltd., Japan). The imaged sample originated from an earlier fabrication batch compared to the samples used in other tests.

Resistance Measurements. After evaporating magnesium onto the fibers, their resistance was measured using a digital multimeter (AxioMET AX-572) by gently pressing the probes onto the Mg layer. The lengths of the magnesium coatings, defined by the tapes in the evaporation phase, were measured using a ruler. The resistances per centimeter were calculated for each conductive fiber ($n = 21$). The measurements and calculations were repeated after extrusion coating in order to evaluate the effect of the coating process to the wire resistance. Excessive PCL coating was first melted and skimmed off the tip of the wires, after which the multimeter probes were pressed through the residual PCL film. A paired Student's t test was applied for the statistical analysis, where $p < 0.05$ was considered significant.

After the dry resistance measurements, the tips of the wires were treated with two layers of conductive silver epoxy adhesive (8331−14G; MG Chemicals, Canada) to ensure a measurement point for the water immersion tests. The bioresorbable wires ($n = 5$) were attached to 50 mL falcon tubes, leaving the Ag epoxy coated wire tips in air and the rest of the wire immersed in prewarmed Sörensen buffer solution. The samples were stored in an incubator at +37 °C and their resistances were measured with a multimeter using hook clip probes.

Bending and Resonator Coils. Flexibility is essential for implantable wires. However, bending should not compromise their conductivity. This aspect was tested by wounding the wires around a glass rod with a diameter of 7 mm as shown in Figure 1a. The resistances of the wires ($n = 5$) were measured with a multimeter before and after the bending experiment.
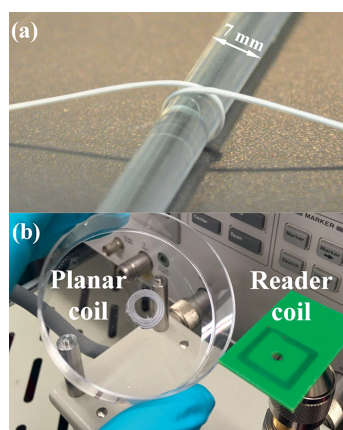

Figure 1. Wire flexibility demonstrations showing (a) a wire coiled around a glass rod with a 7 mm diameter and (b) a planar coil with an inner diameter of 7 mm. The external reader coil was used for the wireless resonance measurements.
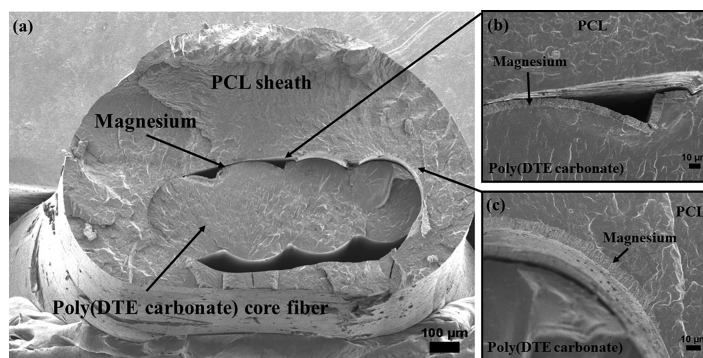
Figure 2. Cross-section of the conductive wire showing (a) the whole cross-section, (b) magnesium film on top of the core fiber, and (c) magnesium attached to the PCL sheath.

One of the simplest functional structures that can be fabricated from conductive insulated wires is a coil. These coils are sensitive to their environment[14] and can be used for example as sensors. The self-resonance frequencies of the coils can be wirelessly estimated by measuring a reader coil that is inductively coupled with the sensor coil.

Three bioresorbable planar coils with three turns were fabricated from the conductive wires. First, the wires were coiled around a 3D printed template with a diameter of 7 mm. Then, a soldering iron was used to melt the PCL coating, which acted as an adhesive after cooling. In addition, three nondegradable reference samples were fabricated from insulated copper wire (Flexi-E 0.10, Stäubli Group, Switzerland) using the same template and super glue as an adhesive. This commercial copper-based cable consisted of a nondegradable insulating polyvinyl chloride (PVC) sheath and a stranded Cu core with a conductor diameter of 0.40 mm and a total diameter of 1.0 mm.

The resonance frequencies of all the bioresorbable and nondegradable coils were first wirelessly measured through a plastic Petri dish using an external two-turn reader coil (Figure 1b). An impedance analyzer (Agilent 4396B; 100 kHz to 1.8 GHz) was used to measure the real part of the impedance of the reader coil from 650 MHz to 1 GHz. Thereafter, the reading distances of one bioresorbable coil and one nondegradable coil were tested. The coils with the highest resonance frequencies were chosen for this test. The reading distance was increased in a stepwise manner by adding 1 mm thick microscopy slides between the coil and the reader. The coils were measured after each 1 mm increment.

■ RESULTS AND DISCUSSION

Wire Structure and Processing. Fabrication of the conductive wire started by extruding poly(DTE carbonate) to form the core fiber. On the basis of an SEM image of the wire cross-section (Figure 2), the poly(DTE carbonate) core took accurately the shape of the extruder die. The core located in the lower portion of the PCL sheath with an approximately 50 μm thick coating layer in the thinnest region. As measured using the digital caliper, the average ($n = 50$) width of the core fibers was 0.79 ± 0.03 mm and thickness 0.29 ± 0.02 mm, whereas the same dimensions for the complete wire including the extrusion-coated sheath were 1.05 ± 0.05 mm and 0.73 ± 0.09 mm, respectively. The dimensions in the SEM image differ from these measurements, showing a core fiber width of approximately 0.9 mm. The SEM sample was prepared from a preliminary fibers batch, where the fibers were collected at a lower conveyer speed. The fibers from the preliminary test batch showed similar behavior with the reported fibers. The

dimensions of both the core and the sheath could be tuned by modifying the extruder dies or collecting the fibers at a different rate. For example, Bourke et al. have extruded poly(DTE carbonate) fibers with a diameter of 61 μm.[15]

The e-beam evaporated magnesium layer appeared to have a relatively uniform thickness of 7−8 μm also in the grooves of the core fiber (Figure 2b). Interestingly, some parts of the magnesium had a greater adhesion on PCL than on the poly(DTE carbonate) core (Figure 2c), causing partial detachment of the Mg layer from the core fiber. We estimate that the detached Mg layers have been surrounded by molten PCL in the extrusion coating phase and have possibly detached during the cooling phase of PCL or even later when cutting the SEM sample. However, the PCL sheath was not fully in contact with the core fiber and specifically did not reach the grooves of the core fiber, which should remain conductive even if larger flakes would be detached. This issue might be improved by using adhesion promotion methods such as plasma treatment before metal evaporation.

On the basis of the shape of the sheath, we conclude that the lack of contact at some locations existed already before cutting the wire for the SEM imaging. The lengths of the conductive wires were limited by the Kapton tapes that were used to attach the fibers to the holder in the evaporation phase. Reeling the core fiber onto a spool that rotates in the evaporation chamber would enable fabricating wires with meters of length. Longer continuous wires could be made for example by using a roll-to-roll sputtering deposition[16] process.

Materials Characterization. As an amorphous polymer,[17] poly(DTE carbonate) does not have a melting temperature. Its glass transition temperature (T_g = 99 °C) is higher than the melting temperature of PCL (T_m = 57 °C), enabling the extrusion coating process without damaging the core fiber by excessive heating. Within this constraint ($T_{g, core} > T_{m, sheath}$), the material choices in the wire can be tuned if for example faster degradation is preferred.

The tensile properties of the core fiber were examined to assess the extrusion process. The tensile properties of the extrusion products are illustrated in Table 1. The tensile strength of our fibers (56 ± 3 MPa) was slightly higher than the 44 ± 11 MPa of the first-generation poly(DTE carbonate) fibers of Bourke et al.[15] However, the Young's modulus of our fibers (1.9 GPa) was lower compared with their second-generation fibers (3.1 GPa) with a diameter of 79 μm. Both the

Table 1. Properties of the Plain and Extrusion-Coated Core Fibers as Averages ± Standard Deviations

	Young's modulus (GPa)	tensile strength (MPa)	elongation at break (%)
poly(DTE carbonate) core fiber	1.9 ± 0.1	56 ± 3	4.2 ± 0.2
PCL-coated core fiber	0.9 ± 0.1	25 ± 3	4.0 ± 0.4

Young's modulus and tensile strength were lower in the PCL coated fiber.

The tensile properties of the core fiber could be significantly modified by adding a further drawing step. Orientation of semicrystalline polymer fibers typically increases the Young's Modulus and tensile strength parallel to the drawing direction but reduces the elongation at break, whereas an increase in elongation at break is often noticed in oriented amorphous polymer fibers.[18] As an example, hot drawn poly(L-lactide-co-glycolide) (PLGA) 80/20 monofilament fibers with a diameter of 0.4 mm had a tensile strength of 377 MPa.[19] On the other hand, the relative decrease in the inherent viscosity of our extruded poly(DTE carbonate) fiber (0.58 ± 0.03 dL/g) compared to the raw material (0.89 ± 0.01 dL/g) was 35%, indicating that some polymer degradation has occurred during extrusion. The result is in line with a comprehensive study of oriented PLGA 85/15 fibers reporting relative postextrusion i.v. value decreases between 29% and 56% depending on the processing conditions and raw material batch.[20]

The water uptake properties of PCL (Figure 3) were tested to estimate the water barrier properties of the extrusion
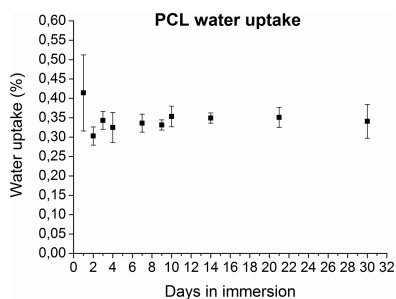
Figure 3. Water uptake behavior of poly(caprolactone) sheets ($n = 5$) immersed in Sörensen buffer solution. The error bars denote standard deviations.

coating. An equilibrium water uptake of PCL was noticed to be around 0.30−0.35 wt %, which is low compared to many other biodegradable polymers whose typical water uptake is in the order of 1 wt %.[21] Correspondingly, PCL water uptake after 60 days has been reported to be 0.5%, whereas the respective value for other tested polymers like poly(butylene succinate) (PBS) and poly(lactic acid) (PLA) were approximately 1.5%.[22] Due to these properties, PCL has been previously described as a good material candidate for encapsulating sensors.[23]

Resistance Measurements. The average electrical resistance of the wires after e-beam evaporation of Mg was 0.9 ± 0.1 Ω cm^{-1}, as shown in Figure 4a. A slight increase in resistance to 1.1 ± 0.2 Ω cm^{-1} was noticed after extruding the PCL sheath onto the wire. This might be due to the detachment of Mg from the core fiber in some locations as seen in the SEM image (Figure 2). All of the tested wires ($n = 21$), however,
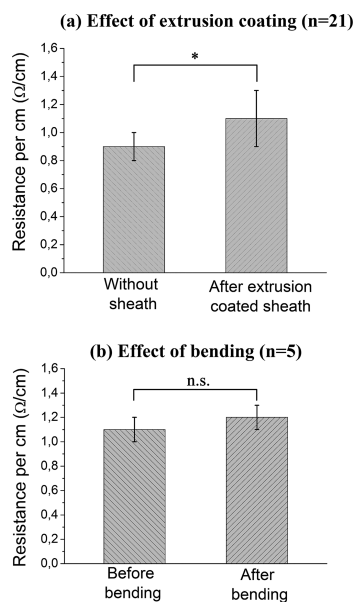
Figure 4. Average resistances of conductive wires (a) before and after extrusion coating as well as (b) before and after bending (bending radius $r = 3.5$ mm). The error bars denote standard deviations. A paired Student's t test was used to assess the statistical significance: *p < 0.05, n.s. = not significant.

remained electrically conductive after the extrusion coating process, addressing the applicability of the fabrication method.

The resistance values of our conductive wires can be considered reasonable, factoring in the electrical properties of magnesium and its dimensions in our application. With thinner Mg layers, the resistance increases, which might be problematic in some applications. For example, a 0.5 μm thick Mg layer on a poly(DTE carbonate fiber) resulted in a resistance of about 10 Ω cm^{-1} (Table S2), which would impair their application as RF coils. On the other hand, a 0.5 μm thick Cu layer on a fiber provided a much lower resistance of approximately 0.5 Ω cm^{-1}. In the literature, the resistance of a copper wire based nonresorbable implantable wire of approximately 0.1 Ω cm^{-1} has been presented.[1] On the other end of the scale, conductive polymer based yarns[24] and wires[25] have been reported with resistances of 77 Ω cm^{-1} to around 2550 Ω cm^{-1}, respectively.

Coiling wires around a glass rod ($r = 3.5$ mm) did not significantly increase the resistance of the wires and none of the tested wires ($n = 5$) were destroyed during the experiment. Thus, the bending radius that the wires withstand without breaking the magnesium layer is 3.5 mm or less, illustrating the flexibility of the prototype wire.

Immersing wires in Sörensen buffer solution was done to evaluate the water barrier properties of the PCL coating and to approximate the functional lifetime of the wires in vitro. The silver epoxy adhesive connection at the tip of the wires was used to protect the thin Mg layer during repeated measurements. However, this connection led to a slight resistance increase in the other samples and a larger effect in sample #4. After the first 24 h of immersion in buffer solution, all the samples showed increased resistances (Figure 5). This was
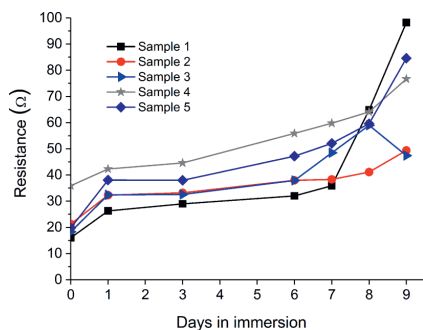
Figure 5. Resistances of PCL-coated conductive wires immersed in Sörensen buffer solution at +37 °C.

probably due to the low amount of absorbed water (∼0.35 wt %) inside the PCL coating. The absorbed water might have initiated the corrosion of Mg or facilitated the delamination of the PCL coating,[21] thus leading to some Mg detachment. For comparison, wires without PCL coating lose their conductivity completely in a few minutes in buffer solution (data not shown).

The samples demonstrated a moderate resistance increase between the first and the sixth day. After 1 week the measurement results started to drift, probably due to the noticed flaking of the silver epoxy adhesive layer. The observed flaking of the Ag epoxy was likely caused by repeated mechanical stress that was derived from the hook clip probes. All the wires were still conductive (<100 Ω) after 9 days. At the 10-day time-point, the first two wires had lost their conductivity (not shown). Three days later, the three remaining samples were still conductive. After 14 days, the hydrolysis was terminated and the conductivities were measured directly from the Mg layer. Only samples #3 and #4 had remained conductive with the resistances of 120 Ω (10.7 Ω cm^{-1}) and 175 Ω (14.1 Ω cm^{-1}), respectively.

The results indicate that water does not penetrate the PCL coating excessively during the first week of immersion. Furthermore, by choosing a more corrosion resistant metal such as iron or zinc, the functional lifetime of the wire could probably be significantly extended. Other tuning possibilities include e-beam evaporating both sides of the core fiber leading to a conductive cable with two separate conductors in one fiber, or using sputter deposition to cover the whole fiber with metal.

Planar Coil RF Measurements. To demonstrate the usability of the developed fabrication methods, we built bioresorbable coils and inductively measured their self-resonance frequencies. Both magnesium- and copper-based coils were clearly readable through the Petri dish, but the copper wire based reference coils produced higher and sharper resonance peaks compared to the bioresorbable coils (Figure 6a). This was an expected result considering the thickness and conductivity of the magnesium layer in comparison with the commercial copper wire with a conductor diameter of 0.40 mm. Correspondingly, one of the key challenges in producing high quality factor biodegradable RF resonators is the conductivity of the materials.[26]

The varying resonance frequencies of the coils were probably caused by the manual assembly; the turns are difficult
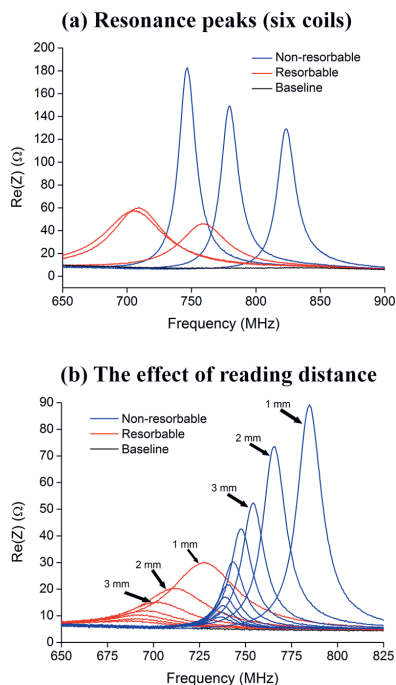

Figure 6. Resonance peaks of (a) all the fabricated planar coils, including three resorbable coils and three nondegradable copper-wire-based reference coils (b) one resorbable and one nonresorbable coil measured with increasing reading distance through glass microscopy slides.

to position identically, which leads to different capacitances between the turns. The changes in capacitance lead to significant changes in the resonance frequency.

The reading distance of the bioresorbable coil was approximately 4−5 mm (Figure 6b), after which it became challenging to distinguish the resonance curve from the background noise. The higher conductivity of the non-degradable coils led to an approximately twice as high reading distance compared to the Mg-based bioresorbable coils. The resonance frequencies increased with decreasing reading distance due to stronger inductive coupling, which is in agreement with previous simulation results.[27]

To use these kind of structures in practical sensor applications, the manual assembly of the coils should be replaced with a more consistent process, for example by using more sophisticated templates. This would minimize the differences in the geometry of the RF coils. In typical applications, the measured quantities are linked to the change of the resonance frequency. In our measurements, the reading distance affected the detected resonance frequency. This phenomenon was caused by the fact that in this setup the self-resonance frequency of the reader coil (not shown) was lower than the measured frequencies. Thus, the readout configuration should be optimized and in addition, the errors could be mitigated by adapting a method for reading distance compensation.[28] In the future, physical changes in the coil dimensions and their effect to the resonance frequency could

be utilized in a wireless sensor for example to monitor the dimensions of stents or tubular organs.

CONCLUSIONS

The design and processing strategy of a bioresorbable implantable wire with minimal metal content has been described. This approach might be beneficial in signal and energy transfer applications where higher metal content would be problematic considering their toxicity, degradation rate or the degradation byproducts. In addition, manually fabricated RF coils were wirelessly readable and their improved versions could be used in the future as biodegradable sensors. The lifetime of the wires immersed in buffer solution was more than 1 week, although only a few micrometers thick layer of extremely fast corroding magnesium was used. To conclude, the presented bioresorbable prototype wires showed promising properties for an application as implantable transient wires.

ASSOCIATED CONTENT

⑤ Supporting Information

The Supporting Information is available free of charge on the ACS Publications website at DOI: 10.1021/acsbiomaterials.8b01292.

> Dimensions of the extruder die, the composition and instructions for preparing the Sörensen buffer solution, resistances for poly(DTE carbonate) fibers with different metal layers (PDF)

AUTHOR INFORMATION

Corresponding Author

*Email: aleksi.hanninen@tut.fi.

ORCID ⊙

Aleksi Palmroth: 0000-0002-8574-6922

Notes

The authors declare no competing financial interest.

ACKNOWLEDGMENTS

REFERENCES

(1) Kim, S.-H.; Moon, J.-H.; Kim, J. H.; Jeong, S. M.; Lee, S.-H. Flexible, Stretchable and Implantable PDMS Encapsulated Cable for Implantable Medical Device. *Biomed. Eng. Lett.* **2011**, *1*, 199−203.

(2) Ong, K. G.; Grimes, C. A.; Robbins, C. L.; Singh, R. S. Design and application of a wireless, passive, resonant-circuit environmental monitoring sensor. *Sens. Actuators, A* **2001**, *93*, 33−43.

(3) Kim, S.; Yoo, S. Comparison of planar type coils for efficient power supply to implantable devices. *Biomed. Eng. Lett.* **2012**, *2*, 179−185.

(4) Kim, D.-H.; Kim, Y.-S.; Amsden, J.; Panilaitis, B.; Kaplan, D. L.; Omenetto, F. G.; Zakin, M. R.; Rogers, J. A. Silicon electronics on silk as a path to bioresorbable, implantable devices. *Appl. Phys. Lett.* **2009**, *95*, 133701.

(5) Nakiri, T.; Kawachi, Y.; Honda, M.; Imoto, K.; Yamakita, T.; Tajitsu, Y. Development of Electric Wire Using Biodegradable Polymer. *IEEE Trans. Ind. Appl.* **2007**, *43*, 1069−1074.

(6) Miyauchi, M.; Miao, J.; Simmons, T. J.; Lee, J.-W.; Doherty, T. V.; Dordick, J. S.; Linhardt, R. J. Conductive cable fibers with insulating surface prepared by co-axial electrospinning of multi-walled nanotubes and cellulose. *Biomacromolecules* **2010**, *11*, 2440−2445.

(7) Kang, S.-K.; Murphy, R. K. J.; Hwang, S.-W.; Lee, S. M.; Harburg, D. V.; Krueger, N. A.; Shin, J.; Gamble, P.; Cheng, H.; Yu, S.; Liu, Z.; McCall, J. G.; Stephen, M.; Ying, H.; Kim, J.; Park, G.; Webb, R. C.; Lee, C. H.; Chung, S.; Wie, D. S.; Gujar, A. D.; Vemulapalli, B.; Kim, A. H.; Lee, K.-M.; Cheng, J.; Huang, Y.; Lee, S. H.; Braun, P. V.; Ray, W. Z.; Rogers, J. A. Bioresorbable silicon electronic sensors for the brain. *Nature* **2016**, *530*, 71−76.

(8) Curry, E. J.; Ke, K.; Chorsi, M. T.; Wrobel, K. S.; Miller, A. N., III; Patel, A.; Kim, I; Feng, J.; Yue, L.; Wu, Q.; Kuo, C.-L.; Lo, K. W.-H.; Laurencin, C. T.; Ilies, H.; Purohit, P. K.; Nguen, T. D. Biodegradable Piezoelectric Force Sensor. *Proc. Natl. Acad. Sci. U. S. A.* **2018**, *115*, 909−914.

(9) Staiger, M. P.; Pietak, A. M.; Huadmai, J.; Dias, G. Magnesium and its alloys as orthopedic biomaterials: A review. *Biomaterials* **2006**, *27*, 1728−1734.

(10) Asgari, M.; Hang, R.; Wang, C.; Yu, Z.; Li, Z.; Xiao, Y. Biodegradable Metallic Wires in Dental and Orthopedic Applications: A Review. *Metals* **2018**, *8*, 212.

(11) Katarivas Levy, G.; Goldman, J.; Aghion, E. The Prospects of Zinc as a Structural Material for Biodegradable Implants—A Review Paper. *Metals* **2017**, *7*, 402.

(12) Lam, C. X. F.; Hutmacher, D. W.; Schantz, J.-T.; Woodruff, M. A.; Teoh, S. H. Evaluation of polycaprolactone scaffold degradation for 6 months in vitro and in vivo. *J. Biomed. Mater. Res., Part A* **2009**, *90A*, 906−919.

(13) Samitsu, S.; Zhang, R.; Peng, X.; Krishnan, M. R.; Fujii, Y.; Ichinose, I. Flash freezing route to mesoporous polymer nanofibre networks. *Nat. Commun.* **2013**, *4*, 2653.

(14) Yousaf, A.; Khan, F. A.; Reindl, L. M. Passive Wireless Sensing of Micro coil parameters in fluidic environments. *Sens. Actuators, A* **2012**, *186*, 69−79.

(15) Bourke, S. L.; Kohn, J.; Dunn, M. G. Preliminary Development of a Novel Resorbable Synthetic Polymer Fiber Scaffold for Anterior Cruciate Ligament Reconstruction. *Tissue Eng.* **2004**, *10*, 43−52.

(16) Park, Y.-S.; Choi, K.-H; Kim, H.-K. Room temperature flexible and transparent ITO/Ag/ITO electrode grown on flexile PES substrate by continuous roll-to-roll sputtering for flexible organic photovoltaics. *J. Phys. D: Appl. Phys.* **2009**, *42*, 235109.

(17) Asikainen, A. J.; Pelto, M.; Noponen, J.; Kellomäki, M.; Pihlajamäki, H.; Lindqvist, C.; Suuronen, R. In vivo degradation of poly(DTE carbonate) membranes. Analysis of the tissue reactions and mechanical properties. *J. Mater. Sci.: Mater. Med.* **2008**, *19*, 53−58.

(18) La Mantia, F. P.; Ceraulo, M.; Mistretta, M. C.; Morreale, M. Effect of Cold Drawing on Mechanical Properties of Biodegradable Fibers. *J. Appl. Biomater. Funct. Mater.* **2016**, *15*, 70−76.

(19) Juuti, H.; Kotsar, A.; Mikkonen, J.; Isotalo, T.; Talja, M.; Tammela, T. L.; Törmälä, P.; Kellomäki, M. The Effect of pH on the Degradation of Biodegradable Poly(L-Lactide-Co-Glycolide) 80/20 Urethral Stent Material In Vitro. *J. Endourol.* **2012**, *26*, 701−705.

(20) Paakinaho, K.; Heino, H.; Väisänen, J.; Törmälä, P.; Kellomäki, M. Effects of lactide monomer on the hydrolytic degradation of poly(lactide-co-glycolide) 85L/15G. *J. Mech. Behav. Biomed. Mater.* **2011**, *4*, 1283−1290.

(21) Lyu, S.; Untereker, D. Degradability of polymers for implantable biomedical devices. *Int. J. Mol. Sci.* **2009**, *10*, 4033−4065.

(22) Correlo, V. M.; Pinho, E. D.; Pashkuleva, I.; Bhattacharya, M.; Neves, N. M.; Reis, R. L. Water Absorption and Degradation Characteristics of Chitosan-Based Polyesters and Hydroxyapatite Composites. *Macromol. Biosci.* **2007**, *7*, 354−363.

(23) Salpavaara, T.; Lekkala, J.; Khan, S.; Ellä, V.; Kellomäki, M. Biodegradable encapsulation for inductively measured resonance

circuit. In *12th International Conference on Bioinformatics & Bioengineering (BIBE)*; IEEE, 2012; pp 323−327.

(24) Amba Sankar, K. N.; Mohanta, K. Dwindling the resistance value of PEDOT:PSS − coated on fabric yarns. *AIP Conf. Proc.* **2015**, *1731*, 120019.

(25) Nagamine, K.; Sato, H.; Kai, H.; Kaji, H.; Kanzaki, M.; Nishizawa, M. Contractile Skeletal Muscle Cells Cultured with a Conducting Soft Wire for Effective, Selective Stimulation. *Sci. Rep.* **2018**, *8*, 2253.

(26) Boutry, C. M.; Chandrahalim, H.; Streit, P.; Schinhammer, M.; Hänzi, A. C.; Hierold, C. Towards biodegradable wireless implants. *Philos. Trans. R. Soc., A* **2012**, *370*, 2418−2432.

(27) Salpavaara, T.; Lekkala, J. A Model Based Analysis of the Measurement Errors in Inductively Coupled Passive Resonance Sensors. In *XXI IMEKO World Congress 'Measurement in Research and Industry'*; IMEKO, 2015.

(28) Salpavaara, T.; Verho, J.; Kumpulainen, P.; Lekkala, J. Readout methods for an inductively coupled resonance sensor used in pressure garment application. *Sens. Actuators, A* **2011**, *172*, 109−116.

Supporting information

Bioresorbable conductive wire with minimal metal content

Aleksi Palmroth[1,], Timo Salpavaara[1], Inari Lyyra[1], Mart Kroon[1], Jukka Lekkala[1], Minna Kellomäki[1,2]*

[1] BioMediTech Institute and Faculty of Biomedical Sciences and Engineering, Tampere University of Technology, Tampere 33720, Finland.

[2] BioMediTech Institute and Faculty of Medicine and Life Sciences, University of Tampere, Tampere 33104, Finland.

*Corresponding author:

Aleksi Palmroth

Tampere University of Technology / Faculty of Biomedical Sciences and Engineering

Korkeakoulunkatu 3
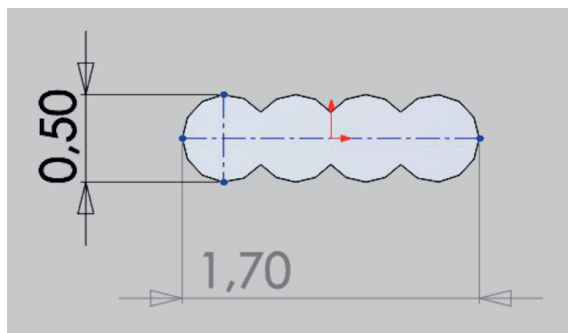
33720 Tampere

aleksi.hanninen@tut.fi

Figure S1. A SolidWorks schematic of the shape and dimensions of the extrusion die. The values are in millimeters.

Sörensen buffer solution with a pH of 7.46 – 7.49 was used in the immersion studies. It was prepared by dissolving the chemicals in distilled water and then diluting the solution to a volume of one liter. The chemicals for the buffer solution were bought from VWR Chemicals.

Table S1. Ingredients for 1l of Sörensen buffer solution (pH 7.46 – 7.49).

Ingredient	Mass	Concentration
$Na_2HPO_4 * 2H_2O$	9.71 g	0.0546 mol/l
KH_2PO_4	1.65 g	0.0121 mol/l
Distilled water		

Table S2 illustrates the resistance values for poly(DTE carbonate) fibers with deposited layers of Mg and non-resorbable Cu. The 0.5-µm thick metal layers were evaporated to obtain test materials for comparing their conductivities with the thicker Mg layer that was used in the study. The evaporation rates for Mg and Cu were 2.0 Å/s and 5.0 Å/s, respectively.

Table S2. Resistances for different metal coatings on poly(DTE carbonate) fibers without further PCL coating.

Deposited metal	Resistance
0.5 µm Cu layer (n=18)	$0.5 \pm 0.03 \ \Omega \ cm^{-1}$
0.5 µm Mg layer (n=18)	$10.1 \pm 1.2 \ \Omega \ cm^{-1}$
7.5 µm Mg layer (n=21)	$0.9 \pm 0.1 \ \Omega \ cm^{-1}$

PUBLICATION
III

Fabrication and Characterization of a Wireless Bioresorbable Pressure Sensor

Aleksi Palmroth, Timo Salpavaara, Jukka Lekkala, Minna Kellomäki

FULL PAPER

Transient Electronics

**ADVANCED
MATERIALS
TECHNOLOGIES**

www.advmattechnol.de

Fabrication and Characterization of a Wireless Bioresorbable Pressure Sensor

Aleksi Palmroth,* Timo Salpavaara, Jukka Lekkala, and Minna Kellomäki

Embedding sensors into orthopedic devices can enable these implants to monitor the progress of the healing process or detect cues of complications. The simple structure of inductor–capacitor (LC) resonance sensors combined with their wireless readout offers a desirable basis for such sensors. A set of eight bioresorbable inductively coupled pressure sensors is fabricated. The conductors are formed by e-beam evaporation of magnesium (7 µm) directly onto the substrates, after which two substrates are adhered to a holed spacer to form an LC sensor. All the sensors show a fairly linear pressure response in the physiological pressure range from 0 to 200 mm Hg with an average pressure sensitivity of −6.0 ± 0.5 kHz mm Hg^{-1}. After the pressure response tests, the effects of known error sources are determined. Finally, the sensor performance in vitro in buffer solution at +37 °C is evaluated. The sensors function tolerably for the first 8 h in immersion, after which they are disabled by mechanical changes in the sensor structure. To conclude, a bioresorbable battery-free wireless pressure sensor architecture with an adequate sensitivity for biomedical applications is described. However, further studies are required to improve the stability of the sensors under physiological conditions.

1. Introduction

As a developing interdisciplinary field, bioresorbable implantable electronics has great potential in acute transitory sensing and stimulation applications.[1–3] In one approach, the electronic devices could be embedded into orthopedic implants like bone fixation plates or screws. This could be done either by using the orthopedic implant as a substrate and fabricating the sensor directly onto the implant, or by mounting a separately fabricated sensor onto an implant. Consequently, such implants could measure physiological events directly at the healing site for a

A. Palmroth, Prof. M. Kellomäki
Biomaterials and Tissue Engineering Group
BioMediTech
Faculty of Medicine and Health Technology
Tampere University
Korkeakoulunkatu 3, 33720 Tampere, Finland
E-mail: aleksi.palmroth@tuni.fi
Dr. T. Salpavaara, Prof. J. Lekkala
Sensor Technology and Biomeasurements Group
BioMediTech
Faculty of Medicine and Health Technology
Tampere University
Korkeakoulunkatu 3, 33720 Tampere, Finland

The ORCID identification number(s) for the author(s) of this article can be found under https://doi.org/10.1002/admt.201900428.

defined period and thereafter disappear via metabolic routes.[4] The sensors could, for example, monitor the cues of inflammatory or infectious complications, the degradation of the implant itself or other physiological variables like pressure.[5–8]

One commonly addressed application for temporary pressure sensors is intracranial pressure (ICP) monitoring.[9–11] An elevated ICP is a life-threatening condition that commonly accompanies severe head trauma and might need surgical intervention.[12] Postoperative ICP monitoring is known to significantly reduce the risk of death after decompressive craniectomy, where parts of the skull are removed to allow space for brain swelling.[13] Another potential application is the detection of acute compartment syndrome, in which the pressure levels inside an osteofascial compartment exceed the pressure of the arteries, leading to limb- and life-threatening emergency if not detected.[14] The condition has many causes, of which bone fracture is the most common. Compartment pressures are usually the highest within close proximity of the fracture,[15] making the bone fixation plate a convenient location for a sensor.

To avoid the inconvenience and increased infection risk caused by transcutaneous wires, a wireless signal transmission is strongly preferred. Low frequency inductive links are commonly used for small distance telemetry in passive implantable sensors.[16] In this method, a coil in the implant communicates with an external reading coil via magnetic coupling.[17] Typically, the sensor creates a resonance peak to the measured impedance of the reading coil at the resonance frequency (f_{max}) of the sensor. The shift of this resonance peak in response to a certain measured variable can be then detected.[18]

Biodegradable materials are typically sensitive to elevated temperatures and many chemicals that are used in conventional microfabrication processes, which makes device fabrication a fundamental challenge in implantable biodegradable electronics.[19] Innovative processing methods have already been developed specifically for the purpose, often relying on transfer printing of separately fabricated conductor or semiconductor patterns onto biodegradable polymer substrates.[4,6,20] Despite the demonstrated functionality of such techniques, their complexity and time-consuming nature encourage seeking alternative processing methods.[21] In addition to their wireless readout, inductively coupled sensors provide an attractive starting point for sensor design due to their simple structure.[22,23]

**ADVANCED
SCIENCE NEWS**
www.advancedsciencenews.com

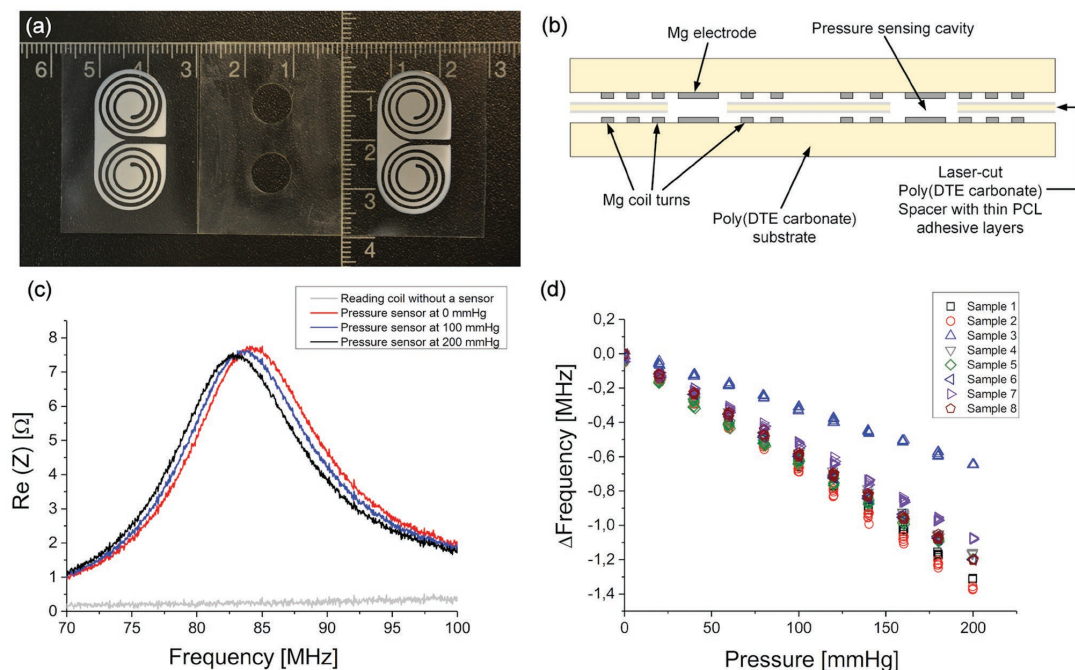**ADVANCED
MATERIALS
TECHNOLOGIES**
www.advmattechnol.de

Figure 1. a) The main components of the sensor including two substrates with Mg patterns and a spacer with laser-cut holes. b) A schematic illustration of the sensor cross-section. c) Graphs of the measured real part of the impedance spectrum as a function of frequency. Each curve corresponds to a single measurement. d) The pressure responses of all the fabricated sensors.

The aim of this study was to develop a wireless bioresorbable pressure sensor architecture with a straightforward assembly scheme and to evaluate the performance of the obtained sensors in vitro. The sensor fabrication yield was good with only one of the eight sensors showing a clearly deviant sensitivity. Furthermore, the sensors were well readable in a lossy buffer solution at a reading distance of 6 mm. Future research efforts are directed toward increasing the stability of the sensors in physiological conditions.

2. Results

Eight wireless pressure sensors were fabricated from bioresorbable materials. The sensors were based on compression molded poly(desamino tyrosyl-tyrosine ethyl ester carbonate) or poly(DTE carbonate) substrates that are known to degrade hydrolytically and resorb in the body.[24,25] Magnesium conductor patterns (7 µm) were electron-beam evaporated directly onto the substrates through 3D printed shadow masks. To form a functional pressure sensor, the substrates were attached to laser-cut spacers using polycaprolactone (PCL) as an adhesive (**Figure** 1b). Wireless measurements were performed using an external reading coil, which was inductively (magnetically) coupled with the sensor to enable short-range wireless data transfer.

The principle of operation for the sensors is demonstrated in Figure 1c, which illustrates the measured graphs of the real part of the impedance spectrum. As pressure was applied, the capacitance of the sensor increased and thus its resonance frequency (f_{max}) decreased, which was noticed as a shifting resonance peak. All the sensors responded to pressure practically linearly in the range from 0 to 200 mm Hg (Figure 1d).

The sensitivities of the sensors in the measured pressure range were estimated from the slope of the linear fit. These results along with the initial resonance frequencies are summarized in **Table 1**. Seven sensors out of eight demonstrated

Table 1. The initial resonance frequencies and sensitivity estimates of the sensors.

	Resonance frequency $f_{max(p=0)}$ [MHz]	Sensor sensitivity [kHz mm Hg^{-1}]
Sample #1	91.50	−6.5
Sample #2	81.85	−6.7
Sample #3	83.98	−3.3
Sample #4	76.96	−5.7
Sample #5	89.04	−5.8
Sample #6	94.20	−6.0
Sample #7	92.28	−5.3
Sample #8	84.49	−5.9
Average	86.79	−6.0[a]
St.dev.	5.93	0.5[a]

[a]Sample #3 excluded.

ADVANCED
SCIENCE NEWS
www.advancedsciencenews.com

ADVANCED
MATERIALS
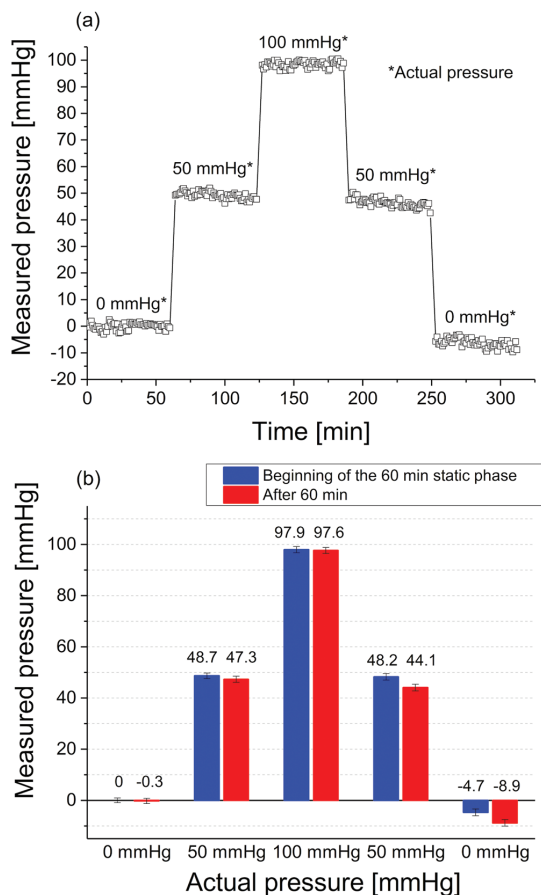TECHNOLOGIES
www.advmattechnol.de

Figure 2. a) The continuous response of the sensor to static pressure. b) The measured pressures before and after each static 60 min pressure step given as average ±SD ($n = 100$).

Figure 3. The temperature sensitivity of the sensors. a) Measurements at set temperatures expressed as average ±SD ($n = 100$). b) f_{max} drifting with respect to changes in the room temperature.

comparable sensitivities in the measurement range. The sensitivity values ranged from −5.3 to −6.7 kHz mm Hg$^{−1}$ except for sample #3 that had a deviant sensitivity of −3.3 kHz mm Hg$^{−1}$. For this reason, sample #3 was excluded from the calculations that resulted in an average sensitivity of −6.0 ± 0.5 kHz mm Hg$^{−1}$.

In the static pressure test (**Figure 2**), the resonance frequency of the sensors did not change significantly during the first 60 min steps at 0, 50, or 100 mm Hg. However, the observed pressure started to drift downward after decreasing the actual applied pressure from 100 to 50 mm Hg and later to 0 mm Hg. The standard deviation of 100 measurements was 1 mm Hg. In addition, the rise time of the system was measured to be 0.2 s (Figure S1b, Supporting Information).

An elevated temperature was noticed to result in an increased f_{max} (**Figure 3**a). Sample #2 showed a nonlinear resonance frequency change of 0.8 MHz in the range from 23 to 40 °C. The two other samples demonstrated a change of about 0.4 MHz.
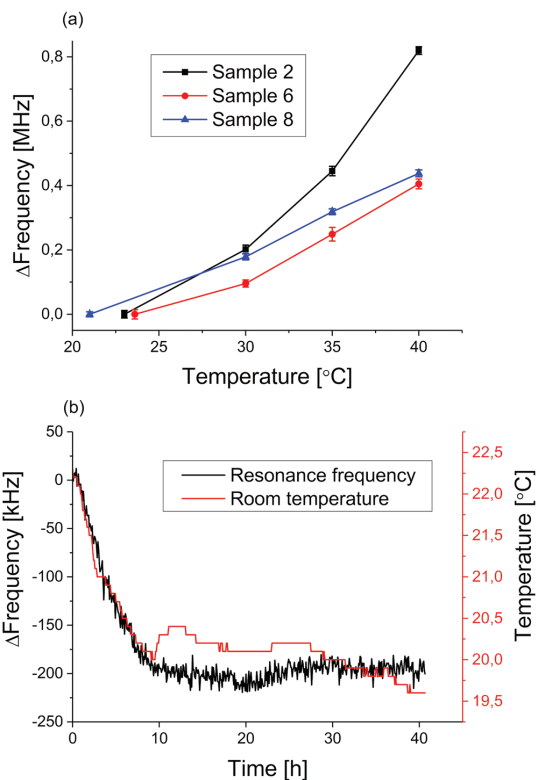
The f_{max} increase was noticed to steepen after 30 °C in all the tested samples. When studying sensor behavior as a function of time (Figure 3b), the resonance frequency seemed to partly follow the changes in the room temperature. During the first 10 h, the temperature decreased by 2 °C and the f_{max} decreased concurrently by 200 kHz. Thereafter, the temperature drifted within 1 °C for 30 h, but no correlation between the f_{max} changes were seen.

In order to see if the wireless reading process increases the sensor temperature, its surface temperature was measured during a 24 h continuous reading at room temperature. However, no changes were noticed, as the sensor surface temperature remained at 23 °C throughout the measurement period. The room temperature remained constant during this test.

In addition to temperature changes, common error sources that may affect the f_{max} of LC sensors include misalignment between the sensor and the reading coil, as well as changes in the reading distance. The results of these measurements are given in Figure S2 (Supporting Information).

A typical sensor behavior after adding Sörensen buffer solution is presented in **Figure 4**. As buffer solution was added to the bottle, the f_{max} of the sensors decreased ≈5–10 MHz. The

**ADVANCED
SCIENCE NEWS**

www.advancedsciencenews.com

**ADVANCED
MATERIALS
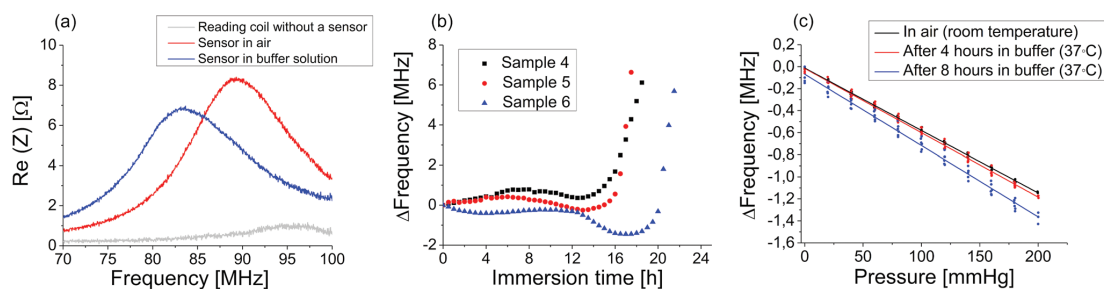TECHNOLOGIES**

www.advmattechnol.de

Figure 4. The characteristics of the sensor in aqueous conditions. a) The impedance resonance peaks of a sensor at +37 °C before and after adding the buffer solution. b) The resonance frequency changes of an immersed sensor as a function of time. c) The pressure responses of sensor sample #4 shown as an example.

resonance frequency f_{max} remained relatively stable within the first 12 h of immersion. However, it started to rapidly increase in all tested sensors after ≈14–18 h of immersion. Finally, the resonance peak drifted outside the measurement range. Therefore, the immersion tests were terminated after 24 h. Practically no magnesium corrosion was noticed at that time.

An example of the sensor sensitivity changes during immersion is shown in Figure 4c. No clear pattern was seen in the sensitivity changes between different sensors, but in all cases the sensitivities remained in the same magnitude during the 4 and 8 h time points compared to the measurements that were performed in air (Table S1, Supporting Information).

The failure mechanism of the immersed sensors was studied using micro-computed tomography (micro-CT) imaging. The results suggest that the substrates have been drawn apart from each other during immersion (**Figure 5**). Moreover, the spacers were partly detached from the substrates. As revealed by the more detailed micro-CT imaging with a pixel size of 2 µm, the distance between the Mg electrodes was about 100 µm in the middle of the cavity of an intact sensor, whereas the corresponding distance in a sensor imaged after the 24 h immersion was more than 180 µm.

3. Discussion

The presented pressure sensor architecture was designed to ease the assembly process, as layer-by-layer processing of bioresorbable materials using solvents or high temperatures may damage the underlying layers. The sensor does not require a galvanic connection between the two conductor layers and it can be assembled using two similar substrates. These factors simplify the fabrication process compared to the previously reported bioresorbable wireless pressure sensors.[6,26] Further, an additional design parameter is that the shadow mask pattern has to be rigid and continuous in order to permit its 3D printing.

The wireless measurement results demonstrated that all the eight fabricated sensors showed nearly linear responses from 0 to 200 mm Hg without any significant hysteresis. Sample #3 had a deviant sensitivity compared to the other seven sensors, which was likely caused by an unsuccessful assembly process, where the PCL adhesive may have partially fixated the capacitor plates in one of the sensing cavities. With an average sensitivity of −6.0 kHz mm Hg^{-1} (sample #3 excluded), the sensors were almost four times more sensitive within this pressure range than the sensors of our alternative design.[26] This sensitivity is well suitable for detecting physiologically relevant pressures.[27]
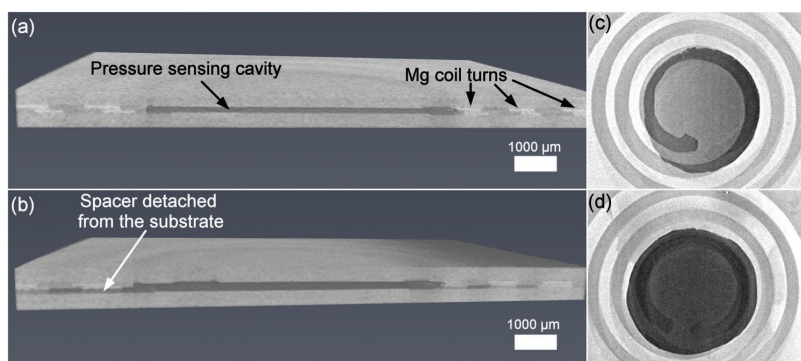

Figure 5. Micro-CT images showing the sensor failure mechanism in immersion. Cropped cross sectional 3D images of a) an intact pressure sensing cavity and b) a cavity after immersing the sensor in buffer solution at +37 °C for 1 d. The illustrations c,d) show the full imaged area around the respective cavities.

By contrast, the biodegradable inductively coupled pressure sensor of Luo et al. was reported having a comparable sensitivity of −5.2 kHz mm Hg^{-1}.[6]

The main parameters in LC sensors are the inductance of the coil and the capacitance of the capacitor, which primarily determine the f_{max} of the sensor.[23] In the currently reported sensors, the $f_{max(p = 0)}$ varied between 76.96 and 94.20 MHz. These differences were caused by variations in the spacer thicknesses and in the assembly phase, both of which probably have affected to the distance between the capacitor plates. In addition, inconsistencies in the 3D printed masks caused small differences in the evaporated coils.

The pressures in the envisioned applications of ICP monitoring or acute compartment syndrome detection are static by nature. In the static pressure tests, the measured pressure was noticed to be 1–2 mm Hg lower than the recorded actual pressure. This was likely caused by the fitting error in the linear approximation of the pressure sensitivity. The drifting of the measured pressure along the gradually decreased pressure was probably related to the mechanical properties of the polymer substrates. This should be taken into account when designing polymer-based implantable pressure sensors. Similar static pressure test results were obtained with our alternative pressure sensor design that was based on the same materials.[26] In applications where the pressure is pulsatile and consequently extremely fast response times are required, replacing the air cavity between the capacitor electrodes with a patterned biodegradable elastomer film could be of advantage.[7]

The error source analysis demonstrated that the sensors were sensitive to temperature, which is a common challenge in implantable pressure sensors.[28] Sample #2 was more sensitive to both temperature and pressure compared to the other tested samples #6 and #8. The temperature sensitivity of the sensors might be explained by heat expansion, which could cause dimensional changes in the substrate and in the adhesive layer. Based on the results, we hypothesize that the capacitors of the more pressure-sensitive sensors would be more susceptible to deformation by temperature as well. Nevertheless, the wireless reading process itself was confirmed not to heat up the sensor, as verified by the sensor surface temperature measurements.

Alignment of the sensor with respect to the reading coil had a significant effect on the detected resonance frequency. The test was performed at a reading distance of 1 mm as an approximated worst case scenario, since the largest errors typically occur when the coupling between the coils is the strongest. Moreover, this setup tests the effects of the possible capacitive coupling between the coil wirings. A displacement of 1 mm in either X- or Y-direction did not alter the measured resonance frequency significantly: a deviance of less than 6 kHz was noticed, which would translate to 1 mm Hg in observed pressure. However, a displacement of 2 mm in the X-direction or 3 mm in the Y-direction shifted the resonance frequency already with 34 kHz. These large shifts were partially caused by overlapping of the sensor and the reading coil in our setup (Figure S3a, Supporting Information).

The sensors were wirelessly readable up to a distance of 14 mm. This would be appropriate in applications where the implant is placed close under the skin, as the skin thickness typically varies from 0.5 to 3.0 mm.[29] The maximum reading distance could be further improved by increasing the conductivity of

the coils. In this case, higher conductivity might be achieved for example by building a thicker magnesium layer.[4] On the other hand, developing bioresorbable materials with higher conductivities has been considered as an important endeavor in the field.[30] Furthermore, the reading distance has been shown to have an effect on the f_{max} in LC resonance sensors due to parasitic capacitances.[31] In our system, the decreasing resonance frequency with reading distances changing from 1 to 4 mm might be due to capacitive coupling between the sensor and the reading coil. The most convenient operating distance for the sensor could be considered to be between 4 and 10 mm, as the effect of the reading distance in that range is relatively marginal.

Upon immersion, an immediate resonance frequency drop was noticed similarly to the inductively coupled sensor of Luo et al., which was measured in normal saline solution (0.9% NaCl in distilled water).[6] The f_{max} drop was partly due to the increased capacitance when the sensors were placed in an ionic solution as well as due to the hydrostatic pressure. Further, the measurement losses are greater in conductive media such as saline or Sörensen buffer solution.[32,33] The errors can be seen in the pressure response measurement results of the immersed sensor as larger deviations compared to the measurements performed in air.

The resonance frequencies were noticed to drift within ±1 MHz during the first 12 h. After 14–18 h of immersion, the resonance frequencies started to rise rapidly, moving ultimately outside the measurement range. In our preliminary tests, LC resonators based on poly-L/D-lactide 96L/4D (PLDLA 96/4) or poly(3-hydroxybutyrate-co-3-hydroxyvalerate) substrates and spacers without any PCL adhesive behaved in a similar manner during immersion. The rapid increase in $f_{max(p = 0)}$ was probably caused by the deformation of the welded substrates by relaxation or swelling processes, which resulted in a decreased capacitance as the capacitor electrodes bended further away from each other. Ultimately, the substrates detached partly from the spacer. The sensor disintegration mechanism was verified by micro-CT imaging.

Prolonging the functional lifetime of bioresorbable sensors without compromising the ultimate bioresorption remains an essential challenge in transient electronics.[10] Concerning the reported sensor architecture, a thicker adhesive layer between the spacer and the substrate might be useful in preventing the deformation of the substrates. Furthermore, thin encapsulation layers made, for example, from MgO or SiO$_2$ have been studied as temporary water barrier layers for prolonging the lifetime of bioresorbable semiconductor based devices.[10,34] Correspondingly, using substrates based on surface erodible polymers such as polyanhydrides or polyorthoesters might be a step toward resolving this issue. In surface eroding polymers, water only penetrates the surface layers of the material that is sequentially eroded.[35] However, the majority of biodegradable polymers are bulk erodible, which means water starts to penetrate into the polymer matrix as soon as the sample is immersed in aqueous media.[36] For example, poly(DTE carbonate) degrades by bulk erosion with a reported water uptake of 2–3 wt% at saturation.[25]

In conclusion, the fabricated sensors showed similar characteristics in air with a sufficient sensitivity for biomedical applications. The most convenient reading distance for the sensors was between 4 and 10 mm, as f_{max} remained relatively constant

within that range. Other parameters to consider when designing and characterizing LC sensors include their possible temperature sensitivity and the alignment of the sensor in relation to the reading coil. In any case, one of the biggest challenges is obtaining a stable performance during the intended functional lifetime under immersion at body temperature. Tackling this challenge would pave the way for inductively coupled capacitive sensors in implant applications.

4. Conclusion

A set of eight bioresorbable pressure sensors was produced and wirelessly measured using inductive coupling as a readout scheme. The yield of the fabrication method was good, as all the resonance sensors functioned, despite one of them showing a deviant pressure sensitivity. The pressure sensitivity of the sensors was relevant for physiological applications. Furthermore, the effects of common error sources were tested. Such parameters include the temperature, alignment between the sensor and the reading coil as well as changes in the reading distance. Finally, sensors were immersed in buffer solution at +37 °C. Their performance remained tolerable for the first 8 h, but the structure of the sensors was noticed to deform in buffer solution, leading to inoperative sensors after the first day of immersion. Future work consists of miniaturizing the sensors and improving their stability in aqueous conditions.

5. Experimental Section

Sensor Fabrication: Poly(DTE carbonate) (Integra LifeSciences, NJ, USA) was first extruded into rods using a corotating twin-screw extruder (Mini ZE 20*11.5 D, Neste Oy, Finland), after which pieces from the rod were compression molded to form substrates (430 µm). Magnesium pellets (99,99%; G-materials, Germany) were electron-beam evaporated onto the substrates through 3D printed masks to form conductor patterns (7 µm). The average DC resistance ($n = 8$) between two capacitor plates in the Mg pattern (Figure 1a) was 15 Ω, as measured from compression molded substrates with a digital multimeter (Fluke 115 TRMS). A simplified electrical design of a similar resonator without a pressure sensing function, as well as the shape of the evaporated Mg pattern have been described previously.[37]

Compression molded poly(DTE carbonate) spacers with thicknesses ranging between 65 and 95 µm were used between two substrates to form a structure of four coils and two varying capacitors. The spacers contained two laser-cut holes with a diameter of 8 mm and a distance between the center points of 14.3 mm.

To attach the substrates to the spacer, ≈7 µm thick PCL (Purac Biochem B.V., Gorinchem, the Netherlands) films were first spin coated onto glass substrates using cyclohexanone (VWR, Fontenay-sous-Bois, France) as a solvent. The PCL films were then transferred onto both sides of the spacer by melting the films and then compressing the spacer onto the melt. After the subsequent cooling phase, the excessive PCL was removed from the laser-cut holes with a scalpel. The magnesium-patterned substrates were then attached to the spacer by heating the sandwich structure at 80 °C under gentle pressure. This temperature is sufficient to melt the PCL layers without deforming the poly(DTE carbonate) substrates that have a glass transition temperature close to 100 °C.[38] The structure was finally sealed from the sides using a heat sealer (Hawo HPL ISZ, Obrigheim, Germany) and the welded seams were trimmed using scissors. Sensors with final dimensions of ≈1 mm by 25 mm by 35 mm were obtained. A total of eight bioresorbable sensors was fabricated.

Pressure Measurements: The sensors were attached onto the bottom of a 250 mL glass bottle (VWR, Leuven, Belgium) using Kapton tape. The pressure measurements were wirelessly performed through the bottle, leading to a reading distance of 6 mm. An external single turn coil with a diameter of 33 mm connected to an impedance analyzer (Agilent 4396B) was used to read the sensor as shown in a schematic illustration of the measurement setup (Figure S4, Supporting Information).

The pressure response measurements were performed from 0 to 200 and back to 0 mm Hg by recording single measurement samples at intervals of 20 mm Hg. Three cycles per sensor were measured at room temperature.

Static pressure testing was performed stepwise from 0 to 100 mm Hg and back to 0 mm Hg at intervals of 50 mm Hg by keeping the pressure constant for 60 min in each step and recording single measurement samples once in a minute. In addition, 100 measurement samples were recorded in the beginning and at the end of each 60 min step. This was done to compare the measured average pressures before and after each static pressure phase. In the calculations, the initial resonance frequency $f_{max(p = 0)}$ was chosen as the average of the first 100 measurements without any applied pressure. The obtained resonance frequencies were translated to pressure values using the linearly approximated sensor sensitivities as a basis.

As opposed to all other measurements, the rise time of the measurement system was assessed with an in-house built reader device[32] that was capable of faster measurements compared to the impedance analyzer. The bottle was pressurized to 150 mm Hg while recording 50 measurement samples per second, after which the pressure was released. The resonance frequency was identified from the magnitude curve (f_{dip}) as opposed to the Re (Z) peak (f_{max}) in all other measurements. The rise time of the system was defined as the time required for the response of the sensor to reach from 10% of the final value to 90%.

Some of the sensors (Table S1, Supporting Information) were tested in aqueous conditions by adding prewarmed Sörensen buffer solution (100 mL) into the bottle at +37 °C. The utilized Sörensen buffer solution[38] was prepared according to the standard "ISO 15 814:1999(E): Implants for surgery—Copolymers and blends based on polylactide—In vitro degradation testing." The $f_{max(p = 0)}$ of the immersed sensors was recorded every 30 min. In addition, the pressure response of the sensors was tested at predetermined time points in a similar manner than in air.

Error Source Measurements: The effects of potential error sources were tested in air. Unless otherwise stated, all the following experiments were done by recording and averaging 100 measurement samples at each test point. First, the temperature sensitivity of the sensors was tested in the range from room temperature (21–24 °C) to 40 °C at set intervals. In addition, the response of the sensor to changing room temperature was studied by recording one measurement of the $f_{max(p = 0)}$ every 5 min for 40 h and measuring the room temperature changes with an indoor weather station (Netatmo, France).

In order to confirm that the sensor does not heat up during the wireless process, the surface temperature of the sensor was measured with an infrared thermometer (Fluke 62 Mini IR thermometer) from five different locations before wireless reading and after 2, 4, 6, and 24 h of continuous reading. The sensor was placed directly onto the reading coil and the room temperature was measured (Vaisala HM40 hand-held humidity and temperature meter, Finland) to rule out its effects on the results.

The error caused by the displacement between the sensor and the reading coil was tested separately in X and Y directions in the plane of the reading coil as illustrated in Figure S3a (Supporting Information). The Z direction was kept constant at 1 mm by placing a microscopy slide between the reading coil and the sensor. The Mg pattern of the sensor was initially positioned to the middle of the reading coil, after which the sensor was moved stepwise 1 mm at a time and measured at each position.

The error caused by the changing reading distance, or the distance between the sensor and the reading coil in vertical direction was tested. This was done by adding 1 mm thick microscopy slides stepwise (Figure S3b, Supporting Information) between the sensor and the reading coil and measuring the sensor after every added 1–2 mm until the resonance peak was not clearly readable. The sensor was positioned to the center of the reading coil in the reading distance test.

ADVANCED
SCIENCE NEWS
www.advancedsciencenews.com

ADVANCED
MATERIALS
TECHNOLOGIES
www.advmattechnol.de

Micro-CT: Micro-computed tomography (Xradia MicroXCT-400, Zeiss, USA) imaging was utilized to study the appearance of the pressure sensing cavities before and after hydrolysis. The imaged area of 10 by 10 mm with a pixel size of 20 µm was sufficient to illustrate one of the two cavities per sensor. Additional micro-CT images with an imaged area of 2 by 2 mm and a 2 µm pixel size were taken to obtain more accurate quantitative data about the distance between the 2 Mg electrodes that formed the varying capacitors.

Supporting Information

Supporting Information is available from the Wiley Online Library or from the author.

Acknowledgements

Conflict of Interest

The authors declare no conflict of interest.

Keywords

[1] S.-K. Kang, J. Koo, Y. K. Lee, J. A. Rogers, *Acc. Chem. Res.* **2018**, *51*, 988.

[2] X. Yu, W. Shou, B. K. Mahajan, X. Huang, H. Pan, *Adv. Mater.* **2018**, *30*, 1707624.

[3] G. D. Cha, D. Kang, J. Lee, D.-H. Kim, *Adv. Healthcare Mater.* **2019**, *8*, 1801660.

[4] S.-W. Hwang, X. Huang, J.-H. Seo, J.-K. Song, S. Kim, S. Hage-Ali, H.-J. Chung, H. Tao, F. G. Omenetto, Z. Ma, J. A. Rogers, *Adv. Mater.* **2013**, *25*, 3526.

[5] T. Salpavaara, A. Hänninen, A. Antniemi, J. Lekkala, M. Kellomäki, *Sens. Actuators, B* **2017**, *251*, 1018.

[6] M. Luo, A. W. Martinez, C. Song, F. Herrault, M. G. Allen, *J. Microelectromech. Syst.* **2014**, *23*, 4.

[7] C. M. Boutry, A. Nguyen, Q. O. Lawal, A. Chortos, S. Rondeau-Gagné, Z. Bao, *Adv. Mater.* **2015**, *27*, 6954.

[8] C. M. Boutry, L. Beker, Y. Kaizawa, C. Vassos, H. Tran, A. C. Hinckley, R. Pfattner, S. Niu, J. Li, J. Claverie, Z. Wang, J. Chang, P. M. Fox, Z. Bao, *Nat. Biomed. Eng.* **2019**, *3*, 47.

[9] S.-K. Kang, R. K. J. Murphy, S.-W. Hwang, S. M. Lee, D. V Harburg, N. A. Krueger, J. Shin, P. Gamble, H. Cheng, S. Yu, Z. Liu, J. G. McCall, M. Stephen, H. Ying, J. Kim, G. Park, R. C. Webb, C. H. Lee, S. Chung, D. S. Wie, A. D. Gujar, B. Vemulapalli, A. H. Kim, K.-M. Lee, J. Cheng, Y. Huang, S. H. Lee, P. V Braun, W. Z. Ray, J. A. Rogers, *Nature* **2016**, *530*, 71.

[10] J. Shin, Y. Yan, W. Bai, Y. Xue, P. Gamble, L. Tian, I. Kandela, C. R. Haney, W. Spees, Y. Lee, M. Choi, J. Ko, H. Ryu, J.-K. Chang, M. Pezhouh, S.-K. Kang, S. M. Won, K. J. Yu, J. Zhao, Y. K. Lee, M. R. MacEwan, S.-K. Song, Y. Huang, W. Z. Ray, J. A. Rogers, *Nat. Biomed. Eng.* **2019**, *3*, 37.

[11] L. Y. Chen, B. C.-K. Tee, A. L. Chortos, G. Schwartz, V. Tse, D. J. Lipomi, H.-S. P. Wong, M. V. McConnell, Z. Bao, *Nat. Commun.* **2014**, *5*, 5028.

[12] L. Rangel-Castilla, S. Gopinath, C. S. Robertson, *Neurol. Clin.* **2008**, *26*, 521.

[13] D.-R. Kim, S.-H. Yang, J.-H. Sung, S.-W. Lee, B.-C. Son, *J. Korean Neurosurg. Soc.* **2014**, *55*, 26.

[14] J. M. Flynn, W. N. Sankar, S. W. Wiesel, *Operative Techniques in Pediatric Orthopaedic Surgery*, 2nd ed., Wolters Kluwer Health, Philadelphia, PA **2015**.

[15] T. Whitesides, M. Heckman, *J. Am. Acad. Orthop. Surg.* **1996**, *4*, 209.

[16] R. Bashirullah, *IEEE Microwave Mag.* **2010**, *11*, S14.

[17] C. O'Connor, A. Kiourti, *J. Bio. Tribo Corros.* **2017**, *3*, 20.

[18] C. M. Boutry, H. Chandrahalim, P. Streit, M. Schinhammer, A. C. Hänzi, C. Hierold, *Sens. Actuators, A* **2013**, *189*, 344.

[19] S.-W. Hwang, J.-K. Song, X. Huang, H. Cheng, S.-K. Kang, B. H. Kim, J.-H. Kim, S. Yu, Y. Huang, J. A. Rogers, *Adv. Mater.* **2014**, *26*, 3905.

[20] S.-W. Hwang, D.-H. Kim, H. Tao, T. Kim, S. Kim, K. J. Yu, B. Panilaitis, J.-W. Jeong, J.-K. Song, F. G. Omenetto, J. A. Rogers, *Adv. Funct. Mater.* **2013**, *23*, 4087.

[21] X. Huang, *Bioresorbable Materials and Their Application in Electronics*, Cambridge University Press, Cambridge **2017**.

[22] T. Salpavaara, J. Verho, P. Kumpulainen, J. Lekkala, *Procedia Eng.* **2010**, *5*, 216.

[23] Q. A. Huang, L. Dong, L. F. Wang, *J. Microelectromech. Syst.* **2016**, *25*, 822.

[24] A. J. Asikainen, M. Pelto, J. Noponen, M. Kellomäki, H. Pihlajamäki, C. Lindqvist, R. Suuronen, *J. Mater. Sci.: Mater. Med.* **2008**, *19*, 53.

[25] V. Tangpasuthadol, S. M. Pendharkar, R. C. Peterson, J. Kohn, *Biomaterials* **2000**, *21*, 2379.

[26] A. Hänninen, T. Salpavaara, J. Lekkala, M. Kellomäki, *Proceedings* **2018**, *2*, 914.

[27] J. F. Drazan, M. T. Wassick, R. Dahle, L. A. Beardslee, N. C. Cady, E. H. Ledet, in *38th Annual Int. Conf. on IEEE Engineering in Medicine and Biology Society (EMBC 2016)*, IEEE, Piscataway, NJ **2016**, pp. 1890–1893.

[28] L. Yu, B. J. Kim, E. Meng, *Sensors* **2014**, *14*, 20620.

[29] L. J. Skandalakis, J. E. Skandalakis, P. N. Skandalakis, *Surgical Anatomy and Technique: A Pocket Manual*, Springer, New York, NY **2009**.

[30] C. M. Boutry, H. Chandrahalim, P. Streit, M. Schinhammer, A. C. Hänzi, C. Hierold, *Philos. Trans. R. Soc., A* **2012**, *370*, 2418.

[31] M. Demori, M. Baù, M. Ferrari, V. Ferrari, *Micromachines* **2018**, *9*, 449.

[32] T. Salpavaara, *Ph.D. Thesis*, Tampere University of Technology **2018**.

[33] N. Xue, S. P. Chang, J. B. Lee, *J. Microelectromech. Syst.* **2012**, *21*, 1338.

[34] S.-K. Kang, S.-W. Hwang, H. Cheng, S. Yu, B. H. Kim, J.-H. Kim, Y. Huang, J. A. Rogers, *Adv. Funct. Mater.* **2014**, *24*, 4427.

[35] M. J.-L. Tschan, N. S. Ieong, R. Todd, J. Everson, A. P. Dove, *Angew. Chem., Int. Ed.* **2017**, *56*, 16664.

[36] S. Lyu, D. Untereker, *Int. J. Mol. Sci.* **2009**, *10*, 4033.

[37] T. Salpavaara, V. Ellä, M. Kellomäki, J. Lekkala, in *8th Int. Conf. on Biomedical Electronics and Devices (BIODEVICES 2015)*, SciTePress, Setúbal, Portugal **2015**, pp. 127–131.

[38] A. Palmroth, T. Salpavaara, I. Lyyra, M. Kroon, J. Lekkala, M. Kellomäki, *ACS Biomater. Sci. Eng.* **2019**, *5*, 1134.

ADVANCED MATERIALS TECHNOLOGIES

Supporting Information

Fabrication and Characterization of a Wireless Bioresorbable Pressure Sensor

Aleksi Palmroth,* Timo Salpavaara, Jukka Lekkala, and Minna Kellomäki

Supporting Information

Fabrication and Characterization of a Wireless Bioresorbable Pressure Sensor

Aleksi Palmroth*, Timo Salpavaara, Jukka Lekkala, Minna Kellomäki

Supporting Information

Table S1. Sensitivity changes of the sensors immersed in buffer solution.

Sensitivity	Sample #1	Sample #4	Sample #5
In air (room temperature)	6.5 kHz mmHg^{-1}	5.7 kHz mmHg^{-1}	5.7 kHz mmHg^{-1}
After 4 hours of immersion (+37 °C)	5.5 kHz mmHg^{-1}	5.8 kHz mmHg^{-1}	4.7 kHz mmHg^{-1}
After 8 hours of immersion (+37 °C)	4.3 kHz mmHg^{-1}	6.5 kHz mmHg^{-1}	5.3 kHz mmHg^{-1}

The rise time was defined as the time required to reach from 10 % to 90 % of the final value $f_{dip(p=150)}$, which was set to the average frequency of the measurements between 12-17 seconds (Figure S1a). As shown in Figure S1b, the rise time for the system used in this study was 0.2 s. However, this metric included the inevitable delays in the bottle pressurization caused by the measurement setup, which was not optimized for quick pressure changes.
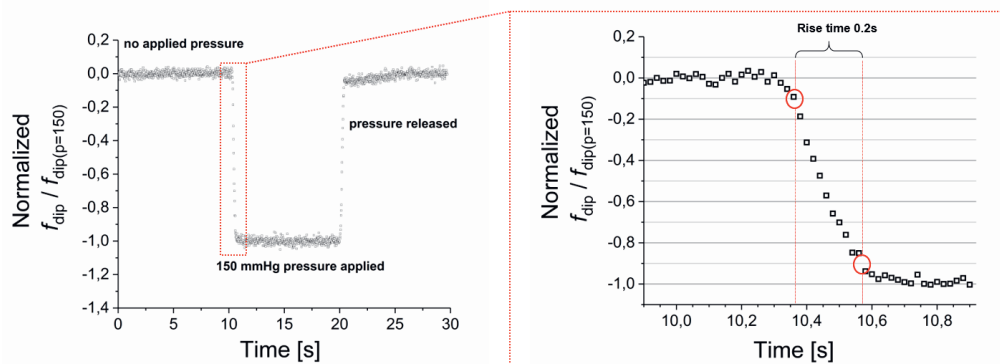

Figure S1. (a) The rise time measurement was performed by pressurizing a bottle including the wireless sensor into 150 mmHg and releasing the pressure. The time (from about 21 to 25 seconds) needed for the system to reach the initial level after pressure release is probably caused by the bottle de-pressurization delay of the measurement setup. (b) A zoomed view of the pressure increase step.

Figure S2 illustrates the effect of misalignment of the sensor and the reading coil as well as the effect of a changing reading distance. An illustration of the measurement details is given in Figure S3. The f_{max} started to decrease after a displacement of more than 2 mm in the Y-direction. In the X-direction, a displacement of 2 mm resulted in an f_{max} shift of more than 30 kHz compared to the initial value. A rapid f_{max} increase was seen when the X-displacement was more than 3 mm.

A decrease of around 300 kHz was noticed after adding the first microscopy slide between the reading coil and the sensor. Increasing the reading distance by stacking microscopy slides between the reading coil and the sensor resulted in a relatively rapid decrease in resonance

frequency up to a distance of 4 mm. The f_{max} remained relatively stable between reading distances from 4 mm to 10 mm, after which it started to increase. The standard deviations of 100 resonance frequency measurements at reading distances of 1 mm, 6 mm, 8 mm and 10 mm were 5.5 kHz, 7.5 kHz, 13.2 kHz and 22.6 kHz, respectively. The sensor was readable up to 14 millimeters although the resonance peak was considerably attenuated at that distance.
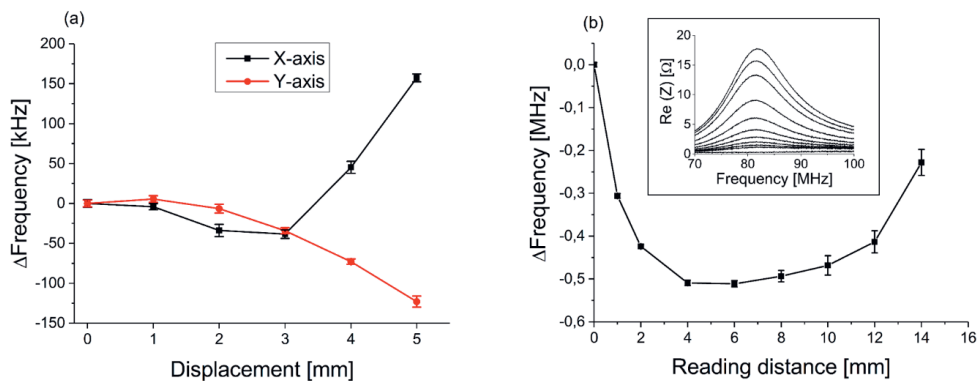

Figure S2. The effects of typical measurement error sources on the resonance frequency $f_{max(p=0)}$:
(a) displacement of the sensor with respect to the coil in X- and Y-directions and (b) alterations in the reading distance of the sensor. The attenuation of the resonance peak with increasing reading distance is shown in the inset figure.
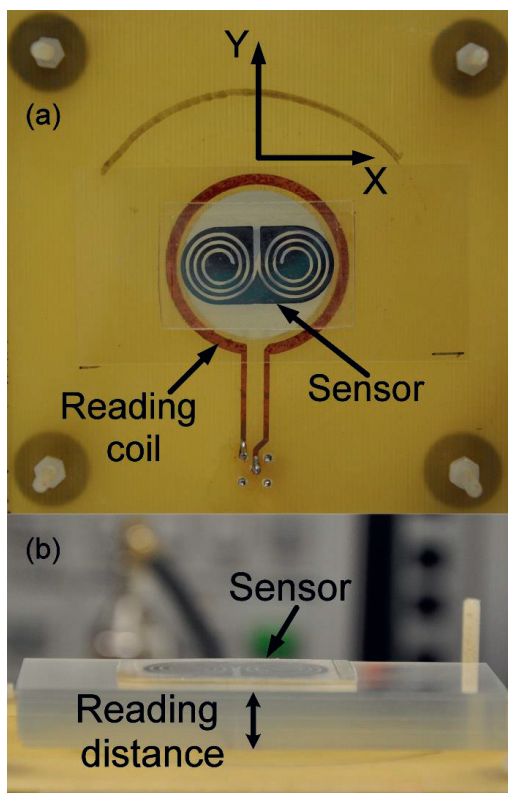
Figure S3. Illustration of the error source measurements. (a) The starting point for the displacement tests. The sensor was moved stepwise 1 mm at a time and measured at each position. X and Y directions were tested separately. (b) An example of the reading distance measurement, where glass slides were stepwise stacked between the reading coil and the sensor to alter the reading distance.
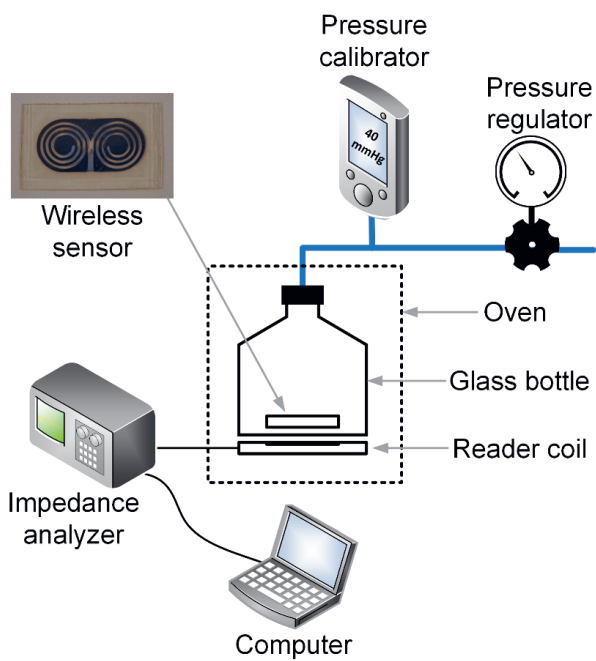
Figure S4. The setup used in the pressure measurements.

PUBLICATION
IV

Materials and Orthopedic Applications for Bioresorbable Inductively Coupled Resonance Sensors

Aleksi Palmroth, Timo Salpavaara, Petri Vuoristo, Sanna Karjalainen, Tommi Kääriäinen, Susanna Miettinen, Jonathan Massera, Jukka Lekkala, Minna Kellomäki

ACS APPLIED MATERIALS & INTERFACES

Research Article

Materials and Orthopedic Applications for Bioresorbable Inductively Coupled Resonance Sensors

Aleksi Palmroth,* Timo Salpavaara, Petri Vuoristo, Sanna Karjalainen, Tommi Kääriäinen, Susanna Miettinen, Jonathan Massera, Jukka Lekkala, and Minna Kellomäki

Cite This: *ACS Appl. Mater. Interfaces* 2020, 12, 31148−31161

Read Online

ACCESS | Metrics & More | Article Recommendations | Supporting Information

ABSTRACT: Bioresorbable passive resonance sensors based on inductor−capacitor (LC) circuits provide an auspicious sensing technology for temporary battery-free implant applications due to their simplicity, wireless readout, and the ability to be eventually metabolized by the body. In this study, the fabrication and performance of various LC circuit-based sensors are investigated to provide a comprehensive view on different material options and fabrication methods. The study is divided into sections that address different sensor constituents, including bioresorbable polymer and bioactive glass substrates, dissolvable metallic conductors, and atomic layer deposited (ALD) water barrier films on polymeric substrates. The manufactured devices included a polymer-based pressure sensor that remained pressure responsive for 10 days in aqueous conditions, the first wirelessly readable bioactive glass-based resonance sensor for monitoring the complex permittivity of its surroundings, and a solenoidal coil-based compression sensor built onto a polymeric bone fixation screw. The findings together with the envisioned orthopedic applications provide a reference point for future studies related to bioresorbable passive resonance sensors.

Bioresorbable bone fixation plate
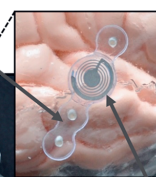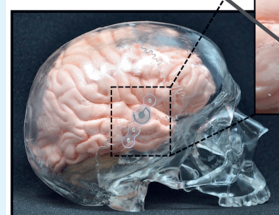
Wireless bioresorbable sensor

1. INTRODUCTION

Implantable sensors have been used for research purposes as part of orthopedic fixation devices for decades, but their clinical usage has remained scarce. The early smart implant systems utilized percutaneous wires for power and data transfer, but the wires are known to increase infection risks and may constrain the device usage to hospital surroundings.[1−3] One approach for wireless sensor systems involves inductively coupled passive resonance sensors, which essentially consist of a parallel circuit of an inductor (L) coil and a capacitor (C). Such sensors operate without batteries, which reduces their size and complexity, thus making them easier to integrate into orthopedic implants.[4] As a recent approach, sensors made from bioresorbable materials are designed to operate for a defined time under physiological conditions, after which they degrade into nontoxic substances that can be eliminated from the body.[5,6]

The operational principle of the sensors is based on inductive coupling between the LC circuit and a reader coil, whereupon a resonance curve is created at a given frequency range. The resonance curve may form a peak or a dip, depending on whether the real part of the impedance or the phase of the impedance is measured, respectively. Typically, the capacitance or inductance of the sensor changes in response to a measured variable, which shifts the resonance curve. This can be detected by estimating the frequency of the maximum or minimum value of the curve (depending on whether the resonance curve is a peak or a dip, respectively). A review by Huang et al. discusses the operational principle and state-of-the-art of these sensors in more detail.[7]

A typical resonance sensor consists of a planar or solenoidal inductor coil connected to an interdigital or parallel-plate capacitor, which is often used as the sensing element. In addition, the sensors comprise a certain resistance (R) and may contain separate resistive components, which is why the term RLC circuit is sometimes used. Passive resonance sensors enable a variety of measurement applications, including but not limited to pressure, strain, pH, temperature, and biochemical sensing.[7]

Bioresorbable sensors are, by definition, only suitable for short-term applications. For example, after an open reduction and internal fixation (ORIF) of broken bones, the sensors could be added into the fixation devices to temporarily
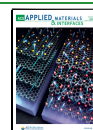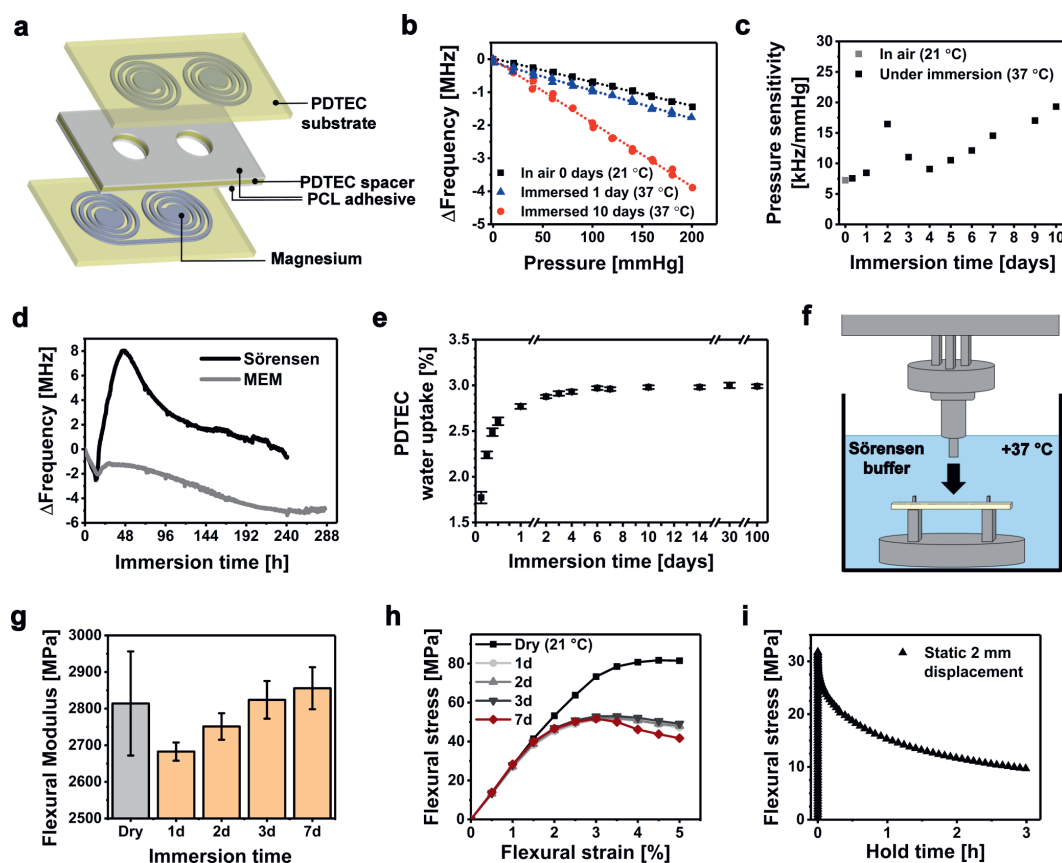
Figure 1. (a) Architecture of the wireless bioresorbable Mg pressure sensors, whose initial resonance frequencies in air are presented later in Table 1. (b) Examples of the pressure response of the sensor in air before immersion and in Sörensen buffer solution after 1 and 10 days of immersion. (c) Measured pressure sensitivities of the sensor immersed in Sörensen buffer. (d) Drifting of the pressure sensor resonance frequency under immersion without applied pressure. (e) Water uptake properties of PDTEC. (f) Measurement setup for all the mechanical tests, where the three-point bending of the PDTEC samples was performed under immersion at +37 °C. (g) Flexural moduli of the immersed PDTEC samples. The initial, day 0 dry value was measured at +21 °C. (h) Flexural stress−strain curves of PDTEC as tested under immersion at various time points. (i) Stress relaxation behavior of PDTEC in aqueous conditions under a static 2 mm displacement.

monitor parameters like temperature for early signs of infection, intratissue pressure for cues of acute compartment syndrome, or strain to measure the stiffness of the fracture callus or to personalize tendon rehabilitation processes.[4,8−10] Furthermore, intraoperative load sensors have provided improved results in total knee replacements by guiding the surgeon toward correct knee loading.[11] Similar sensor-guided operations could be performed with smart implants where a bioresorbable sensor would be integrated into the orthopedic implant. These kinds of applications could reduce unnecessary patient discomfort and facilitate massive savings by detecting adverse events early or by reducing revision surgeries and expensive imaging procedures.[4,12]

One of the main challenges in bioresorbable sensors is their fabrication. In many cases, the bioresorbable substrates are incompatible with conventional microfabrication processes like electrodeposition, photolithography, and etching.[13,14] The process steps may involve spin-coating materials with organic

solvents, baking at high temperatures, or immersing the substrates into electrodeposition solutions or lift-off chemicals. The associated conditions may damage the substrates or already prepared functional layers, which complicates the assembly of bioresorbable sensors.

The aim of this study is to provide an overall materials perspective on bioresorbable passive resonance sensors by discussing different material options, fabrication methods, and sensor architectures. The experimental novelty of the work lies in two original sensors, new material combinations and discussion of in vitro testing methods. Furthermore, an improved version of a previously published pressure sensor is utilized to discuss the effect of polymer substrates on the sensor performance as well as to compare physical vapor deposited (PVD) magnesium (Mg) and zinc (Zn) conductors. The novel sensor architectures include the first bioactive glass-based wireless resonance sensor and a molybdenum (Mo) wire-based compression sensor with a solenoidal design. The

performance of the devices is demonstrated with wireless sensor measurements, on top of which the material properties of the components are evaluated in simulated physiological conditions. Finally, the water barrier materials are addressed by evaluating atomic layer deposited (ALD) encapsulation films, which are deposited on bioresorbable polymer substrates. In addition to the experimental results, several potential orthopedic applications are suggested for wireless bioresorbable sensors.

2. RESULTS AND DISCUSSION

2.1. Bioresorbable Polymer-Based Pressure Sensors.
Bioresorbable wireless pressure sensors reported so far are mostly based on polymeric substrates.[3,15−18] This is rational because bioresorbable polymeric bone fixation plates have been used for decades especially in pediatric patients, where permanent fixation might hinder bone growth.[19] Thus, fabricating the sensors directly onto the orthopedic plates offers one simple possibility for integrating the sensors onto the implants. In this study, the material attributes of a recently reported polymer-based bioresorbable pressure sensor[18] were adjusted regarding the adhesive layers and Mg conductor patterns. This section involves testing these Mg pressure sensors and characterizing the water uptake and flexural properties of the substrate material in simulated physiological conditions.

The Mg pressure sensors were fabricated by attaching two poly(desaminotyrosyl−tyrosine ethyl ester carbonate) (PDTEC) substrates (430 μm) with e-beam evaporated Mg conductor patterns (7.5 μm) onto a holed spacer by using molten polycaprolactone (PCL) films (∼15 μm) as an adhesive (Figure 1a). The working principle of the sensor is based on variable capacitors formed by the Mg electrodes on the substrates; as pressure is increased, the electrodes bend toward each other in the two cavities that are confined by the substrates and the holes in the spacer. This increases the capacitance of the LC circuit, which is detected as a shifting resonance peak (or decreased resonance frequency) as illustrated earlier.[18] In this study, the adhesive PCL layer that attaches the substrates into the spacer was about twice as thick than in the previous version. This was assumed to increase the functional lifetime of the pressure sensor because in the anterior publication the substrates were noticed to detach from the spacer during immersion. In addition, the evaporation masks were now fabricated from laser-cut metal sheets instead of 3D-printed polymers that were used in the earlier study.[18] The masks were redesigned to remove excessive Mg from around the coils to reduce possible stray capacitances.

In this study, the sensor remained readable and responded to pressure changes under immersion in the Sörensen buffer solution for 10 days, after which the resonance peak (∼101 MHz) was largely attenuated and the test was terminated. The Sörensen buffer was chosen to reliably compare the sensor behavior with our previously reported pressure sensor, which had failed during the first 24 h of immersion.[18] In addition, a similar sensor was now immersed in Minimum Essential Medium (MEM) to more accurately simulate the contents of physiological solutions.[20] The sensor was readable in MEM for up to 12 days. Thereafter, the detection of the resonance frequency (∼88 MHz) was not reliable anymore due to resonance peak attenuation, which increased the uncertainty in estimating the resonance frequency. The attenuation was caused by the corroding Mg conductors, which increased the

electrical resistance in the circuit. Furthermore, the increasing resistance may decrease the resonance frequency.[21] The effects of the resistance on the resonance frequency are often neglected in conventional applications where the resistances are diminutive, but should be taken into account in biodegradable devices where the resistances and their changes can be more significant.

Bacterial growth was noticed as a film on top of the MEM solution upon test termination after 14 days, which may potentially have accelerated Mg corrosion via acidification.[22] As discussed later in section 2.3, the differences in the simulated physiological conditions have a significant impact on the metal corrosion. On the other hand, the contamination risks and increased complexity of the test setups advocate for using simpler buffer solutions than cell culture media in sensor measurements, where the conductors are encapsulated. This is because the encapsulation layers diminish the effect of proteins and other nonpermeable substances on the metal corrosion.

The initial resonance frequencies of the immersed sensors in Sörensen and MEM were 101.89 MHz (106.57 MHz in air) and 92.76 MHz (98.67 MHz in air), respectively. The resonance frequencies decreased during the first 12 h (Figure 1d), caused by the capacitance increase due to water diffusion into the PDTEC substrates. Thereafter, the resonance frequency of the sensor started to rise, which is earlier shown to result from the outward bending of the substrates.[18] This could have been caused by relaxation or swelling of the substrates or possibly by hydrogen gas generation arising from the corrosion of Mg.[20] Furthermore, the corrosion increased the resistance of the conductors, which can be considered as one of the factors that contribute to the drifting. The small amount of water that diffused into the polymer matrix could have slowly initiated the dissolution of Mg, possibly explaining why no clear corrosion was noticed after 24 h of immersion.[18] The materials testing revealed that the water uptake of PDTEC was 2.5 wt % after 12 h, in contrast to the final equilibrium state of 3.0 wt % after a few days (Figure 1e). The water uptake remained at the same level during the rest of the 100 days test period, which is consistent with the reported slow degradation rate of PDTEC.[23]

The pressure response measurements (Figure 1b) showed that the initial sensitivity of the nonimmersed sensor was around −7 kHz/mmHg, which is in the same range compared to the previously reported set of sensors.[18] The pressure sensitivity of the sensor was noticed to drift as a function of immersion time (Figure 1c). In comparison, the bioresorbable LC circuit-based pressure sensor of Luo et al. showed also slight sensitivity drifts under immersion, but the changes were much smaller.[15] The three-point bending test showed only a modest increasing trend in the flexural Young's modulus of PDTEC during the first week, as tested under aqueous conditions at 37 °C (Figure 1f,g). Thus, the changes in the mechanical properties of PDTEC do not explain the nonlinear sensitivity drifting. Instead, the drifting was likely attributed to structural changes between the substrates and the adhesive PCL layers, possibly due to hydrogen generation inside the sensor. It can be concluded that the diffused water caused changes in the dielectric properties of the capacitors, dimensional changes in the substrate, and corrosion of the conductors, all of which are undesirable regarding sensor stability. The drifting of the sensor would require frequent calibration in practical implant applications. Thereby, we suggest that in this kind of sensor architecture the water
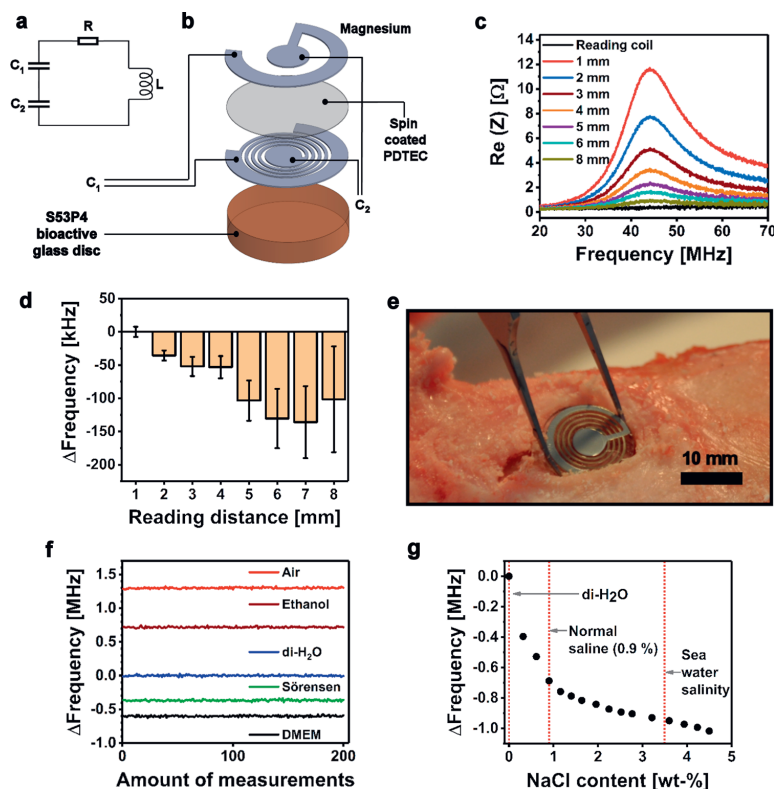
Figure 2. (a) A simplified lumped element model and (b) schematic structure of the bioactive glass-based resonance sensor. (c) Illustration of the resonance peaks at varying reading distances. (d) Effect of reading distance onto the resonance frequency (~44 MHz). The results are presented relative to the reading distance of 1 mm and given as mean ± standard deviation ($n = 100$). (e) An envisioned application of the sensor as a sensor-containing bone graft disc shown in a cadaveric porcine tibia. (f) Relative resonance frequency behavior of a parylene-coated sensor embedded in different media, where the mean of 200 measurements in deionized water (di-H_2O) has been set as the zero point. (g) Effect of increasing NaCl content in the resonance frequency of the coated sensor embedded in di-H_2O.

diffusion into the polymer matrix should be ideally fully prevented during the functional lifetime of the sensor, regardless of the degradation rate of the conductor material. This could be achieved for example with an appropriate bioresorbable encapsulation layer.

The PDTEC samples tested in dry conditions exhibited increased flexural strength compared to the wet samples (Figure 1h). While dry samples maintained the same stress values beyond the yield point, the immersed samples showed strain softening. The stress needed to flex the PDTEC samples to a constant displacement of 2 mm under aqueous conditions decreased significantly within 3 h of testing (Figure 1i). The stress relaxation behavior could be of significance in applications where the pressure is static. In addition to the mechanical properties, the response of human fibroblasts to compression-molded PDTEC discs was evaluated (Figure S1, Supporting Information), indicating that their biocompatibility was at least comparable to, if not better than, that of poly-L/D-lactide 96L/4D (PLDLA 96/4) discs or untreated polystyrene well plates.

Possible applications for bioresorbable pressure sensors include detecting adverse conditions during or after the surgery. For example, craniosynostosis is a malformation of an infant's skull caused by premature ossification of cranial sutures, which is often treated with a cranial vault remodeling by using bioresorbable plates and screws. Elevated intracranial pressure (ICP) levels after surgery may potentially require further treatment, which is why wireless postoperative ICP monitoring would be desirable.[24] Detecting acute compartment syndrome (ACS), which is caused by elevated pressure inside muscle compartments, is another attractive application for temporary pressure sensors. The diagnosis usually relies in clinical symptoms such as disproportionately severe pain and paresthesia, but delays between initial assessment and diagnosis are still frequent, leading to irreversible ischemic damage in 6−8 h if the condition is not properly treated.[25] Implantable pressure sensors could be used to detect cues of ACS in unresponsive or sedated patients or to complement clinical assessment in other risk groups. Finally, sensors could be used to guide surgeons during the operation. For example, pressure sensors could be used to avoid periosteal necrosis and subsequent osteopenia, which may arise from applying too much compression on a bone fixation plate.[26] Embedding such sensors onto fixation plates could aid in the adoption of the

technology, as there would be fewer modifications to the surgical techniques compared to external sensors that are removed in the end of the operation.

2.2. Bioactive Glass-Based Wireless Resonance Sensors. Bioresorbable glasses and ceramics offer underrepresented yet fascinating substrate materials for wireless resonance sensors. Invented by Larry Hench, bioactive glasses can create a strong bonding interface with bone or even with soft tissues by releasing soluble ions upon immersion in water.[27] These ions stimulate osteogenic cells and contribute to the formation of a bonelike apatite layer onto the glass surface, due to which such glasses are clinically used for example as synthetic bone grafts. The dissolution kinetics of bioactive glasses can be adjusted by their composition, and certain glass compositions are fully bioresorbable. Even though fast dissolving borate glasses have been proposed as sensor substrates, the interest toward bioactive glasses in biodegradable electronics has been scarce.[28,29] Herein, we present the first wirelessly measured bioactive glass-based resonance sensor with S53P4 (Bonalive) glass disc substrates, dissolvable Mg conductors, and spin-coated bioresorbable polymer dielectric layer.

A simplified electrical design and the schematic structure of the bioactive glass-based resonance sensor are presented in Figure 2a,b. The sensor architecture consisted of spin-coated PDTEC dielectric layers ($\sim$1 μm) and Mg conductors (7.5 μm) that were e-beam evaporated through 3D-printed stencil masks. Figure 2c presents the measured graphs of the impedance spectrum with increasing reading distances. Because no batteries are needed in the sensors, the most critical limiting factor for their miniaturization is the size of the coil, which has a strong effect on the reading distance of the device.[2,7] The bioactive glass-based sensor showed a detectable but attenuated resonance peak ($\sim$44 MHz) at a distance of 8 mm, which is in line with the previously reported 14 mm reading distance for the Mg pressure sensors with larger coils.[18] For comparison, the reading distance for nondegradable intraocular resonance pressure sensors with a diameter of 6 mm have been reported at 30 mm already in 1967 by Collins.[30] A more recent example with 4 × 4 mm^2 pressure sensors reached a 15 mm reading distance by using Cu conductors.[31]

The uncertainty in detecting the resonance frequency from the attenuated peaks increased along with the increasing reading distance (Figure 2d). In addition, the determined resonance frequency changed with the increasing reading distance due to parasitic capacitances between the sensor and the reader coil.[32] This feature might require compensation in practical applications.

One potential application for passive resonance sensors is monitoring complex permittivity changes in their close proximity.[33,34] This feature is attributed to the electrical field in the capacitor, which partly reaches the environment of the sensor. Changes in the permittivity of the immediate sensor environment affect its capacitance and thus shift the resonance frequency of the device. For example, nondegradable sensors with interdigital capacitors (finger electrodes) as sensing elements have been earlier tested for monitoring the degradation behavior of bioresorbable polymers as well as for distinguishing different tissues.[35,36] The finger electrodes offer the possibility to confine most of the interactions between the electrical field and the sensor surroundings near these electrodes.[34]

The fabricated bioactive glass-based resonance sensors were used to demonstrate the complex permittivity sensing capability by distinguishing different media in which the sensor was embedded (Figure 2f). The sensors were first coated with nondegradable parylene (13 μm) to eliminate the effect of Mg corrosion during the tests. The standard deviations of the estimated resonance frequencies ($n = 200$) in air, ethanol, and di-H$_2$O were 9.7, 9.5, and 9.4 kHz, respectively. Correspondingly, those of Sörensen buffer and Dulbecco's Modified Eagle Medium (DMEM) with high glucose were 10.8 and 10.7 kHz. The $\sim$15% higher standard deviations in Sörensen or DMEM solutions compared to di-H$_2$O can be explained by their ionic content. In another test, a nonlinear resonance frequency decrease was observed as saline was gradually added into di-H$_2$O where the sensor was immersed (Figure 2g). The result was caused by the capacitance increase originating from the addition of sodium and chloride ions.

A highly desirable potential application (Figure 2e) for resonance sensors made from bioactive glass would be monitoring the formation of the apatite layer and the subsequent bonding of bone onto the glass. The sensors could be integrated onto bioactive glass plates that have been clinically used for repairing orbital floor fractures and nasal septal perforations.[37] A similar sensing method could be of benefit also in nondegradable implants like total hip prostheses. This kind of quick osseointegration measurement could complement or even replace conventional imaging procedures and aid in personalizing rehabilitation.

To conclude, glass substrates contain several advantages over polymeric alternatives, such as better compatibility with conventional microfabrication processes.[29] For example, bioactive glasses tolerate solvents like acetone and elevated temperatures that may be required for lithography processes utilizing photoresist masks. A recent study demonstrated dry fabrication methods for Mg microcoils and heaters on float glass substrates, requiring only four steps: Mg deposition, photolithography for pattern definition, ion beam etching of Mg, and resist stripping with oxygen plasma and acetone.[38] This is one example of methods that could be useful with bioactive glass substrates for fabricating devices with detailed conductor patterns.

2.3. Fabrication and Properties of Bioresorbable Conductor Metals. The prevalent bioresorbable conductor materials are metals such as Mg, Zn, Mo, iron (Fe), and tungsten (W), out of which all but W are dietary minerals. Yin et al. have reported the electrical and corrosion properties of various dissolvable metal thin films (40−300 nm) because their properties might be very different compared to bulk materials.[39] Nevertheless, more studies are needed to cover the relevant behavior of bioresorbable metal films, especially in radio-frequency (RF) applications where the films are typically measured in micrometers rather than nanometers and their electrical properties may be affected by the skin effect. In this section, the fabrication, structure, electrical properties, and corrosion behavior of a few micrometers thick Mg and Zn thin films are discussed, including the drastic effect of different corrosion test conditions. In addition, alternative fabrication methods for bioresorbable conductors are briefly summarized.

In LC circuits, lower electrical resistance of the inductor coil generally enables higher quality resonators with longer reading distances.[2] However, at high frequencies, the skin effect may restrict the current flow on the surface of the conductors.[40] For
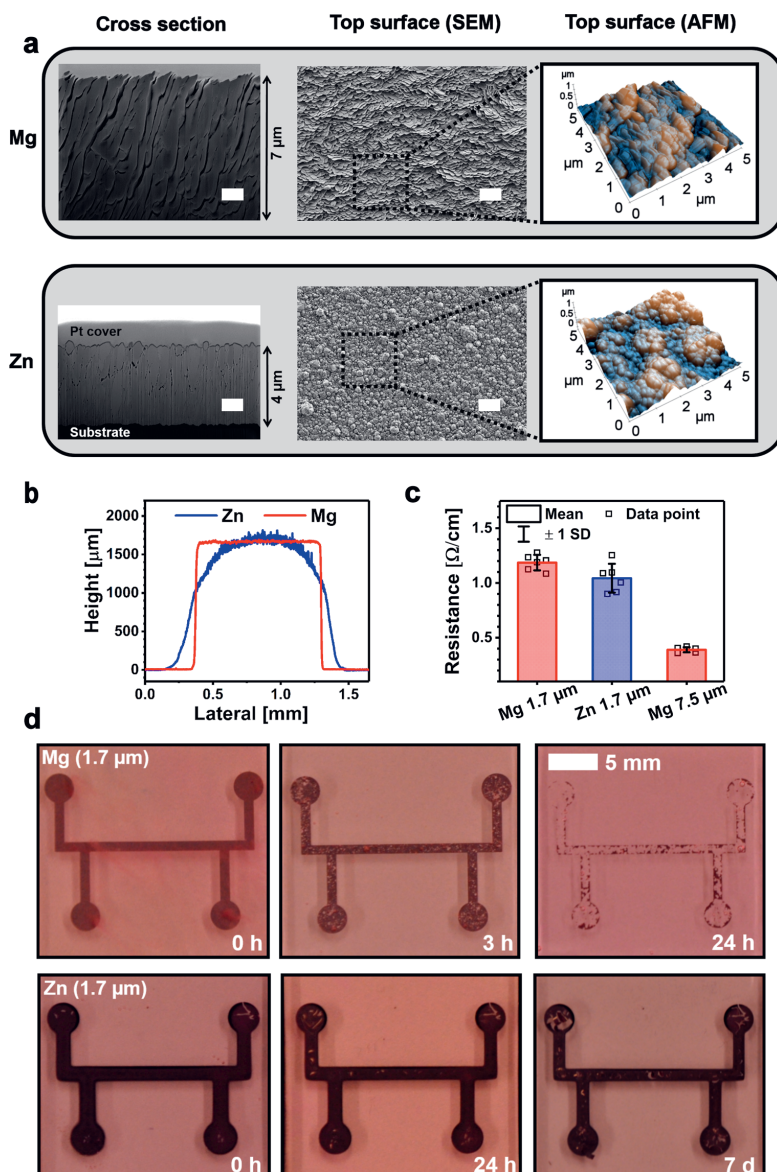
Figure 3. (a) Structure of the evaporated Mg (7.5 μm) and sputtered Zn films (~4 μm) illustrated by FIB-SEM, FE-SEM, and AFM techniques. White scale bars 1 μm. (b) Cross-sectional profiles of the 1.7 μm thick Mg and Zn films. (c) Electrical resistances of the ~1 mm wide Mg and Zn films given as mean ± standard deviation (*n* = 6). (d) Photographs of the metal films in cell culture medium at +37 °C in 5% CO_2.

instance, pure Fe has been considered as a poor conductor choice for LC resonators due to its low skin depth.[15,41] Table S1 summarizes the skin depths of Mg, Zn, Fe, and Mo at different frequencies. The recommended maximum conductor thickness in RF applications is about 3−5 times the skin depth because conductors much thicker than this do not result in significant increases in the Q-factor.[42]

Physical vapor deposition (PVD) methods are attractive for fabricating conductors because they can be utilized without transfer printing, and the techniques can be readily applied onto many types of substrates. In this study, e-beam evaporation was used for Mg deposition, as it is known to be a capable method for producing Mg films at the micrometer scale.[43−45] On the contrary, the Zn films were magnetron sputtered because the high vapor pressure of Zn results easily

in undesirable wall deposits in evaporation systems.[46] Evaporated Mg (7.5 μm) and sputtered Zn ($\sim$4 μm) films were first deposited on bioresorbable PDTEC substrates to study the morphology of the conductors. A prolonged Zn sputtering process was noticed to heat the PDTEC substrates over their glass transition temperature (T_g = 99 °C), which impaired obtaining thicker Zn films. In addition, both metals (1.7 μm) were deposited on glass substrates to compare their electrical characteristics and corrosion rates with minimal influence of the substrate.

The Mg film surface morphology (Figure 3a) consisted of similar facets as described recently with sputtered Mg.[47] The Zn film surfaces comprised individual grains together with larger clusters. The cross-sectional focused ion-beam SEM (FIB-SEM) images revealed that the Mg films had a coarse columnar structure compared to the denser structure of Zn. The structure could explain why the Zn films (1.7 μm) showed comparable or even slightly lower electrical resistances compared to Mg films of same thickness (Figure 3c). Comparing the approximated mean bulk resistivity of the 1.7 μm thick sputtered Zn films (180 nΩ·m) with that of the evaporated Mg films (200 nΩ·m) of similar thickness demonstrates that the fabrication method dominated the electrical properties of the films over intrinsic material properties. This can be concluded by comparing literature bulk resistivity values, which suggest that Zn (59 nΩ·m) should be less conductive than Mg (44 nΩ·m). The results illustrate the differences between thin films and bulk materials, which should be taken into account when choosing the conductor materials and their fabrication method.

The sharper profile of the Mg conductors (Figure 3b) originated from the directional nature of evaporation, where the material was deposited in a line of sight manner in contrast to more nondirectional sputtering, which resulted in an arched Zn film contour.[48] The sputtering masks should thus be in a close contact with the substrate, as a short circuit might otherwise form between the coil turns. The disadvantages of fabricating the conductor patterns by using PVD together with shadow masks are related to limited resolution and the required vacuum conditions.[14] Higher precision can be achieved by using lithographic masks, but transfer printing from a provisional substrate is often needed because most bioresorbable polymers do not tolerate the associated chemicals and temperatures.[49] Alternative fabrication techniques include approaches, where patterned metal films are formed by micromachining or wet etching of metal foils.[3,50−53] The advantage of these top-down methods is the easiness in obtaining thicker films compared to PVD or most other bottom-up processes. On the other hand, several tens of micrometers thick Mg and Zn microstructures have been obtained by electroplating the conductor patterns onto a temporary substrate and subsequently transfer printing them onto bioresorbable substrates.[15,54] Further approaches include conductive ink printing methods that do not require vacuum technology and would thus be beneficial for scaling the manufacturing processes.[14,55] These methods are currently under development, but the nonconductive surface oxide layers on biodegradable metal particles make their development challenging.

Yin et al. concluded that thin films of Mg, Mg alloy AZ31B, and Zn degrade significantly faster compared to Fe, Mo, or W.[39] Figure 3d elucidates the degradation rate differences of Mg and Zn films (1.7 μm) in cell culture medium (MEM

supplemented with 10% fetal bovine serum and 1% antibiotics) at +37 °C with 5% CO_2 supply, which is the recommended practice for in vitro corrosion testing of magnesium, as stated by Gonzalez et al. in their position paper.[20] Mg started to visibly degrade immediately upon immersion with corrosion pits present after 3 h, and most of the film dissolved within the first 24 h. Testing of thicker Mg films (7.5 μm) revealed the dramatic difference in the degradation behavior between different conditions (Figure S2), which should be recognized when studying unprotected bioresorbable metal films. For example, the Mg samples in di-H_2O and Sörensen buffer did not show similar pitting corrosion as those immersed in cell medium. Furthermore, mere addition of 5% CO_2 accelerated the corrosion of the films in di-H_2O. The Sörensen buffer resulted in a significantly faster degradation compared to cell culture medium, possibly due to lack of proteins and differences in the buffering system.

The Zn film surface appeared black, which may be caused by the observed Zn nanoclusters on top of the films.[56] The dissolution of the Zn films was much slower compared to Mg, but Zn flakes detached from the film already during the first 24 h. The slower degradation rate could be a benefit in applications where a longer sensor lifetime is desired. The corrosion of bulk Zn and Mg in simulated body fluid (SBF, pH 7) has been estimated to occur at a pace of 50 and 220 μm year^{-1}, respectively.[57] Correspondingly, the dissolution rate for sputtered Zn thin films (300 nm) has been estimated at 120−170 nm day^{-1} (44−62 μm year^{-1}) in di-H_2O, with an observation that the films lose their electrical conductivity 10 times faster than it takes for the thickness to decrease to zero.[39] Thus, nonpassivated Mg and Zn thin films are not considered practical in bioresorbable electronics. Instead, slower dissolving Mo was suggested for applications where the electrodes are in direct contact with biological tissues.

2.4. Bioresorbable Conductor Metals in Passive Resonance Sensors. Most bioresorbable inductively coupled devices reported so far utilize Mg as the conductor material.[3,18,38,51,58] On the contrary, the first fully biodegradable resonance pressure sensor presented by Luo et al. was based on 50 μm thick electroplated Zn films on top of a 5−10 μm Fe layer. In this section, the performances of Mg- and Zn-based pressure sensors are compared. The schematic structure of the sensors is presented in Figure 1a with Mg conductors. Furthermore, the properties of wirelessly readable compression sensors with thick Mo wire (200 μm) conductors around polymeric screws are presented.

The results indicate that magnetron sputtered Zn ($\sim$4 μm) was sufficient for producing wireless pressure sensors with similar, virtually linear pressure responses compared to sensors made from 7.5 μm thick Mg (Table 1). However, a practical

Table 1. Characteristics of the Fabricated Mg and Zn Pressure Sensors, Whose Pressure Responses Are Illustrated in Figure 4

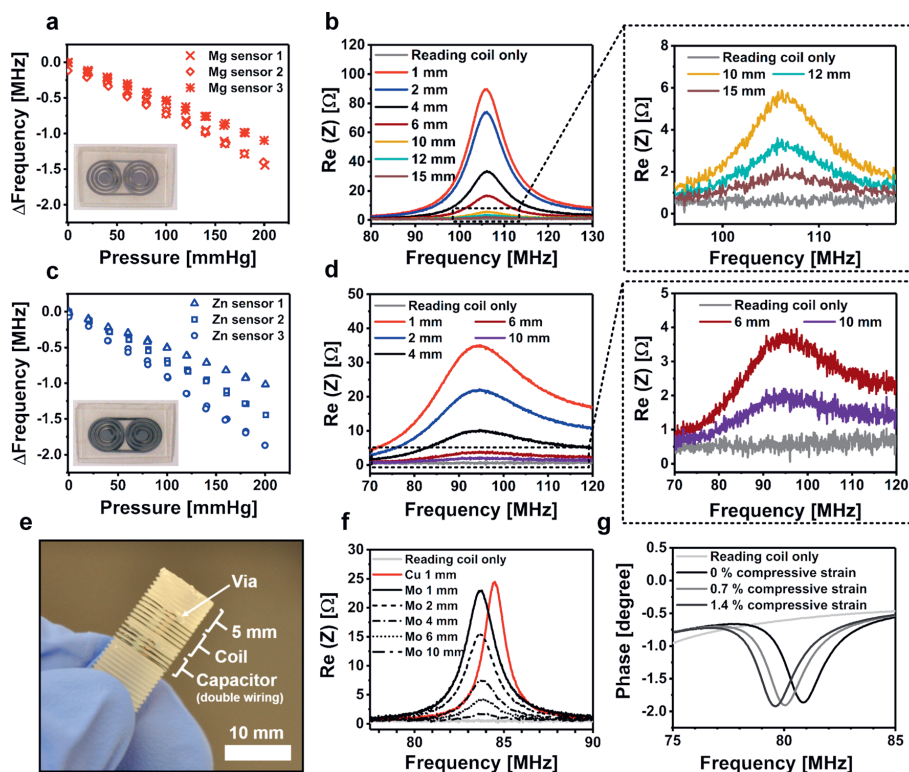| sample	initial resonance frequency (MHz)	pressure sensitivity (kHz mmHg^{-1})
Mg sensor 1	106.57	−7.2
Mg sensor 2	99.57	−6.7
Mg sensor 3	98.67	−5.4
Zn sensor 1	84.58	−5.1
Zn sensor 2	95.79	−7.2
Zn sensor 3	88.32	−9.4

Figure 4. (a) Pressure responses of the bioresorbable Mg pressure sensors, as measured through a glass bottle from a reading distance of 6 mm. A photograph of the sensor is shown in the inset. (b) Graphs of the impedance spectrum measured by increasing the reading distance of the Mg sensor, including rescaled graphs of the largest reading distances (on the right). The testing was performed by stacking 1 mm thick microscopy slides one by one between the sensor and the reader coil to stepwise increase the reading distance. (c, d) Corresponding Zn pressure sensor data. (e) Structure of the Mo wire compression sensor with a solenoidal coil. (f) Impedance spectrum of the Mo compression resonance sensor with an increasing reading distance, including a reference measurement using a similar sensor made from Cu wire. In our measurement setup, the tip of the polymer screw adds another 5 mm to the indicated distance between the sensor coil and the reading coil. (g) Impedance phase graphs at various axial compressive strains, showing a decrease in the resonance frequency as estimated from the minimum value of the phase.

reading distance for the Zn pressure sensors was only about 6 mm (Figure 4d), whereas the Mg pressure sensors were relatively effortlessly readable at a distance of 10 mm. The poorer performance of the Zn pressure sensors was likely caused by their lower conductor thickness, which resulted in a higher electrical resistance. Another potential reason is the arched cross-sectional profile of the Zn films, which may have decreased the quality of the resonance sensor due to increased parasitic capacitances or resistances.

The resonance peak of the Zn-based sensors attenuated so considerably in Sörensen buffer solution that their resonance frequency was difficult to detect under immersion. Along with different corrosion behavior, this is another important reason why in vitro testing of bioresorbable LC circuits should not be performed in di-H_2O. Photographs illustrating the differences in sensor degradation are presented in Figure S3.

Although planar inductor coils are often used for flat resonance sensor architectures, orthopedic screws facilitate the implementation of solenoidal coil-based resonators. A similar idea has been demonstrated with nondegradable materials by embedding an LC circuit-based temperature sensor inside an

interference screw for early detection of infections.[8] In our study, a resonance compression sensor constructed by using parylene-insulated Mo wire (diameter 200 μm) is presented in Figure 4e. A reference sensor was fabricated by using commercial insulated Cu wire (diameter 180 μm).

The capacitor in the compression sensor composed of two turns of a double-stranded wire that was coiled along the screw threads, whereas the inductor coil was formed from a single Mo wire strand. Compressing the screw brings the turns between the wirings closer in both the inductor coil and the capacitor wirings, which leads to increased capacitances in the structure, which is noticed as a decreasing resonance frequency shift. For example, an axial compressive strain of 0.7% decreased the resonance frequency from 80.9 to 80.1 MHz with a further drop to 79.6 MHz at a strain of 1.4% (Figure 4g). This sensing capability could be applied for monitoring the dimensional changes in self-reinforced bioresorbable polymer screws, which are expected to swell and shorten 1–2% after implantation, thereby allowing improved compression at the bone fracture line.[59]
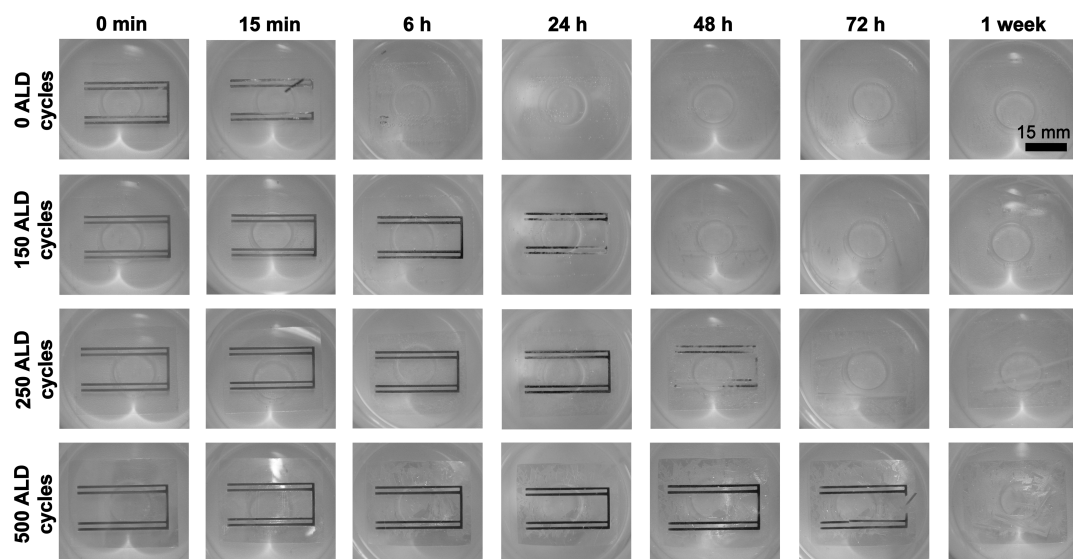
Figure 5. Atomic layer deposition (ALD) coated Mg conductors immersed in Sörensen phosphate buffer solution (pH 7.48) at +37 °C. The Mg conductors (7.5 μm) were deposited onto PLDLA 96/4 substrates and coated with different thicknesses of TiO$_2$. One ALD cycle corresponded to ~1 Å.

The resonance peak of the Mo-based device was noticed to be comparable to the Cu reference sensor (Figure 4f). The Mo-based LC resonator was effortlessly readable with 10 mm of glass between the reader coil and the resonator. In this measurement setup, the tip of the screw (Figure 4e) increased the actual reading distance by 5 mm. The inductance and capacitance of the resonator can be increased by adding more windings to the coil or the capacitor, respectively. Based on a preliminary immersion test using Sörensen buffer solution (37 °C), uncoated Mo wires retained their electrical conductivity for ~4 weeks, after which the resistance started to increase (Figure S4). The first wire broke after 14 weeks of immersion. A previous immersion testing of Mo wire (10 μm) in bovine serum has shown only a minor resistance increase during the 16 day test period.[51] These findings demonstrate the potential of Mo in applications where a slow conductor degradation is preferred.

2.5. Encapsulation Layers. Achieving clinically relevant stable operation times of multiple days or weeks remains a challenge with implantable bioresorbable sensors. The dissolution or fracture of the conductors are among the main reasons for an untimely device failure along with disintegration of the device structure.[14,49,60] Water penetration into the device is a common denominator for all of these breakdown mechanisms, for why separate water barrier layers have been studied to improve the stability of bioresorbable sensors.[61,62] There is a great demand for encapsulation layers that could be applied onto bioresorbable polymer substrates because the deposition of inorganic coatings often requires elevated temperatures. In this section, the pros and cons of low-temperature atomic layer deposited (ALD) TiO$_2$ films on polymeric substrates are discussed. In addition, other options for increasing the functional lifetime of bioresorbable sensors are recapitulated.

Typical water barrier layers involve inorganic ceramic coatings like SiO$_2$, MgO, and Si$_3$N$_4$ that are used in conventional electronics as well. Such coatings can be deposited for example by evaporation, sputtering, thermal oxidation, plasma-enhanced chemical vapor deposition (PECVD), or atomic layer deposition (ALD) methods.[61,62] Kang et al. have studied different encapsulation layers and their combinations on silicon wafers, suggesting that some pinholes and other defects may be expected with PECVD deposited films despite their conformal nature, whereas ALD provides a means for reducing the amount of defects.[61]

Conventional PECVD processes are usually operated at temperatures around 250−350 °C, even though room temperature processes have been also developed.[61,63,64] Many ALD processes can be performed at lower temperatures, facilitating the use of polymeric substrates that typically require temperatures below 100 °C.[65,66] However, there are only few studies where ALD coatings have been performed on biodegradable polymer substrates.[67,68] In this study, the protective effect of ALD TiO$_2$ on a Mg layer (7.5 μm) evaporated onto bioresorbable PLDLA 96/4 substrates was studied. TiO$_2$ was chosen as the coating material due to its excellent water corrosion resistance properties.[69] The samples with different amounts (0, 150, 250, and 500) of ALD process cycles and thus different TiO$_2$ thicknesses (0, 15, 25, and 50 nm, respectively) were immersed in Sörensen buffer. The coatings were peeled off from the ends of the substrate (Figure S5) by using tape to enable water diffusion into the polymer, while keeping the coating on top of the Mg patterns intact. This simulated a realistic scenario, where the surgical insertion of an ALD coated implant would be difficult to perform without damaging the coating.

The noncoated Mg pattern disintegrated within the first minutes and was almost fully dissolved after 6 h of immersion (Figure 5). The ALD-coated Mg samples showed reduced

dissolution rates with increasing TiO_2 thicknesses, where the thickest coating (∼50 nm) resulted in an intact Mg pattern after 2 days of immersion. However, a black Mg surface layer possibly consisting of $Mg(OH)_2$ was noticed earlier as a sign of corrosion, as described in Mg corrosion studies performed in atmospheric conditions.[20] The corrosion could have been caused by the equilibrium water uptake into the PLDLA 96/4 substrates. Based on previous studies, using composite coatings formed from two or more different coating materials might provide improved water barrier properties.[61,69] Nonetheless, more studies are needed using bioresorbable substrates, as they significantly contribute to the functionality of the protective layer. For example, any dimensional changes in the substrates may potentially crack the coatings, as shown with an LC resonator formed using ALD-coated polymer substrates (Figure S6). Hence, in this kind of fully immersed and highly delicate sensor applications, ALD coatings might be more compatible with rigid substrates such as bioactive glasses. Inorganic coatings on rigid nondegradable wafers have been previously discussed in the literature.[61,62,70]

To avoid the challenges related to mechanical fragility of inorganic coatings, natural waxes have been described as a potential biodegradable encapsulation material option.[51,71] The most promising reported candidate was candelilla wax that showed hardly any water uptake during the first 2 weeks of immersion. A 300 μm thick wax layer helped Mg patterns retain their conductivity for more than 7 days in phosphate buffer solution (PBS).[71] Further advances have been recently reported by blending different waxes. The combination of transfer printed monocrystalline silicon layers together with edge-sealing wax barriers enabled accurate ICP measurements in rats for up to 3 weeks using a wired bioresorbable sensor.[72] Furthermore, recent advances in gas-phase polymerization of hydrolytically degradable polymers could in the future provide bioresorbable conformal coatings similar to nondegradable parylene, which has already been utilized in passivation coatings of implanted devices.[73]

A common scheme for protecting bioresorbable circuitry is to use sensor substrates as encapsulation layers. Most of the reported bioresorbable polymers are bulk-degrading, which means that water diffuses into the polymer matrix at a faster speed than the polymer erodes.[74] For example, the equilibrium water uptake of immersed polyesters is around 1 wt %.[36] Even such a small amount of water leads to corrosion of the metal conductors over time and may affect the dimensional properties of the polymer. One interesting possibility to circumvent this problem is to use surface-eroding polymers like poly(ortho esters) or polyanhydrides, where water diffusion into the polymer matrix is slower than the erosion rate of the material.[74] As an example, polyanhydride coating (120 μm) has been shown to enable a stable operation of 3 days for a silicon semiconductor-based pressure sensor.[10] Nevertheless, the effects of surface-eroding substrates on wireless LC circuit-based sensors remains to be tested.

3. EXPERIMENTAL SECTION

3.1. Device Fabrication. The Mg and Zn pressure sensors whose structure was illustrated in Figure 1a were fabricated by extruding PDTEC powder (Integra LifeSciences, Princeton, NJ) and compression-molding pieces of the extruded rod into plates (430 μm). PDTEC spacers (50−70 μm) were compression-molded and laser-cut as described earlier.[18] Compression-molded PCL layers (15−20 μm) were melted onto both sides of the spacer, and excessive

PCL was removed from the laser-cut holes. E-beam-evaporated Mg (7.5 μm) or magnetron-sputtered Zn (4 μm) conductors were deposited onto the PDTEC substrates through laser-cut steel masks, after which the substrates were attached onto the spacer by heating the structure to 80 °C and using the molten PCL layers as an adhesive. The sides of the sensors were finally heat sealed (Hawo HPL ISZ, Obrigheim, Germany) and trimmed with scissors to yield sensors sized approximately 1 mm by 25 mm by 35 mm. A simplified electrical model of a resonator based on a similar pattern has been reported earlier.[75]

The wireless compression sensors (Figure 4e) based on parylene-coated Mo wire (200 μm) conductors were fabricated by extruding PLDLA 96/4 into a rod (ϕ = 10 mm), threading the PCL rod, and cutting it into billets. The Mo wire was coated with nondegradable parylene C (10 μm; Galentis S.r.l., Italy) to prevent short circuit. Two holes were drilled through each billet to provide electrical vias for the construct and to aid in fixing the wire to the threaded billet. A solenoidal coil was formed by winding Mo wire around the billet (5.5 turns). The capacitor was formed by coiling double-stranded wire along the threads (2 turns). The loose double-stranded wire ending was attached to the billet by using molten PCL as an adhesive. Reference resonators were fabricated in a similar manner using commercial enamel insulated Cu wire (180 μm).

The bioactive glass resonance sensors (Figure 2b) were made from silicate S53P4 glass that was prepared by a conventional glass melting method in platinum crucible. The nominal oxide composition of S53P4 is 53 wt % SiO_2, 23 wt % Na_2O, 20 wt % CaO, and 4 wt % P_2O_5.[76] In this study, proportional amounts of SiO_2, $CaCO_3$, Na_2CO_3, and $CaHPO_4·2H_2O$ raw materials were used. The mixture was melted at 1450 °C, cast and quenched in a prewarmed (350 °C) graphite mold, and annealed at 520 °C for 5 h. The resulting S53P4 bioactive glass rods (ϕ = 14 mm) were sliced into discs (h = 2 mm) which were polished. E-beam-evaporated Mg (7.5 μm) formed the first conductor layer, after which PDTEC solution (12%) in cyclohexanone (VWR Chemicals, Fontenay-sous-Bois, France) was spin-coated onto the discs. 3D-printed masks were used to define the Mg patterns. Another Mg layer (7.5 μm) was evaporated onto the dielectric PDTEC layer to complete the resonator. The resonators were finally parylene coated (13 μm) to enable studying the resonator behavior in aqueous conditions without constraints related to Mg corrosion.

3.2. Physical Vapor Deposition. E-beam evaporation of Mg granules (99.99%; G-materials, Germany) was performed at less than 7×10^{-6} Torr with substrate rotation. The source-to-substrate distance was 31 cm. The Zn films were deposited from a Zn target (99.99% Zn; Kurt J. Lesker Company, Hastings, UK) by using direct current (DC) magnetron sputtering. The vacuum level was 5×10^{-6} Torr with a working Ar gas pressure of 10 mTorr. The sputtering current and voltage were 1 A and 560 V, respectively. The sputtering target-to-substrate distance was 10.5 cm. No substrate rotation was used.

3.3. Thin Film Characterization. The cross-sectional structure of the Mg (7.5 μm) and Zn (4 μm) films on bioresorbable PDTEC substrates was analyzed with a scanning electron microscope (SEM) combined with focused ion beam milling (FIB-SEM; Zeiss Cross-Beam 540) from a working distance of 5.2 mm with an electron high tension (EHT) of 3.0 kV. A platinum cover was applied onto the target films before gallium ion milling. The surface of the metal films was imaged with a high-resolution field emission SEM (FESEM; Zeiss UltraPlus) from a working distance of 5.0 ± 0.2 mm and with an EHT of 1.5 kV. The surface topography of the metal films was further characterized by using a noncontact atomic force microscope (AFM; XE-100, Park Systems Inc., USA) equipped with silicon probes (ACTa, Applied NanoStructures Inc., USA). The imaged area with the AFM was 5×5 μm^2.

The height and the cross-sectional profile of the Mg and Zn films (1.7 μm) on glass slides (Figure 3b) was measured by using a mechanical profiler (Dektak XT Stylus, Bruker Corporation). The electrical resistance (Ω/cm) of these films was calculated by dividing the measured resistance of the deposited 4-wire patterns (n = 6) by the distance between the inner lines of the pattern (Figure 3c). Mean

bulk resistivity of the 1.7 μm thick films was approximated by multiplying the mean electrical resistance values with the estimated conductor cross-sectional area. Based on the profilometer data, the width of the Mg conductor films was estimated at 1 mm, and the cross-sectional area of the Zn films was considered similar to that of the Mg films. Finally, the samples were immersed in 25 mL of cell culture medium (MEM; Sigma-Aldrich supplemented with 10% fetal bovine serum and 1% antibiotics) at +37 °C with a 5% CO_2 supply and photographed at predetermined time points for corrosion behavior comparison (Figure 3d). In addition, thicker Mg samples (7.5 μm) were immersed in similar cell culture conditions as well as in 25 mL of di-H_2O and Sörensen buffer (+37 °C) to compare different corrosive environments (Figure S2).

3.4. Wireless Measurements. The reading distance of all LC circuit-based sensors was investigated by using the same measurement setup, which included a double-turn square reader coil (diameter about 20 mm) on a printed circuit board (PCB).[45] The reading distance was stepwise increased by adding 1 mm glass slides between the reader coil and the sensor. After each 1 mm increment, the real part of the impedance of the reader coil was measured with an impedance analyzer (Agilent 4396B). Furthermore, the miniaturized bioactive glass-based sensor was measured 100 times at each discrete distance to obtain the mean and standard deviation of the resonance frequency, similarly to our previous Mg pressure sensor.[18]

The other wireless measurements were performed by using setups that were constructed on occasion depending on the type of measurement. The reader coils were chosen to increase the coupling coefficients between the sensors and the reader coils. The Mg and Zn pressure sensors were measured using a similar setup as described earlier, where a single-turn copper reader coil (ϕ = 33 mm) was located inside an oven and connected to the impedance analyzer with a cable.[18] The sensors were taped onto the bottom of a glass bottle, which was pressurized from 0 to 200 mmHg applied pressure in increments of 20 mmHg by using a manual pressure regulator connected to a pressure calibrator. The reading distance through the glass bottle was ~6 mm. The immersion tests were performed by pouring 100 mL of buffer solution into the bottle and measuring the resonance frequency every 15 min. In addition, the pressure response of the sensor was measured during immersion at predetermined time points.

The wireless compression sensor built onto a PLDLA 96/4 screw was axially compressed in a vise by using an electrically insulating Teflon block between the reader coil and the metallic vise jaw. As opposed to other measurements that were performed with an impedance analyzer, the resonance frequency of the compression sensor was determined by using an in-house built portable reader device.[77] The reader coil was a single turn aluminum coil with a diameter of 30 mm on a poly(ethylene terephthalate) (PET) sheet. The measurements were performed by using the phase-dip method, where the resonance frequency was the estimated minimum value in the phase of impedance.[77] The compression was measured by using a digital caliper.

The parylene-coated bioactive glass resonance sensors were measured through a 1 mm thick Petri dish by using the double-turn rectangular reader coil. The resonators were first immersed in di-H_2O and measured, after which 9% NaCl solution was stepwise added until the solution reached a NaCl concentration of 4.5%. After each addition of the NaCl solution, the mixture was gently suspended using a pipet to ensure that the solution was homogeneous. The response of the sensor was recorded after each NaCl addition step. To test the effect of the immersion media onto the sensor, 200 measurement samples were recorded in air and under immersion in di-H_2O, Sörensen phosphate buffer, DMEM with high glucose (Sigma-Aldrich, United Kingdom), and 96% ethanol (VWR Chemicals). The sensor was rinsed with di-H_2O and tapped dry with tissue paper between each solution.

3.5. Water Uptake Testing of Polymers. The water uptake properties of PDTEC were evaluated by using samples (n = 5) with a size of $50 \times 10 \times 0.4$ mm³. The samples were dried in a vacuum, weighed, and then immersed in Sörensen buffer solution at 37 °C. At predetermined time points, the samples were gently wiped with tissue paper and weighed. The wet weights were compared to the initial dry weight. After 100 days of immersion, the hydrolysis was terminated by rinsing the samples with di-H_2O, drying them thoroughly in a vacuum, and weighing to ensure that no mass loss had occurred.

3.6. Mechanical Testing. Flexural characteristics of PDTEC were determined by testing the stress−strain and the stress relaxation behavior of the material with an Instron Electropuls E1000 testing machine (High Wycombe, UK) equipped with a 50 N load cell. The span length of the three-point bending setup was 30 mm, and the sample size was $50 \times 10 \times 0.9$ mm³. The stress−strain behavior of samples (n = 3) was obtained by bending the samples with a 5 mm/min crosshead speed until 5% flexure strain was reached. The tests were performed in ambient laboratory conditions as well as in aqueous conditions (Figure 1f) after different immersion times. Young's moduli were calculated from the linear portion of the acquired stress−strain curves. The stress relaxation behavior of the PDTEC samples (n = 3) was tested under immersion (Sörensen buffer, +37 °C) by bending the sample rapidly to 2 mm displacement and holding it for 3 h. The stress needed to hold the displacement was recorded with respect to time.

3.7. ALD Coating. The 7.5 μm thick Mg patterns were e-beam evaporated onto compression-molded PLDLA 96/4 substrates (0.4 mm × 30 mm × 40 mm). Thereafter, ALD TiO_2 coatings were deposited onto the metallized substrates at 60 °C by using a Beneq TFS 200 ALD reactor. ALD TiO_2 films were grown from titanium tetrachloride ($TiCl_4$) (Sigma-Aldrich) and water, both vaporized from the source at 20 °C. One deposition cycle for TiO_2 consisted of a 0.5 s $TiCl_4$ pulse, a 20 s N_2 purge, a 0.5 s water pulse, and a 20 s N_2 purge. The ALD TiO_2 film thickness was varied by alternating the number of ALD cycles. The amount of cycles was 150, 250, and 500. Each ALD cycle corresponded to about 1 Å. The film thicknesses were measured from silicon (100) witness pieces by using spectroscopic ellipsometry (J.A. Woollam Co., Inc., model M-2000FI).

4. CONCLUSIONS AND FUTURE CONSIDERATIONS

This study summarizes the prospects and caveats in the assembly, testing, and performance of wireless inductor−capacitor (LC) resonance sensors fabricated by using bioresorbable materials, as well as outlines several potential orthopedic applications for such devices. The reported Mg-based pressure sensors were wirelessly readable and pressure responsive for 10 days in aqueous conditions, but water diffusion into the bulk-degrading polymer substrates resulted in sensitivity and baseline resonance frequency drifting. Using surface-eroding materials or separate encapsulation layers to hinder water diffusion into the substrates should thereby be considered to enable stable operation during the functional lifetime of the sensor. In our opinion, bioactive glasses possess tremendous undiscovered potential in bioresorbable sensors, including possible improvements in their stability. Moreover, these glasses tolerate conventional microfabrication techniques better than most biodegradable polymers, which provides prospective opportunities for device fabrication and assembly. The reported resonance sensors operate at distances that are sufficient for applications close beneath the skin. Longer reading distances could be achieved for instance by using thicker conductors or developing bioresorbable materials with improved electrical conductivities. However, depending on the material, thick films may be difficult to produce by physical vapor deposition (PVD), and the obtained thin film conductivities are often lower than those of the bulk materials. Thus, PVD might not be the ideal conductor fabrication method for maximizing the reading distances. Although Mg is the most studied biodegradable metal with the highest conductivity in this material group, Zn and Mo provide slower

corroding options whose potential should be more thoroughly investigated.

ASSOCIATED CONTENT

🄢 Supporting Information

The Supporting Information is available free of charge at https://pubs.acs.org/doi/10.1021/acsami.0c07278.

> Cell culture results, discussion and experimental methods; skin depths of common bioresorbable materials; corrosion testing of magnesium films (7.5 μm); in vitro degradation of wireless Mg and Zn pressure sensors; molybdenum wire (200 μm) immersion test; illustration of the peeled-off area of the ALD coatings; ALD-coated substrates in an LC resonator (PDF)

AUTHOR INFORMATION

Corresponding Author

Aleksi Palmroth − *BioMediTech, Faculty of Medicine and Health Technology, Tampere University, Tampere 33720, Finland;* ⦿ orcid.org/0000-0002-8574-6922; Email: aleksi.palmroth@tuni.fi

Authors

Timo Salpavaara − *BioMediTech, Faculty of Medicine and Health Technology, Tampere University, Tampere 33720, Finland*

Petri Vuoristo − *Materials Science and Environmental Engineering, Faculty of Engineering and Natural Sciences, Tampere University, Tampere 33720, Finland*

Sanna Karjalainen − *BioMediTech, Faculty of Medicine and Health Technology, Tampere University, Tampere 33720, Finland*

Tommi Kääriäinen − *Department of Chemistry, University of Colorado Boulder, Boulder, Colorado 80309, United States*

Susanna Miettinen − *BioMediTech, Faculty of Medicine and Health Technology, Tampere University, Tampere 33720, Finland*

Jonathan Massera − *BioMediTech, Faculty of Medicine and Health Technology, Tampere University, Tampere 33720, Finland;* ⦿ orcid.org/0000-0002-1099-8420

Jukka Lekkala − *BioMediTech, Faculty of Medicine and Health Technology, Tampere University, Tampere 33720, Finland*

Minna Kellomäki − *BioMediTech, Faculty of Medicine and Health Technology, Tampere University, Tampere 33720, Finland*

Complete contact information is available at:
https://pubs.acs.org/10.1021/acsami.0c07278

Notes

The authors declare no competing financial interest.

ACKNOWLEDGMENTS

REFERENCES

(1) Ledet, E. H.; D'Lima, D.; Westerhoff, P.; Szivek, J. A.; Wachs, R. A.; Bergmann, G. Implantable Sensor Technology: From Research to Clinical Practice. *J. Am. Acad. Orthop. Surg.* **2012**, *20* (6), 383.

(2) Boutry, C. M.; Chandrahalim, H.; Streit, P.; Schinhammer, M.; Hänzi, A. C.; Hierold, C. Towards Biodegradable Wireless Implants. *Philos. Trans. R. Soc. A Math. Phys. Eng. Sci.* **2012**, *370* (1967), 2418−2432.

(3) Boutry, C. M.; Beker, L.; Kaizawa, Y.; Vassos, C.; Tran, H.; Hinckley, A. C.; Pfattner, R.; Niu, S.; Li, J.; Claverie, J.; Wang, Z.; Chang, J.; Fox, P. M.; Bao, Z. Biodegradable and Flexible Arterial-Pulse Sensor for the Wireless Monitoring of Blood Flow. *Nat. Biomed. Eng.* **2019**, *3* (1), 47−57.

(4) Ledet, E. H.; Liddle, B.; Kradinova, K.; Harper, S. Smart Implants in Orthopedic Surgery, Improving Patient Outcomes: A Review. *Innov. Entrep. Heal.* **2018**, *5*, 41−51.

(5) Li, R.; Wang, L.; Kong, D.; Yin, L. Recent Progress on Biodegradable Materials and Transient. *Electronics. Bioact. Mater.* **2018**, *3* (3), 322−333.

(6) La Mattina, A. A.; Mariani, S.; Barillaro, G. Bioresorbable Materials on the Rise: From Electronic Components and Physical Sensors to In Vivo Monitoring Systems. *Adv. Sci.* **2020**, *7* (4), 1902872.

(7) Huang, Q. A.; Dong, L.; Wang, L. F. LC Passive Wireless Sensors Toward a Wireless Sensing Platform: Status, Prospects, and Challenges. *J. Microelectromech. Syst.* **2016**, *25* (5), 822−841.

(8) Karipott, S. S.; Veetil, P. M.; Nelson, B. D.; Guldberg, R. E.; Ong, K. G. An Embedded Wireless Temperature Sensor for Orthopedic Implants. *IEEE Sens. J.* **2018**, *18* (3), 1265−1272.

(9) Boutry, C. M.; Kaizawa, Y.; Schroeder, B. C.; Chortos, A.; Legrand, A.; Wang, Z.; Chang, J.; Fox, P.; Bao, Z. A Stretchable and Biodegradable Strain and Pressure Sensor for Orthopaedic Application. *Nat. Electron.* **2018**, *1* (5), 314−321.

(10) Kang, S.-K.; Murphy, R. K. J.; Hwang, S.-W.; Lee, S. M.; Harburg, D. V.; Krueger, N. A.; Shin, J.; Gamble, P.; Cheng, H.; Yu, S.; Liu, Z.; McCall, J. G.; Stephen, M.; Ying, H.; Kim, J.; Park, G.; Webb, C.; Lee, C. H.; Chung, S.; Wie, D. S.; Gujar, A. D.; Vemulapalli, B.; Kim, A. H.; Lee, K.-M.; Cheng, J.; Huang, Y.; Lee, S. H.; Braun, P. V.; Ray, W. Z.; Rogers, J. A. Bioresorbable Silicon Electronic Sensors for the Brain. *Nature* **2016**, *530* (7588), 71−76.

(11) Gustke, K. A.; Golladay, G. J.; Roche, M. W.; Jerry, G. J.; Elson, L. C.; Anderson, C. R. Increased Satisfaction after Total Knee Replacement Using Sensor-Guided Technology. *Bone Joint J.* **2014**, *96-B* (10), 1333−1338.

(12) O'Connor, C.; Kiourti, A. Wireless Sensors for Smart Orthopedic Implants. *J. Bio- Tribo-Corrosion* **2017**, *3* (2), 20.

(13) Allen, M. G. Micromachined Endovascularly-Implantable Wireless Aneurysm Pressure Sensors: From Concept to Clinic. In *The 13th International Conference on Solid-State Sensors, Actuators and Microsystems, 2005. Digest of Technical Papers. TRANSDUCERS '05*; 2005; Vol. *1*, pp 275−278 .

(14) Yu, X.; Shou, W.; Mahajan, B. K.; Huang, X.; Pan, H. Materials, Processes, and Facile Manufacturing for Bioresorbable Electronics: A Review. *Adv. Mater.* **2018**, *30* (28), 1707624.

(15) Luo, M.; Martinez, A. W.; Song, C.; Herrault, F.; Allen, M. G. A Microfabricated Wireless RF Pressure Sensor Made Completely of Biodegradable Materials. *J. Microelectromech. Syst.* **2014**, *23*, 4−13.

(16) Hänninen, A.; Salpavaara, T.; Lekkala, J.; Kellomäki, M. An Inductively Coupled Biodegradable Capacitive Pressure Sensor. *Proceedings.* **2018**.

(17) Luo, M.; Shen, W.; Allen, M. G. Microfabricated PLGA/PVA-Based Completely Biodegradable Passive RF Pressure Sensors. In *2015 Transducers - 2015 18th International Conference on Solid-State*

Sensors, Actuators and Microsystems (TRANSDUCERS); 2015; pp 101−104.

(18) Palmroth, A.; Salpavaara, T.; Lekkala, J.; Kellomäki, M. Fabrication and Characterization of a Wireless Bioresorbable Pressure Sensor. *Adv. Mater. Technol.* **2019**, *0* (0), 1900428.

(19) Eppley, B. L. Use of Resorbable Plates and Screws in Pediatric Facial Fractures. *J. Oral Maxillofac. Surg.* **2005**, *63* (3), 385−391.

(20) Gonzalez, J.; Hou, R. Q.; Nidadavolu, E. P. S.; Willumeit-Römer, R.; Feyerabend, F. Magnesium Degradation under Physiological Conditions − Best Practice. *Bioact. Mater.* **2018**, *3* (2), 174−185.

(21) Chen, P.; Saati, S.; Varma, R.; Humayun, M. S.; Tai, Y. Wireless Intraocular Pressure Sensing Using Microfabricated Minimally Invasive Flexible-Coiled LC Sensor Implant. *J. Microelectromech. Syst.* **2010**, *19* (4), 721−734.

(22) Marco, I.; Feyerabend, F.; Willumeit-Römer, R.; Van der Biest, O. Degradation Testing of Mg Alloys in Dulbecco's Modified Eagle Medium: Influence of Medium Sterilization. *Mater. Sci. Eng., C* **2016**, *62*, 68−78.

(23) Tangpasuthadol, V.; Pendharkar, S. M.; Peterson, R. C.; Kohn, J. Hydrolytic Degradation of Tyrosine-Derived Polycarbonates, a Class of New Biomaterials. Part II: 3-Yr Study of Polymeric Devices. *Biomaterials* **2000**, *21* (23), 2379−2387.

(24) Seruya, M.; Oh, A. K.; Boyajian, M. J.; Posnick, J. C.; Keating, R. F. Treatment for Delayed Presentation of Sagittal Synostosis: Challenges Pertaining to Occult Intracranial Hypertension. *J. Neurosurg. Pediatr.* **2011**, *8* (1), 40−48.

(25) Schmidt, A. H. Acute Compartment Syndrome. *Injury* **2017**, *48*, S22−S25.

(26) Popkov, A. V.; Popkov, D. A.; Kononovich, N. A.; Gorbach, E. N.; Tverdokhlebov, S. I.; Bolbasov, E. N.; Darvin, E. O. Biological Activity of the Implant for Internal Fixation. *J. Tissue Eng. Regener. Med.* **2018**, *12* (12), 2248−2255.

(27) Jones, J. R. Review of Bioactive Glass: From Hench to Hybrids. *Acta Biomater.* **2013**, *9* (1), 4457−4486.

(28) Unda, K.; Mohammadkhah, A.; Lee, K.; Day, D. E.; O'Keefe, M. J.; Kim, C. Sensor Substrates Based on Biodegradable Glass Materials. *2016 IEEE SENSORS* **2016**, 1−3.

(29) Adnan, S.; Lee, K.-M.; Ghasr, M. T.; O'Keefe, M. J.; Day, D. E.; Kim, C.-S. Water-Soluble Glass Substrate as a Platform for Biodegradable Solid-State Devices. *IEEE J. Electron Devices Soc.* **2016**, *4* (6), 490−494.

(30) Collins, C. Miniature Passive Pressure Transensor for Implanting in the Eye. *IEEE Trans. Biomed. Eng.* **1967**, *BME-14* (2), 74−83.

(31) Chen, L. Y.; Tee, B. C.-K.; Chortos, A. L.; Schwartz, G.; Tse, V.; J. Lipomi, D.; Wong, H.-S. P.; McConnell, M. V.; Bao, Z. Continuous Wireless Pressure Monitoring and Mapping with Ultra-Small Passive Sensors for Health Monitoring and Critical Care. *Nat. Commun.* **2014**, *5*, 1−10.

(32) Baù, M.; Demori, M.; Ferrari, M.; Ferrari, V. Contactless Readout of Passive LC Sensors with Compensation Circuit for Distance-Independent Measurements. *Proceedings* **2018**, *2*, 842.

(33) Ong, K. G.; Grimes, C. A.; Robbins, C. L.; Singh, R. S. Design and Application of a Wireless, Passive, Resonant-Circuit Environmental Monitoring Sensor. *Sens. Actuators, A* **2001**, *93* (1), 33−43.

(34) Salpavaara, T.; Järveläinen, M.; Yli-Hallila, T.; Seppälä, S.; Levänen, E.; Vilkko, M.; Lekkala, J. Passive Resonance Sensor Based Method for Monitoring Particle Suspensions. *Sensors Actuators B. Chem.* **2014**, *219*, 324−330.

(35) Yvanoff, M.; Venkataraman, J. A Feasibility Study of Tissue Characterization Using LC Sensors. *IEEE Trans. Antennas Propag.* **2009**, *57* (4), 885−893.

(36) Salpavaara, T.; Hänninen, A.; Antniemi, A.; Lekkala, J.; Kellomäki, M. Non-Destructive and Wireless Monitoring of Biodegradable Polymers. *Sens. Actuators, B* **2017**, *251*, 1018−1025.

(37) Peltola, M.; Kinnunen, I.; Aitasalo, K. Reconstruction of Orbital Wall Defects With Bioactive Glass Plates. *J. Oral Maxillofac. Surg.* **2008**, *66* (4), 639−646.

(38) Rüegg, M.; Blum, R.; Boero, G.; Brugger, J. Biodegradable Frequency-Selective Magnesium Radio-Frequency Microresonators for Transient Biomedical Implants. *Adv. Funct. Mater.* **2019**, 1903051.

(39) Yin, L.; Cheng, H.; Mao, S.; Haasch, R.; Liu, Y.; Xie, X.; Hwang, S.-W.; Jain, H.; Kang, S.-K.; Su, Y.; Li, R.; Huang, Y.; Rogers, J. A. Dissolvable Metals for Transient Electronics. *Adv. Funct. Mater.* **2014**, *24* (5), 645−658.

(40) Kim, Y.-J.; Allen, M. G. Surface Micromachined Solenoid Inductors for High Frequency Applications. *IEEE Trans. Components, Packag. Manuf. Technol. Part C* **1998**, *21* (1), 26−33.

(41) Boutry, C. M.; Chandrahalim, H.; Streit, P.; Schinhammer, M.; Hänzi, A. C.; Hierold, C. Characterization of Miniaturized RLC Resonators Made of Biodegradable Materials for Wireless Implant Applications. *Sens. Actuators, A* **2013**, *189*, 344−355.

(42) Zeng, J.; Wang, C.; Sangster, A. J. Theoretical and Experimental Studies of Flip-Chip Assembled High-Q Suspended MEMS Inductors. *IEEE Trans. Microwave Theory Technol.* **2007**, *55* (6), 1171−1181.

(43) Hwang, S.-W.; Huang, X.; Seo, J.-H.; Song, J.-K.; Kim, S.; Hage-Ali, S.; Chung, H.-J.; Tao, H.; Omenetto, F. G.; Ma, Z.; Rogers, J. A. Materials for Bioresorbable Radio Frequency Electronics. *Adv. Mater.* **2013**, *25* (26), 3526−3531.

(44) Lee, C. H.; Kang, S.-K.; Salvatore, G. A.; Ma, Y.; Kim, B. H.; Jiang, Y.; Kim, J. S.; Yan, L.; Wie, D. S.; Banks, A.; Oh, S. J.; Feng, X.; Huang, Y.; Troester, G.; Rogers, J. A. Wireless Microfluidic Systems for Programmed, Functional Transformation of Transient Electronic Devices. *Adv. Funct. Mater.* **2015**, *25* (32), 5100−5106.

(45) Palmroth, A.; Salpavaara, T.; Lyyra, I.; Kroon, M.; Lekkala, J.; Kellomäki, M. Bioresorbable Conductive Wire with Minimal Metal Content. *ACS Biomater. Sci. Eng.* **2019**, *5*, 1134.

(46) Martin, P. M.. *Handbook of Deposition Technologies for Films and Coatings: Science, Applications and Technology*; William Andrew: 2009.

(47) Moens, F.; Schramm, I. C.; Konstantinidis, S.; Depla, D. On the Microstructure of Magnesium Thin Films Deposited by Magnetron Sputtering. *Thin Solid Films* **2019**, *689*, 137501.

(48) Rossnagel, S. M. Thin Film Deposition with Physical Vapor Deposition and Related Technologies. *J. Vac. Sci. Technol., A* **2003**, *21* (5), S74−S87.

(49) Hwang, S.-W.; Song, J.-K.; Huang, X.; Cheng, H.; Kang, S.-K.; Kim, B. H.; Kim, J.-H.; Yu, S.; Huang, Y.; Rogers, J. A. High-Performance Biodegradable/Transient Electronics on Biodegradable Polymers. *Adv. Mater.* **2014**, *26* (23), 3905−3911.

(50) Lee, C. H.; Kim, H.; Harburg, D. V.; Park, G.; Ma, Y.; Pan, T.; Kim, J. S.; Lee, N. Y.; Kim, B. H.; Jang, K.-I.; Kang, S.-K.; Huang, Y.; Kim, J.; Lee, K.-M.; Leal, C.; Rogers, J. A. Biological Lipid Membranes for On-Demand, Wireless Drug Delivery from Thin, Bioresorbable Electronic Implants. *Npg Asia Mater.* **2015**, *7*, 1−9.

(51) Koo, J.; MacEwan, M. R.; Kang, S.-K.; Won, S. M.; Stephen, M.; Gamble, P.; Xie, Z.; Yan, Y.; Chen, Y.-Y.; Shin, J.; Birenbaum, N.; Chung, S.; Kim, S. B.; Khalifeh, J.; Harburg, D. V.; Bean, K.; Paskett, M.; Kim, J.; Zohny, Z. S.; Lee, S. M.; Zhang, R.; Luo, K.; Ji, B.; Banks, A.; Lee, H. M.; Huang, Y.; Ray, W. Z.; Rogers, J. A. Wireless Bioresorbable Electronic System Enables Sustained Nonpharmacological Neuroregenerative Therapy. *Nat. Med.* **2018**, *24* (12), 1830−1836.

(52) Allen, D.; Simpkins, M.; Almond, H. A Novel Photochemical Machining Process for Magnesium Aerospace and Biomedical Microengineering Applications. *J. Micromech. Microeng.* **2010**, *20*, 105010.

(53) Guo, Q.; Koo, J.; Xie, Z.; Avila, R.; Yu, X.; Ning, X.; Zhang, H.; Liang, X.; Kim, S. B.; Yan, Y.; MacEwan, M. R.; Lee, H. M.; Song, A.; Di, Z.; Huang, Y.; Mei, Y.; Rogers, J. A. A Bioresorbable Magnetically Coupled System for Low-Frequency Wireless Power Transfer. *Adv. Funct. Mater.* **2019**, *0* (0), 1905451.

(54) Tsang, M.; Armutlulu, A.; Herrault, F.; Shafer, R. H.; Allen, S. A. B.; Allen, M. G. Development of Electroplated Magnesium Microstructures for Biodegradable Devices and Energy Sources. *J. Microelectromech. Syst.* **2014**, *23* (6), 1281−1289.

(55) Lee, S.; Koo, J.; Kang, S.-K.; Park, G.; Lee, Y. J.; Chen, Y.-Y.; Lim, S. A.; Lee, K.-M.; Rogers, J. A. Metal Microparticle − Polymer

Composites as Printable, Bio/Ecoresorbable Conductive Inks. *Mater. Today* **2018**, *21* (3), 207–215.

(56) Abduev, A. K.; Akhmedov, A. K.; Asvarov, A. S.; Alikhanov, N. M.-R.; Emirov, R. M.; Muslimov, A. E.; Belyaev, V. V. Gas-Phase Clusterization of Zinc during Magnetron Sputtering. *Crystallogr. Rep.* **2017**, *62* (1), 133–138.

(57) Vojtěch, D.; Kubásek, J.; Šerák, J.; Novák, P. Mechanical and Corrosion Properties of Newly Developed Biodegradable Zn-Based Alloys for Bone Fixation. *Acta Biomater.* **2011**, *7* (9), 3515–3522.

(58) Tao, H.; Hwang, S.-W.; Marelli, B.; An, B.; Moreau, J. E.; Yang, M.; Brenckle, M. A.; Kim, S.; Kaplan, D. L.; Rogers, J. A.; Omenetto, F. G. Silk-Based Resorbable Electronic Devices for Remotely Controlled Therapy and in Vivo Infection Abatement. *Proc. Natl. Acad. Sci. U. S. A.* **2014**, *111* (49), 17385–17389.

(59) Zamora, R.; Jackson, A.; Seligson, D. Correct Techniques for the Use of Bioabsorbable Implants in Orthopaedic Trauma. *Curr. Orthop. Pract.* **2016**, *27* (4), 469–473.

(60) Kang, S.-K.; Hwang, S.-W.; Yu, S.; Seo, J.-H.; Corbin, E. A.; Shin, J.; Wie, D. S.; Bashir, R.; Ma, Z.; Rogers, J. A. Biodegradable Thin Metal Foils and Spin-On Glass Materials for Transient Electronics. *Adv. Funct. Mater.* **2015**, *25* (12), 1789–1797.

(61) Kang, S.-K.; Hwang, S.-W.; Cheng, H.; Yu, S.; Kim, B. H.; Kim, J.-H.; Huang, Y.; Rogers, J. A. Dissolution Behaviors and Applications of Silicon Oxides and Nitrides in Transient Electronics. *Adv. Funct. Mater.* **2014**, *24* (28), 4427–4434.

(62) Shin, J.; Yan, Y.; Bai, W.; Xue, Y.; Gamble, P.; Tian, L.; Kandela, I.; Haney, C. R.; Spees, W.; Lee, Y.; Choi, M.; Ko, J.; Ryu, H.; Chang, J.-K.; Pezhouh, M.; Kang, S.-K.; Won, S. M.; Yu, K. J.; Zhao, J.; Lee, Y. K.; MacEwan, M. R.; Song, S.-K.; Huang, Y.; Ray, W. Z.; Rogers, J. A. Bioresorbable Pressure Sensors Protected with Thermally Grown Silicon Dioxide for the Monitoring of Chronic Diseases and Healing Processes. *Nat. Biomed. Eng.* **2019**, *3* (1), 37–46.

(63) Hwang, S.-W.; Kim, D.-H.; Tao, H.; Kim, T.; Kim, S.; Yu, K. J.; Panilaitis, B.; Jeong, J.-W.; Song, J.-K.; Omenetto, F. G.; Rogers, J. A. Materials and Fabrication Processes for Transient and Bioresorbable High-Performance Electronics. *Adv. Funct. Mater.* **2013**, *23* (33), 4087–4093.

(64) Alonso, J. C.; Ortiz, A.; Falcony, C. Low Temperature SiO$_2$ Films Deposited by Plasma Enhanced Techniques. *Vacuum* **1992**, *43* (8), 843–847.

(65) Hoivik, N. D.; Elam, J. W.; Linderman, R. J.; Bright, V. M.; George, S. M.; Lee, Y. C. Atomic Layer Deposited Protective Coatings for Micro-Electromechanical Systems. *Sens. Actuators, A* **2003**, *103* (1), 100–108.

(66) Lahtinen, K.; Maydannik, P.; Johansson, P.; Kääriäinen, T.; Cameron, D. C.; Kuusipalo, J. Utilisation of Continuous Atomic Layer Deposition Process for Barrier Enhancement of Extrusion-Coated Paper. *Surf. Coat. Technol.* **2011**, *205* (15), 3916–3922.

(67) Kääriäinen, T. O.; Maydannik, P.; Cameron, D. C.; Lahtinen, K.; Johansson, P.; Kuusipalo, J. Atomic Layer Deposition on Polymer Based Flexible Packaging Materials: Growth Characteristics and Diffusion Barrier Properties. *Thin Solid Films* **2011**, *519* (10), 3146–3154.

(68) Lahtinen, K.; Johansson, P.; Kääriäinen, T.; Cameron, D. C. Adhesion of Extrusion-Coated Polymer Sealing Layers to a Fiber-Based Packaging Material with an Atomic Layer Deposited Aluminum Oxide Surface Coating. *Polym. Eng. Sci.* **2012**, *52* (9), 1985–1990.

(69) Abdulagatov, A. I.; Yan, Y.; Cooper, J. R.; Zhang, Y.; Gibbs, Z. M.; Cavanagh, A. S.; Yang, R. G.; Lee, Y. C.; George, S. M. Al2O3 and TiO$_2$ Atomic Layer Deposition on Copper for Water Corrosion Resistance. *ACS Appl. Mater. Interfaces* **2011**, *3* (12), 4593–4601.

(70) Song, M.-K.; Namgung, S. D.; Sung, T.; Cho, A.-J.; Lee, J.; Ju, M.; Nam, K. T.; Lee, Y.-S.; Kwon, J.-Y. Physically Transient Field-Effect Transistors Based on Black Phosphorus. *ACS Appl. Mater. Interfaces* **2018**, *10* (49), 42630–42636.

(71) Won, S. M.; Koo, J.; Crawford, K. E.; Mickle, A. D.; Xue, Y.; Min, S.; McIlvried, L. A.; Yan, Y.; Kim, S. B.; Lee, S. M.; Kim, B. H.; Jang, H.; MacEwan, M. R.; Huang, Y.; Gereau, R. W., IV; Rogers, J. A.

Natural Wax for Transient Electronics. *Adv. Funct. Mater.* **2018**, *28* (32), 1801819.

(72) Yang, Q.; Lee, S.; Xue, Y.; Yan, Y.; Liu, T.-L.; Kang, S.-K.; Lee, Y. J.; Lee, S. H.; Seo, M.-H.; Lu, D.; Koo, J.; MacEwan, M. R.; Yin, R. T.; Ray, W. Z.; Huang, Y.; Rogers, J. A. Materials, Mechanics Designs, and Bioresorbable Multisensor Platforms for Pressure Monitoring in the Intracranial Space. *Adv. Funct. Mater.* **2020**, *30*, 1910718.

(73) Xie, F.; Deng, X.; Kratzer, D.; Cheng, K. C. K.; Friedmann, C.; Qi, S.; Solorio, L.; Lahann, J. Backbone-Degradable Polymers Prepared by Chemical Vapor Deposition. *Angew. Chem., Int. Ed.* **2017**, *56* (1), 203–207.

(74) Middleton, J. C.; Tipton, A. J. Synthetic Biodegradable Polymers as Orthopedic Devices. *Biomaterials* **2000**, *21* (23), 2335–2346.

(75) Salpavaara, T.; Ellä, V.; Kellomäki, M.; Lekkala, J. *Biodegradable Passive Resonance Sensor: Fabrication and Initial Testing.* In BIODEVICES 2015 - 8th International Conference on Biomedical Electronics and Devices; SCITEPRESS: 2015; pp 127–131.

(76) Massera, J.; Fagerlund, S.; Hupa, L.; Hupa, M. Crystallization Mechanism of the Bioactive Glasses, 45S5 and S53P4. *J. Am. Ceram. Soc.* **2012**, *95* (2), 607–613.

(77) Salpavaara, T. *Inductively Coupled Passive Resonance Sensors: Readout Methods and Applications*; Tampere University of Technology: 2018.

Supporting Information

Materials and Orthopedic Applications for Bioresorbable Inductively Coupled Resonance Sensors

Aleksi Palmroth[a,*], Timo Salpavaara[a], Petri Vuoristo[b], Sanna Karjalainen[a], Tommi Kääriäinen[c,†], Susanna Miettinen[a], Jonathan Massera[a], Jukka Lekkala[a], Minna Kellomäki[a]

[a]BioMediTech, Faculty of Medicine and Health Technology, Tampere University. Korkeakoulunkatu 3, Tampere 33720, Finland.

[b]Materials Science and Environmental Engineering, Faculty of Engineering and Natural Sciences, Tampere University. Korkeakoulunkatu 6, Tampere 33720, Finland.

[c]Department of Chemistry, University of Colorado, Boulder, Colorado 80309, United States.

*Corresponding author: aleksi.palmroth@tuni.fi

Contents

1. Cell culture results and discussion

The cytotoxicity of PDTEC was evaluated by culturing a human fibroblast cell line (ATCC, CRL-2429) on compression molded discs using standard polystyrene 24-well plates (Nunc, Denmark*)* as a control and PLDLA 96/4 discs as a bioresorbable reference material. Based on the crystal violet staining (Figure S1a-b), the cell growth on PDTEC was comparable if not superior to the reference materials. The result is in agreement with earlier cell data using rat lung fibroblasts, where the cytotoxicity level of PDTEC was estimated to be comparable to glass and hydrophilic modified polystyrene.[1] The Live/Dead images showed a rather spherical fibroblast shape during the first days of culture (Figure S1c). The alive cells were colored green, whereas no red color (indicating dead cells) were noticed in the images. After 7 days, the amount of elongated cells increased.
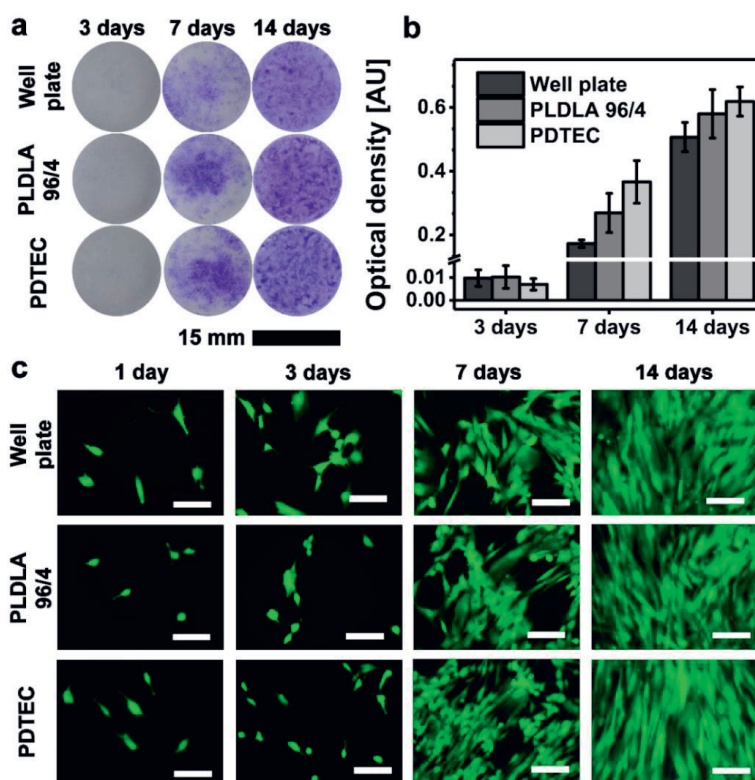

Figure S1. The in vitro cytotoxicity assessment of different materials using (a) Crystal violet staining (b) Quantitative crystal violet staining (n=8), where the bound dye was solubilized in 10 % acetic acid and its optical density in absorbance units (AU) was measured at 590 nm. The optical density correlates to the number of cells. (c) Live/Dead staining where green color depicts alive cells. Dead cells would have been shown in red. The scale bars are 100 µm.

2. Cell culture methods

PDTEC and PLDLA 96/4 sheets were compression molded against glass to yield a smooth surface. Polymer discs (Ø = 14 mm) were punch-cut from the sheets, washed in 2-propanol (VWR Chemicals), dried and sterilized by gamma irradiation (BBF Sterilisationsservice GmbH, Kernen im Remstal, Germany) with a minimum dose of 25 kGy.

Human foreskin fibroblasts (ATCC, CRL-2429) at passage 12 were seeded onto the bioresorbable polymer discs as well as directly onto the polystyrene 24-well plates (Ø = 15 mm; Nunc, Roskilde, Denmark) by first adding 1 ml of cell culture medium onto each well and then pipetting 1000 cells in 50 µl of cell suspension onto each well. The cell culture medium consisted of DMEM/F-12 (DMEM/F-12 1:1; Gibco by Life Technologies, United Kingdom) supplemented with 10 % fetal bovine serum (FBS; Gibco by Life Technologies), 1 % L-glutamine (GlutaMAX I; Thermo Fischer Scientific, USA) and 1 % antibiotics (100 U/ml penicillin; 100 U/ml streptomycin; Lonza, Switzerland). The fibroblasts were cultured at 37 °C in 5 % CO_2 and the medium was changed twice a week.

The viability of the fibroblasts was evaluated with Live/Dead staining probes (Invitrogen Molecular Probes, USA) after 1, 3, 7 and 14 days of culture.[2] The fibroblasts were incubated in 0.25 mM EthD-1 (Molecular Probes) and 0.5 mM calcein AM (Molecular Probes) in Dulbecco's Phosphate Buffered Saline (DPBS; Sigma Aldrich, United Kingdom) for 45 minutes and then imaged with a phase-contrast microscope (Olympus IX51, Japan) with fluorescence optics. The fibroblast imaging was done by transferring the bioresorbable substrate discs onto clean well plates, whereas well plate controls were imaged directly from the polystyrene wells.

The relative cell number was determined with a quantitative crystal violet staining method with slight modifications.[3] The fibroblasts were fixed onto their substrates with 5% glutaraldehyde in 0.1 M PBS. The washed and dried substrates were then incubated for 20 minutes with 250 µl of 0.1 % crystal violet stain (Merck) in H_2O (milli-Q). The fibroblasts were then washed with H_2O until the washing solution was clear, after which the substrates were allowed to dry. The samples were then photographed before solubilizing the dye bound in the cell nuclei in 10 % acetic acid (J.T. Baker, Deventer, the Netherlands). The amount of acetic acid was calculated based on the substrate culture area, using 550 µl for the reference wells (Ø = 15 mm) and 480 µl for the bioresorbable polymer discs (Ø = 14 mm).[4] The optical density (590 nm) was measured from each well using Victor 1420 multilabel plate reader (Wallac, Turku, Finland). This resulted in relative cell numbers given as absorbance units. Eight parallel samples were measured to calculate the mean optical density ± standard deviation for each

material at each time point. Stained substrates without cells were used as a baseline by subtracting their optical density values from the adjacent time-point measurements (3, 7 and 14 days) containing cells.

3. Skin depths of common biodegradable metals

Table S1 summarizes the skin depth values of the most commonly used biodegradable conductor metals. The values were calculated using the equation:

$$Skin\ depth\ \delta = \sqrt{\frac{\rho}{\pi f \mu_0 \mu_r}}$$

where ρ is the electrical resistivity of the material, f the frequency and μ_0 the permeability constant ($4\pi \times 10^{-7}$ H/m).[5] The relative permeability μ_r was approximated as 1 for all other metals except for Fe, whose μ_r estimation was 5500.[6]

Table S1. The electrical characteristics of the most common biodegradable metals.

Material	Electrical resistivity at 295 K ($\Omega \times 10^{-8}$m)	Skin depth @ 10 MHz	Skin depth @ 50 MHz	Skin depth @ 100 MHz	Skin depth @ 500 MHz
Magnesium (Mg)	4.3	33 µm	15 µm	10 µm	5 µm
Zinc (Zn)	5.9	39 µm	17 µm	12 µm	5 µm
Iron (Fe)	9.8	0.7 µm	0.3 µm	0.2 µm	0.01 µm
Molybdenum (Mo)	5.3	37 µm	16 µm	12 µm	5 µm

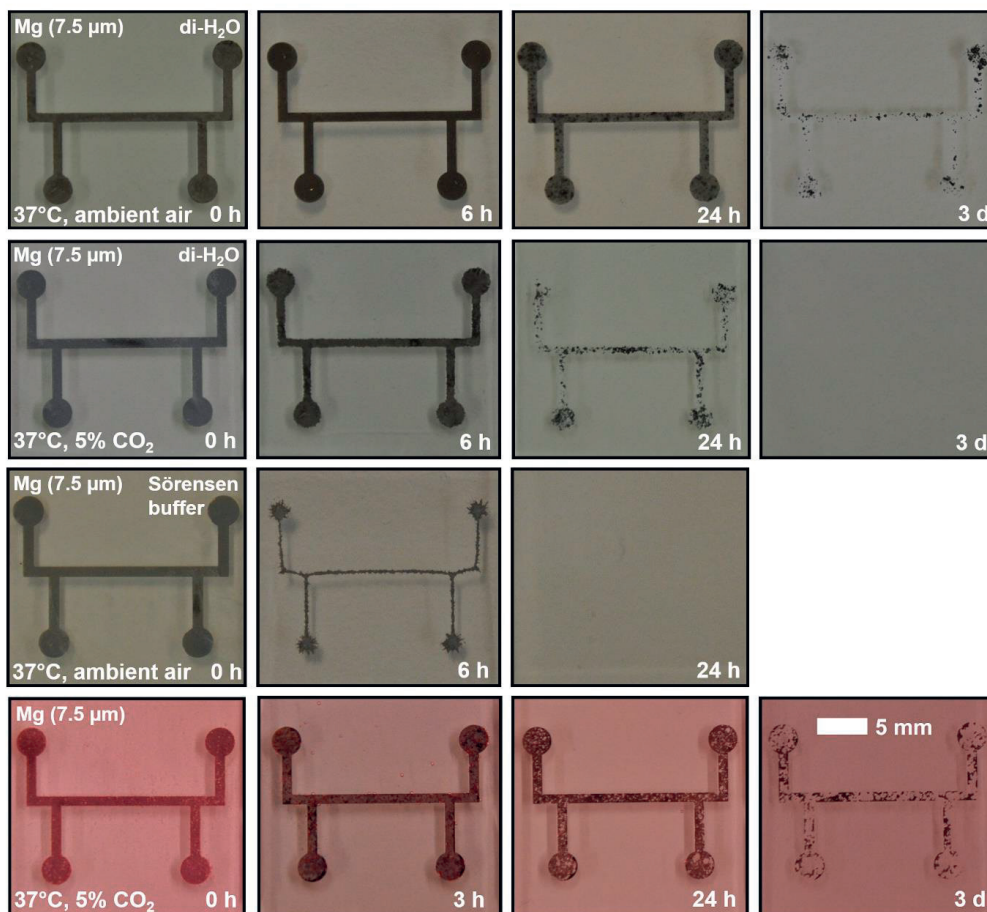## 4. Corrosion testing of magnesium films (7.5 μm)

Figure S2. Comparison of the corrosion behavior of Mg films (7.5 μm) in different immersion environments at +37 °C. The undermost row shows samples immersed in cell culture media, which consisted of Minimum Essential Medium supplemented with 10 % FBS and 1 % antibiotics.

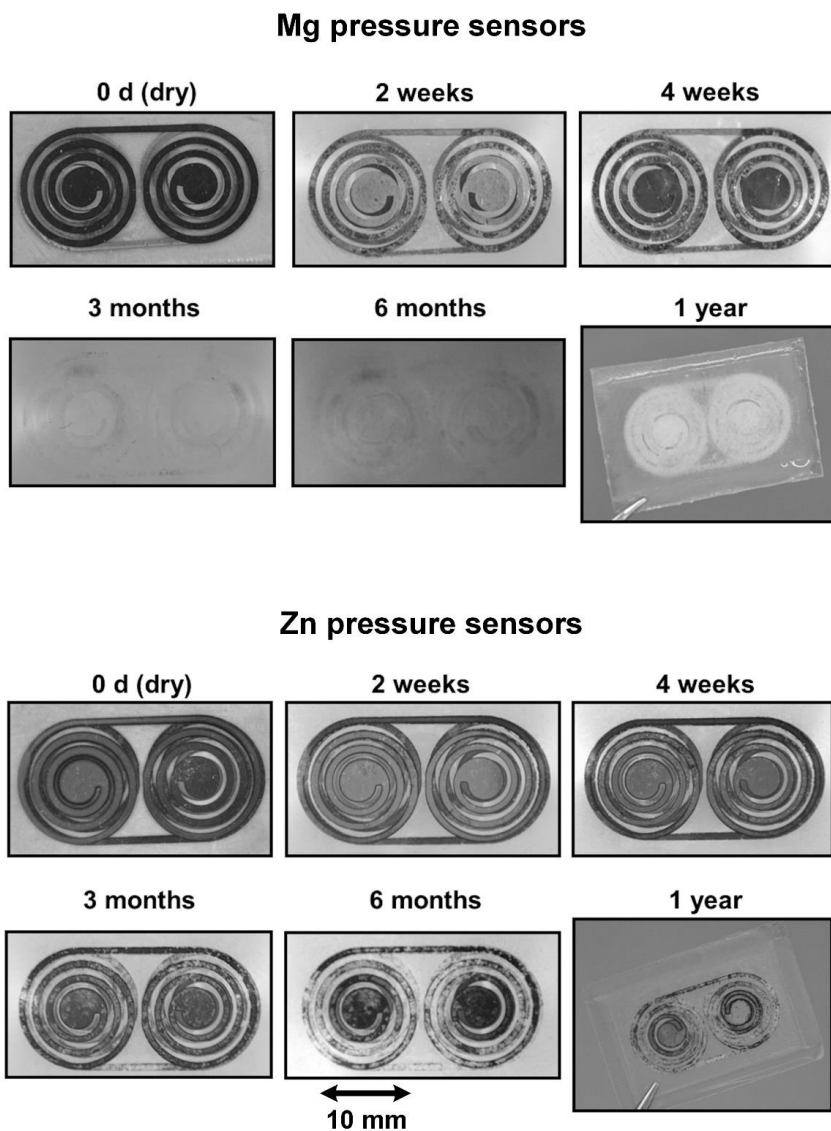## 5. In vitro degradation photographs of the wireless Mg and Zn pressure sensors

Mg pressure sensors

Zn pressure sensors

Figure S3. Photographs of the Mg and Zn pressure sensors immersed in Sörensen buffer (+37 °C). The conductors are encapsulated inside the PDTEC substrates as illustrated in the 1-year images.
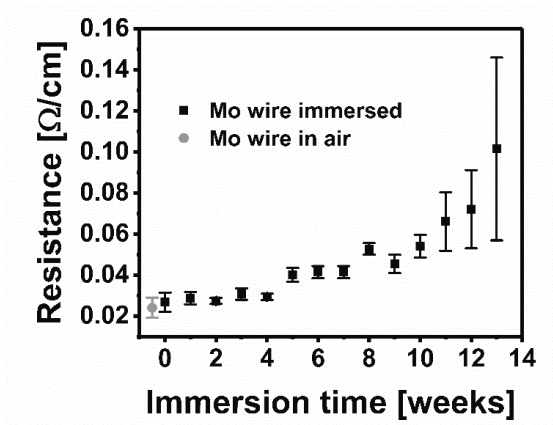
6. Molybdenum wire immersion test

Figure S4. The electrical resistance of uncoated molybdenum wires (200 µm) immersed in Sörensen buffer solution at +37 °C. The tips of the 30 cm wires were attached to the lid of 50 ml falcon tubes for reliable non-immersed measurement points.

7. Illustration of the peeled-off area of the ALD coatings
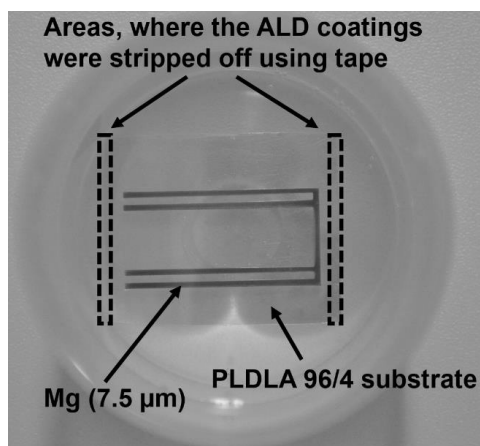

Figure S5. The image illustrates the areas, from where the ALD coatings were peeled off using tape. This was done to see the possible effects of water diffusion into the substrate.

8. ALD coated substrates in an LC resonator

LC resonators were formed using ALD coated (500 cycles or 50 nm) PLDLA 96/4 substrates (430 µm) with Mg conductors (7.5 µm) that were e-beam evaporated onto the ALD coatings as shown in Figure S6a. Two substrates were separated with a compression molded PLDLA 96/4 spacer (80 µm) and the whole structure was then melt welded from the sides. The resonator architecture was based on the design by Salpavaara et al. with the exception of the insulating polymer spacer instead of evaporated SiO_2 dielectric layers.[7]

The behavior of the resonator with ALD coated substrates under immersion (Sörensen buffer, +37 °C) was similar to earlier reported non-coated resonators in the sense that the resonance frequency of the device started to increase steeply within the first 24 hours.[7,8] In this case, after 10 hours of immersion, the resonance frequency of the sensor increased from less than 70 MHz to over 100 MHz in 1.5 hours. Furthermore, after 24 hours of immersion, the ALD coatings showed clear cracks (Figure S6c).

The increasing resonance frequency indicates that the polymer substrates have undergone dimensional changes and bended away from each other. This could have been due to their swelling, or due to H_2 generation inside the resonator caused by the corroding the Mg conductors. Thus, with this kind of resonator structure where the water is allowed to diffuse into the polymer matrix from the welded sides, the ALD coating did not provide benefits in terms of stable operation. Further studies where a complete resonator is ALD coated would be interesting, even though in practical implant applications their defect-free insertion might be challenging.
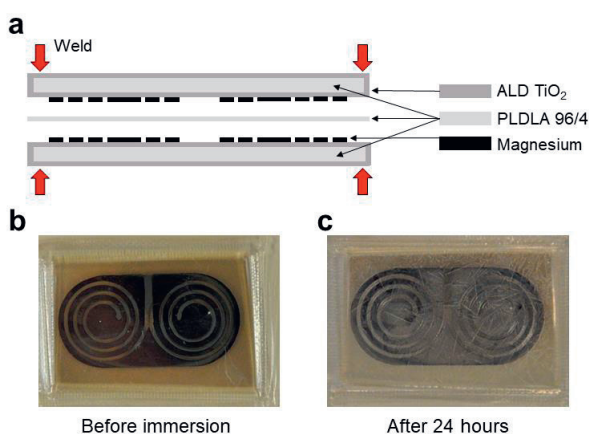

Figure S6. (a) Schematic image of the LC resonator structure, where the substrates were first ALD coated, then metallized and in the end heat sealed from the sides, as pointed by the red arrows. (b) A photograph of a resonator before immersion. (c) The resonator after 24 hours of immersion in Sörensen buffer solution, showing cracks in the ALD layer.

9. References

(1) Ertel, S. I.; Kohn, J. Evaluation of a Series of Tyrosine-Derived Polycarbonates as Degradable Biomaterials. *J. Biomed. Mater. Res.* **1994**, *28* (8), 919–930. https://doi.org/10.1002/jbm.820280811.

(2) Tirkkonen, L.; Halonen, H.; Hyttinen, J.; Kuokkanen, H.; Sievänen, H.; Koivisto, A.; Mannerström, B.; Sándor, G. K. B.; Suuronen, R.; Miettinen, S.; Haimi, S. The Effects of Vibration Loading on Adipose Stem Cell Number, Viability and Differentiation towards Bone-Forming Cells. *J. R. Soc. Interface* **2011**, *8* (65), 1736–1747. https://doi.org/10.1098/rsif.2011.0211.

(3) Kueng, W.; Silber, E.; Eppenberger, U. Quantification of Cells Cultured on 96-Well Plates. *Anal. Biochem.* **1989**, *182* (1), 16–19. https://doi.org/10.1016/0003-2697(89)90710-0.

(4) Miettinen, S.; Ahonen, M. H.; Lou, Y.-R.; Manninen, T.; Tuohimaa, P.; Syvälä, H.; Ylikomi, T. Role of 24-Hydroxylase in Vitamin D3 Growth Response of OVCAR-3 Ovarian Cancer Cells. *Int. J. Cancer* **2004**, *108* (3), 367–373. https://doi.org/10.1002/ijc.11520.

(5) Shaltout, A. H.; Gregori, S. Conformal-Mapping Model for Estimating the Resistance of Polygonal Inductors. In *2016 IEEE International Symposium on Circuits and Systems (ISCAS)*; 2016; pp 1274–1277. https://doi.org/10.1109/ISCAS.2016.7527480.

(6) Edwards, T. C.; Steer, M. B. Appendix B: Material Properties. In *Foundations for Microstrip Circuit Design*; Wiley Online Books; John Wiley & Sons, Ltd, 2016; pp 635–642. https://doi.org/doi:10.1002/9781118936160.app2.

(7) Salpavaara, T.; Ellä, V.; Kellomäki, M.; Lekkala, J. Biodegradable Passive Resonance Sensor: Fabrication and Initial Testing. In *BIODEVICES 2015 - 8th International Conference on Biomedical Electronics and Devices*; SCITEPRESS, 2015; pp 127–131. https://doi.org/10.5220/0005255901270131.

(8) Palmroth, A.; Salpavaara, T.; Lekkala, J.; Kellomäki, M. Fabrication and Characterization of a Wireless Bioresorbable Pressure Sensor. *Adv. Mater. Technol.* **2019**, *0* (0), 1900428. https://doi.org/10.1002/admt.201900428.